# Cast iron cannonballs of the *Mary Rose*: quantifying corrosion rates to inform management of the collection

Jerrod H. Seifert

Thesis submitted to Cardiff University in candidature
for the degree of PhD
June 2021

# SUMMARY

Managing heritage collections requires understanding of their response to storage and display environments. For heritage iron artefacts, and especially those from marine contexts, this environmental response is influenced by corrosion-instigating chlorides that remain after conservation treatments designed to remove them have been completed. Previous studies have shown that measuring chlorides extracted during treatment does not accurately inform on how many chlorides remain. Artefacts are then placed on display or in storage under the assumption it is safe to do so, when in fact their environment may be causing them to deteriorate at a rate that compromises their structural integrity and cultural value.

It is this problem that faces the 1248 cast iron cannonballs from the *Mary Rose,* Henry VIII's Tudor-era warship that sank in 1545 and was excavated beginning in 1971. Many treatment methods have been employed on the cannonballs to mitigate their corrosion, yet they continue to show visible signs of corrosion in a range of humidities. Nearly all of the cast iron cannonballs are now in desiccated or passivating storage, robbing the public of crucial context their display would otherwise provide.

This study set out to determine the corrosion rates of 56 variously treated cannonballs from the *Mary Rose*, to inform on and determine their best practices for their ongoing care. Using non-invasive oxygen consumption monitoring to determine their corrosion rates confirmed earlier studies on wrought iron showing the escalating risk faced with escalating humidity. All cannonballs exhibited negligible gains from 20–40% RH, followed by substantial increases at 50% RH and again at 60% RH. Selected cannonballs were then retreated in order to determine if their corrosion rates could be reduced. The results showed that not only did retreatment fail to reduce corrosion rates, doing so caused those rates to increase for most of the samples that underwent the procedure, thereby ruling out retreatment as a viable option until new methods are assessed.

By using the methodology and data presented in this study, the Mary Rose Trust is now able to ascertain the risk to each of their cast iron cannonballs post-treatment, and can use that knowledge to mitigate the deterioration of the assemblage.

# ACKNOWLEDGMENTS

I am deeply indebted to my advisors Nicola Emmerson and David Watkinson for their gracious and unceasing assistance, input in laboratory practice and insight in data analysis, supervision, guidance, mentorship, their belief in this work, and their belief in me.

Many thanks to the Mary Rose Trust and to Mark Jones, Eleanor Schofield, and David Pearson for providing the sample material that made this study possible, and for unreservedly answering any and all questions about their treatment and storage histories. I owe no small amount of gratitude to Jesse Wolfhagen for his insight and expertise in statistical analysis.

At Cardiff University, thanks to Jane Henderson and Phil Parkes for their constant support, Ian Dennis and Kirsty Harding for help with graphics and unmitigated use of their laboratory, Richard Madgwick and Jacqui Mulville for providing opportunities for this work to reach a broader audience, John Hines for his help with PhD annual reviews, and to Ashley Lingle for her unwavering compassion and friendship. I was at one time or another a student of all of these people, and I am humbled and honoured to be ending this journey as their colleague. Additional thanks go to Johanna Thunberg and Sam Johnson for their help and patience in the lab, and Peter Meehan for his knowledge and providing invaluable reference material.

Finally, my deepest thanks to my friends and family for their steadfast, unqualified encouragement and support, especially my partner Pinar, my brother Leigh and his partner Emily, and my parents David and Yvonne.

# DEDICATION

For my sister Byrony Frances Seifert and our niece, Evelyn Frances.

## TABLE OF CONTENTS

# LIST OF FIGURES

# LIST OF TABLES

# LIST OF EQUATIONS

# 1 INTRODUCTION

## 1.1 THE *MARY ROSE*

When Henry VIII ascended to the throne of England in 1509, he immediately sought to increase the military armament and prowess of the country (Teesdale, 1991: 12). He commissioned the building of the *Mary Rose* in the same year, as part of a larger coastal and marine defence build-up (Rule, 1982: 22), one of 29 ships he either acquired or commissioned between 1509 and 1514 (Teesdale, 1991: 12). A clinker-built carrack (Figure 1.1) the *Mary Rose* was completed and first sailed in 1511. She was considered Henry's flagship and saw regular naval action in the ensuing decades (Hildred, 2011: 9).

In 1536, she was drydocked in Portsmouth and underwent an extensive rebuild, including retrofitting the clinker construction for carvel planking (Figure 1.1)and a continuous gun deck, a feature that allowed for a massive increase in firepower and had since become a necessity of any modern warship (Figure 1.2) (Rule, 1982: 25).

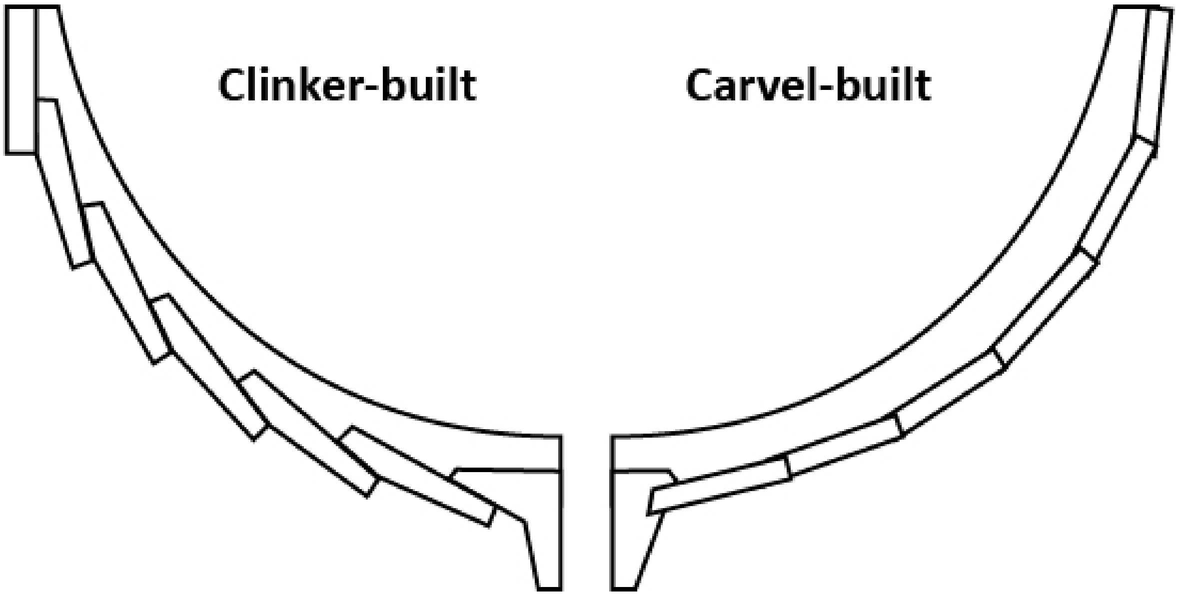

**Figure 1.1:** Clinker and carvel construction. From Wikipedia.org

Following the ex-communication of Henry VIII from the Roman Catholic Church, France and Spain (at the urging of the Pope) increased the military force against England. In 1545, France had a fleet of some 225 ships and 30000 men anchored off the southern coast of England with a goal of invading Portsmouth, destroying the shipyards, and burning Henry's ships as they were moored in their own docks (Rule, 1982: 33).

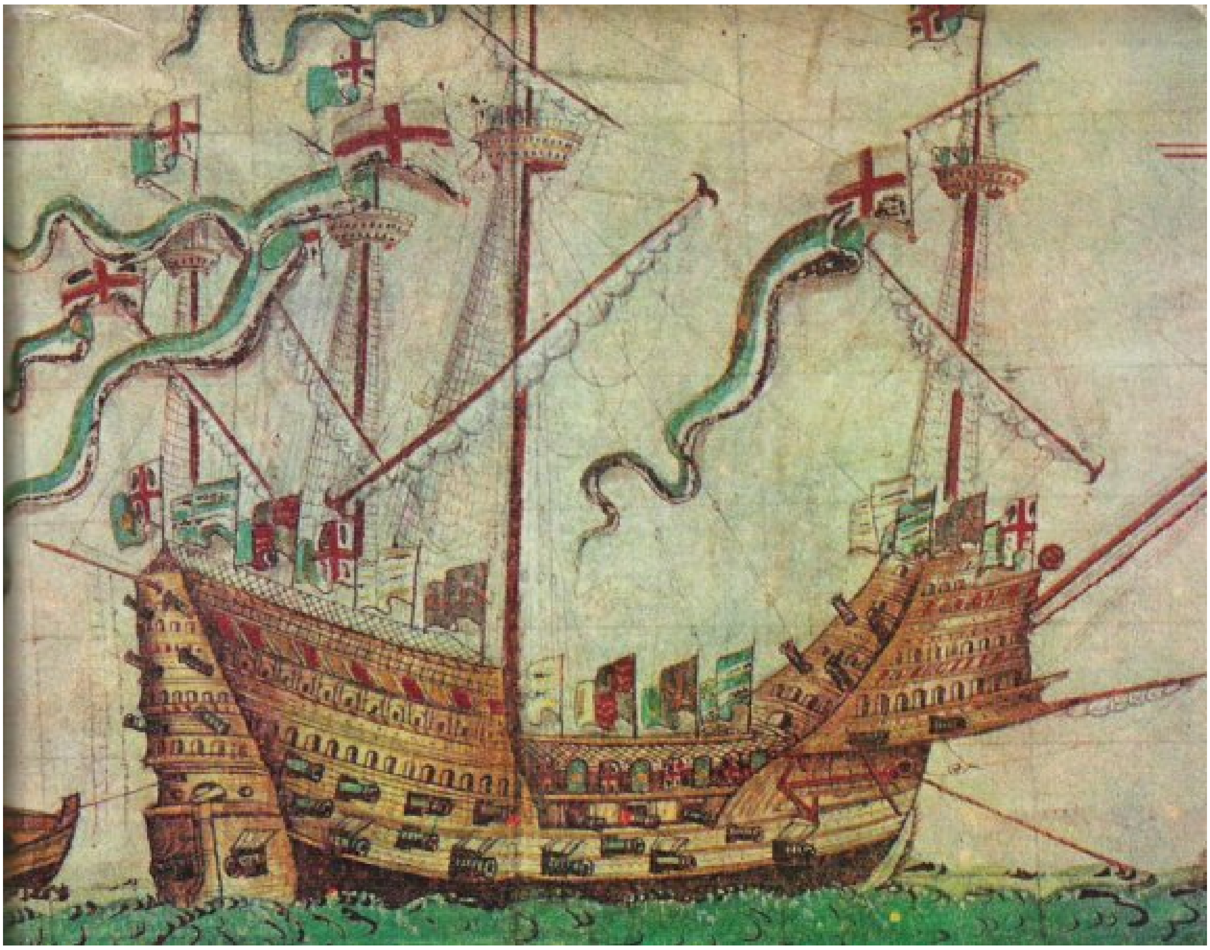

**Figure 1.2:** The *Mary Rose,* as depicted in 1546 in the Anthony Roll. From Rule (1982: 26).

Henry himself was at Portsmouth when, on July 19th 1545 whilst preparing to engage the French navy in the Solent, the *Mary Rose* heeled and capsized. Sinking rapidly on her starboard side, she embedded into the clay deposits at the bottom of the sea. Over 400 crewmen lost their lives with only an estimated 40 survivors. The cause of the rapid sinking lies in the rebuild: the continuous gunport meant that the ship was overburdened with ordnance, and the ports being lashed open allowed a rush of water into the hull. The French claimed a shot from one of their cannons sunk her, though no evidence for this was observed during excavation. The *Mary Rose* held a complement of up to 60% foreign nationals pressed into Henry's service, and it has been speculated that miscommunication amongst the crew led to a failed manoeuvre, causing the ship to keel (Bell et al., 2009).

Once on the ocean floor, the embedded starboard side quickly filled with silt, as the port side acted as a shield against stronger currents and provided a calm internal burial environment. Eventually, the port side collapsed and either washed away in currents or fell into surrounding pits (Rule, 1982: 40).

## 1.2 SALVAGE AND EXCAVATION

At least three attempts were made to retrieve the wreckage of the *Mary Rose* in the immediate aftermath of her sinking, in 1545, 1547, and 1549. A tow cable was found during the 1982 field season, suggesting one such attempt. Further attempts at salvage were scrapped after the main mast was ripped out, as that would have been required to lash any salvage rigging. Divers removed whatever guns could be retrieved, and the *Mary Rose* lay undisturbed until the 19th century (Rule, 1982: 41).

In 1836, divers John and Charles Deane were hired by local fisherman to survey an area in the Solent where their lines kept snagging. Over the next four years, the pioneering Deane brothers used their prototype diving suits and removed several large bronze and wrought iron breech guns (Figure 1.3), yew longbows, and small objects (Rule, 1982: 46). They abandoned their salvage operations in 1840, most likely due to any further findspots requiring extensive sediment removal.

**Figure 1.3:** Wrought iron gun recovered from the *Mary Rose* by The Dean Brothers in 1836.

The wreckage of the *Mary Rose* was rediscovered in 1971 after a five-year search. Excavations grew in size and duration, and increasing public interest brought more substantial funding. In 1978, The Mary Rose Trust (MRT) was formed, with the goal of quickly yet methodically excavating the wreck site *in situ*. The Trust hoped for the recovery of an intact hull, with its remains featuring as the centrepiece of a new museum (Rule, 1982: 72).

From 1979 to 1982 the bulk of the finds in and around the wreck were excavated and lifted. In October 1982, the remaining starboard hull was lifted (Figure 1.4) and removed to the Number 3 dock at Portsmouth Royal Naval Base (Figure 1.5), where it remains to this day (Rule, 1982: 214). If the excavation and lifting had not proceeded at the rate it did, the exposed timbers most likely would have broken away from current perturbations.

**Figure 1.4:** Raising of the *Mary Rose* hull in October 1982. From Rule (1982: 219).

**Figure 1.5:** The *Mary Rose* after being placed in Dry Dock #3, as the Prince and Princess of Wales look on. From Rule (1982: 230).

## 1.3 ASSOCIATED ARTEFACTS

The artefacts recovered from the wreckage provide a window into Tudor-era maritime life, at a time when England had recently become a formidable naval power. The finds include organic and inorganic materials, animal and human remains, military weaponry, and personal effects Table 1.1.

The heavy cannon aboard the ship is of note, as cast foundries had only been established in England 50 years prior (Teesdale, 1991: 10). The cast munitions from the ship represent one of the earliest mass gunfounding operations in Europe (Teesdale, 1991: 12), and their ammunition stockpile accounts for a large percentage of the total finds. For instance, of the ~19000 finds, 1248 – or 6.5% - of them are cast iron cannonballs alone (Hildred, 2011: 314). The large number of recovered cast iron shot may have something to do with their mass, as many organic and less dense artefacts (such as arrows) deteriorated or were swept away.

| Material | Typology | Find Types |
|---|---|---|
| **Wood** | poplar | arrows, handguns, tampion, lantern |
| | oak | stool, hull, tankard |
| **Human and Faunal (non-leather)** | bone | human remains |
| | | animal (dog) remains |

| | | |
|---|---|---|
| | pine | chest, spatulas, tankard |
| | boxwood | beads, sundial, combs |
| | chestnut | handles |
| | yew | longbows |
| | ash | ram head |
| | cherry | feeding bottle |
| | beech | shovel |
| | apple | linstock |
| | walnut | parrel ball |
| | maple | spoons |
| | elm | |
| | | |
| **Leather** | deerskin, sheepskin, calfskin, goatskin | jerkins, shoes, straps, bucket |
| | | |
| **Textile** | hemp | rope/rigging |
| | wool | clothing, dyed/ornamented clothing |
| | silk | cordage |
| | | |
| **Ceramic** | earthenware | flask |
| | unglazed | cooking pot |
| | tin-glazed | jug |
| | stoneware | jar |

| | | |
|---|---|---|
| | | beef bones (butchery) |
| | | carvings |
| | | pig bone |
| | horn | inkpot, bow points |
| | ivory | archer wrist guard, comb |
| | beef tallow | candles |
| | | |
| **Other Organic** | wicker | bottle wrapping |
| | paper | book |
| | | |
| **Glass** | | hourglass, beads, mirrors, windows, compass, bottles |
| | | |
| **Metals** | iron | armaments, nails, fittings |
| | copper (alloy) | fittings, cooking utensils, candle snuffer |
| | brass | navigational dividers |
| | gold | coins, jewellery |
| | silver | coins, weights, jewellery |
| | bronze | armaments |
| | leaded brass | maille |
| | lead | weights |

**Table 1.1:** Materials, typology, and find types of artefacts from the Mary Rose. The find types listed are not representative of every artefact.

## 1.4 CONSERVATION OF THE *MARY ROSE*

Conservation treatments applied to marine artefacts are rarely completed quickly, as removing harmful salts from within objects and preparing them for a life in the atmosphere after 500 years in the ocean can take months or even years, depending on the material type (North, 1987). The scope of the project provided for several treatment timelines. Artefacts were treated rapidly at the Portsmouth City Museum where a hugely curious public could view them, maximising project funding (Rule, 1982: 93). As incoming finds increased and concerns about hull stabilisation grew, artefacts that required immediate treatment were given priority over those objects that could be placed in passive storage to await treatment (Jones, 2003: 35). This allowed coordinators the time needed to both analyse artefacts and treat them, without worrying about rapid deterioration post-excavation. Nearly 50 years after her discovery, finds from the *Mary Rose* are still being treated.

### 1.4.1 CONSERVATION OF THE HULL

It took ten years to excavate and lift the *Mary Rose*, and a further 34 years to treat her (Jones, 2003: 74). After removal to her dry dock, the hull was sprayed (Figure 1.6), initially with water and later with polyethylene glycol (PEG). This polymer replaced water within degraded wood cells (Björdal and Nilsson, 2001) with initial spraying of low molecular weight (MW) ($\leq$ 600 g/mol) PEG penetrating any remaining cell walls and subsequent application of higher MW ($\geq$ 1500 g/mol, and usually in the 3500-4000 range) PEG bulking larger voids in the cellular structure. Controlled drying removed the remaining water from the hull structure with the PEG content of the wood preventing its shrinkage and distortion on drying.

**Figure 1.6:** Hull of the *Mary Rose* during treatment. From Jones (2003: 76).

This was a lengthy process; determining the best method for PEG treatment method took ten years alone, as extensive research first had to be carried out on PEG molecular weight variability to ensure optimal outcomes (Jones, 2003: 68). A two-part program was eventually settled upon. Water spraying prior to PEG treatment ensured the hull did not dry out and deteriorate. A 30% PEG 200 solution was sprayed on the hull from 1994 – 2003, with PEG 2000 and 4000 used from 2003 – 2010. The hull underwent controlled drying from 2010 – 2015.

### 1.4.2 CONSERVATION OF ASSOCIATED ARTEFACTS

The conservation program for the associated artefacts grew from being part of the Portsmouth City Museum to a requisitioned Grade II-listed Victorian warehouse in the Portsmouth Royal Naval Base. The facilities include large-scale treatment tanks, lifting cranes, walk-in climate chambers, climate-controlled storage lockers, and large freeze dryers (Figure 1.7 – Figure 1.8). The unprecedented number of finds and the decades-long treatment regime has resulted in the *Mary Rose* becoming a document of the evolution of conservation. Treatments employed in one decade were discontinued in the next (Jones, 2003: 95). The immediate necessities of the project (increase publicity, awareness, and funding) impacted initial treatment pathways. Staff turnover no doubt altered treatment directives. Documentation began in a pre-digital era when treatment reports were not required to be as comprehensive as they are today. These are all to be expected for a project of such breadth, and it remains impressive that despite these obstacles, project conservators have maintained such continuity over 50 years.

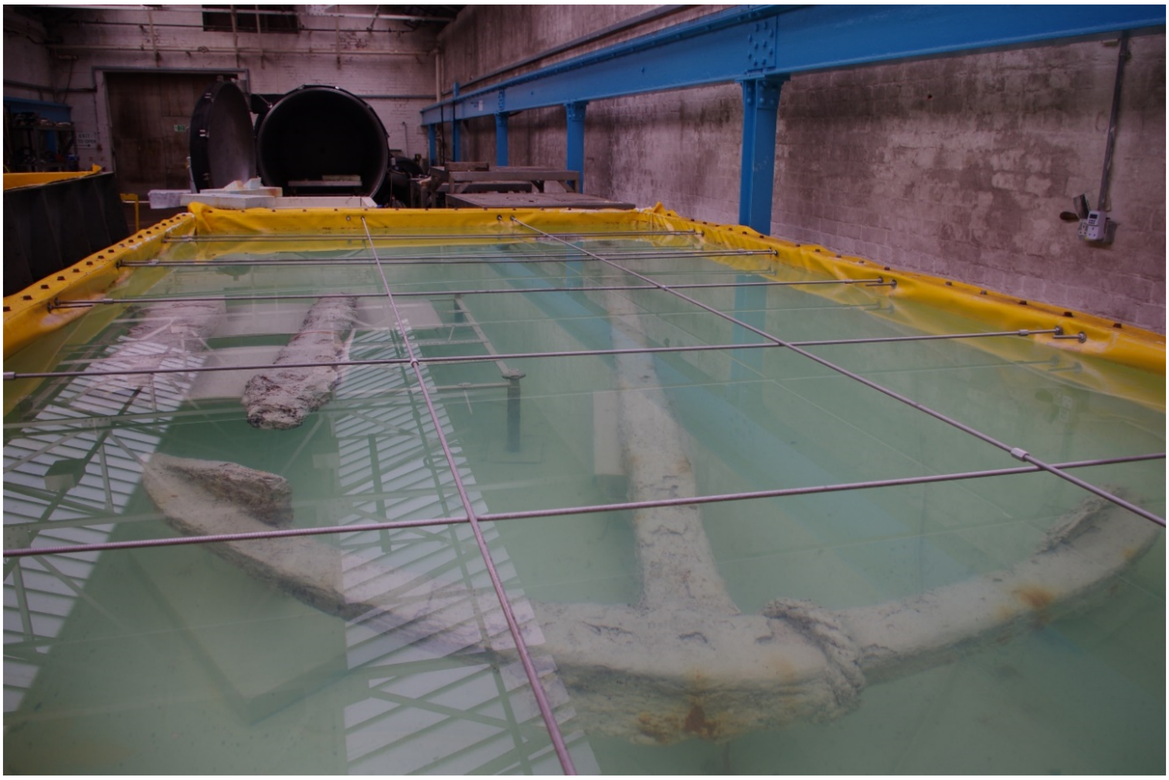

**Figure 1.7:** Large desalination tank at the *Mary Rose* conservation laboratory with anchor and cannon.

**Figure 1.8:** One treatment area of the *Mary Rose* conservation laboratory with treatment tanks, freeze-drier and hoist.

The work is not yet finished. Though majority of the 19000+ finds have been treated but many remain in passive storage, awaiting conservation (Jones, 2003: 1; Pearson, 2020). Most of these are mass-produced items found in large quantities in the wreckage, such as cannonballs (Figure 1.9) and arrows. Some parts of the waterlogged hull remain in fresh water until they can undergo PEG and freeze-drying treatment.

**Figure 1.9:** Untreated cast-iron shot held in passivating storage, awaiting treatment.

### 1.4.3 CONSERVATION SCIENCE AND RESEARCH

The vast number of artefacts and materials recovered from the site has allowed for, and often necessitated, a portfolio of dedicated conservation research. The willingness of the MRT to encourage researchers to use the collection has resulted in significant advances within the field of heritage material preservation. Studies involving the *Mary Rose* have included using nanoparticles (Schofield et al., 2011; Chadwick et al., 2012b; Schofield et al., 2016) and X-ray absorption spectroscopy (Wetherall et al., 2008; Berko et al., 2009; Chadwick et al., 2016) to treat degraded wood timbers, a synchrotron to study material composition and degradation (Chadwick et al., 2012a; Simon et al., 2019), and scanning electron microscopy to determine metallographic profiles (Starley and Hildred, 2002). Biological growth on and within waterlogged wood (Jones and Jones, 1993; Pointing et al., 1996; Preston et al., 2012; Preston et al., 2014) has been studied to understand deterioration processes. Impact of the marine environment on the prevalence and ability of these fungi and microbes to damage archaeological wood was examined (Pournou et al., 2001). Techniques were developed to quantitatively, non-destructively analyse composite metal artefacts (Walker and Hildred, 2000). The practice of freeze-drying archaeological wood has been greatly advanced (Jones et al., 2009).

These are only examples of conservation research carried out on the *Mary Rose.* Archaeological, zooarchaeological, and osteoarchaeological studies on the ship and her remains have combined to produce a body of work of incalculable academic and scientific value.

## 1.5 DISPLAY AND STORAGE OF ARTEFACTS

Post-treatment care and management of collections is a delicate balancing act requiring both an understanding of how materials react in given environments and the ability to manipulate and sustain those environments. The extent of the *Mary Rose* collection and the nature of the materials comprising it have presented a challenge for the design of safe storage and display since their excavation.

### 1.5.1 THE *MARY ROSE* MUSEUM 1984 - 2013

The first museum dedicated to the *Mary Rose* opened to the public in 1984 in Boathouse No. 5, a short walk from Dry Dock No. 3 (Figure 1.10). The original plan to house the ship and her finds was to develop a site in Eastney, Portsmouth (Figure 1.11) (Rule, 1982: 227).

However, the decision was made to further develop the Royal Naval Base as her home and include the Tudor warship alongside the *HMS Victory,* Nelson's flagship (Jones, 2003: 116). The hull was sealed inside a temporary structure that would allow for both controlled treatment and safe public viewing (Figure 1.12).

**Figure 1.10:** The original *Mary Rose* Museum, in Boathouse No. 5. From Jones (2003: 117).

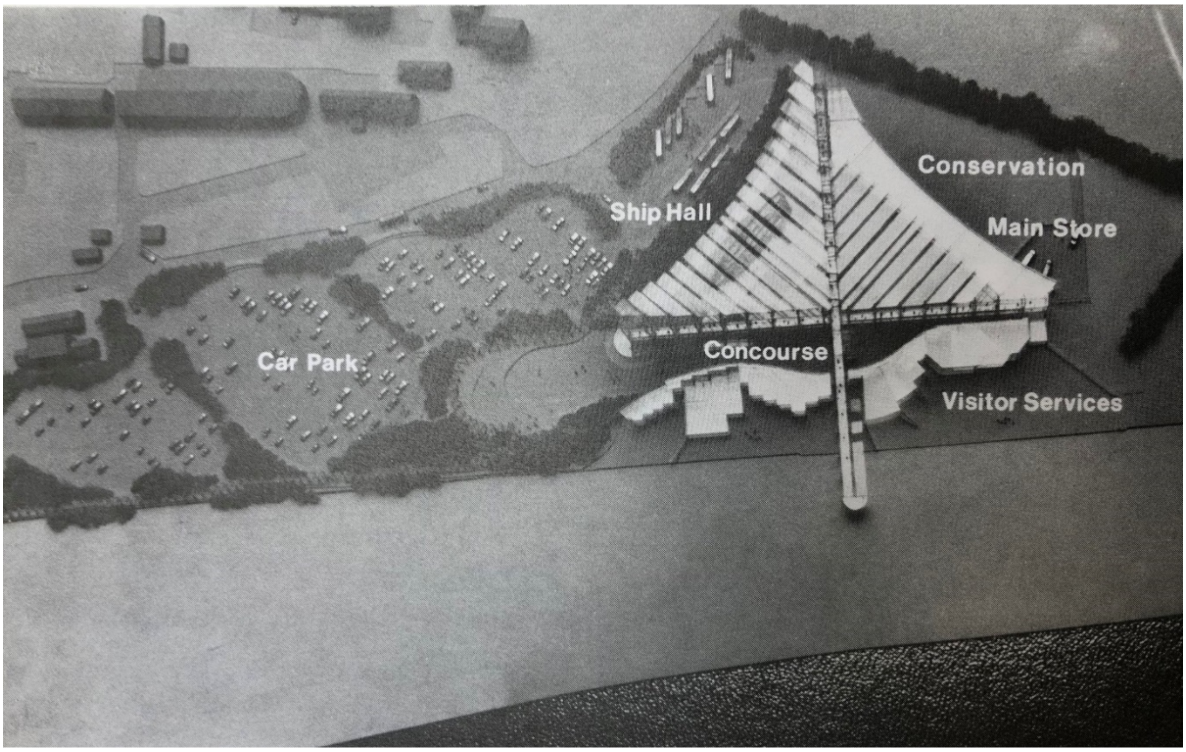

**Figure 1.11:** Original plan for a new-build *Mary Rose* Museum. The project was abandoned in favour of building over and around Dry Dock 3. From Rule (1982: 212).

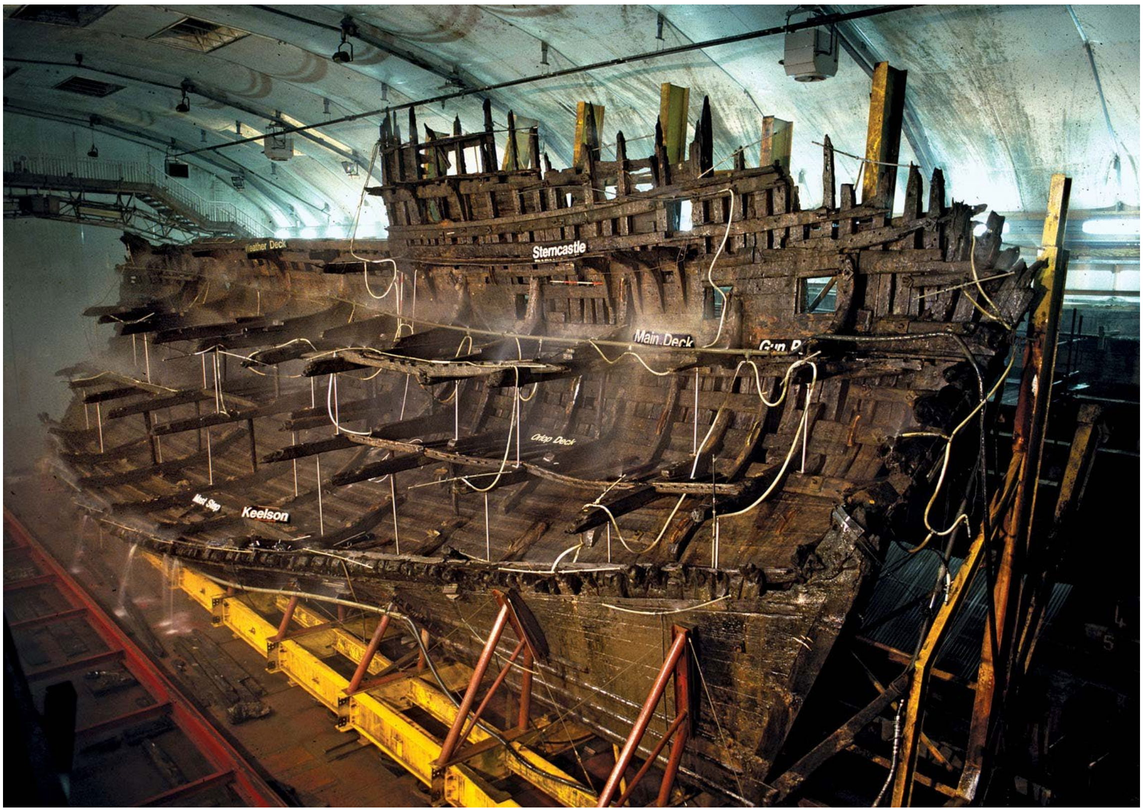

**Figure 1.12:** The *Mary Rose* as seen in the old shiphall prior to 2009, whilst still undergoing treatment. From Encyclopaedia Britannica (Tikkanen, 2020). Online.

As the listed building had to be retrofitted to become a museum, conservators and conservation scientists developed a design brief to safeguard the objects whilst maintaining a consistent historical narrative. An HVAC system was installed to maintain temperature, whilst measures to reduce or avoid biological, ultraviolet, and humidity deterioration were taken. Display cases were custom built to include air filtration and were sealed to limit exposure to external contaminants. Organic and mixed materials displays were held at 55-58% RH, whilst metals were kept in separate showcases at 40% RH (Jones, 2003: 121). The museum was designed to optimise collections care and maintain what was considered best practice at the time of its opening.

Though capable of housing and displaying objects, the Boathouse museum lacked a linking contextual thread between the ship and her finds. Removed as it was from the hull, the museum could never place the magnificent artefacts with the rest of the ship. This severely undercut the impact of the breadth and magnitude of the wreck upon the viewing public, especially considering that so many of the finds could not be displayed in the much smaller Boathouse.

### 1.5.2 STORAGE

Object stores are split between the museum and the conservation laboratory. The laboratory holds larger artefacts, untreated objects, and objects that do not require climate control, such as stone shot. The laboratory is also the home for sensitive artefacts in danger of accelerated deterioration. Sensitive metallic artefacts, including many of the cast-iron cannonballs, are held in a large climatic chamber that keeps objects at 20% RH (Figure 1.13), as it is assumed corrosion is negligible at that value. Two climate-controlled walk-in stores contain objects that tolerate low-mid RH values (30-40%) and require stable environmental conditions. These are usually organic artefacts, such as treated wooden arrows. Organic artefacts adsorb and desorb water in fluctuating environments, accelerating their deterioration, and so a stable environment is required to ensure their safety. Additionally, larger metallic objects that do not fit into the climate chamber are also held within these stores. The 30-40% range is a compromise between the organic and inorganic artefacts, as it a bit dry for the former and a bit humid for the latter.

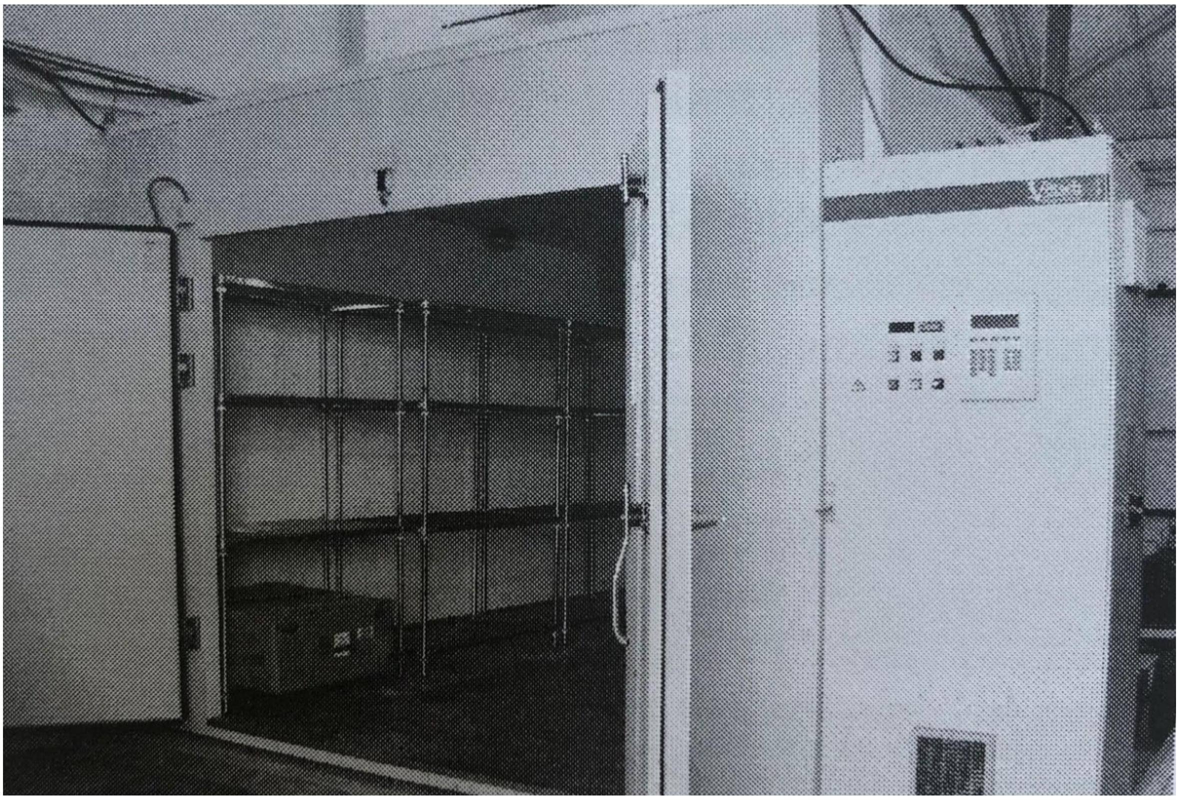

**Figure 1.13:** The climatic chamber in the *Mary Rose* conservation lab, where environmentally sensitive objects are kept. From Jones (2003: 72).

### 1.6 THE CAST IRON CANNONBALLS OF THE *MARY ROSE*

The 1248 cast iron cannonballs excavated from the wreck site represent over 6% of the total finds and well over half of all the ~2000 cannonballs recovered (Hildred, 2011: 307). This quantity renders the cannonballs both impressive and mundane. As a singularity, the collection of cast iron cannonballs is magnificent, but individually each is nearly indistinguishable from the other. In the environs of the old Boathouse museum where space was limited, displaying all the cannonballs was neither possible nor necessary. Conservation labour time, space, and funds had to be inclusive of all find types, as well as focused on those objects that were not capable of being put in passivating storage and those that were deemed unique or high value (Jones, 2020). To date, hundreds of cannonballs remain untreated, due in part to both their number and their unmitigated corrosion post-treatment (Figure 1.14). Most of those recovered are in physically satisfactory state with densities that confirm they retain metal.

**Figure 1.14:** Untreated *Mary Rose* cast iron cannonballs held in passivating storage.

With the development of the new museum (opening in April 2013) and its extensive context gallery (the largest showcase in Europe at that time) replicating the gun deck, the number of cannonballs available meant that they could be displayed in large clusters to emphasise the scale of the armaments. Cast iron cannonballs treated by a range of conservation methods were placed in the new museum displays in April 2013, prior to its opening (Figure 1.15).

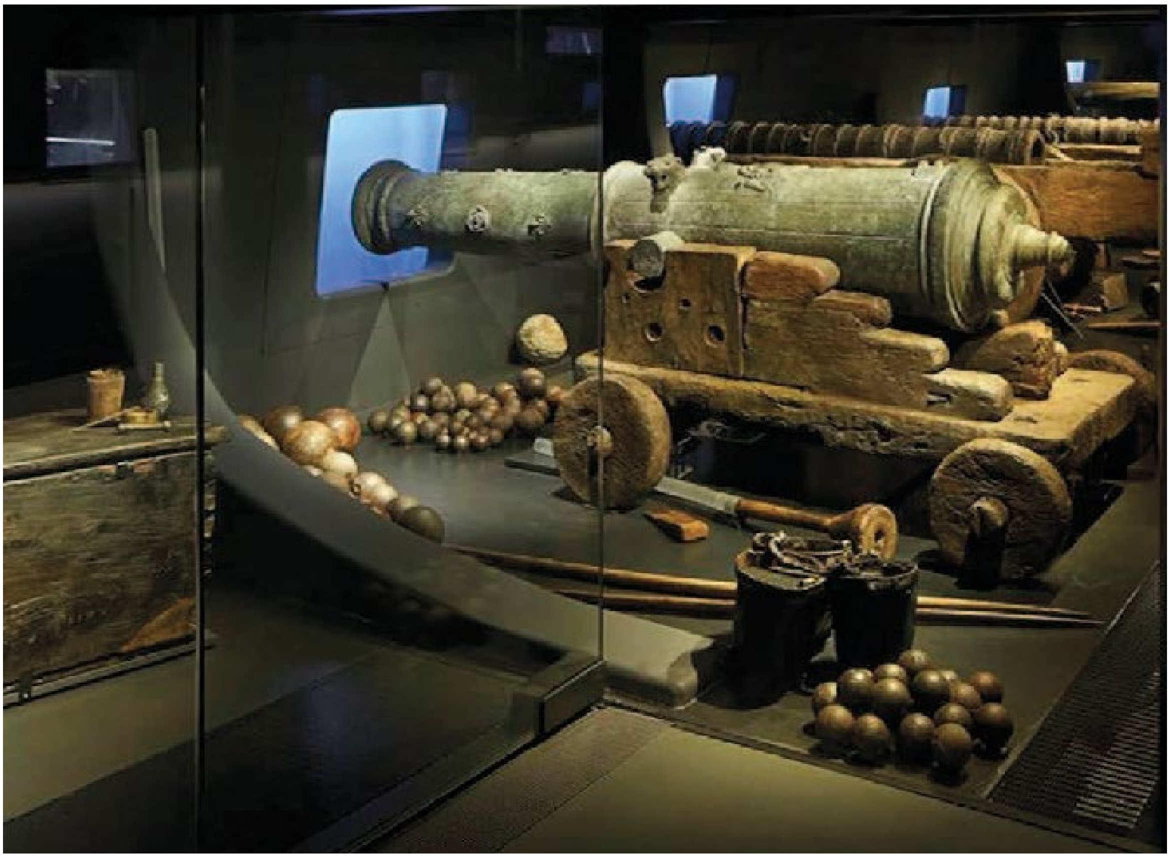

**Figure 1.15:** Cast iron cannonballs on display in the context gallery of the new *Mary Rose* museum.

Soon after the opening of the museum, staff observing the condition of the artefacts noticed cracking of the cast iron cannonballs on display (Figure 1.16). Realising that this was likely to be related to the relative humidity of the showcase (c. 55% RH) being higher than recommended for heritage iron (Commission, 1992), particularly from a marine environment, the cannonballs were removed from display to desiccated storage (Jones, 2020). By July 2014, the only cannonballs that remained on display were those treated by hydrogen reduction (Trust, 2015) which anecdotally appeared to be unaffected.

**Figure 1.16:** Cannonballs from the *Mary Rose* that exhibit damage and loss of function due to accelerated corrosion. The left has been intentionally left on display in the *Mary Rose* Museum to show how these artefacts break apart. On the right is MRT #83A-0447 as it arrived at Cardiff University in February 2015.

## 1.7 DEFINING THE PROBLEM

Attracting visitors and preserving collections are primary goals for museums. New and novel ways of making collections appealing to the visitor are often a necessity for maintaining the visitor numbers required to produce the income to support self-funding museums like the Mary Rose Trust. How to present collections to the public in a manner that preserves the objects while engaging the public can be a difficult balancing act.

The Mary Rose provides the allure of being Henry VIII’s flagship but its artefacts are a unique record of a point in time when the ship sank. Life on board the ship is recreated in the museum using original objects in a single 40 metre long display case. The corrosion and physical disintegration of cast iron cannonballs in the display exemplified why 55% RH is far from ideal for the metals present. Yet the popularity of such mixed displays with the public reveals their importance for attracting visitors who bring income into the Trust. Developing an evidenced management strategy that minimises risk to objects within a mixed display requires understanding of how the materials present react to their environment.

From investigating the corrosion rate of cast iron cannonballs excavated from the Mary Rose as a function of relative humidity, it will be possible to decide if they can ever be displayed in anything other than low humidity environments. This information can justify unpopular management decisions to display replicas rather than risk the destruction of original cannonballs. Alternatively, it may be that corrosion rates are slow until a specific humidity value, in which case there may be options for compromise when setting showcase RH. If this is high enough, perhaps a showcase RH of less than 55% could be chosen if the ongoing corrosion of the cannonballs remains slow and the set RH does not cause the wood to shrink. Once rate of corrosion is known, it may be possible to assign a display lifespan to cannonballs, accepting their eventual loss in exchange for displaying genuine objects to the public. The effectiveness of past treatments applied at the MRT to slow the corrosion rate of cannon balls is unknown. By exploring how treated cannonballs respond to RH may be possible to identify treatment groups that are less prone to ongoing corrosion and therefore safer to display. The possibility of retreating cannonballs to reduce their corrosion rates by extraction of further corrosion-promoting chlorides has been suggested. Is this a viable option for the *Mary Rose* collection?

At the moment, the MRT recognises it cannot display cannonballs at 55% RH without them incurring damage. Investigating the corrosion rates of cannon balls will identify risk as a function of environmental RH to inform their display and storage, allowing management to produce informed decisions on the level of risk they are prepared to accept in order to display the cannonballs.

Since 2010, Cardiff University conservation has established itself as the world leader in the non-invasive determination of heritage iron corrosion rates (Watkinson and Rimmer, 2013; Watkinson et al., 2013b; Emmerson, 2015; Watkinson et al., 2016; Lawson, 2016; Nordgren, 2016; Emmerson and Watkinson, 2016; Watkinson et al., 2019). Extensive research has been conducted using the in-house climate chambers to simulate real-world environments (Lingle, 2019; Thunberg et al., 2020; Johnson, 2020). This robust research culture combined with a dedicated climate impact lab is an ideal surrounding to conduct this investigation.

The MRT contacted the Department of Archaeology and Conservation at Cardiff University in 2010 to propose a project to determine best conservation practices and develop a plan for the safe storage and display of the cannonballs.

### 1.7.1 THE *MARY ROSE* MUSEUM 2013 – CURRENT

After Dock No. 3 became the permanent home of the *Mary Rose,* plans were made to build a custom museum around her, one that incorporated state of the art climate and visitor controls, narrative design, and architecture. The treatment timeline for the hull allowed for the raising of funds over several decades and the Boathouse museum ensured visitors would continue to engage with the ship during construction. In 2009, as treatment of the hull neared completion, the shiphall was closed to the public as the new museum was constructed (Figure 1.1**Error! Reference source not found.**).

**Figure 1.17:** The new *Mary Rose* Museum in 2013, built over Dry Dock #3.

The new £35 million museum opened in 2013, at around the same time as PEG treatment of the hull was completed and air drying commenced (Corporation, 2013). Hull drying was completed in 2016 and the museum again closed for nine months to remove the drying system, treatment hotbox, and public barriers (at an additional cost of £5.4 million). Visitors can now view the interior starboard side without encumbrance (Figure 1.18**Error! Reference source not found.**) and, turning over their opposite shoulder, see a recreation of how the gun deck would have looked (Figure 1.19**Error! Reference source not found.**). The display case encompasses deck-sized areas, cordoned off from the public with floor-to-ceiling glass and completely climate-controlled. More traditional display cases occupy areas at the bow and stern ends of the ship (Figure 1.20**Error! Reference source not found.**). All display cases are climate controlled and monitored, with mixed displays populated by artefacts that require the same climatic conditions. Access to the main hall is through an automated airlock system, ensuring that both the climate around the ship and the display halls are maintained. The hull is kept in a strict 55% RH environment, which is higher than in other parts of the museum.

**Figure 1.18:** The *Mary Rose* as seen in 2020, 5 years after completion of treatment.

**Figure 1.19:** Deck-length mixed display set up to simulate how the deck may have looked. From nationalhistoricships.org.uk (©Johnny Black).

**Figure 1.20:** Mixed display of stone and lead shot, and wrought iron at the *Mary Rose* Museum.

## 1.8 THESIS AIM AND STRUCTURE

By recording the post-treatment stability of marine cast iron artefacts, using a remote sensing oxygen technique to determine their corrosion rate, this study produces a data set to inform management practice for the treatment and care of marine cast iron.

The structure of this thesis is designed to provide a scholarly background and context to the research before discussing experimental design, method and results. The historical narrative introduced in this chapter is followed in Chapter 2 by an explanation of iron corrosion mechanics, with emphasis on the influence of the marine environment, cast iron composition, and post-excavation atmosphere on corrosion product formation. Chapter 3 examines external factors that conservators must consider when choosing treatment plans, summarises treatments that have been employed on heritage iron, and under what conditions those treatments are considered successful or discontinued. Experimental design and methodology are discussed in Chapter 4. Experimental results are shown in Chapter 5 and discussed in Chapter 6. Chapter 7 concludes the thesis by looking ahead to the possibilities raised by it.

# 2 HERITAGE CAST IRON – COMPOSITION AND CORROSION

Properties of iron artefacts such as strength, flexibility, ductility, flow, and compactness are determined by alloying materials and method of production. For example, wrought iron involves the smelting of ore and shaping solid iron, whereas cast iron is made from pouring liquid iron into moulds (Scott, 1992: 5). The alloying materials required to produce a molten iron capable of being cast create a fundamentally different product than hammered and folded wrought iron. The production process also produces distinctive metallographic profiles. Wrought iron carries slag inclusions within its structure, whilst the carbon content of cast iron results in a network of graphite nodules and flakes (Reynaud, 2010). These compositional differences significantly impact both pre- and post-depositional corrosion, treatment efficacy, and after-treatment care.

The focus of this research is on cast iron, and cannonballs specifically, from a marine environment. Understanding the history, production, composition, corrosion and consequent physical break up of cast iron, as well as how the marine environment affects it, is necessary to understanding how it can ultimately be preserved.

## 2.1 HISTORY AND PRODUCTION OF CAST IRON THROUGH THE 15TH CENTURY AD

The first iron artefacts were most likely crafted from meteorites; 'AN.BAR', the first recorded 'word' for iron is composed of the Sumerian pictographs for sky and fire (Stefanescu, 2017), well before the establishment of any forges or foundries. The high nickel content of meteoritic iron makes it difficult to cold work, as the composition is brittle and easily cracks (Tylecote, 1976: 2). Still, meteoric iron was worked and smithed into artefacts. Worked meteoric beads from Egypt date to ~3200 BC (Figure 2.1), and the skill required for production suggests metalsmiths had been working with this material well before this date (Rehren et al., 2013).

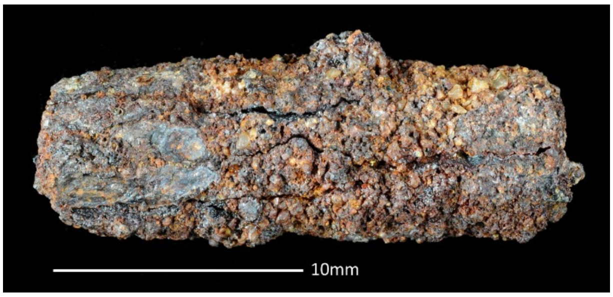

**Figure 2.1:** A meteoric iron bead from Gerzeh, Egypt, the earliest known iron artefact. From: Johnson et al. (2013).

The first wrought iron artefacts were not produced for at least another 500 years in Asia Minor (Tylecote, 1976: 40). Iron smelting is thought to derive as a by-product of copper smelting, where iron ore would have been used as a flux (Tylecote, 1976: 40; Stefanescu, 2017). Early smelting attempts in the early 2nd millennium resulted in smaller objects that were poorly joined. However, the method had become widespread throughout the Anatolian-Iranian region with the advent of the so-called Iron Age, at around 1500 BC, with large-scale manufacturing operations taking place as early as 1200 BC (Tylecote, 1976: 40).

Whilst the production of wrought iron had by 800 BC slowly spread to most of Eurasia, the earliest produced functional cast iron was only just being poured in China (Stefanescu, 2017). The earliest discovered sand casting moulds and iron requisitions date to the mid-7th and 6th centuries BC, respectively (Stefanescu, 2017). By the time of the Western Han dynasty in 200 BC, cast iron was widespread, utilised for objects both ornate and mundane (Scott and Eggert, 2009: 1). Though the Greeks and Romans both experimented with casting iron, the process was not being used throughout Europe until the 11th century AD. This disparity in technological adaptation can be ascribed to the earlier development of the box-bellows furnace, which allowed for the heating of ore to the melting point of iron at 1530°C, then adding large amounts of carbon and holding it at 1170°C. This caused the mixture to become liquid and be poured and cast at a temperature lower than bronze (Scott and Eggert, 2009: 10; Stefanescu, 2017).

Though iron casting did take place in Europe before the 2nd millennium AD (Stefanescu, 2017), it was not widely used until the 15th century when the blast furnace was developed (McNeil, 2002: 149). The size of the furnace allowed for mass production of cast pig iron, which would later be refined into wrought iron by burning off the excess carbon (Figure 2.2). It was also possible to create curvilinear objects in a single cast, such as cannon and cannonballs. The first blast furnace in England appeared in Sussex in 1496 at the behest of Henry VII (Schubert, 1957: 163), with cannonballs being produced at that forge the same year (Teesdale, 1991: 11).

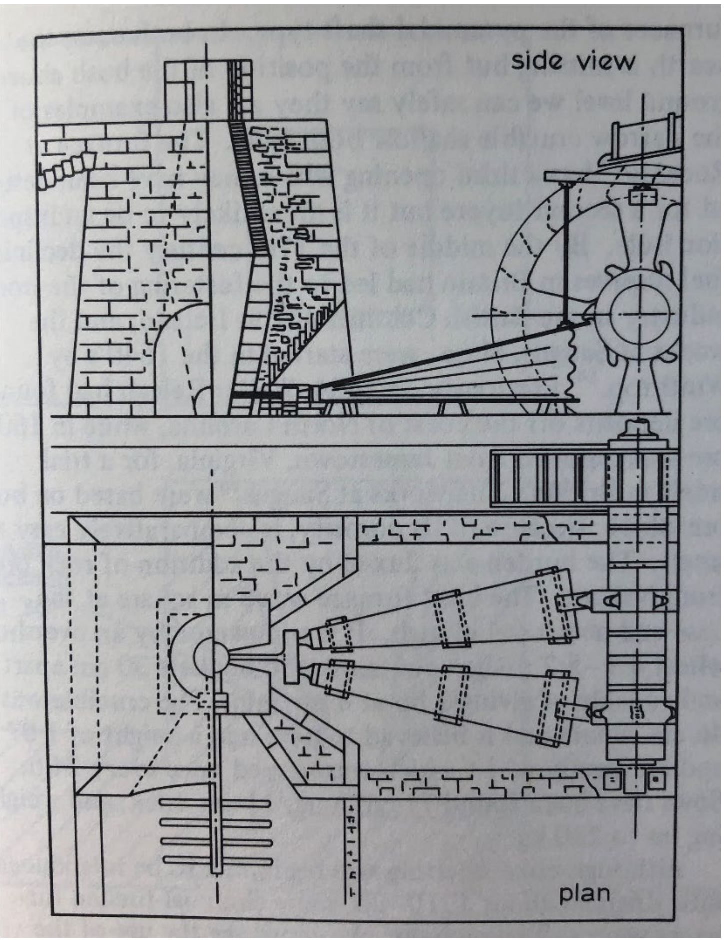

**Figure 2.2:** Diagram of an early blast furnace. From Tylecote (1976: 83)

### 2.1.1 PRODUCTION OF CAST IRON CANNONBALLS FROM THE *MARY ROSE*

Henry VIII's pugnacious attitude toward both his neighbours France and the Papacy resulted in an incredible demand for iron projectiles and guns, with 457 iron shot '*of diverse sortes*' and 120 crossbar shot listed in the 1514 royal inventory (Hildred, 2011: 309). When the *Mary Rose* sank in 1545, she had on board at least 1248 cast iron cannonballs, a testament to how rapidly the royal armament came to rely on the material (Hildred, 2011: 314).

Though cannonballs could have been sand-cast (Stefanescu, 2017), the number required for munitions stockpiles meant most were probably mould-cast, either in plaster of Paris or brass (Starley and Hildred, 2002; Hildred, 2011: 383). The liquid iron was poured into a tong-supported mould, where it could be cooled, opened, and quickly reused (Figure 2.3). Stone moulds could also have been used for production, where multiple cannonballs could be produced within a single mould.

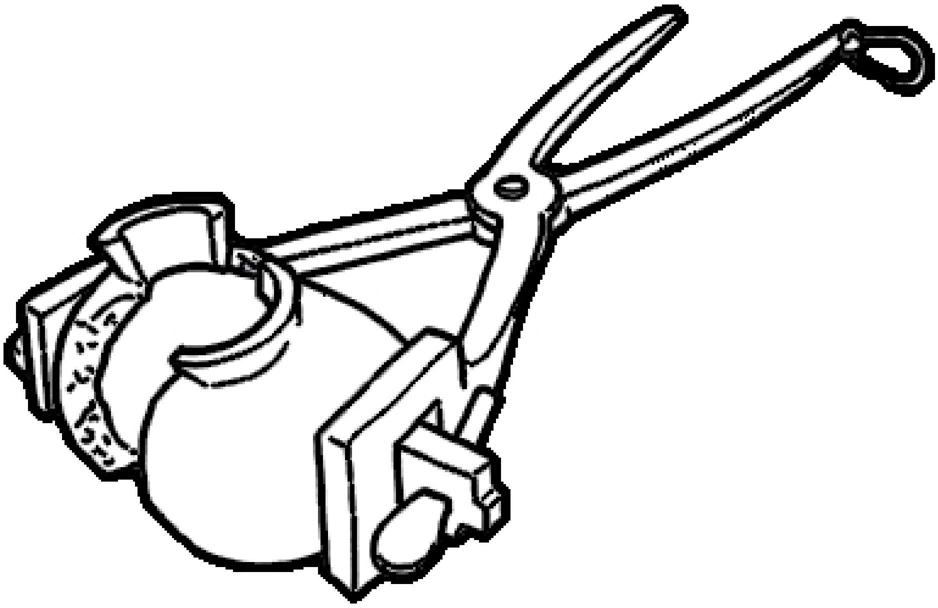

**Figure 2.3:** Drawing of a tongs with moulds. From Hildred and Fontana (2011: 383).

The casting process results in excess metal building up where it is poured in (Figure 2.4). This is called sprue (Figure 2.5). The excess is then cut off after cooling and the cannonball ground and finished. Casting flaws most certainly happened, either due to differential cooling of the cannonball or trapped oxygen unable to bubble out (Figure 2.6) (Williams and Johnson, 2000).

**Figure 2.4:** An example of a cannonball immediately after casting. From Williams and Johnson (2000).

**Figure 2.5:** An example of casting sprue on MRT 82A-4362.

Whilst the cannonballs from the *Mary Rose* could theoretically have been produced any time prior to its sinking, it remains likely that the bulk of 1200+ cannonballs were produced between 1540-1545, as England remained under threat of war from both France and Spain, at the urging of the Papacy (Teesdale, 1991: 12). This resulted in a massive increase in military defence spending, with Henry having spent an estimated £376,000 (£317 million in 2019 currency) on shoring up England's southern defences (Teesdale, 1991: 14), including rebuilding the *Mary Rose* in 1536 to accommodate a continuous gunport and the increase in cannon that this required (Rule, 1982: 21). Disputed accounts say that 1543 saw the production of cast iron cannons and cannonballs on a scale never previously seen (Teesdale, 1991: 17). Either way, Henry VIII's gunmaker sent 1100 cannonballs to Portsmouth in 1545 (before or after the *Mary Rose* met her fate is unknown), in addition to being paid £500 (£337,000 adjusted) for additional iron cannonball production (Teesdale, 1991: 18). An inset 'H' appears on 431 of the recovered iron cannonballs, most likely meaning they were produced at the same foundry (Hildred, 2011: 315).

**Figure 2.6:** An example of a casting flaw within a cannonball. This is ½ of a newly cast cannonball following bifurcation. From Williams and Johnson (2000).

## 2.2 COMPOSITION OF CAST IRON

The high carbon content of cast iron of 2-5% is what sets it apart from wrought iron (Mentovich et al., 2010). The lower carbon percentage of wrought iron ($\leq$ 0.8%) keeps it from flowing, and so cannot be cast. Wrought must hammered to shape it, and the combination of this, the higher temperature, and the tempering creates a product with different metallographic properties than cast iron (Scott, 1992: 31). The inclusion of carbon during the production process drops the melting point of the iron from 1538°C, creating a new eutectic mixture (a mixture of separate components that have a lower melting point when combined than individually) with a corresponding eutectic point of 1148°C. Other constituent elements common in cast iron in the Tudor era, particularly sulfur, phosphorus and silicon, will further lower its melting point to around 960°C (Scott, 1992: 38), allowing it to be cast into metal moulds (Hildred, 2011: 383). Modern cast irons have more controlled levels of such impurities and may be deliberately alloyed with elements such as chromium and nickel to develop adventitious properties (Scott, 1992: 37).

The carbon content of cast iron also results in its characteristic physical properties and a metallographic profile wholly distinct from that of wrought iron. Cast iron has a lower density than wrought and is porous and brittle, with considerable compressive, but poor tensile, strength. Metallurgically, carbon precipitates within the substrate as graphite or as iron carbide ($Fe_3C$, cementite). Cementite is a brittle, thermodynamically unstable combination of iron (93.3%) and carbon (6.67%) and is formed during casting. Pearlite (a mixture of ferrite and cementite) also appears. Cast formation is discussed in more detail in the following section (Reynaud, 2010; Hack, 2010).

### 2.2.1 CAST IRON TYPOLOGY

The microstructure of cast iron objects is determined by the amount of alloying material added during processing and the rate at which the iron cooled after casting (Scott, 1992: 37). Historic cast iron appears in three distinct forms: grey cast iron, white cast iron, and mottled cast iron. The names refer to the colour that precipitated carbon imparts to the microstructure, as the graphite flakes in grey cast iron give it a dull grey hue. Graphite flakes do not precipitate out in white cast, instead appearing entirely as cementite, producing a 'whiter' hue. Slower cooling rates favour grey cast formation, as the longer ferrite and cementite are in contact with each other, the more ferrite will decarburise metastable cementite, leaving ferrite and graphite (Bhadeshia, 2020). Faster cooling rates prevent this. Mottled cast, as one might guess, is a mixture of the two, usually occurring due to differential cooling between the exterior of an object and its interior.

These differences in microstructure give cast iron types different properties. Graphite is much softer than cementite – 1-2 Mohs hardness compared to 6.5 for cementite (Shimura, 1930) – resulting in white cast iron being much harder but much more brittle than grey. Higher carbon and silicon (> 1% wt) content favour ferritic (i.e. grey) formation, higher sulfur stabilises cementite and promotes white (Hack, 2010; Ashkenazi et al., 2012). Smaller amounts of phosphorous can also create steadite, a phosphide eutectic with a melting point of 960°C, which is low enough to favour grey cast iron formation (Scott, 1992: 38). As alloying can greatly impact functionality and corrosion resistance, modern alloys such as austenite cast irons that contain a high percentage of nickel (Reynaud, 2010) or those containing chromium are not discussed here. Figure 2.7 displays cross-sections of cast irons types.

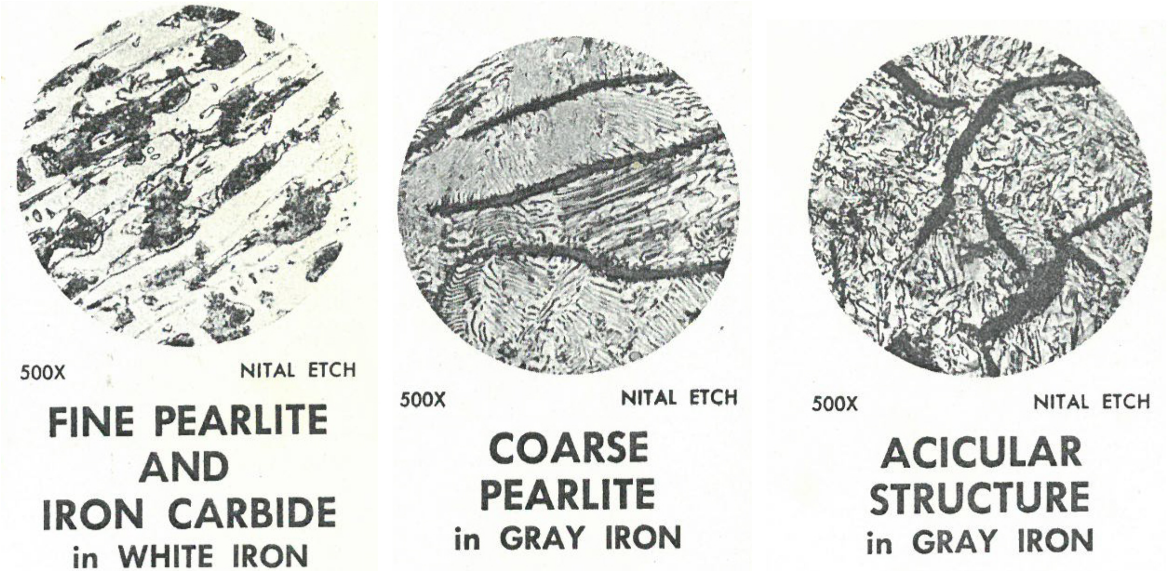

**Figure 2.7:** Metallographic structures of white and grey cast iron. From Zimmerman and Eppelsheimer (1963: 1.6).

## 2.3 CORROSION OF HERITAGE IRON

### 2.3.1 PRINCIPLES OF CORROSION

A considerable amount of energy is required to refine metallic iron from its ore and in the presence of oxygen and moisture it oxidises to reach lower energy states, forming iron corrosion products (Trethewey and Chamberlain, 1995: 69). The electrode potential of iron (-0.409V) and the nature of its corrosion products make it an inherently unstable metal. There are two pathways for the oxidation of iron: either directly at very high temperatures (Pinder et al., 2010) or electrochemically involving water and electrolytes (Shreir, 2010). Only the latter is relevant to this study. Electrolytic oxidation of iron requires three components: an anode, a cathode, and an electrolytic medium (Turgoose, 1993). There must be an energy difference between the anode and cathode, as well as solid phase contact to enable the transfer of electrons between them. Oxidation of iron occurs at the anode and the resulting electrons travel to the cathode through the solid phase, where they are consumed by a reduction reaction according to the prevailing environment. The anode and cathode must be connected by an electrolyte to facilitate the movement of ions produced at the anode into solution and to enable reactions at the cathode to occur, as well as allowing charge balance to take place.

Elemental iron (Fe) readily oxidises and the resulting electrons are passed to the cathode:

$$\mathrm{Fe} \rightarrow \mathrm{Fe}^{2+} + 2\mathrm{e}^{-} \qquad \textbf{Equ. 2.1}$$

pH at the cathode rises due to $OH^-$. In aerated conditions above a pH of 4, the energetically preferred cathode reaction is the reduction of water, and the cathode is provided by the other components:

$$O^2 + 2H_2O + 4e^- \rightarrow 4OH^- \qquad \textbf{Equ. 2.2}$$

The ferrous ($Fe^{2+}$) ions are free to react with other components and form new compounds, such as reaction with cathodically generated hydroxyl ions to form iron hydroxides ($Fe(OH)_2$). Hydrogen ($H^+$) ions can also exist in this solution due to the hydrolysis of Fe2+ ions (Turgoose, 1985):

$$Fe^{2+} + H_2O \rightarrow Fe(OH)^+ + H^+ \qquad \textbf{Equ. 2.3}$$

$$Fe(OH)^+ + H_2O \rightarrow Fe(OH)_2 + H^+ \qquad \textbf{Equ. 2.4}$$

While $Fe^{2+}$ is a corrosion product, for it to form solid phase products cations must meet anions and precipitate. This is governed by the ability of the ions to form solid compounds in the prevailing conditions, which will also determine the oxidation states and the composition of the compound formed. Delocalisation of ions from anodes and cathodes may be difficult due to diffusion difficulties, producing a build-up of ions which interferes with corrosion rate as concentration polarisation (North and MacLeod, 1987).

Continued production of ferrous ions ($Fe^{2+}$) at the anode requires local electroneutrality (charge balance) and encourages the diffusion of anions such as chloride towards the anodic regions. At higher pH, $Fe^{2+}$ will precipitate as ferrous hydroxide that may be oxidised further to ferric hydroxide (Equ. 2.5). Alternatively, at lower pH oxidation of ferrous to ferric ($Fe^{3+}$) can occur in solution. Subsequent hydrolysis of the ferric ion, encouraged by the presence of chloride, and releasing $H^+$, lowers the pH and results in precipitation of hydrated iron oxide (Equ. 2.6):

$$Fe(OH)_2 + \frac{1}{2}H_2O + \frac{1}{4}O_2 \rightarrow Fe(OH)_3 \qquad \textbf{Equ. 2.5}$$

$$2Fe^{2+} + 3H_2O + \frac{1}{2}O_2 \rightarrow 2FeOOH + 4H^+ \qquad \textbf{Equ. 2.6}$$

Availability of oxygen will facilitate oxidation of $Fe^{2+}$ to $Fe^{3+}$, which in turn encourages the formation of oxyhydroxides and ferric oxides further away from the metal surface (Equ. 2.7) (Scott and Eggert, 2009: 102).

$$Fe(OH)_2 + \frac{1}{2}H_2O + \frac{1}{4}O_2 \rightarrow Fe(OH)_3 \qquad \textbf{Equ. 2.7}$$

The metal core retreats further into the object as corrosion progresses and corrosion products build on the metal surface. If oxygen ingress to cathodes is limited and pH falls to 4 or lower due to hydrolysis the energetically favoured cathode reaction is reduction of hydrogen ions. This instead results in the formation of hydrogen gas as the reducing reaction (Equ. 2.8). This is more likely to occur in strongly reducing burial conditions where oxygen is limited:

$2\mathrm{H_2O} + 2\mathrm{e}^- \rightarrow \mathrm{H_2} + 2\mathrm{OH}^-$ (water reduction) **Equ. 2.8**

It is clear that pH and the concentration of oxygen and dissolved ions influence which corrosion products occur and whether they will be in solid or liquid phase. Pourbaix (1974; 1977) utilised these factors to produce thermodynamic data plotted onto diagrams that revealed the stability field of corrosion products according to prevailing pH, Eh and concentration of dissolved species (Figure 2.8). These Pourbaix or thermodynamic phase stability diagrams can be used as a guide to the likely occurrence of corrosion products in known environments. Water oxidises or reduces outside of its region of stability, resulting in the formation of different corrosion products. The limitations of the diagrams are that they are constructed for fixed temperature, pressure and ionic concentrations and do not offer information on kinetic data (McNeil and Odom, 1994).

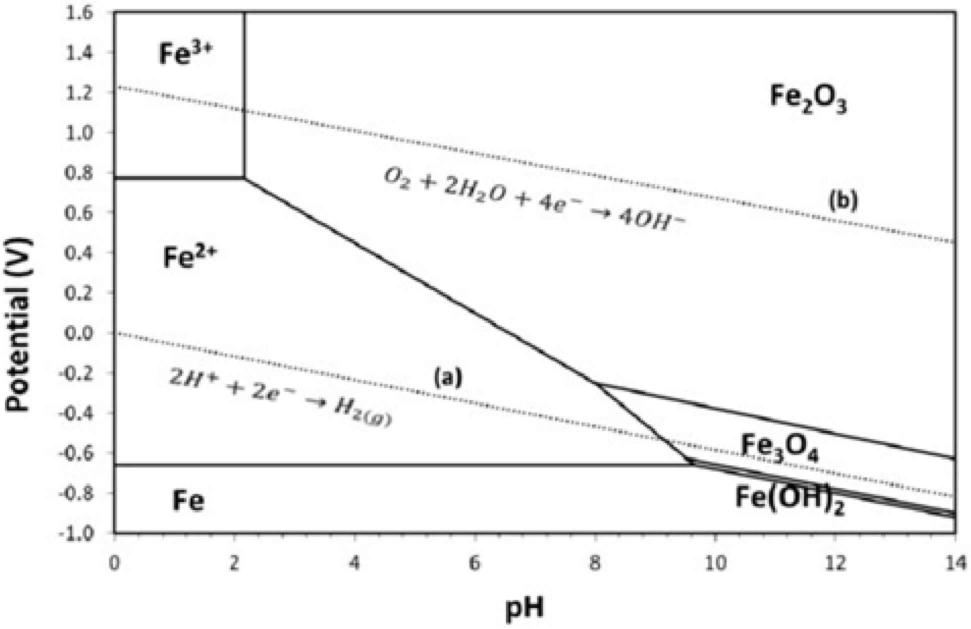

**Figure 2.8:** Pourbaix diagram of iron ions in water. Concentration of $Fe^{2+}$ is $10^{-6}$ M.

### 2.3.2 CORROSION OF CAST IRON

The high carbon content of cast iron causes it to corrode differently from other iron alloys. Graphite is cathodic to iron, resulting in the preferential corrosion of iron. This, combined with the inclusion of silicon creates two distinct corrosion layers: the topotaxial and epitaxial layers (Figure 2.9) (Reynaud, 2010). The topotaxial is the ‘base layer’ of corrosion, an area which begins at the original casting surface and extends to the metal interface. Above this lies the epitaxial layer, where oxidised ferrite is deposited and precipitates as various products after corroding outward toward the cathodes, sited on the graphite due to its more positive corrosion potential (Reynaud, 2010). What is left behind is a network of crystalline graphite with the surrounded spaces formerly occupied by ferrite now filled with corrosion products. Much like wrought iron, the original surface is preserved as corrosion deposited outside of it. In surface contexts, this can result in delamination and spalling of the surface layers. In marine contexts, the original object is retained as a soft and porous graphite matrix, rather than a fully corroded outline.

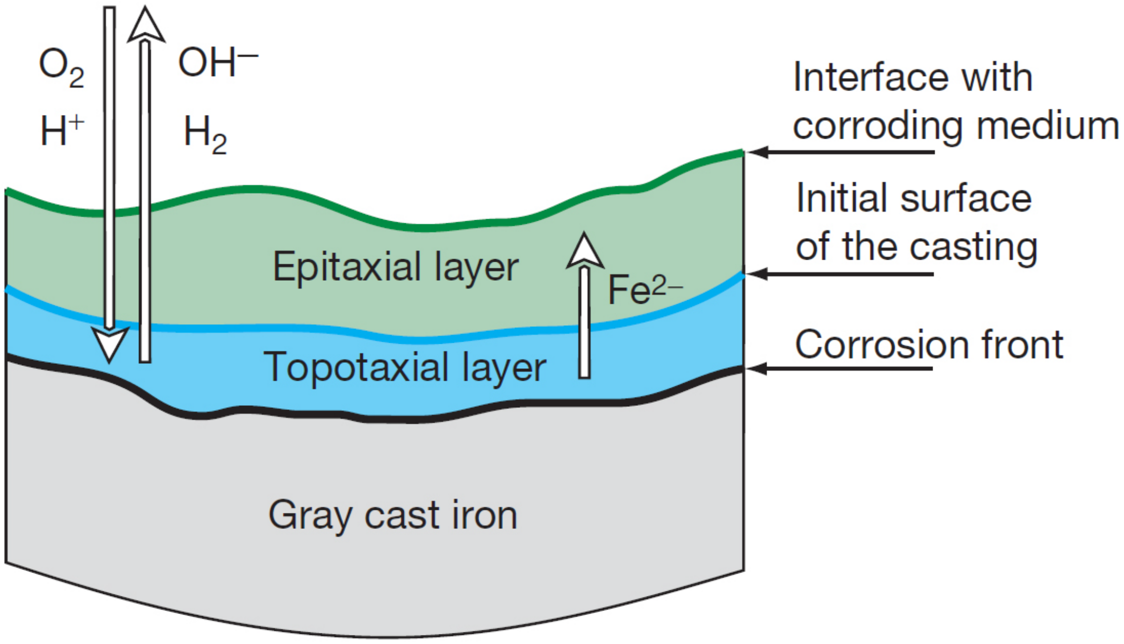

**Figure 2.9:** Schematic of corrosion layers on grey cast iron. From Reynaud (2010).

This area of graphitisation increases as the metal surface corrodes inward and is known as the ‘graphitised zone’ (perhaps more properly called the ‘layer of graphitic corrosion residue’) (Reynaud, 2010). The area is less dense than ferrite/graphite/cementite and is prone to fracturing under too much pressure. If conditions allow it, the formation of voluminous corrosion products that are denser than graphite can form in the graphitised zone, causing fissures through the substrate and surface. This is discussed in-depth later in this chapter.

The alloying and metallographic structure of cast iron can result in galvanic coupling, though this depends on the species typology (insulating, conducting) and if it is electrochemically active. The homogeneous alloying places nodules of cementite and other eutectics (steadite, sulfides) in contact with each other, graphite, and ferrite (Reynaud, 2010). As ferrite has lower reduction potential, it is the first to corrode, followed by iron-containing eutectic mixtures. As graphite acts as a cathode, the size of the graphite inclusions affects this rate (Hack, 2010; Reynaud, 2010). Flaws within the casting itself can result in localised corrosion. Silicon inclusions, slag, blowholes, etc. can all result in pitting or crevice corrosion (Reynaud, 2010).

### 2.3.3 INFLUENCE OF THE MARINE ENVIRONMENT ON HERITAGE IRON CORROSION

Corrosion of iron is highly dependent on its surroundings. This includes archaeological iron, where the burial environment greatly influences corrosion pathways. Marine iron is subjected to wholly different environmental conditions compared to iron in the atmosphere or the ground. Marine geo- and biochemistries greatly influence the corrosion of heritage iron deposited in these environments. Seawater includes large amounts of biological organisms, salts, and dissolved gases. Currents can erode and cover objects with sediment. The environment on the seafloor allows for an abundance of corrosion-inducing particles to find their way into iron, though without any uniform consistency (North and MacLeod, 1987).

#### 2.3.3.1 CHARACTERISING THE MARINE ENVIRONMENT

The complexity of the marine environment results in no two locations behaving in the same manner. Depth and equatorial proximity can influence temperature which will in turn influence biological growth and oxygen concentration. Sulfur-spewing volcanic activity alters local ecosystems, with thermo and haloclines influencing component concentration (dissolved gasses, biomatter, calcareous depots) and vice versa (MacLeod, 2011). Strong underwater currents effect particulate movement and deposition.

The influence of each factor on the other results in the marine environment being a ‘living medium’ (Phull, 2010). If an area is brackish (less salty) than another, for instance, it may result in higher localised deposition due to the lesser buoyancy of the water. The composition of brackish and saline water strongly influences the corrosion of metals. The most important influence is the concentration of dissolved oxygen followed by the conductivity of the water as these, respectively, influence the cathodic reaction rate, and the electrical resistance between cathode and anode. Calcium carbonate precipitation may slow corrosion while production of hydrogen sulfide and other metabolites from marine organisms can increase corrosion."

### 2.3.3.2 COMPONENTS

Nitrogen, carbon dioxide, and oxygen are the most abundant gases in seawater (Chester, 2009: 163) and their concentration is influenced by temperature, salinity and pressure (Chester, 2009: 165). Generally, oxygen concentration decreases with increasing temperature and salinity (Figure 2.10) (Phull, 2010) and is also depleted by aerobic organisms and by reactions with inorganic materials (Florian, 1987: 4). This depletion can result in an anoxic environment on, or immediately below, seafloor beds, which will influence metallic corrosion there. Whilst chlorides and salinity are important, it is dissolved oxygen that is the greatest determinant of corrosion pathways to maritime artefacts (Phull, 2010). Oxygen is either absorbed from the atmosphere or dissolved from photosynthesis, resulting in shallower depths ($\leq$ 100m) being much more saturated with oxygen than lower depths.

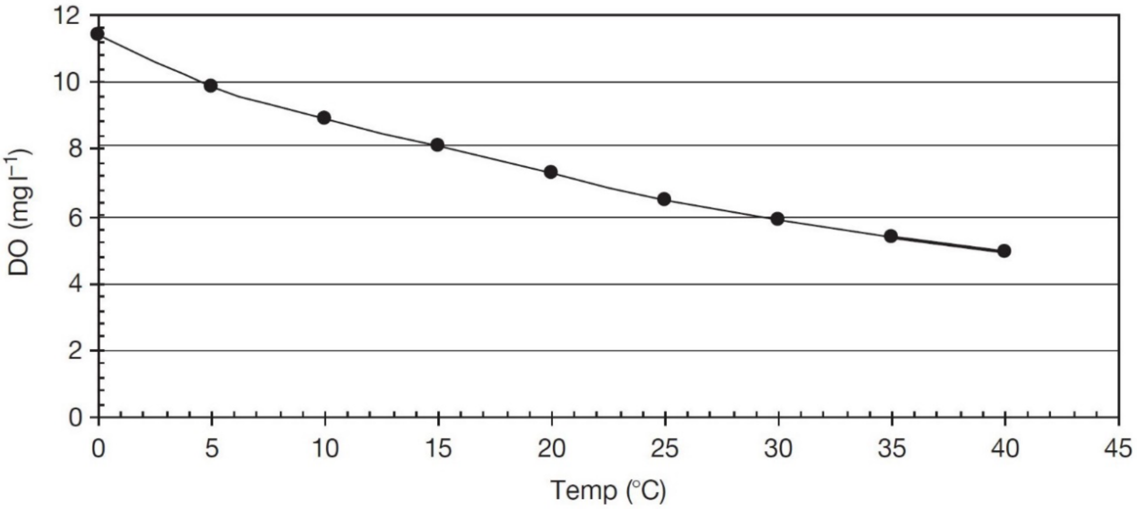

**Figure 2.10:** Dissolved oxygen versus temperature in 35% salinity seawater, 1 atm. From Phull (2010).

Calcium carbonate ($CaCO_3$) covers nearly 25% of the global seafloor, mostly due to calcareous deposits from biological organisms (Chester, 2009: 354). Calcium, combined with high concentrations of dissolved $CO_2$, acts to buffer seawater to pH ~8.1 but local oceanic environments can vary this (pH 7.5 – 8.4) (Florian, 1987: 6). Calcareous deposits also settle on object surfaces, impacting on corrosion mechanics (see below) (Phull, 2010). Since solubility of calcium compounds have lower solubility in higher temperatures, warmer oceans are likely to build thicker deposits.

Marine environments are highly saline, with an average $Cl^-$ concentration of 19.35 g/kg, or nearly 48x more than $Ca^{2+}$ ions (Florian, 1987: 3). Their solubility is not affected by pH or *E*h, though temperature can affect concentration and salinity is influenced by river outflows, as fresh water reduces salt concentration and evaporation due to higher temperatures increases it. For example, the Arabian Sea is nearly 8x more saline than the Baltic Sea (Phull, 2010). Littoral areas (river outflows, deltas) affect corrosion patterns, by altering salinity and introducing high amounts of organic and inorganic waste (Phull, 2010). Salinity of seawater produces low electrical resistance, allowing anode-cathode reactions to occur over greater distances, which, increases corrosion rates (Phull, 2010).

Iron artefacts from marine contexts may contain a range of sulfur compounds due to the abundance of sulfur in seawater. Its many oxidation states (+6, +5, +4, +3, +2, +1, -1, -2) mean it can be present in many forms and susceptible to both oxidative and reductive processes (Cornwell and Morse, 1987). Marine volcanic activity is thought to be the primary contributor to the abundance of the sulfate ion ($SO_4^{2-}$) in seawater (2.712 g/kg) (Chester, 2009: 140). This supports sulfate-reducing bacteria (SRB) that play a vital role in the ocean sulfur cycle (Little et al., 2000) and their role in iron corrosion is discussed later.

Sodium ($Na^+$), magnesium ($Mg^{2+}$), and potassium ($K^+$) are other ions present in large amounts in seawater (Florian, 1987: 3), with manganese ($Mn^+$), copper, lead, nickel, zinc, and cadmium being present in smaller amounts (Chester, 2009: 271). Magnesium, sodium, and potassium can form salt complexes, though the literature does not address these cations forming corrosion products with iron (North and MacLeod, 1987). Although manganese is highly soluble and has multiple oxidation states and, like $Fe^{2+}$ ions, can react with sulfur and oxygen, it is only present in trace amounts (Chester, 2009: 269). Silicon is abundant in sediment.

Temperature is an overarching factor that can affect corrosion mechanisms and their rates. Higher temperatures increase resistivity and promote biomatter but decrease dissolved oxygen concentrations and calcium solubility (Phull, 2010). Colder oceanic waters may induce faster corrosion, as the oxygen content will be higher due to lower temperatures and less biomatter. Additionally, protective concretions may form at slower rates in cold water due to calcium being more soluble (see Section 2.3.3.4 below for more on concretion formation).

#### 2.3.3.3 CORROSION IN MARINE CONTEXTS

Though the composition of seawater makes it highly corrosive, this depends on external factors, concentration gradients, and geography. The velocity of currents affects the deposition of sediment and calcareous components, as sediment layers affect the rate of oxygen diffusion to the metal surface. These will fall out of currents and settle if velocity is too slow; however, the velocity required to remove settled sediment from surfaces is far greater than is necessary to keep them suspended. A reduction in settled deposits leaves artefacts exposed to open environments and faster corrosion, as calcareous deposits can act as a barrier to oxygen renewal at cathode sites. Increased current velocity also directly delivers more dissolved oxygen to the metallic surface, as well as increasing erosion (Phull, 2010). Although salinity affects corrosion rates, as more chlorides equate to a more productive electrical cell, oxygen access is the determining factor in marine corrosion. Oxygenated seawater oxidises $Fe^{2+}$ to $Fe^{3+}$ as it migrates outwards from the metal surface towards the object/seawater horizon (North, 1982).

#### 2.3.3.4 CONCRETION FORMATION

One of the defining characteristics of iron artefacts found on the seafloor is the formation of concretions on their exterior surfaces (North, 1976; North and MacLeod, 1987). Occurring on objects both beneath and lying on the seafloor, concretions form by corrosion products interacting with surrounding seawater components as iron is not toxic to marine life. Iron is dissolved at the anode electrochemically via Equation 2.1. Organisms can then coat object surfaces, combining with calcareous deposits to create a layer of calcium carbonate. Egressing $Fe^{2+}$ and $Fe^{3+}$ ions interact with this deposit, precipitating within it. Concretions trap water within the concretion and the corrosion products beneath it, oxygen is depleted and hydrolysis of $Fe^{2+}$ occurs at anode sites via Equation 2.3, lowering the pH to 4.8. Charge balance for the iron and hydrogen ions is achieved by ingress of $Cl^-$ ions. The acidic solution removes impurities, usually sulfide, phosphide, and alkaline metals, from the material as it passes, depositing them at the $CaCO_3$ interface, and in the case of cast iron leaving behind graphitised carbon. This deposition indicates the position of the original surface of artefacts. The lower pH solution dissolves the $CaCO_3$ adjacent to this corrosion layer. If the concretion is buried, the oxidation state of the iron will be lower, resulting in $Fe_2O_3$. If exposed, ferric ions can then form hydrated ferric oxide and oxyhydroxides (North and MacLeod, 1987). $FeCO_3$ has also been reported, though this is not common. When exposed to external seawater with a higher pH, $CaCO_3$ reforms, incorporating surrounding sediment into its matrix. This can continue indefinitely until all the metallic iron within the object has passed into the concretion layer (Figure 2.11), producing a very lightweight object that retains the shape of the cannonball. Rate of formation is dependent on current density, velocity, temperature, and *E*h (Phull, 2010). Inorganic $CaCO_3$ can form in the absence of microbial activity if the surrounding seabed contains calcium carbonate (North and MacLeod, 1987). The acidic, iron-containing solution comes into contact and dissolves $CaCO_3$, starting the concretion cycle.

**Figure 2.11:** An iron concretion (left) excavated from the *Mary Rose* wreckage. Seen after concretion removal (right) and stabilisation (bottom). From Jones (2003: 74).

These factors also contribute to which product formation is preferred. Different polymorphs of $CaCO_3$ (calcite and aragonite) form preferentially when the pH increases around the cathode:

$$Ca^{2+} + HCO_3^- + OH^- \rightarrow CaCO_3 + H_2O \qquad \textbf{Equ. 2.9}$$

Under cathodic overprotection conditions, formation of magnesium hydroxide is favoured (Phull, 2010):

$$\mathrm{Mg^{2+} + 2OH^- \rightarrow Mg(OH)_2}$$ **Equ. 2.10**

$Mg^{2+}$ in seawater can inhibit the formation of $CaCO_3$. However, as $CaCO_3$ decreases in solubility with increasing temperature, $CaCO_3$ is preferred in warmer waters and $Mg(OH)_2$ in colder (Phull, 2010). Though possible, it should be noted that $Mg^{2+}$ is not as relevant for corroding marine iron as it is for industrial complexes (offshore wind turbines, etc).

These products, both within concretions and objects, construct complex matrices that act as a barrier to restrict the diffusion of reactive species, particularly dissolved oxygen, to the underlying metallic surface. In the absence of oxygen, the cathodic reaction rate becomes dependent on the water reduction reaction, which is very slow. Under anaerobic conditions, hydrolysis of ferrous ions to ferrous hydroxide becomes important, reducing the local pH adjacent to the metal surface (North, 1976).

### 2.3.3.5 SULFATE-REDUCING BACTERIA

As explained above, sulfate-reducing bacteria (SRB) are abundant in seawater. These microorganisms can filter through sediment, concretions and corrosion layers, reducing dissolved sulfate held within the pores of the concretions and corrosion product layers generating sulfide species and lowering pH resulting in the formation of hydrogen sulfide, which is highly corrosive (Phull, 2010). Sulfate-reducing bacteria is a term used to define the anaerobic, heterotrophic and mixotrophic bacteria present in seawater. SRB-induced corrosion was known and reported before SRB were even characterised (Little et al., 2000). Autotrophic bacteria are capable of metabolising inorganic compounds, utilising energy from chemolithic (chemical-based) sources. When autotrophic and heterotrophic (organisms that must intake and metabolise secondary organic sources) bacteria metabolise simultaneously, the process is called mixotrophy. Acidophilic autotrophic bacteria can utilise inorganic compounds, including those of sulfur and iron, for metabolic reactions at a low pH (Little et al., 2000).

SRB ingest a small amount of sulfur, reducing $SO_4^{2-}$ to $S^{2-}$ whilst the rest is distributed back into the oceanic ecosystem (Little et al., 2000). Human pollution can also affect sulfur concentrations (Phull, 2010). In anoxic environments such as when objects are covered in concretions and buried in sediment on an ocean floor that is already low in dissolved oxygen. In anoxic conditions, water reduction is the main cathodic reaction:

$2H_2O + 2e^- \rightarrow H_2 + 2OH^-$ (water reduction) **Equ. 2.8**

Sulfate reduction by SRBs proceeds stepwise to sulfur, involving an increase in pH:

$SO_4^{2-} + 4H_2O + 6e^- \rightarrow S + 8OH^-$ **Equ. 2.11**

Then to sulfide:

$S + 2e^- \rightarrow H_2 + 2OH^-$ **Equ. 2.12**

Although sulfate cannot act as a cathodic reactant, reduced sulfur compounds, particularly sulfur itself, can. The end product, sulfide, is reactive to ferrous ions rapidly producing ferrous sulphide:

$Fe^{2+} + S^{2-} \rightarrow FeS$ **Equ. 2.13**

Which can be either oxidised easily to ferric oxide or, in anaerobic conditions, acts as an electrocatalyst for the cathodic reaction. Both of these processes substantially increase the corrosion of iron.

A more comprehensive proposed model for SRB microbial-induced corrosion (MIC) comes from Enning and Garrelfs (2014) (Figure 2.12):

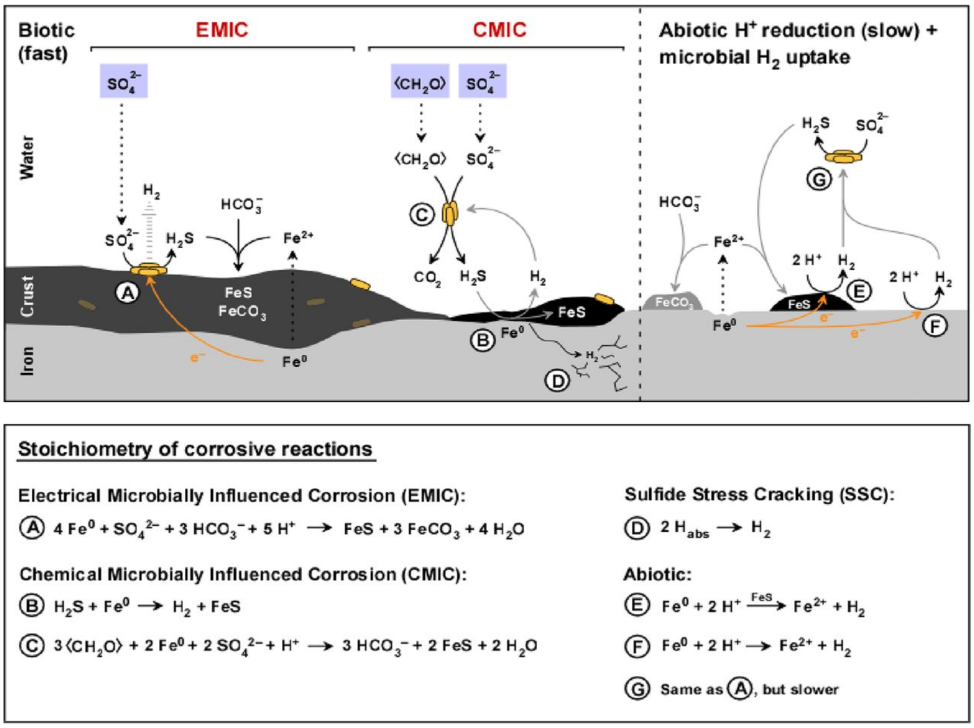

**Figure 2.12:** Model of SRB corrosion. From Enning and Garrelfs (2014).

Studies have shown that sulfate-containing environments can form sulfate green rust ($GR(SO_4^{2-})$) complexes in marine iron (Refait et al., 2003b). A corrosion product in deoxygenated environments, $GR(SO_4^{2-})$ quickly transforms into iron oxyhydroxides (FeOOH) when contacting oxygen. In aqueous environments, $GR(SO_4^{2-})$ can form and be formed by oxyhydroxides. Close to anodes, $GR(SO_4^{2-})$ remains in a dissolved state, producing $Fe^{2+}$ ions that migrate outward toward the exterior, where they further oxidise and form oxyhydroxides.

$$\mathrm{Fe_4^{II}Fe_2^{III}(OH)_{12}SO_4 + \frac{3}{4}O_2 \rightarrow 5FeOOH + Fe^{2+} + SO_4^{2-} + \frac{7}{2}H_2O} \qquad \textbf{Equ. 2.14}$$

Then the ferric species in the outer rust layers are reduced into GR (green rust), and DIRB (dissimilatory iron reducing bacteria) reduce any FeOOH present into $Fe_{aq}^{2+}$ (Refait et al., 2003b). The reaction:

$$\mathrm{2FeOOH_s + 4Fe_{aq}^{2+} + 2H_2O + SO_4^{2-} + 6OH^- \rightarrow Fe_4^{II}Fe_2^{III}(OH)_{12}SO_4} \qquad \textbf{Equ. 2.15}$$

Hence, when marine iron is exposed to atmosphere, $GR(SO_4^{2-})$ is available in both outer and inner corrosion horizons. Langumier et al. (2009) also noted that $GR(SO_4^{2-})$ in the presence of $CO_2$ and further sulfates could form the ferric sulfide (FeS) mackinawite on marine iron, though mackinawite can form through inorganic processes as well.

### 2.3.4 POST-EXCAVATION BEHAVIOUR AND CORROSION OF HERITAGE IRON

After excavation, artefacts are subjected to atmospheric corrosion processes. Rates of corrosion post-excavation can be controlled through understanding the co-dependency of the three constituents responsible for it: oxygen, water and chlorides. Removing one will effectively stop the corrosion process; however, once removed from aquatic burial environments, post-excavation corrosion can proceed at an accelerated rate and quickly destroy otherwise intact artefacts (Turgoose, 1993).

Whilst corrosion takes place in deposition, metastable products can give way to products that are only capable of forming in the atmosphere (Neff et al., 2007). Drying artefacts can cause $Cl^-$ to precipitate and concentrate, whilst atmospheric moisture can initiate corrosion. Corrosion product formation can be determined by concentrations of these constituents, as can corrosion rates. Compounds that migrated from the burial environment can alter corrosion paths. How these objects are stored or displayed post-excavation is crucial for controlling corrosion, conditions that minimise factors such as oxygen and/or moisture access should be sought. Treatments that aim to remove corrosion drivers by physical intervention, such as washing out electrolytes, can contribute to reducing corrosion rates. Understanding the corrosion process and its products is central to optimising the effectiveness of treatments.

### 2.3.4.1 WATER

Water is held in the atmosphere, meaning heritage iron will always be subjected to it, both indoors and outdoors, unless steps are taken to remove it. Relative humidity (RH) is the percentage ratio of water vapour pressure in a gas atmosphere to the saturated water vapour pressure in the same atmosphere at a given temperature. It is a thermodynamic quantity representing the chemical activity of water vapour in that environment and is used as a metric for liminal display and storage zones (Blades et al., 2000a). Water can adsorb on metallic surfaces, creating thin films. These films can increase in thickness with increasing RH (Leygraf et al., 2016: 8). Hydroxyls will form almost immediately on the metallic surface (Cole, 2010). Clustering of water molecules rather than even film formation is common on metallic surfaces. Layers of 1-2 monolayers thick can induce localised corrosion, though rates are relatively low, as a continuous layer of moisture is not yet present (Cole, 2010). One to two monolayers will form on 'clean' metallic surfaces up to 40% RH, with up to 5 at 60% (Cole, 2010). Figure 2.13 shows monolayer formation at given RH values.

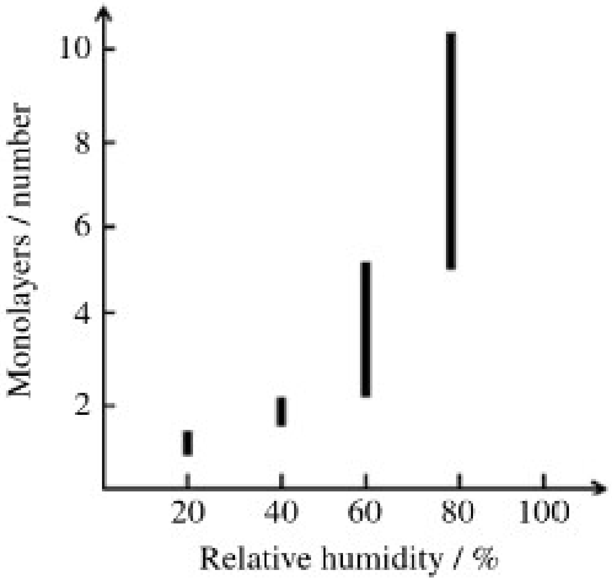

**Figure 2.13:** Monolayer formation at escalating RHs. From Leygraf (2016: 9).

When the RH reaches a critical point, surface wetness occurs, i.e. a continuous surface-covering film of water develops (Dean and Reiser, 1995). This value lies somewhere between 80-90% RH (Vernon, 1935). However, that value can be lower depending on the metal, any alloying material, metallurgical grains, boundaries, and defects, and salts and pollutants (dust, grease) present on the surface (Dean and Reiser, 1995; Leygraf et al., 2016). Water can also condense at 50% RH in structural capillaries as small as 1.5nm starting at the metal surface (Garverick, 1994).

The presence of salt contamination on a surface lowers the RH for condensation to the deliquescence point of the salt. In other words, liquid water is thermodynamically more stable (has a lower RH) when it contains dissolved salt species. A study by Watkinson and Lewis (2005a) showed that iron from chloride-containing environments begins corroding in RHs as low as 12%. Turgoose (1982a) showed how hydration states of ferrous chloride impact corrosion formation: $FeCl_2 \cdot 2H_2O$ forms at 15% RH and $FeCl_2 \cdot 4H_2O$ at 20% RH. Increases in RH from 20% correspond with increases in corrosion rates (Watkinson and Lewis, 2008). A further study of wrought iron found that corrosion rates increase slowly but steadily from 20% to 40% RH with a noticeable increase at 50% RH and a dramatic rise above this value (Figure 2.14) (Watkinson et al., 2019). Though $Cl^-$ and other pollutants (discussed below) can impact corrosion rates, the increases in rates relative to RH values remains the same.

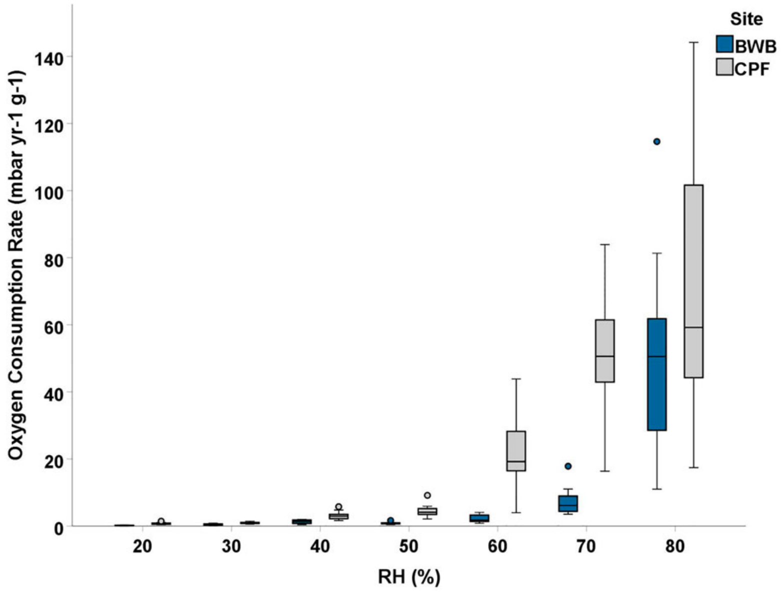

**Figure 2.14:** Corrosion rates of Roman nails from two different archaeological sites, as determined by oxygen consumption. The danger of increasing humidity on corrosion rates is clear. From Watkinson et al. (2019).

### 2.3.4.2 OXYGEN

Oxygen interaction with moisture at object surfaces and diffusion through substrates influences corrosion typology and rates of formation. The partial pressure of oxygen ($pO_2$) in the atmosphere is 20%, which at standard conditions (25°C and 1 atm) equates to 275 mg/l, with a freshwater electrolyte having an oxygen content of 8.3 mg/l under the same conditions (Florian, 1987: 6). This solubility decreases as water temperature rises (North and MacLeod, 1987: 74). Only an increase in temperature or a severe rise in altitude can reduce the amount of oxygen held within the electrolyte, meaning that there are no practical ways to reduce the amount of oxygen an object will be subjected to (barring placing it in an anoxic environment). There are, however, ways to reduce the ability of that oxygen to reach object surfaces. Surface porosity affects oxygen diffusion. Hydrophobic coatings such as waxes or polymers can reduce water and oxygen transport to metal surfaces, limiting the anodic reaction (Emmerson, 2015). Limiting moisture also limits the amount of oxygen it carries (though the pathway for diffusion and replenishment becomes longer with increasing monolayer thickness). This can also occur at points of failure in coatings, as moisture can egress and become trapped, reducing oxygen below the failure point, with adjacent areas acting as a cathode (Figure 2.15) (Greenfield and Scantlebury, 2000).

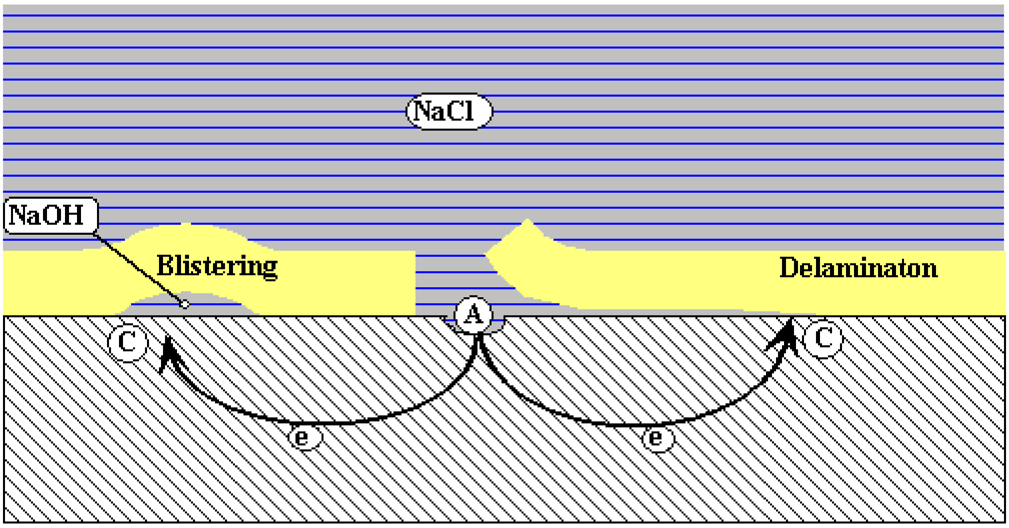

**Figure 2.15:** Drawing of corrosion underneath a failed protective coating. ‘A’ is the anode, ‘C’ are the cathodes, and ‘e’ are the flow of electrons. From Greenfield and Scantlebury (2000).

In most storage and display scenarios, moisture (and its conductivity) and not oxygen becomes the rate-determining factor, as oxygen cannot be reduced (Trethewey and Chamberlain, 1995: 281). Unlike in maritime environments, SRB do not contribute to atmospheric corrosion. Corrosion mechanisms cease in sealed, air-tight vessels once all the oxygen within it has been utilised. It is at this point of its near-depletion when oxygen becomes the rate-determining factor when the rate of corrosion slows in oxygen-suppressed environments.

#### 2.3.4.3 POLLUTANTS

##### 2.3.4.3.1 SULFUR-CONTAINING COMPOUNDS

Sulfur containing components can induce corrosion and influence product formation in standard atmospheric conditions, in both indoor and outdoor locations. The most aggressive of these is sulfur dioxide ($SO_2$), a compound present in air due to human industrial activities (Tidblad, 2013). Other sulfur compounds include hydrogen sulfide ($H_2S$), dimethyl sulfide (DMS), carbon sulfide (CS2), and carbonyl sulfide (OCS) (Cole, 2010). DMS can oxidise into $SO_2$, and OCS can react with oxygen atoms in atmosphere to convert to $SO_2$. CS2 can oxidise into OCS, resulting in further $SO_2$ production. It must be noted however that these, with the except of $SO_2$ and $H_2S$, are of little consequence in storage conditions.

The solubility of $SO_2$ in water is 0.2 g $SO_2$/1000 g water at 20°C (Terraglio and Manganelli, 1967). $SO_2$ can then act as a depolarising agent and increase metal dissolution. Ferrous ions can form complexes with oxidised sulfur compounds, including iron sulfate ($FeSO_4$), which can then lead to γ-FeOOH formation (Xia and Chunchun, 2006). Iron sulfate can then dissolve and hydrolyse, decreasing pH and increasing metal dissolution at the anode. Sulfate and hydrogen radicals will form sulfuric acid, which will also increase the dissolution of the metal surface (Cole, 2010).

Atmospheric pollution is largely irrelevant for most archaeological materials from marine contexts. The biggest threat comes from sulfur compounds generated in the marine environment and embedded in corrosion layers. The multiple oxidation states of sulfur allow it to oxidise readily into other compounds, most notably sulfates ($SO_4^{2-}$) and hence sulfuric acid. Sulfides will react with oxygen and new sulfur bearing compounds will be formed that produce an acidic environment. GR($SO_4^{2-}$) can quickly oxidise to form ferric oxides and oxyhydroxides, including α- and γ-FeOOH (Refait et al., 2003b).

#### 2.3.4.3.2 CHLORIDES

Chlorides from aqueous and terrestrial burial environments can be retained within objects after their excavation. They can also be deposited on surface exteriors in open air, uncontrolled environments, increasing with proximity to bodies of saltwater, but are not considered to be an air-borne pollutant within indoor environments (Blades et al., 2000b). Their high solubility makes them easily transported through corrosion product layers, acting as electrolytes and facilitating corrosion (North and Pearson, 1978b; North and MacLeod, 1987). Many chloride containing compounds are hygroscopic and will draw moisture to surfaces they are adsorbed on, increasing water monolayers and lowering critical corrosion thresholds (Leygraf et al., 2016).

Residual chlorides can balance ferrous ion production at the anode and form iron chlorides and hydroxychlorides $Fe_2(OH)_3Cl$, which can both produce oxyhydroxides (Neff et al., 2007). Chlorides are also a component of green rust $GR(Cl^-)$, which can oxidise to several differing compounds, depending on oxygen concentration and exposure (Refait et al., 2003a). Chloride concentration can determine what compounds can form, as higher concentrations have been shown to lead to β-FeOOH akaganeite (Rémazeilles and Refait, 2007), a product with chlorides adsorbed on its surface and locked within its structure. These products are discussed in the following section.

#### 2.3.4.3.3 OTHER POLLUTANTS

Atmospheric corrosion can be instigated by other pollutants (e.g. organic acids from the decay of wood- and paper-based materials) that are available within museums, displays, and object stores. Modern cast irons include alloying materials that are more resistant to organic acid attack; however, unalloyed cast iron like that from the *Mary Rose* is susceptible to corrosive organic gases (Reynaud, 2010). Acetic acid ($CH_3COOH$) is off-gassed by wood composites, sealants, and adhesives (Blades et al., 2000b) and will initiate corrosion by attacking metal surfaces. Anodic polarisation increases with temperature and acid concentration, increasing corrosion rates (Singh and Mukherjee, 2010).

Choosing storage materials is important, as wood composites, adhesives, and binding agents can also off-gas formic acid, inducing corrosion in the same manner as acetic acid (Singh and Gupta, 1996). Formaldehyde is introduced into internal environments via adhesive-soaked wood composites such as MDF. This can then oxidise into formic acid (Blades et al., 2000b).

## 2.4 CORROSION PRODUCTS AND FORMATION

Corrosion product formation can lead to stifling of further corrosion, though this is dependent upon the morphology of its layer and environment. Some products are considered ‘stable’, due to their low solubility and ongoing stability. Others are metastable, existing in specific environments (such as aqueous) and rapidly transforming once that environment changes. For marine cast iron post-excavation, variation in concentration of species inside a rust/corrosion product will give rise to a concentration cell which produces separated anodes and cathodes and drives the corrosion process. No protective corrosion product layers are formed, as they are all voluminous and powdery, with their growth pressuring overlying corrosion product layers and breaking them up. The products that are present can determine what stabilising action is taken, as well as how successful that action is. The presence of any one product does not preclude the presence of others, as several different anode/cathode reactions can take place throughout an object. If one area of an object is more ‘protected’ than another, moisture and oxygen ingress could be altered, leading to the concurrent formation of separate products within the same artefact and local concentrations of chlorides may influence the products formed.

Neff et al. (2007) illustrate this product differentiation, showing how multiple products will form within a single substrate, given their proximity to the low pH anode and an oxygen-rich cathode (Figure 2.16). Therefore, variability of product formation results in no two objects following the same corrosion pathway. This unpredictability underscores the challenge conservators face when determining treatment effectiveness.

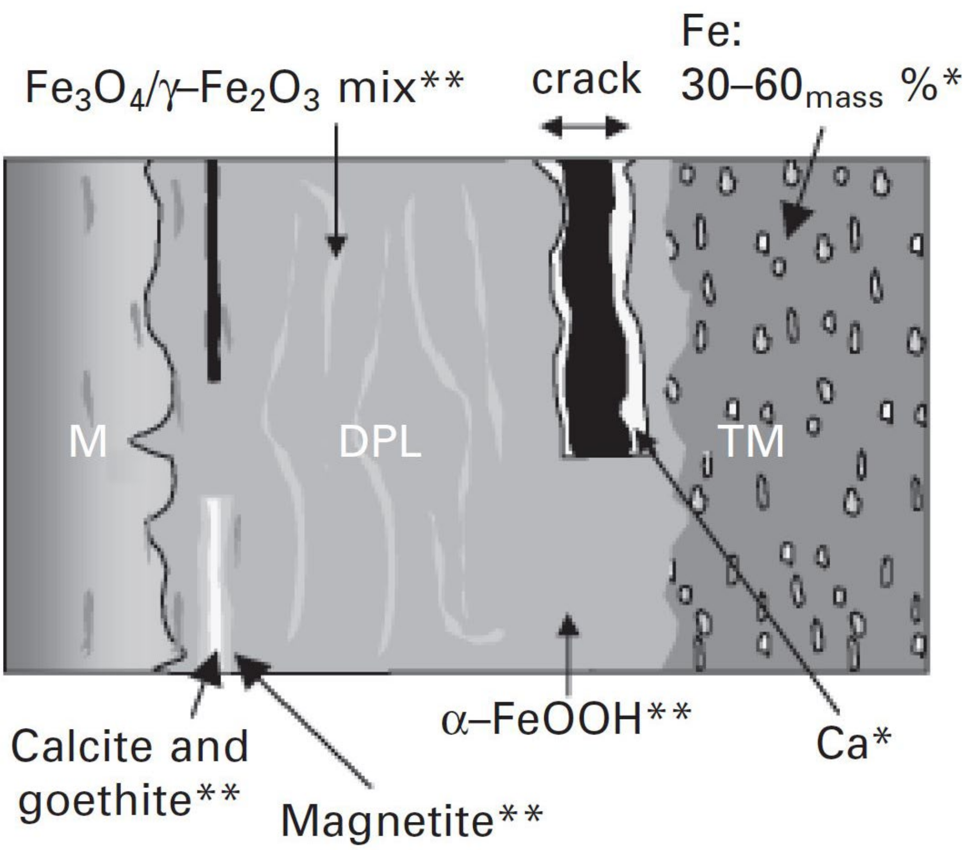

**Figure 2.16:** Corrosion product variability within a single metallographic profile. From Neff et al. (2007).

### 2.4.1 MAGNETITE

Magnetite $Fe_3O_4$ (or $Fe_2O_3$ FeO) is a $Fe^{2+}/Fe^{3+}$ balanced, ferrimagnetic oxide that is black in appearance and forms closer to the metal surface, though can also appear adjacent to the concretion zone in marine iron (Cornell and Schwertmann, 2003; Memet, 2007a). The compound is precipitated in mixed solutions of $Fe^{2+}$ and $Fe^{3+}$ ions and oxidised by either green rust or $Fe(OH)_2$ (Cornell and Schwertmann, 2003: 346). In aqueous solutions, magnetite is one of only two stable, solid corrosion products, the other being goethite (α-FeOOH, see below) (Turgoose, 1993). The formation of magnetite is preferred in buried, anoxic marine iron (Angelini et al., 2013), whereas goethite forms in areas of higher oxygen concentration. Both may form concurrently, though magnetite will underlay goethite in the corrosion profile, as goethite blocks access to oxygen (Turgoose, 1982a). The crystalline structure of magnetite (with areas occupied by $Fe^{III}$, others occupied by $Fe^{II}$ and $Fe^{III}$) allows it to appear as either a dense phase or voluminous powder, depending on formation (Schwertmann and Cornell, 2008: 9).

Magnetite has the lowest resistivity of any iron oxide, allowing it to act as a cathode in certain situations (Cornell and Schwertmann, 2003: 117). It is capable of reducing oxygen and thus increasing corrosion rates as more of it forms (Cornell and Schwertmann, 2003: 500). This low resistivity and its ability to adsorb and concentrate $Cl^-$ on its surface allow it to be a source of mobile chlorides within objects. Taken in combination with its cathodic ability, magnetite is both a determinate of other product formation and capable of being reduced (to Fe(OH)2) and oxidised into others (such as FeOOH) (Cornell and Schwertmann, 2003: 6).

### 2.4.2 GOETHITE

Goethite (α-FeOOH) is the most stable of the five oxyhydroxide polymorphs and one of the most thermodynamically stable iron oxides, forming either first within a corrosion cycle, or the final product after many transformations (Cornell and Schwertmann, 2003: 300). This results in goethite being the most abundant corrosion product in most iron substrates. Slower supply of hydrolysed components favour the formation of goethite, as it has a large crystal structure and slow formation results in larger crystals (Cornell and Schwertmann: 347). Goethite will typically form in oxygen-rich environments where chloride and $Fe^{2+}$ concentrations are intermediate and (Refait and Génin, 1997; Rémazeilles and Refait, 2007) and in a neutral to alkaline pH (Turgoose, 1982a). Turgoose (1982a) states that in aqueous conditions, eventually β, γ, δ FeOOH compounds convert to α-FeOOH, meaning the presence of the other polymorphs in archaeological artefacts is a result of post-excavation atmospheric corrosion. Sulfate presence promotes goethite formation in favour of lepidocrocite (Cornell and Schwertmann, 2003: 500).

### 2.4.3 AKAGANEITE

Akaganeite (β-FeOOH) is a voluminous, hygroscopic, and acidic corrosion product, a combination that can result in object degradation and destruction, even at low humidities (Watkinson and Lewis, 2005a). The crystal structure of akaganeite differs from the other hydroxychlorides, in that it holds $Cl^-$ within its matrix in a hollandite-type tunnel, and also adsorbs $Cl^-$ on its surface (Figure 2.17) (Ståhl et al., 2003). Akaganeite forms with a transformation of $Fe(OH)_2$ to iron hydroxychloride β-$Fe_2(OH)_3Cl$, further followed by oxidation to GR($Cl^-$), though only if $Cl^-$ concentrations are high enough (Refait and Génin, 1997). Though this is possible to simulate in oxygenated aqueous conditions, akaganeite usually forms upon removal of chloride containing artefacts from aqueous and deoxygenated burial environments to a more oxygenated atmosphere. This means akaganeite is a distinctly post-excavation/atmospheric phenomenon of heritage iron (Turgoose, 1982b), with wet/dry cycles promoting its formation (Hœrlé et al., 2004; Dillmann et al., 2004).

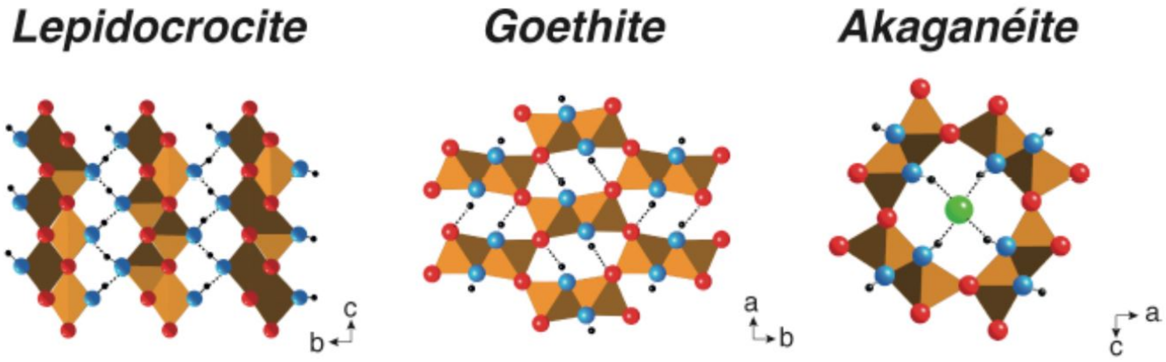

**Figure 2.17:** Crystal structures of various FeOOH iron oxyhydroxides. Note the locked chloride (in green) in the centre of the akaganeite structure. From Song (2013).

Apart from chloride within its structure, it has anywhere from 1.3% to 17% surface adsorbed chloride (Childs et al., 1980). Its hygroscopic nature (Watkinson and Lewis, 2005b) promotes mobility of the surface chloride to provide an electrolyte, which takes part in the corrosion of iron it contacts with. Akaganeite is not hygroscopic at low RH%, however. The rate of corrosion remains slow until 40%, with rates significantly increasing at 50-60% RH as more water is adsorbed, increasing mobility of the chloride (Watkinson and Lewis, 2004). Thickett and Odlyha (2013) report that β-FeOOH formed at high humidities lowers this critical threshold, resulting in higher corrosion rates at lower RH, although it is not clear why. Akaganeite has been known to transform to goethite, releasing $Cl^-$ which can support further corrosion and formation of new akaganeite crystals (Thickett and Odlyha, 2013). The hygroscopicity of akaganeite and its adsorbed $Cl^-$ ions will lower the surrounding pH, increasing $Fe^{2+}$ production and forming ferrous chloride $FeCl_2$; however, akaganeite is less hydrated than ferrous chloride, with the latter deliquescing at ~55% RH (Lin, 2014). This results in the crystallised β-FeOOH forming on the surface with soluble $FeCl_2$ forming in the acidified area beneath it (Réguer et al., 2007). This results in 'blister' formations. When these akaganeite 'skins' break, a weeping effect is observed (Watkinson and Lewis, 2005b).

### 2.4.4 LEPIDOCROCITE

Lepidocrocite (γ-FeOOH) commonly forms post-excavation on archaeological iron. Lepidocrocite is unstable compared to goethite, yet will persist within objects (Cornell and Schwertmann, 2003: 5). It is a common oxidation product of $Fe^{2+}$, though its formation is dependent upon the same factors as the other oxyhydroxides: pH, and concentrations of $Fe^{2+}$, $Cl^-$, and oxygen (Turgoose, 1982a; Cornell and Schwertmann, 2003: 5). γ-FeOOH will form preferentially to α-FeOOH in strongly oxidising conditions, or when $Fe^{2+}$ and $Cl^-$ concentrations are low (Rémazeilles and Refait, 2007). Both GR($Cl^-$) and GR($SO_4^{2-}$) oxidise to γ-FeOOH, with the latter capable of further transforming into α-FeOOH (Refait et al., 1998; Refait et al., 2003b). γ-FeOOH both forms and is reduced during wet-dry cycles (common in uncontrolled atmospheres). Hœrlé et al. (2004) state lepidocrocite is an oxidiser in rust layers, and can then be reduced with $Fe^{2+}$ 'doping', allowing it to reoxidise quickly. Cornell and Schwertmann (2003: 500) explain that during the wetting of a dry surface, lepidocrocite is reduced by an intermediate (most likely GR) to ferrous hydroxide, with corrosion of the metal occurring simultaneously. Upon drying, oxygen re-enters via the porous oxide layer, oxidising the magnetite to maghemite. However, lepidocrocite is the final product if reduction stops during the intermediate state.

The constant wet/dry cycles and continual transformation result in poor adhesion of corrosion to underlying substrates, resulting in larger surface porosity and inhomogeneity, increasing corrosion rates.

### 2.4.5 MAGHEMITE

Maghemite (γ-$Fe_2O_3$) is a red coloured, ferrimagnetic iron oxide that could be considered a fully oxidised magnetite (Cornell and Schwertmann, 2003: 6; Schwertmann and Cornell, 2008: 9). As maghemite is a $Fe^{3+}$ ferric oxide and $Fe^{3+}$ ions are less soluble, it will form at a greater distance from the metal surface than other products, including magnetite (Memet, 2007b). It can form through oxidation of magnetite (Cornell and Schwertmann, 2003: 403; Neff et al., 2007), especially during atmospheric wet/dry cycles (Hœrlé et al., 2004).

### 2.4.6 HEMATITE

Hematite (α-$Fe_2O_3$) is found either as a blood-red or greyish-black mineral, depending on the crystal structure. It is, along with goethite, considered the most stable of iron corrosion products (Cornell and Schwertmann, 2003: 345). In heritage artefacts, it can develop from ferrihydrite in aqueous environments in the 6-8 pH range, though this is unlikely, as the reaction requires higher temperatures (85°C) and the dry dehydration of an FeOOH species (Cornell and Giovanoli, 1990). This may explain its appearance in artefacts subjected to subcritical stabilising treatments (see 3.2.6.2) (Cornell and Schwertmann, 2003: 367).

Oxidation from magnetite can occur, but only at higher temperatures, leaving maghemite to be the favoured ferric oxide in heritage iron.

### 2.4.7 IRON CHLORIDES, HYDROXYCHLORIDES, AND FERRIHYDRITE

Iron$^{II}$ hydroxychoride $Fe_2(OH)_3Cl$ is thought to be the main chloride-containing product formed during anaerobic corrosion. Its formation is specific to pH and high $Cl^-$ concentration, as $Fe(OH)_2$ forms if the pH is higher than 7.51 (Rémazeilles et al., 2009). This suggests formation closer to the metal surface, where larger quantities of soluble ferrous ions subside. This product is especially prone to oxidation in atmosphere, forming iron$^{III}$ oxyhydroxides. Ferrous chlorides $FeCl_2$ also form within heritage iron. $FeCl_2$ is a progenitor for akaganeite formation, as it is composed entirely of $Fe^{2+}$ and $Cl^-$ ions (Refait and Génin, 1997). Turgoose (1993) suggests it could form upon drying of artefacts but this has rarely been confirmed by analysis. Iron chlorides have a low pH, creating an acidic environment that can dissolve metal, resulting in pit formation and blistering, as described earlier in this chapter. Oxidation of either $FeCl_2$ or $Fe_2(OH)_3Cl$ first forms a $GR(Cl^-)$ intermediary, followed by further oxidation to oxyhydroxide. The resultant FeOOH species depends on the concentration of $Cl^-$ ions (Refait et al., 1998). Ferric chlorides may also be present and are hygroscopic, causing akaganeite to form as low as 13% RH (Thickett and Odlyha, 2013)

Ferrihydrite $Fe_5O_8H \cdot H_2O$ is a poorly crystalline compound that can dissolve and reprecipitate in aqueous solutions. It can transform into akaganeite (high $Cl^-$ content, low pH), goethite (pH 3-14), or lepidocrocite (Cornell and Schwertmann, 2003: 366). The values of $OH^-$ and $H_2O$ are variable, with conditions dictating formula. Ferrihydrite can form from $GR(Cl^-)$ when $OH^-$, $Cl^-$, and larger amounts of dissolved oxygen are present (Refait et al., 2003a).

### 2.4.8 SULFUR PRODUCTS

As discussed above, sulfate is present in marine contexts, with SRB increasing iron corrosion in anoxic environments noting that on evaporation most of the sulfate is seawater precipitates as gypsum. Sulfonated green rust GR ($SO_4^{2-}$) can lead to oxyhydroxide formation, as well as mackinawite (Langumier et al., 2009). Iron sulfate $FeSO_4$ can also lead to oxyhydroxides. Amorphous iron sulfide (FeS) is usually present as mackinawite or pyrrhotite (Cornwell and Morse, 1987; Walker, 2001). Anaerobic conditions in the burial environment cause sulfides to be most present near metal surfaces, where they react readily with ferrous ions (Little et al., 2000). This usually occurs around the concretion zone of iron artefacts, where $Fe^{2+}$ ions are abundant. Sulfide ions must still move inward to be present near the metal core. As a result, sulfide products are rarely seen in the graphitised zone of maritime cast iron artefacts (North, 1982).

Elemental sulfur has been observed in maritime cast iron corrosion (North, 1976), a possible reaction being:

$$3H_2S + 2FeOOH \rightarrow S^0 + 2FeS + 4H_2O \qquad \textbf{Equ. 2.16}$$

The disproportionation results in both reduction of iron ($Fe^{3+} \rightarrow Fe^{2+}$) and oxidation of sulfur ($S^{2-} \rightarrow S^0$). If the artefact is still in a marine environment, SRB can then react with FeS and $S^0$ to form $FeS_2$ pyrite (Jørgensen and Nelson, 2004). When $Fe_2O_3$ is present, sulfate reduction can result in precipitation of $CaCO_3$ and FeS (Gardner, 1973).

In atmospheric conditions of 50% RH and above, corrosion of iron in the presence of sulfate increases dramatically, with 60% RH considered critical (Turgoose, 1993), though it is likely that chloride-bearing species at this humidity pose a greater risk to heritage iron. Chlorides deliquesce at RH lower than sulfates, by the time the deliquescence levels for sulfates are reached the environment is corrosive anyway (Rimmer and Watkinson, 2011).

### 2.4.9 CARBONATE PRODUCTS

Calcium carbonate is a primary constituent of iron concretions and precipitates from seawater at raised pH typically present at cathodic sites. Siderite ($FeCO_3$) has been observed (Matthiesen et al., 2003; Rémazeilles et al., 2009). The nature of concretion products allows for carbonate ions to exchange their $Ca^{2+}$ partners for $Fe^{2+}$ ions, or from carbonic acid (Matthiesen et al., 2003). Siderite is not generally found other than on the surface of an object, nor does it form in solutions containing higher sulfide concentrations (North and MacLeod, 1987) It does form when oxygen levels are severely low and carbonates are present, or in high temperatures with nearly saturated concentrations of $CO_2$ (Neff et al., 2007). Siderite can oxidise to α and γ-FeOOH, though Turgoose (1982b) points out that both these oxyhydroxides are less voluminous than siderite, so will not physically damage corrosion product layers, and the presence of the carbonate post-oxidation will prevent pH from dropping. $CO_3^{2-}$ can, in the same way as $Cl^-$ and $SO_4^{2-}$ complexes, for green rust $GR(CO_3^{2-})$. $GR(CO_3^{2})$ will then follow same path as the other $Fe^{II}/Fe^{III}$ hydroxysalts and transform into α or γ-FeOOH (Antony et al., 2008; Rémazeilles and Refait, 2009). Iron hydroxycarbonate $Fe_2(OH)_2CO_3$ chukanovite, though its occurrence is rare,can form in the presence of excess carbonate and $Fe^{2+}$ ions and has been suggested as forming from $Fe(OH)_2$ during long corrosion periods, driven by dissolution/reprecipitation cycles (Rémazeilles and Refait, 2009).

### 2.4.10 MANGANESE

Manganese is present in marine water and sediments (Chester, 2009: 269) and will find its way into heritage iron. Its multiple oxidation states can cause it to form a variety of compounds and oxides. Manganese ions ($Mn^{2+}$) are preferred over manganese oxides and carbonates at low pH and reduction potentials. The presence of $S^{2-}$ sulfide ions in solution can cause MnS to form. However, for this to happen the concentration of sulfide must be more present than carbonate by a factor of 100 (Krauskopf, 1995: 364). The typical wt% of $CO_3^{2-}$ ions to $S^{2-}$ in marine artefact concretions is nearly 4-1 (Florian, 1987: 12). $MnCO_3$ would precipitate in more basic, less reducing environments, while $MnO_2$ would be preferred when both redox potential and pH are higher. Krauskopf (1995: 365) states that manganese compounds will only form when $Mn^{2+}$ content is 'abnormally high'. When iron is present, hematite is preferred over $MnO_2$ formation over a wide Eh/pH range. However, the possibility remains that MnS can form further in from the surface, where few $CO_3^{2-}$ ions are found. It should be noted, however, that the likelihood of these reactions is small and manganese is unlikely to be of any significance.

## 2.5 CHARACTERISATION AND CORROSION OF THE *MARY ROSE* CANNONBALLS

### 2.5.1 METALLOGRAPHIC PROFILE

Cannonballs from the *Mary Rose* have been characterised in earlier studies (Starley and Hildred, 2002; Seifert, 2015; Simon et al., 2018; Simon et al., 2019) confirming a white/grey cast iron mixture, with the former diminishing in favour of the latter when moving from the exterior surface inward. This is due to differential cooling rates during casting, with the outside cooling quickly and forming white, whilst the interior features a slower cooling rate, favouring grey. Figure 2.18 shows SEM photos of three separate MRT cannonballs, acquired at different times by different people. All have nearly identical metallographic profiles. The dark nodules are areas of corrosion, whilst graphite flakes are visible as thin black strands. The less dense, graphite-rich corrosion area starts formation ~1.5 mm below the exterior surface (Simon et al., 2019), though is not a uniformly corroded zone. Figure 2.19 is a composite cross section (via SEM) of MRT cannonball #83A-0449 (Seifert, 2015). The composition of the cannonball visibly changes as it moves from the exterior surface (on the left) to the interior. The densities of these areas vary. The graphite-rich corrosion area near the exterior is less dense than the adjacent, further in white cast iron, which in turn is denser than the grey cast iron in the furthest interior.

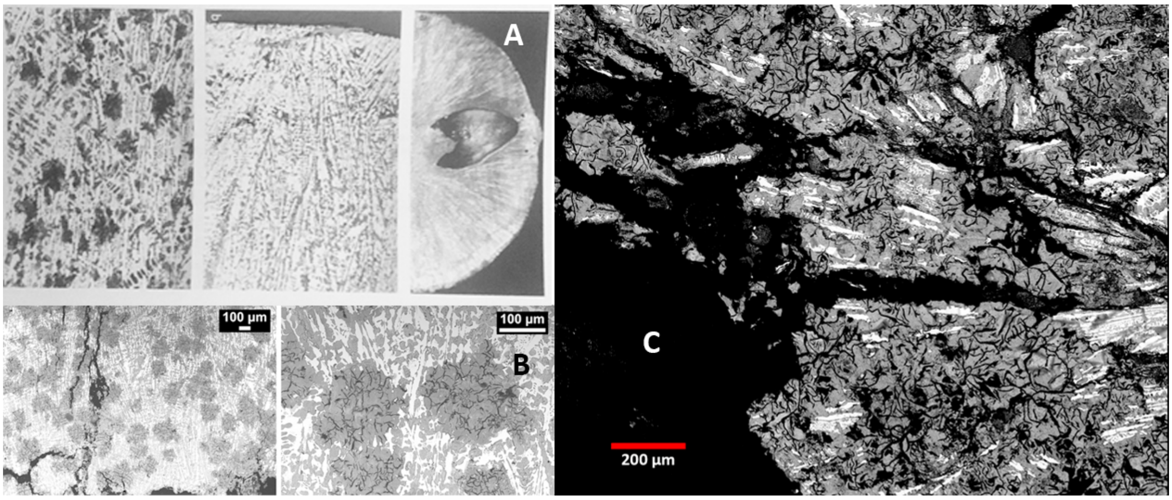

**Figure 2.18:** Scanning electron microscope images of cross sections from three different Mary Rose cannonballs. A) from Starley (2002); B) from Simon et al. (2019), C) from Seifert (2015).

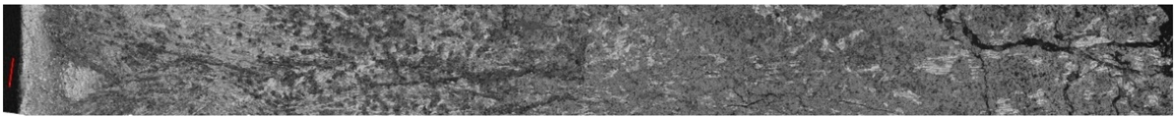

**Figure 2.19:** A cross section profile of MRT cannonball #83A-0449, from the outer surface to the middle. Note how the composition, and thus density, changes moving from the exterior (left) to the interior (right).

### 2.5.2 CORROSION

Understanding how the production, metallurgy, burial environment, and storage can affect and induce highly specific corrosion pathways, one can synthesise a probable corrosion profile for the *Mary Rose* cannonballs. During their time on the seafloor, the mottled cast iron cannonballs became inundated with aerated seawater which quickly instigated corrosion. The iron metal surface began to retreat from the exterior of the cannonballs, leaving behind a mix of iron oxyhydroxides, green rusts, and carbon-rich graphite products, as shown in Figure 2.18. As concretions slowly formed around the cannonballs, oxygen became limited, slowing corrosion rates. Once the majority of oxygen had been consumed by corrosion, the corrosion product network restricted further diffusion and essentially anoxic conditions prevailed where slow water reduction, or faster microbially induced (e.g.

by SRB) corrosion prevailed. This rate was significantly slower, allowing the iron cannonballs that were quickly buried in sediment and concreted over to be significantly more stable than other cannonballs that were exposed to aerated seawater for longer periods. Other factors, such as galvanic response between metals in contact with each other, salinity gradients, and biosphere contribution also resulted in these objects of identical morphology to corrode at different rates. This would account for the variable masses of the cannonballs once excavated.

Once excavated and exposed to the atmosphere, the cannonballs underwent rapid oxidation. Upon drying, green rusts, ferrous chlorides, and hydroxy chlorides converted to oxyhydroxides (including akageneite) and oxides, dependent upon $Cl^-$ content and pH (Simon et al., 2019). The rates of transformation are fuelled by atmospheric moisture content. The graphite-rich corrosion nodules and flakes act as localised cathodes, inducing localised corrosion events (Simon et al., 2019). The corrosion products formed are much more voluminous than their hydrated progenitors. This formation takes place throughout the graphite-heavy corrosion matrix, and the variability of densities between it and the white and grey cast iron results in an internal build-up of pressure. The soft, porous, and less dense graphite-rich corrosion matrix then buckles and cracks, leading to damage visible on object exteriors. Depending on the resultant network of cracks, a spalling effect is possible, leading to the exfoliation and ultimate destruction of the objects (Figure 2.20).

**Figure 2.20**: Spalling and exfoliation of MRT #83A-0180, a result of continued corrosion post-treatment.

The cannonballs from the *Mary Rose* underwent treatments aimed at preventing further post-excavation corrosion. Although no corrosion of the cannonballs has been identified while stored in the dedicated low-humidity facility, visible corrosion damage occurred during exposure to higher humidities while on display. A consideration of these treatments and the factors that influence their implementation and success may be beneficial in understanding the continued deterioration of the cannonballs.

# 3 TREATMENT OF HERITAGE IRON

Decision-making in preservation of cultural heritage is complex and conservators must employ a holistic approach to designing interventive and preventive treatment strategies. Comprehending material chemistry, composition and decay processes is central to treatment design but cannot be divorced from practical and ethical concerns. Having considered the intricacies of cast iron production and corrosion, this discussion focuses on conservation treatments employed on heritage iron and the complex decision-making pathways that conservators navigate when selecting them.

## 3.1 TREATMENT CONSIDERATIONS, DECISION MAKING, AND COMPLEXITY OF CHOICE

The ideal conservation route (Figure 3.1) is an oversimplification of a complex decision tree that starts not from the point of excavation, burial, use life, or even manufacture, but from the materials and technology that were available for its production, with material composition informing decay and survival during interment.

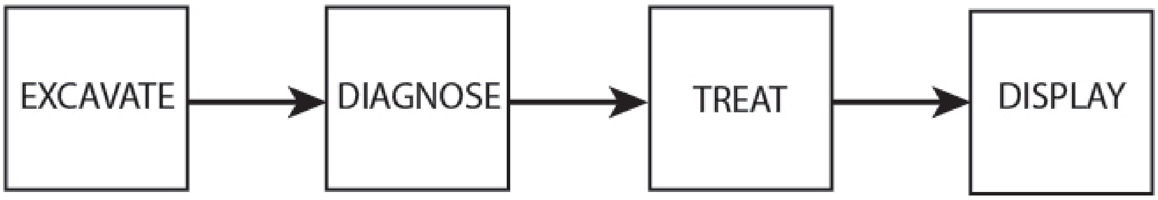

**Figure 3.1:** The idealised version of a conservation treatment.

Post-excavation survival of artefacts is likewise heavily dependent on the materials and technology available to preserve it, in addition to a myriad of interrelated factors that are subjective and may be uncontrollable (Figure 3.2). Successful treatment design relies on navigation of these factors and is no different for heritage iron than for any other material.

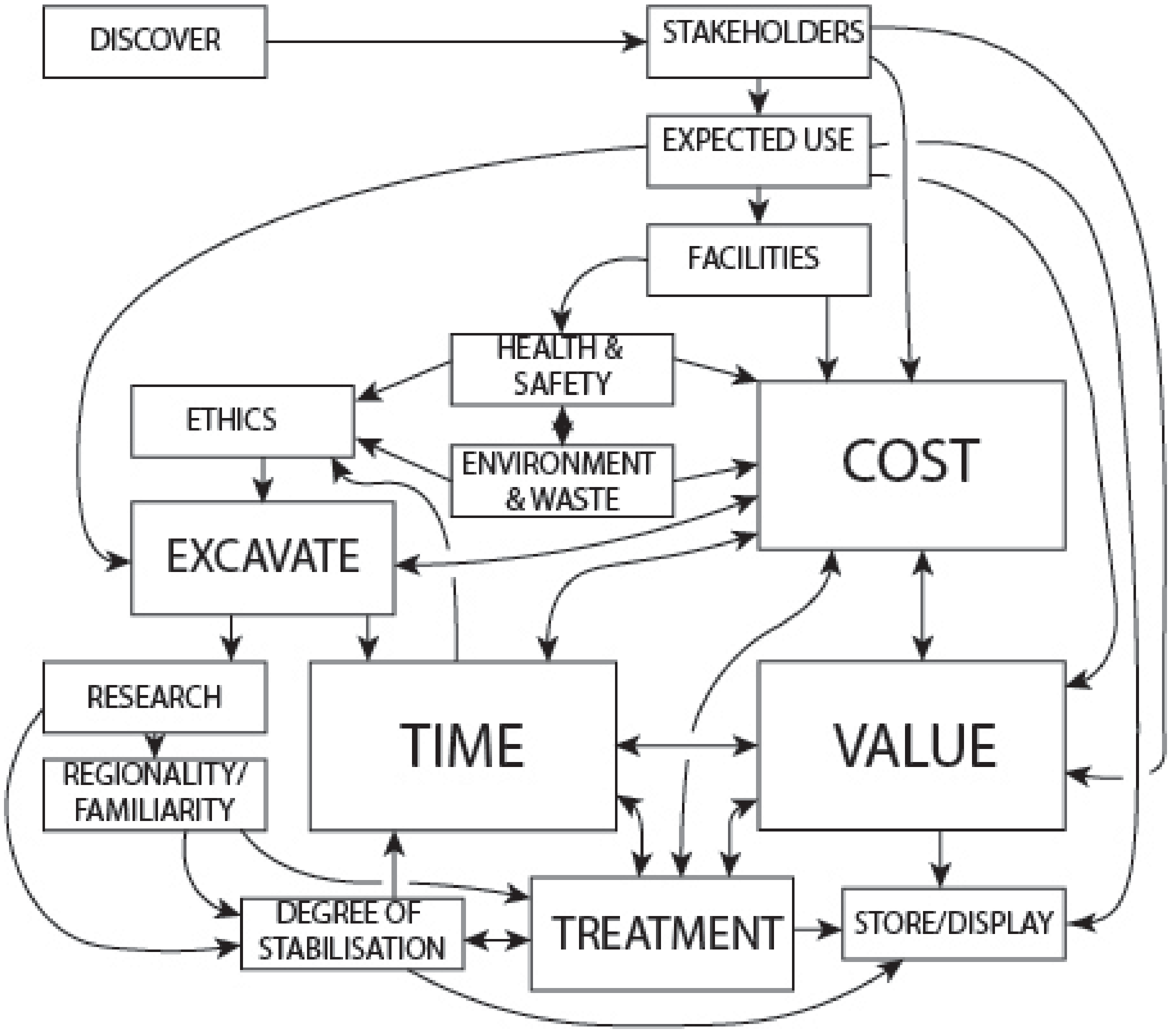

**Figure 3.2:** Decision diagram of factors that may determine the treatment path of an object.

### 3.1.1 STAKEHOLDERS

An important factor influencing many treatment decisions is who is invested in the preservation of an artefact or collection. Stakeholders can include governments, museums, cultural groups and ethnicities, religions, funding bodies, and the public at large. Conservators must consider the impact a treatment may have on those who have a stake in an object. Likewise, the stakeholders often determine available funds, facilities, and time scales for treatment.

### 3.1.2 COST

The financial investment needed to undertake and complete a treatment must be considered, as well as any ongoing costs arising from it. The willingness of stakeholders to provide treatment funds usually depends on the intrinsic and perceived value of the object or collection and a cost-benefit assessment of the projected outcome.

Calculating the financial cost of a treatment is complex. Treatment materials may be relatively inexpensive but the process requires significant input of specialist time. Conversely, treatment set up could be prohibitively expensive but the process swift or requiring little specialist oversight over a longer time frame. The ongoing costs associated with an interventive treatment may relate to treatment lifetimes and the need to retreat (as seen with the application of protective coatings to metals) or the need to maintain a particular environment around an artefact post-treatment. Calculating these costs relies on a prediction of treatment outcomes, effectiveness and longevity which in turn relies on practical experience or targeted research.

The cost-benefit of a treatment can also refer to the maintenance, enhancement or loss of cultural value of an artefact or collection. What is the cost of a treatment to the object? If the treatment results in loss or alteration of original material but is judged to increase the lifetime of an object, should that treatment be considered viable? These ethical considerations are often subjective and controversial.

### 3.1.3 TIME

The duration of a treatment will influence decisions around its suitability for use. All other factors being equal, conservators will select a shorter treatment, as more time usually costs more money. All other factors are rarely (if ever) equal, however. Consider the scenario in which Treatment A is a longer treatment which requires more funding initially than the shorter Treatment B. Treatment B will only preserve an object under a specific set of parameters and only for a short time. The time it takes to carry out Treatment A makes it unviable, yet it gives the object a longer survival time than the time it takes to carry out the only other possible treatment.

Can an object be put in stasis until such time as funding is raised, or facilities built, or methods developed? Does the project timeline allow for treatment? By how much time does any treatment extend object lifetimes?

### 3.1.4 FACILITIES

Treatment facilities must be tailored to the dimensions of the objects under treatment. This is undoubtedly the case with shipwrecks such as the *Mary Rose*, USS *Monitor, H.L. Hunley* and the *Vasa,* as the facilities and space required to conserve entire structures are extensive (Figure 3.3). Facilities are not limited to laboratory space. Appropriate storage is vital in the safeguarding of heritage artefacts.

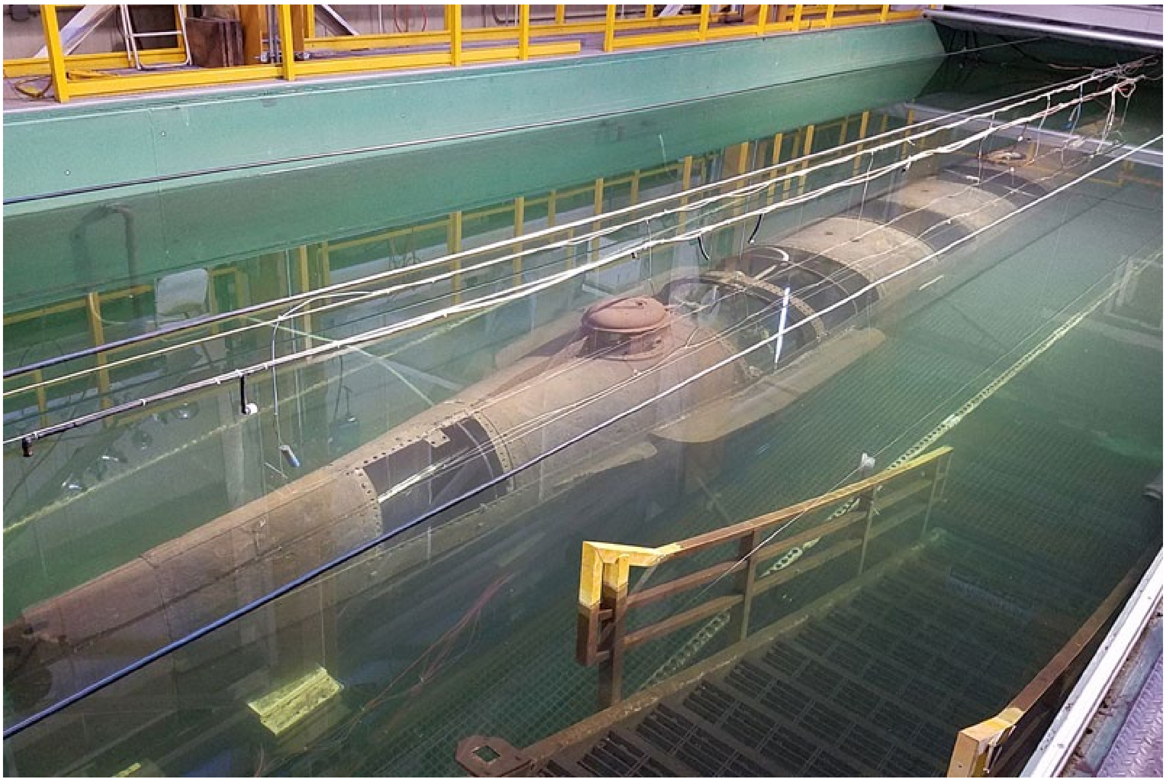

**Figure 3.3:** *H.L. Hunley* in stabilising treatment at the Warren Lasch Conservation Center in South Carolina, USA. Photo from hunley.org

### 3.1.5 HEALTH AND SAFETY

Conservators are bound by organisational and governmental restrictions to reduce workplace hazards (Institute of Conservation, 2016). For example, benzene was employed in conservation for decades but was shown to be a carcinogen and is no longer used widely. Even common solvents such as acetone are also considered to pose a risk to health and exposure limits must not be exceeded (Health and Executive, 2018).

Large projects (the *Mary Rose, H.L. Hunley,* USS *Monitor,* etc.) bring their own set of safety protocols, as cranes, barges, large tanks of volatile desalination solutions, rigging, lifts and trolleys all require risk mitigation strategies. Rigorous health and safety planning is essential when devising conservation treatments and strategies, regardless of the size of the project. An inability to mitigate the risks posed by a treatment will result in it being rejected as a viable option despite a projection of excellent results for the artefact.

### 3.1.6 ENVIRONMENT AND WASTE

Conservation treatments can have a considerable impact on the environment. Volatile and toxic chemicals used in conservation treatments may deleteriously affect aquatic and marine life (if improperly disposed of in sinks), off-gas noxious fumes, or simply be insoluble and remain in landfills for centuries. Conservation ethics (see 3.1.7) state that treatments should be both reversible and as minimally impactful as possible, and this remains true of the waste generated by treatments. It violates the spirit of conservation principles if the treatment is minimally impactful to the object but greatly impactful to the environment (Avrami, 2009). Likewise, if a treatment leaves an object too toxic to handle safely (such as arsenic treatments of the past (Sharma, 2016)), it has no place in the profession.

In addition to waste produced and its disposal, environmental considerations include indoor environment creation and monitoring, and $CO_2$ production. Heating, ventilation, and air conditioning (HVAC) systems are a vital component in the preservation of heritage materials, though they can have a great environmental cost (Neuhaus, 2013). The energy needed to maintain controlled climates is considerable, and the combined carbon footprint from energy production and climate generation can and should inform conservation decisions, treatments, and long-term care.

### 3.1.7 ETHICS

Ethical considerations in conservation are a mandate of the profession. Preserving cultural heritage and its value for future generations requires an understanding of how any treatment meant to preserve that value may impact it. If, for instance, an action meant to ensure the continued survival of an object fundamentally changed its structure, other actions should be considered, or no action taken at all (Institute of Conservation, 2020). This latter point is especially relevant to the *Mary Rose* cannonballs. Many remain in passive storage awaiting treatment, as their safety post-treatment can no longer be assured. In this case, no action is the most suitable response. Additionally, appropriate documentation is required of every action taken to ensure future practitioners both know what interventions were taken and the intent and reasoning behind their application. For example, treatment records for the *Mary Rose* cannonballs provide invaluable context for their continued corrosion.

However, the very nature of conservation treatments results in the irreversible removal of certain components (dirt, concretions, disassociated fill material) that may be causing damage. Conservation ethical codes understand this, allowing for treatment risks and consequences to be weighed against the benefits it provides (Institute ofConservation, 2020). The non-binding nature of conservation ethics is an advantage to the field, as following directives step-by-step reduces conservation to a formulaic, hierarchical technique. Doing so makes conservation a recipe to be followed, rather than a holistic, encompassing scholarship founded upon science, art, history, creativity, and skill (Institute of Conservation, 2016). However, a system open to such interpretation can undoubtedly be manipulated to justify for or against any decision or outcome. Conservation ethics are no different than any other ethical system: open to interpretation by the individual implementing it.

### 3.1.8 DESIRED OUTCOME AND EXPECTED USE

1 The objects at the bottom of this case have not been conserved. In contrast all the other objects here have been conserved in a number of ways. They all belonged to an archer.

His wristguard [1], made of elephant ivory, has survived because ivory is very hard

2–6 The straps which held the wristguard on the archer's arm were leather, as were his jerkin [2], shoes [3] and his belt [4]. After washing, the water in the cells of the leather was replaced with an oil blend and then freeze-dried.

Wooden objects, like the comb [5] tucked

**Figure 3.4:** A mixed-materials display case from the *Mary Rose* Museum featuring a cannonball intentionally left to corrode. This pathway of non-treatment was explicitly chosen to inform the public on the deterioration of the collection.

The post-treatment lives of heritage materials are not limited to either being on display or in store. The expected use of an object after treatment can determine what that treatment will be (Figure 3.4) (Gerrish and McDonald, 2004). Is the object going to be used in a handling collection? Will it be displayed outside, and if so, will it be near the sea? Treatment plans must envisage such parameters from their outset, as simple oversights (an inappropriate coating, an epoxy without UV protection) could prove catastrophic to objects. The *in-situ* conservation of a wrought iron gate usually has the desired outcome of keeping the gate functioning as a gate. The desired outcome of conserving a cannonball, however, is not to restore it to a state where it is once again a fireable projectile. One is preserving the functionality of an object, and the other assumes that functionality is lost.

### 3.1.9 FAMILIARITY AND REGIONALITY

Treatments can be region-specific. Professional bodies, training, and universities within separate geographic regions can prefer one system to another. Large institutions such as national museums will continue to utilise older treatments even when they can afford to invest in new ones, as a means of treatment continuity across their collections (Keene, 2012: 176). Institutional methodology is then disseminated throughout those areas and to the conservators that are dependent upon those institutions (Buck, 1974). Many of these smaller institutions then become reliant on long-standing familiarity and infrastructure, as the investment required to incorporate new methods (financially, temporally, structurally, instructionally, communally, etc.) may not be possible.

## 3.2 TREATMENT OF HERITAGE IRON

Comprehensive methods used to prevent the corrosion and destruction of cultural artefacts composed of iron were established by the mid-19th century (Rathgen, 1905: 89). Observation of destructive corrosion led to experimentation with mitigation techniques, such as thermal reduction and wax coating. As the field of chemistry expanded and the scientific method became more refined, those charged with the care of heritage artefacts began incorporating more scientifically rigorous methods.

Today, the field of heritage iron conservation combines theoretical approaches with pragmatic considerations of what constitutes the most effective and efficient treatments. Understanding that debate, and ultimately how to determine and quantify effectiveness, requires knowledge of treatments that have been employed on heritage iron and the chemical processes that facilitate them.

### 3.2.1 PRE-TREATMENT IMAGING

Heritage iron must first go through preparatory steps in order to determine a proper course of treatment. Though historically not always possible, imaging methods warrant mentioning here as conservators routinely employ them to determine the best course of action.

Imaging includes those techniques used to identify objects and their composition. X-radiography is used to determine the condition of objects, such as ascertaining how much metal core is remaining within an artefact or identifying cracks and construction flaws (Corfield, 1982). X-radiography is also used to identify objects within concretions.

Optical photography is used to document objects prior to conservation. Optical microscopy aids in understanding surface topography and corrosion layers. Scanning electron microscopy is also used to determine metallographic composition (Meeks, 1987).

### 3.2.2 MECHANICAL CLEANING

Mechanical cleaning includes any process by which conservators remove deposits (concretions) or corrosion layers from the surface of an object by mechanical means such as scalpels, abrasive- and dry ice-blasting (Hoffman and King, 2019). Removing such deposits and visible corrosion aides in the effectiveness of treatments by facilitating access of treatment solutions to object surfaces and interiors.

### 3.2.3 CONTROLLING CORROSION

The corrosion process (Chapter 2) requires three constituents: water, oxygen, and an electrolyte (North and MacLeod, 1987). Every treatment employed on heritage iron substrates has sought to remove or limit its exposure to one or all of these, with the reduction of remaining destructive corrosion products to less unstable forms.

#### 3.2.3.1 REMOVAL OF ELECTROLYTES

The removal of electrolytes, specifically chloride ions, has arguably been the most common method of interventive treatment for archaeological iron. As chloride facilitates corrosion, its removal from the equation should mitigate the process. Reducing the number of chloride ions within an object slows its corrosion rate, prolonging its life expectancy (Rimmer et al., 2013). However, as corrosion begins at the exterior surface of an object, the longer corrosion is active, the further in the corrosion/metal interface will be (Neff et al., 2007). This includes chlorides, and so their removal from an object becomes increasingly difficult the more corroded an object becomes. This is compounded by some corrosion products utilising chlorides in their composition, including akaganeite and $Fe_2(OH)_3Cl$ (Rémazeilles and Refait, 2007). Removing chlorides involves both their removal from these corrosion products and their diffusion through corrosion layers.

The effectiveness of desalination treatments is determined by the amount of chloride removed from, not remaining within, an object (Watkinson et al., 2013b), and so the post-treatment condition of objects is unquantified.

### 3.2.3.2 DESICCATION

Much the same as chloride removal, desiccation involves removing moisture from an object and its environment. The amount of water present will dictate (along with available $Cl^-$) the rate of the reaction. As iron corrosion begins at ~12% RH, drying an object and maintaining an atmosphere at or below this level should result in the total cessation of corrosion as long as the object remains within this low RH environment (Watkinson and Lewis, 2005a).

Maintaining this level of desiccation can be problematic, as keeping an atmosphere to such a low humidity can be expensive, impractical (for storage, viewing, handling), costly (carbon footprint of HVAC equipment), or all three.

### 3.2.3.3 OXYGEN REMOVAL

Preventing objects from coming into contact with oxygen stops corrosion but may be unrealistic as a long-term treatment plan. Oxygen-barring materials such as ESCAL$^{TM}$ sheeting exist, but any time an object needs to be handled, it will encounter oxygen, restarting the corrosion process.

Oxygen removal can be done either in an aqueous medium combined with a chemical oxygen scavenger, or as a coating applied to the surface. Again, maintaining a deoxygenated environment is impractical, especially as a post-treatment option, and barrier coatings are prone to the same failures as inhibiting coatings (Gabe et al., 2010).

#### 3.2.3.4 OXIDE REDUCTION AND CHLORIDE REMOVAL

Reduction is the process of treating heritage iron by transforming unstable corrosion products into less harmful, more stable ones. There are a number of ways to achieve this. Electrochemical reduction uses electric current to facilitate the electrolytic movement of chlorides and alter the electric field of an object (Wihr, 1975). Gaseous reduction relies on the interaction of volatile, free gaseous ions to interact with $Cl^-$ in a high-temperature environment (Barkman, 1977). High temperature reduction processes can alter the metallographic profile of objects under treatment.

### 3.2.4 EARLY TREATMENTS

The first treatments employed on heritage iron can be defined by their speed and their severity. The concept of conservation as a field of study and profession was in its infancy. The development of concepts of ‘original surface’, ‘non-destructive’, and ‘reversibility’ were direct responses to unsuccessful early conservation efforts. Nevertheless, many of these methods were used well into the 20th century, depending largely on regionality.

Planned treatments were rarely carried out at first, as most objects were pulled from the sea and left to stand (as a reference, the cannon shown in Figure 1.3 has received no treatment) (Pearson, 2020). Rathgen (1898; 1905) lists several substances ‘appropriate’ for impregnating iron with, including wax (paraffin or bees’), shellac in alcohol, isinglass, rubber in carbon bisulfide , copal varnish in turpentine, copal varnish with linseed oil, just linseed oil, linseed varnish, and vaseline. Vegetable pitch, lead white, and sodium silicate were also used at various points (Scott and Eggert, 2009: 132). So many impregnation methods were utilised due to the belief that by putting a substance into objects, they would no longer fall apart. There was also an understanding that impregnating materials into iron both limited oxygen exposure and caused a chemical reaction that would form a less unstable compound (Rathgen, 1905: 89).

While the majority of the impregnation methods mentioned above have long been discontinued, washing iron to remove soluble electrolytes remains in use today. It was first recommended by Krause (Rathgen, 1905: 92)  who advocated washing iron with water. After several washes, the temperature of the bath was then raised to boiling, often with alkaline substances added (Rathgen advises against this, however, as he believed it to form insoluble iron hydroxides that ‘closes the interstices’ and limits access of water). Objects were steeped according to the thickness of their corrosion layers and the number of fissures running through them. Cracks were viewed as beneficial in producing a less unstable product. The process could take up to ‘several weeks’ (Rathgen, 1905: 93). Objects were then dried either in the air, an oven, or in alcohol, then coated/impregnated with paraffin, a celluloid lacquer, or dammar. Simple boiling treatments were used in the UK as late as 1979 (Keene and Orton, 1985).

Ekhoff (Rathgen, 1905: 96) also placed objects in water baths with the addition of quicklime. Following drying, objects were placed in petroleum baths that were slowly heated to 105$^{o}$C. Treatment was finished when bubbles were no longer observed rising out of the object. Beeswax or paraffin coatings followed. This is an interesting approach, as the washing of iron in alkali baths remains the focus of the modern day approach to washing iron.

Straberger’s method involved placing freshly excavated objects in linseed oil to limit moisture access. They were then wrapped in oil-saturated cloths, packed into sawdust, and shipped to a treatment laboratory. Artefacts were washed in caustic soda-containing water, followed by the mechanical removal of ‘blisters’. Objects were then smoked over a candle and smoothed with India rubber. The smoking was thought to coat objects in petroleum by products and soot, which would limit their exposure to oxygen and moisture (Rathgen, 1905: 97).

A little over a decade later, most of these methods were deemed insufficient, with only the ‘heating to redness’ method seeing further development by Rosenberg (1917). Iron artefacts were heated to 800°C for 15 minutes and put in a sodium or potassium carbonate solution whilst still red. At the time, the heating was thought to ‘open the crevices’ and allow the salts to leach out. Artefacts were then placed in boiling water baths to remove any remaining chlorides, dried, and impregnated with wax. The method was in use in Denmark with little variation (Eriksen and Thegel, 1966) into the early 1980s, though it was subjected to heavy criticism before its retirement (Jakobsen, 1984). A study conducted by Salomonsen (1977) showed at least 20% of artefacts treated in this way were unstable, as it left too many $Cl^-$ within the substrate.

Krefting introduced a basic electrochemical treatment using a solution metallic zinc and sodium hydroxide. Rathgen (1905: 108) mentions its use, and Rosenberg (1917) implemented it on fragile, inlay-decorated objects. Its use subsided after observing that it significantly damaged objects, though was still implemented as late as the 1950s (Jakobsen, 1984). Early conservators in Spain adopted the method after observing that boiling, heating to red, and impregnating artefacts left them susceptible to continued corrosion. Objects were electrochemically cleaned in 50°C solutions of granulated zinc and 5% caustic soda (Barrio et al., 2009). The *Museo Arqueológico Nacional* (National Archaeological Museum) of Spain as early as 1930 employed a specialist in electrolysis to treat their iron finds. However, the process was not suitable to badly corroded artefacts, or those saturated with $Cl^-$. Blistering corrosion resulted in material loss and instability.

### 3.2.5 NOVEL AND RETIRED TREATMENTS

The prolonged use of boiling and impregnation showed that there was an acceptance within the conservation field of the shortcomings of these methods and their ratio of successes to failures. Post-war innovation was largely applied to electrolytic reduction as that, reportedly, showed the most promise (Plenderleith and Werner, 1971: 286). These methods and their anecdotal evidence of success eventually began to be viewed as unacceptable in a burgeoning conservation field that was forced to watch as iron objects that had undergone these treatments continued to deteriorate, requiring extensive upkeep and harmful retreatments.

A response to this status quo came in the form of analytical chemistry. The application of methodological, laboratory-based science to produce quantified outcomes led to numerous innovations in metals conservation. Many were redeveloped from earlier treatments that had been used in conservation for decades, and others applied newly available commercial products that had been developed by chemical companies and were in use in other fields. Some of these treatments were suggested, trialled, and found to be unfit, whilst others were only recently discontinued (Table 3.1).

| Method | Reference | Years Active |
|---|---|---:|
| Boiling in caustic/sesquicarbonate | (Scott, 1922) | 1920s-70s |
| Sodium Sesquicarbonate | (Plenderleith and Werner, 1971: 286) | 1960s-80s |
| Lithium hydroxide | (Bresle, 1974) | 1974-1982 |
| Anhydrous ethanol | (Bleck, 1978) | 1978 |
| Anhydrous liquid ammonia | (Gilberg and Seeley, 1982) | 1982 |
| Ionophoresis | (Fenn and Foley, 1975) | 1960s-80s |
| Heating to red | (Rathgen, 1905) | 1900s-1970s |
| ammonium carbamate/hydroxide | (Ladeburg, 1973) | 1970s |
| Vilhar' method | (Vilhar, 1978) | 1970s |
| Hydrogen reduction | (Rathgen, 1905; Kendell, 1982) | 1890s; 1960s-80s |

| | | |
|---|---|---:|
| Gas plasma | (Duncan, 1986) | 1980s-2000s |
| Ion-exchange resin | (Keene and Orton, 1985) | 1985 |
| Pressure steamed | (Keene and Orton, 1985) | 1980s-2000s |
| Sodium benzoate | (Mercer, 1979) | 1979 |
| Ethylenediamine | (Argo, 1982) | 1980s-1990s |
| Ethylene Oxide | (Duncan, 1986) | 1986 |
| Fertan | (Weaver, 1987) | 1980s |
| Hostacor-IT | (Argyropoulos et al., 1999) | 2000s |
| Bacteria/microbial | (Albini et al., 2016) | 2010s |

**Table 3.1:** Obsolete and experimental treatment methods employed on heritage cast iron.

### 3.2.5.1 ALKALINE TREATMENTS

Most likely spurred on by both the chemistry of alkaline substances to stabilise iron corrosion (see Chapter 2.3) and by early treatments that involved alkaline components that were (likely visually) assessed as being stable, such as combining electrolytic reduction in caustic soda (Plenderleith and Werner, 1971: 286), many of these 'modern' treatments relied on desalination through an aqueous alkaline medium. Scott (1922) installed a laboratory in the British Museum in 1920 and began publishing results soon after. His recommendation to remove chlorides was to boil objects in caustic soda or sodium sesquicarbonate, followed by washing, and then electrolysis in dilute sulfuric acid or an alkaline medium. Objects were considered stable when silver nitrate in nitric acid tests detected very little $Cl^-$ remaining in the treatment solution. Plenderleith and Werner later stated the process was only suitable for those objects that were not 'too frail' (1971: 286).

Plenderleith and Werner (1971) continued to propose boiling iron objects in caustic soda, but also said that a 5% solution of sodium sesquicarbonate left at room temperature with solution changes daily to weekly was sufficient for stabilisation. This latter method was first proposed by Scott and later recommended by Oddy and Hughes (1970). The authors stated that the aqueous medium dissolved and removed $Cl^-$, whilst the sesquicarbonate passivated the iron and, due to the alkaline pH, prevented rusting. Treatment endpoints were based on Organ's method (1955; 1961) and further elaborated that any test that failed to show $Cl^-$ was proof that none remained with the artefact under examination, and that it was therefore completely stable in any environment.

Oddy and Hughes (1970) say most iron objects were stable after 7-10 weeks of washing in a 5% solution, observing that $Cl^-$ concentrations fell to 5 ppm (using a mercuric thiocyanate colourimetry method for determination), so those $Cl^-$ remaining within the object must be equivalent. The acceptable desalination threshold was stated as being at or less than 10 ppm. If it was above this, washes would continue. However, in 1987 Oddy and Black revisited an object treated with sodium sesquicarbonate in 1975 and found the method to be 'haphazard' and say it is little used at that point (Oddy and Black, 1987). Sodium sesquicarbonate is still employed today on heritage copper (Leyssens et al., 2005), as a passivating storage solution for heritage iron (Jones, 2003; Simon et al., 2019), and for use in copper/iron composites (Devaud et al., 2016), though not as a primary stabilising treatment of objects composed solely of iron.

Lithium hydroxide was first proposed by Bresle (1974; 1976) and enjoyed a brief period of use (Fabech and Trier, 1978). Objects are placed in low 0.2% concentrations of lithium hydroxide in an alcohol medium (ethanol, methanol, isopropanol, and iso/methanol were all used, depending on the practitioner). The non-aqueous environment would inhibit further corrosion whilst the LiOH reacts with free $Cl^-$ to form highly soluble LiCl (Bresle, 1974). Residual lithium hydroxide forms insoluble lithium carbonate, which was argued to create an alkaline environment near the surface of an object, further passivating atmospheric corrosion. North and Pearson (1978a) stated $Cl^-$ extraction times made it insufficient as a treatment on marine iron, and Watkinson (1982) showed NaOH desalination to be twice as efficient and have a greater capacity for extraction than LiOH. Combined with higher price points and greater safety issues, desalinating objects in LiOH/alcohol solutions ceased to be used as a primary stabilising treatment.

Anhydrous liquid ammonia was proposed by Gilberg and Seeley (1982) as a more efficient method of $Cl^-$ extraction, one that was potentially less harmful to iron artefacts and required far less treatment time. Using cannonballs recovered from the Solent (though do not say if from the *Mary Rose*), they successfully showed that pretreating with liquid ammonia followed by washing with water baths extracted 'a great deal' of $Cl^-$ (measured using a $Cl^-$ ion meter). They do not compare samples from the same wreck site to other treatment methods and fail to quantify any corrosion rates of samples. They instead say that after a week at 100% RH, the 'metal core' (no measurements given) began perspiring ferric chloride droplets. This vague analytical description no doubt did not assist in the method becoming widespread, nor did the safety hazards and equipment required by it. Liquid ammonia boils at -33.4°C, requiring objects to be put in sealed containers kept to ~-40°C, or within pressure vessels above this. The substance can be extremely harmful if not handled properly, causing skin and (if allowed to go into its vapour state) lung burns, as the substance is highly toxic. Though capable of removing $Cl^-$, the method never overcame its shortcomings and failed to develop further.

Ionophoresis involves using a charged electric field to allow cations to move to the anode and anions to move to the cathode (Oddy and Black, 1987; Selwyn and McKinnon, 2006). In principle, the electric field is employed through an electrolyte and encourages $Cl^-$ ions to migrate out of an object and toward an anode set up outside of it, usually a stainless-steel rod. The method was employed in the late 1960s into the 1970s. Fenn and Foley (1975) used it and showed there was still $Cl^-$ remaining within objects (following their pulverisation) after readings were consistently negative, even after subjecting them to boiling afterwards. Keene and Orton (1985) compared artefacts treated with ionophoresis in a 5% sodium benzoate electrolyte, saying objects were treated until $Cl^-$ was undetected (using silver nitrate analysis) in the electrolyte bath. Visual assessment was the only metric used to determine instability. Oddy and Black (1987) re-examined an object (a cast iron cannonball) that underwent ionophoresis with a lithium hydroxide electrolyte and found the method efficient and effective, stating that the cannonball was stable and nearly visually unchanged ten years later. They do not provide quantification of its stability, though visually compare it to a cannonball treated at the same time with sodium sesquicarbonate, noting the latter to be in a poor state (Figure 3.5).

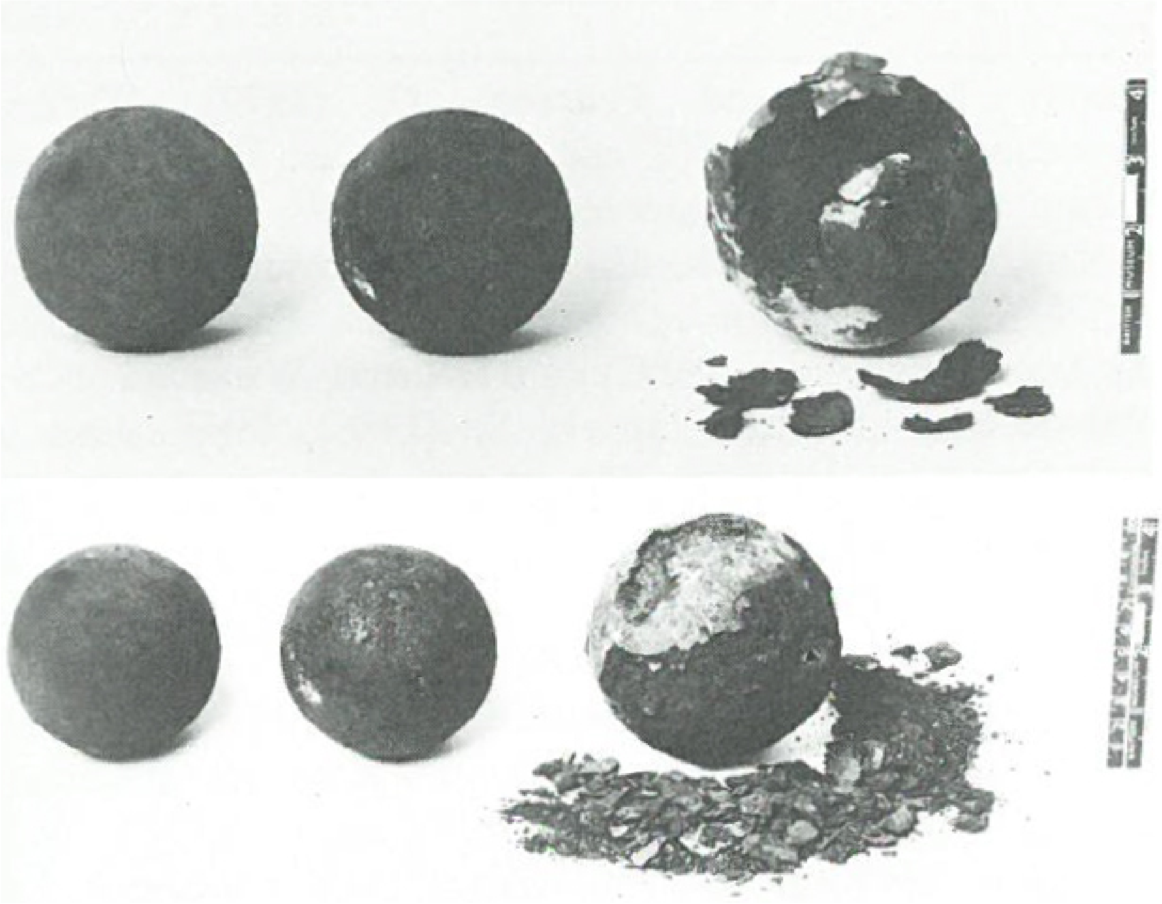

**Figure 3.5:** Cannonballs under study in Oddy and Black (1987). The top row shows cannonballs in 1977 immediately post-treatment, and the bottom shows the same shot in 1987. Anecdotal evidence was used to determine their stability.

Ethylenediamine (EN) was developed as a treatment in the early 1980s (Argo, 1982). The complex $H_2N\text{-}CH_2\text{-}CH_2\text{-}NH_2$ works by protonating in water and raising the pH to inhibit the cathodic reaction. Chloride ions are then presumably freed from their role in facilitating electrochemical balance, are withdrawn into the solution, and can combine with either the EN complex or remain free. Extracted $Cl^-$ is measured, and end-of-treatment is determined when measured $Cl^-$ has fallen below a determined threshold (< 20 ppm by one method). The method found some use during the 1980s, particularly at the CCI. A follow-up study published in 2005, however, showed that EN solutions were not as effective as sodium hydroxide washes, either as a first treatment followed by NaOH or a post-treatment after NaOH soaking (Selwyn and Argyropoulos, 2005). The study also showed that EN dissolved more iron than NaOH, though it was suggested that this is due to the complex's adsorption onto metallic surfaces. This adsorption results in EN being a superior corrosion inhibitor to NaOH, though this is dependent on temperature. Furthermore, EN was shown to stimulate corrosion by forming soluble $[Fe(\mathit{EN})_x]^{2+}$, leading to oxide stripping and exposing bare metal (Busse, 1997). The solution was suggested as a first treatment followed by sodium hydroxide for extremely corroded objects where core metal no longer existed but where outer surface details were important, as NaOH was shown to be damaging to the surfaces of badly corroding objects (Selwyn and Argyropoulos, 2005). Essentially, when used in combination with NaOH solutions, this methodology owes most aspects of its success to the effect of alkali washing by the NaOH.

### 3.2.5.2 THERMAL REDUCTION

The longevity and perceived success of the 'heating to red' method encouraged further development in gaseous reduction treatments. The complete removal of $Cl^-$ within objects via sublimation was seen as worthy of pursuit. The exfoliation and loss of outer layers, and the possible detail and information they provided, was viewed as being the most significant detriment of the method (ethics notwithstanding), a result of heating objects in open atmosphere (Kendell, 1982: 15). In response to this, conservators began subjecting objects to non-oxygen gases in controlled/vacuum environments. Ladeburg (1973) submerged objects in ammonium carbamate and ammonium hydroxide for 14 hours, followed by drying and heating under vacuum to 150°C. Interaction between the ammonium complexes and $Cl^-$ species results in ammonium chlorides which are then sublimated via heat and vacuum. Destructive testing of samples (test panels and nails from the Bremen Cog) claimed complete removal of $Cl^-$, though no reports of further use or development could be found. Vilhar (1978) developed a method where objects were packed in charcoal, wrapped in asbestos, heated to 800°C for an hour, plunged into sodium hydroxide whilst still incandescent and boiled for 2-6 hours (dependent upon volume of the object), boiled in distilled water for 12 hours, and finally boiled for 24 hours in a 50ml/150l NaOH/dH20 solution. Objects are left in a spongy, reduced, carbon-enriched state where soluble $Cl^-$ can freely leave in wash baths. Consolidating with paraffin supports objects post-treatment. The author states the method had up to that point been in use in the Archaeological Museum of Zadar (modern-day Croatia) for ten years with satisfactory results; however, no quantification of objects' conditions or $Cl^-$ measurements are given. The treatment is incredibly severe and invasive and is not mentioned as being used anywhere else.

Hydrogen reduction treatments were first used in the late 19th century by Hartwich (Rathgen, 1905: 117). The method involved placing small objects in a glass tube and heating to red in a 'current' of hydrogen. Rathgen noted there was a significant safety issue, owing to the explosive nature of combusting hydrogen in an oxygen atmosphere. Products would often resemble a conglomeration of loose iron dust rather than stable, dense iron objects, and were actually capable of becoming red hot again due to rapid oxidation when exposed to air. However, the method was developed during the 1960s and saw the greatest use within the field of any gaseous reduction treatment. The process involves placing objects in a reaction chamber flooded with hydrogen gas and heating to high temperatures (anywhere from 400-1200°C). Gaseous hydrogen, which can more easily penetrate into small pores than a liquid reagent, is intended to remove chloride by reaction to form hydrogen chloride gas, which then escapes. The higher the temperature, the greater the rate of reaction, however, higher temperatures also increase the chance of reducing rust from its normal ferric state. Direct reduction of rust in this way will cause a volume change with subsequent re-oxidation causing another volume change. Both processes will potentially reduce structural stability of the artefact. The gas escapes through an effluent which is monitored for $Cl^-$. Treatment is considered finished when $Cl^-$ is no longer observed or is at an appreciably low level (Kendell, 1982: 32). The pH of the effluent also experiences a sharp decrease as it becomes saturated with HCl, with pH mirroring withdrawn chlorides (Barker et al., 1982). The combination of $Cl^-$ sublimation and reduction of corrosion compounds theoretically produces an object that is stable in nearly all climates, both indoors and out, and will be resistant to continued corrosion. Hydrogen reduction was first used in 1964 to treat over 800 artefacts from the Swedish ship *Vasa*, a 17th-century Swedish warship raised from Stockholm's harbour (Arrhenius et al., 1973). Objects were subjected to hydrogen with temperatures raised in excess of 800°C over 72 hours, followed by a 48-hour cooling period (Figure 3.6). The procedure produced stable objects functionally free of $Cl^-$ in only five days. Post-furnace stabilisation with a polymer was required, as volume vacated by $Cl^-$ and FeO-products left objects brittle and prone to damage.

**Figure 3.6:** The hydrogen furnace at the *Vasa* conservation laboratory. From Barkman (1977).

The success of the *Vasa* artefacts led to further development of the method. A Finnish project running concurrently with the *Vasa* (Patoharju, 1975; 1978) treated iron artefacts from a Brackish Sea shipwreck, including a 413 kg cast iron cannon, at 500°C for 12 hours and 800°C for 8 hours, using a 12/88 hydrogen/nitrogen mixture. The treatment was deemed a success based on visual analysis alone. Barkman (1977), continuing on finds from the *Vasa,* found that a temperature of 600°C was best, noting that though reduction was faster in the 800-1000°C range, it caused decarburisation in the rust layer. He stated a range of 300-400°C was also possible if iron objects also contained non-ferrous metals, though it would take longer. Iron finds from the *Mary Rose* were treated in a hydrogen reduction furnace to 850°C for 100 hours, allowed to cool, and injected with epoxy resin (Barker et al., 1982). Figure 3.7 shows the hydrogen reduction furnace used to stabilise iron finds from the *Mary Rose.* Ammonia gas was decomposed by a catalytic cracker into hydrogen and nitrogen gases which were then used to fill the reaction vessel containing the iron objects to be treated. The authors claimed a near complete reduction of iron salts and corrosion products back to metallic iron, with nearly all $Cl^-$ removed. They stated they had not determined $Cl^-$ remaining within objects, as that required destructive analyses, though said a $\leq$7ppm $Cl^-$ content was observed in the final effluent, with peak saturation ~30000ppm (O'Shea et al., 1982). Post-treatment metallurgical analysis showed no metallographic change in temperature up to 400°C, though state that only cast iron objects were subjected to temperatures higher than this.

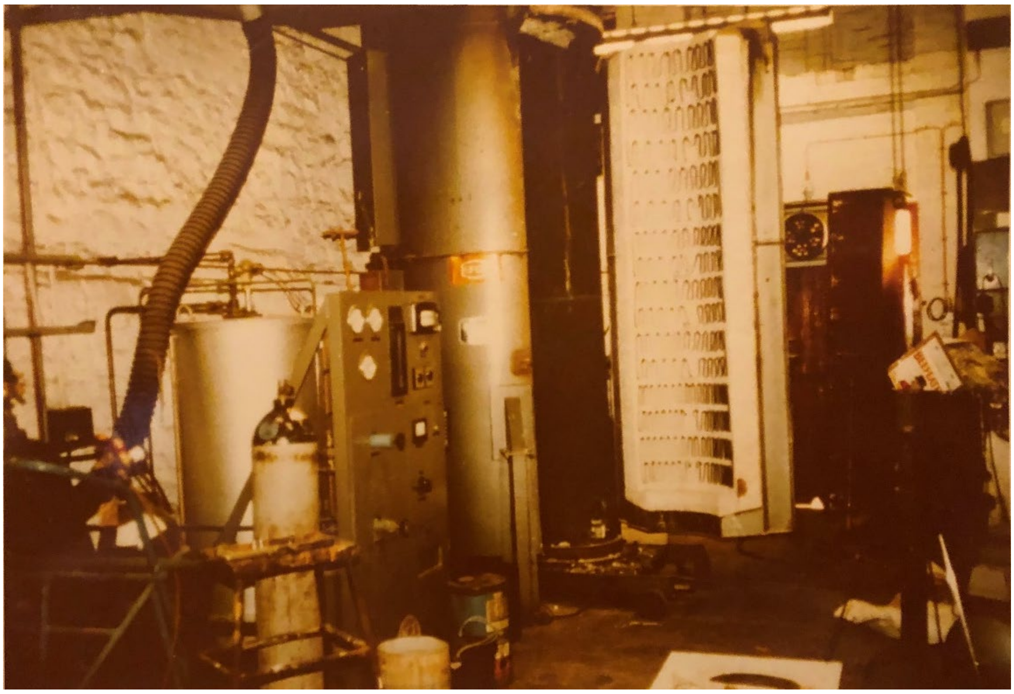

**Figure 3.7:** The hydrogen reduction furnace at the Portsmouth City Museum. From Kendell (1982: 77).

As might be expected, hydrogen reduction was a highly contentious treatment, with the alteration of object metallography the primary focus of dissent. North, Owens, and Pearson (1976) studied the effects of such high temperatures on the metallographic composition of both wrought and cast heritage iron. They found that in grey cast iron, temperatures above 600°C converted pearlite to ferrite, with nearly all pearlite altered at 1000°C. The carbon content remained unchanged, with carbon from $Fe_3C$ cementite merging with corrosion-induced graphite flakes. White cast iron saw the removal of its ledeburite (cementite-pearlite mix), along with carbon migration and loss. Wrought iron saw no metallographic change, even at 1000°C; however, Widmanstatten wrought iron, a wrought with pockets of higher carbon content that contains pearlite and cementite, saw microstructure change at 400°C, with the restructuring of the ferrite/pearlite lattice nearly complete at 1000°C. The authors concluded that although safe for standard wrought iron, there is no way to tell the difference between that and Widmanstatten, and as such hydrogen reduction would only be appropriate up to 400°C. This is not, however, a high enough temperature to achieve full metallic reduction and stabilise objects. Tylecote and Black (1980) showed how thermal reduction results in detail loss and surface alteration, though noted that for badly corroded marine iron this might not matter. What did matter was that objects were known to melt (North, 1987). As a treatment, it also requires a large initial outlay on equipment and significant ongoing costs, as well as major safety challenges due to the risks of oxy-hydrogen explosion. Cost benefit will always play a major role in treatment options within the relatively underfinanced field of heritage.

In addition to object alteration, hydrogen reduction was a serious safety concern. Using heated hydrogen gas requires extreme caution, and reduction chambers required careful operation and control, lest the hydrogen would combust. This limited the facilities that could implement the method, and greatly reduced the number of practitioners capable of carrying it out. Those museums that had been using and pioneered the process quickly phased it out in the early 1980s, and it has not been used since.

Using a gas plasma as a means of removing $Cl^-$ from iron was developed after the procedure was shown to reduce hematite to magnetite, remove silver tarnishing, and convert silver chloride to metallic silver (Daniels et al., 1979; Daniels, 1981). The process involves placing artefacts in a gas-filled, pressurised reaction chamber fitted with electrodes and a power source. As the energy is applied to the field, a potential difference between the two electrodes creates an ionising effect, causing the gas to excite (or 'glow') and the cathode to lose electrons. The charged, ionised gas bombards the artefact, interacting with less stable compounds (such as chlorinated iron species or silver sulfide). Treatment outcomes are dependent upon the type of gas and the amount of energy used. Varying the setup can subject objects to a broad range of temperatures. Using a hydrogen/argon mixture and a 50Hz A/C 300-400v current and 50mA, Duncan (1986) claimed that all $Cl^-$ was removed from the 'metal-oxide interface' of his archaeological iron sample whilst never exceeding 40°C. He noted that the method caused shrinking and cracking of the outer oxide layer, noting that other methods (such as alkaline sulfite) caused no such damage.

Patschieider and Vepřek (1986) altered the setup, using an 80MHz/2Kw that heated objects to 400°C. The resulting reaction reduced hematite to magnetite, as well as free samples of FeOCl species. The authors claimed $Cl^-$ levels were reduced to $\leq$ 10ppm 'relative' to sample mass, as determined by dipping objects in deionised water post-treatment and measuring $Cl^-$ using ion chromatography. Object stability was determined by placing treated and untreated Roman nails in vials filled with deionised water and visually comparing their degradation, finding that the treated nail maintained its integrity and was considered stable. However, this method failed to account for any $Cl^-$ remaining within artefacts, instead viewing the low $Cl^-$ content as a successful removal of nearly all $Cl^-$ rather than a failure to remove substantial amounts of it from the interior of objects. Like hydrogen reduction, heating objects to this temperature causes annealing, altering the metallographic profile. Unlike hydrogen reduction, temperatures induced by plasma reduction are not high enough to cause all $Cl^-$ to volatilise out of substrates, resulting in the visible corrosion of objects after several years (Schmidt-Ott, 1997). Schmidt-Ott and Boissonnas (2002) altered the method to reduce object temperature to 120°C, claiming this caused a reduction in product density and facilitating mechanical cleaning. They also recognised that this results in $Cl^-$ removal being far below what is required for object stability. The method is now only employed on iron as a pre-treatment to desalination. Limitations in size of object and cost of equipment are also major drawbacks of this treatment.

### 3.2.5.3 NON-ALKALINE DESALINATION TREATMENTS

Bleck (1978) attempted using anhydrous methanol to desalinate heritage iron, as the viscosity is lower than water and would allow the methanol better penetration into an object's substrate. He also suggested that iron (III) chloride compounds dissolved more readily in methanol. Objects were placed in a Soxhlet for desalination, dried using magnesium powder, heated to 100°C, and covered with wax. Bleck provides no desalinating concentrations or extraction curves, no treatment times, and no comparison to other methods.

Keene and Orton (1985) placed objects in circulation baths in an ion-exchange resin. This quickly oxidised objects, causing flash rusting and system failures.

Steaming objects in a pressure cooker (Keene and Orton, 1985) was theorised to penetrate iron substrates, allowing high temperature, freshly condensed water to remove $Cl^-$ continually. This was shown not to be the case, as objects were visibly corroding after 'treatment'.

Ethylene oxide was proposed and trialled as a means of removing $Cl^-$ from heritage iron (Duncan, 1986). Objects were fumigated with ethylene oxide under vacuum for 12 hours, with the $CH_2OCH_2$ reacting with $Cl^-$ to form ethylene chlorohydrin. This complex was then removed via vacuum, leaving a $Cl^-$ - reduced object. Visual checks determined stability. Duncan states the method withdrew $Cl^-$ in nearly equal measure to alkaline sulfite, but there was never an experimental follow-up. Safety hazards most likely contributed to it never developing further (Kolman et al., 2002).

#### 3.2.5.4 INHIBITORS

Tannins and tannic acid were proposed in 1966 as a treatment for corroding heritage iron, though were suggested as being suitable to stop rusting on steam boilers in the late 19th century (Pelikán, 1966). Tannic acid is a combination of phenolic-bearing compounds derived from plants and acid, often phosphoric. The low pH complex is dissolved in water and brushed onto the surface of an object, where it interacts with iron oxides and oxygen to form a blocking film of ferric tannate. Ferrous and ferric ions react with carboxyl and hydroxyl groups, creating insoluble surface species that do not oxidise. However, the treatment was never suggested for use on $Cl^-$-infested heritage iron, only as a post-treatment corrosion-inhibiting coating. Complete stability is nearly impossible to achieve, especially when an inhibitor is brushed on a surface (Emmerson, 2015: 55). Limited oxygen can still ingress, encountering a $Cl^-$-rich environment.

This did not stop the use of Fertan (a tannin-based commercially developed rust inhibitor) from being deployed as a treatment for corroding marine iron. The compound works the same way as tannic acid; it reacts with oxidised iron compounds on the surface of an object, passivating the electrochemical process. It was applied by salvaging dive crews to stop rusting of finds pulled from the seafloor, including USS *Holland,* the US Navy's first submarine (Snow, 1984). Anecdotal evidence and visual checks on artefacts treated with the compound (15 months after treatment) deemed it so successful that it was considered by some to be a miracle cure for heritage iron corrosion (Weaver, 1987). However, less than a decade after treatment, USS *Holland* was rapidly deteriorating (Weaver, 2004). The lack of any desalination of the submarine acted as a test case for Fertan, proving that the compound did not stop corrosion, and questioning the validity of using visual monitoring to determine initial treatment success. During the past decade, the use of tannins seems to be remerging within certain areas of conservation. Given the many commercial publications on tannins, there is no doubt they have a place in the arsenal of inhibitors available in corrosion control but remain unproven for the needs of archaeological iron preservation.

Sodium benzoate was proposed as a possible corrosion inhibitor. However, testing showed it to be less effective for cast iron and required a higher concentration of 5% in combination with benzotriazole (Mercer, 1979). A later study showed its use in dechlorinating treatment baths to be less effective than other methods (Keene and Orton, 1985).

Hostacor-IT is an oxygen-inhibiting triethanolamine salt of Hostacor IS, an acylamido carboxylic acid (Figure 3.8). The addition of the salt allows the complex to be soluble in water. The carboxylate reacts with dissolved oxygen in the solution, limiting the cathodic reaction. Both the carboxylate and nitrogen groups interact with ferrous and ferric ions, and the hydrocarbon chain creates a hydrophobic end that limits water access to the metal surface. The excess of hydroxyl ions (OH-) permit ion exchange within the body of the rust, releasing chloride for diffusion out of the structure. The complex is functional in neutral pH, though the pH will increase as ferrous ions are oxidized to ferric. Hostacor-IT has found some use in conservation as a treatment for iron/waterlogged wood composite objects, slowing corrosion during polyethylene glycol soaking (Argyropoulos et al., 2000). There is no published study, however, on its effectiveness as a primary desalination treatment of corroded iron. Hostacor can inhibit iron corrosion, thus avoiding high pH treatments like alkaline sulfite that cause wood to degrade, but its ability to stabilise iron has not been measured. It has been used to treat non-composite iron finds from the *Mary Rose* (Trust, 2015; Watkinson et al., 2016; Simon et al., 2018).

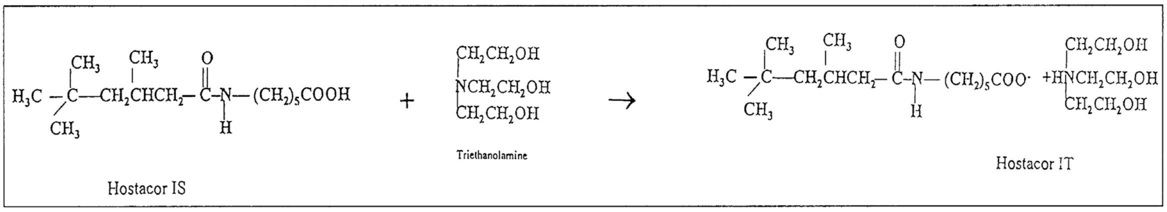

**Figure 3.8:** Hostacor-IT structure, from Argyropoulos et al. (1999).

The use of bacteria and microbial reduction has been proposed as a possible treatment for heritage metals (Albini et al., 2016), including archaeological iron (Comensoli et al., 2017). Certain bacteria have the ability to utilise Fe(III) iron species, including oxyhydroxides, as electron receptors for anaerobic respiration, reducing them to Fe(II) and Fe(II, III) species such as magnetite. The culture medium can influence product formation (Comensoli et al., 2017), and in some cases, the bacteria strain itself can carry polyphosphates, which combine with reduced iron species to form and deposit iron phosphates (Kooli et al., 2018). Though this compound has been suggested as an inhibiting surface on heritage iron and evidence shows that bacteria are capable of reducing $Cl^-$-containing iron species, the method is still in its infancy. No metric of object stability has been provided, nor has any quantified efficiency of $Cl^-$ removal. It remains to be seen how effective bacteria will be in treating heritage iron.

### 3.2.6 CURRENT TREATMENT METHODS FOR HERITAGE IRON

There are few accepted interventive corrosion prevention treatments that are still employed on chloride-infested iron artefacts and scientists continue to seek safer, faster, more effective and more ethical methods. Determining treatment effectiveness is complicated by a lack of non-destructive, quantitative methods that can be used on a large scale to determine the amount of $Cl^-$ remaining in artefacts post-treatment. Instead, treatment endpoints tend to be defined by $Cl^-$ extraction as a function of object mass, confirmed by ion count in desalination baths, and treatment effectiveness by visually checking for corrosion. An overview of published research indicates that there has been more focus on examining the treatments themselves and what they achieve, often in terms of the chloride being removed from objects as determinants of end points, rather than quantitative studies of what has been achieved by assessing the post-treatment rate of corrosion.

#### 3.2.6.1 DESICCATION

Given that iron does not corrode at 12% RH or below (Watkinson and Lewis, 2005a), desiccating objects and maintaining environments below this threshold will guarantee their survival. Iron artefacts can be oven-dried to remove moisture retained in their substrates and placed in controlled stores and displays; however, maintaining an environment this low in atmospheric moisture is logistically challenging, can be prohibitively expensive, and requires constant oversight. Failure of the system can lead to rapid oxidation and formation of corrosion products, so desiccation makes little sense to routinely employ it for small objects that can be stabilised using other means (Watkinson and Lewis, 2008; Thunberg et al., 2020). If the determined value is great enough to justify these financial and time-intensive commitments, desiccation is a valid option that can deliver on desired treatment objectives. The *ss Great Britain* is one such example of desiccation as treatment. The

Brunel-designed, wrought iron ship was once the biggest in the world, but eventually was decommissioned, used as a scrap warehouse, and left to decay. Her retrieval from the Falkland Islands saw it installed in the very dry dock in Bristol, UK where she was built. The chloride-saturated hull was subject to heavy, unceasing corrosion. Several treatment plans were considered (Watkinson et al., 2005), but desiccation remained the only viable choice for long-term stability and maintenance of the ship that also met desired post-treatment objectives (Watkinson and Lewis, 2004; Watkinson and Tanner, 2008). The ship is now a museum, with her deck exposed to atmospheric climate and her hull enclosed in a conditioned environment. A complex desiccation system forces air through and around the lower hull, ensuring a constantly maintained RH that is below the corrosion threshold (Watkinson and Lewis, 2007). As the hull is still saturated with $Cl^-$, any failure in the maintenance system will result in rising RH and corrosion resumption.

### 3.2.6.2 SUBCRITICAL WASHING

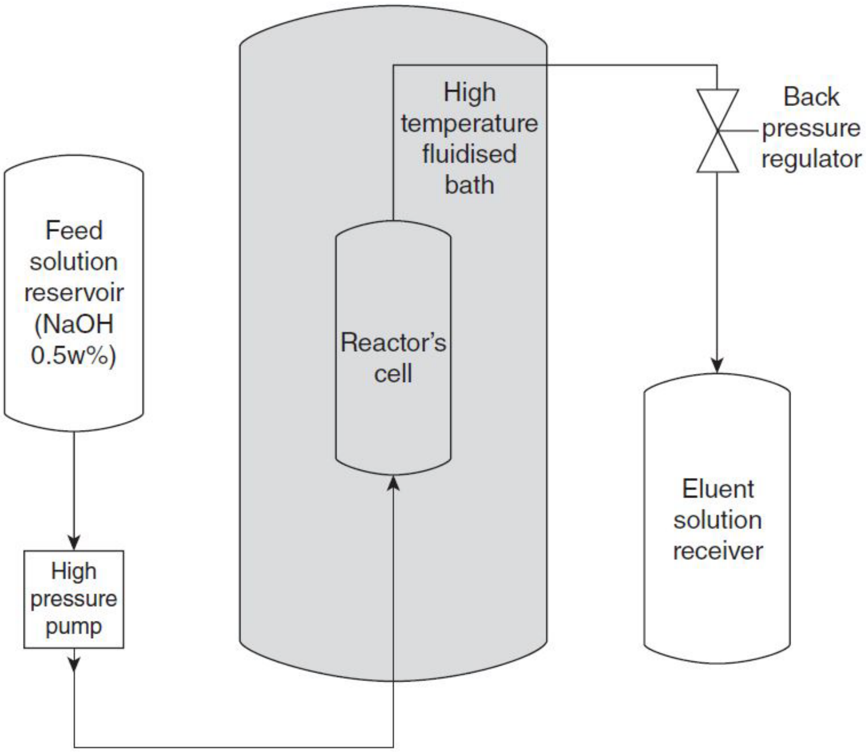

**Figure 3.9:** Subcritical treatment cell schematic. From González et al. (2013).

The subcritical method was first developed to treat iron finds from *H.L. Hunley*, a US Civil War submarine recovered off the coast of South Carolina (Drews et al., 2004). The process involves placing objects in a sealed container with a pressure valve (Figure 3.9). An aqueous sodium hydroxide solution (0.5% wt) is pumped into the chamber, a heating mechanism raises the solution temperature, and the internal pressure is increased. The pressure allows the water in solution to remain liquid up to 374°C before further pressure above 220.5 bar causes it to become a supercritical liquid. The high temperature lowers the viscosity of water, theoretically allowing faster penetration of substrates and dissolution and extraction of chlorides. The alkaline environment encourages passivation of any remaining metallic iron and ion-exchange with residual chloride allowing the latter to diffuse out of the structure. The process also transforms ferrihydrite and akageneite into stable hematite (Bayle et al., 2016a; 2016b). Subcritical treatments are completed within a matter of days, though in some cases objects that have undergone subcritical stabilisation have remained in passivating/pretreatment solutions of sodium hydroxide for several years (González et al., 2013).

**Figure 3.10:** Subcritical treatment equipment at the Warren Lasch conservation laboratory. From González et al. (2013).

The rapid treatment times and transformation of akageneite to stable hematite shows subcritical to be a vast improvement upon standard alkaline desalination methods. However, the setup has only been used in a handful of laboratories, as the custom-built reaction chamber is expensive. Chamber volumes limit the size of objects that can undergo treatment (Figure 3.10). These factors, combined with the process being relatively new compared to alkaline sulfite, have limited its use.

### 3.2.6.3 ELECTROLYTIC REDUCTION

Evolving from early electrochemical treatments, electrolytic reduction (or electrolysis) involves suspending an object in an electrolyte and applying an electrical current, with the object being made the cathode and two electrodes are made anodes in an electrolyte. The object is suspended between them acting as the cathode, completing the circuit (Wihr, 1975). Reduction of oxygen occurs on the internal conductive surface (residual metallic iron or magnetite) generating hydroxide and increasing the local pH while simultaneously causing electro-migration of chloride out of the structure towards the external anode. Electrolysis depends on the voltage between the two electrodes. The electrolyte is changed once its electric potential has diminished and has become saturated with extracted $Cl^-$. Depending on treatment parameters, the electrolyte can be alkaline or neutral pH (Scott and Eggert, 2009: 156).

Electrolysis is commonly used to treat large metal objects lifted from the seafloor, such as cannon (Pearson, 1972), shipwrecks, and submarines (Mardikian, 2004; Nordgren et al., 2007). Early electrolysis treatments were shown to damage extensively corroded objects, particularly those made of cast iron, as hydrogen gas would evolve in the porous substrate and cause exfoliation of layers (Rees-Jones, 1972). The addition of a reference electrode and lower voltages causes a reduction in hydrogen formation, an improvement on the first electrochemical treatments. The process is not recommended for small cast iron finds, where the corroded graphite matrix acts as a cathode and can result in artefact damage.

In addition to post-excavation treatment, electrolysis is routinely employed on *in situ* shipwrecks as a means of slowing corrosion in the marine environment. This is known as cathodic protection and is recommended as a pre-treatment prior to lifting (if lifting is ever done) (Macleod, 1981; 1986; 1989; 1990; 1996; 1998; 2006; 2011; 2016; MacLeod et al., 1986; 2008).

### 3.2.6.4 ALKALINE DESALINATION

The ability of alkaline complexes to slow corrosion rates of iron was known by the time the earliest treatments were performed (Rathgen, 1898; 1905). Though other alkaline solutions have been used, the method currently almost exclusively uses sodium hydroxide. Placing objects in an $OH^-$ saturated alkaline bath results in an ion exchange, causing ferrous hydroxide ($FeOH_2$) to form preferentially to ferrous chloride ($FeCl_2$), allowing free chlorides to be withdrawn from the surface and substrate (Watkinson et al., 2013a).The high pH will passivate any remaining metal. Their use as a treatment was not widely discussed until Pearson used sodium hydroxide as pretreatment for a cannon recovered from the sea (1972). North and Pearson (1978b) discussed how the high pH allowed sodium hydroxide to remove high concentrations of $Cl^-$ more effectively than other aqueous desalination treatments, such as sodium carbonate and sodium sesquicarbonate (North and Pearson, 1978a). However, the oxygenated, aqueous treatment solutions allow objects to corrode during sodium hydroxide desalination.

A method designed to prevent corrosion during treatment is alkaline sulfite desalination (1975a; 1975b). This involves placing objects in an aqueous solution of sodium hydroxide with concentration sufficiently high to maintain pH $\geq$ 13. The addition of sodium sulfite creates an anoxic environment, with the reaction (Rodgers, 1960):

$$2\mathrm{Na_2SO_3} + \mathrm{O_2} \rightarrow 2\mathrm{Na_2SO_4}$$ **Equ. 3.1**

This scavenges oxygen to prevent corrosion during desalination and increases the amount of counter $Cl^-$ ions that can be extracted (Watkinson et al., 2013a). For any corrosion that did occur, there is an excess of $OH^-$ ions to act as counter ions in the corrosion process, freeing up $Cl^-$ from this role and allowing it to diffuse out of the object. Treatments are considered complete when $Cl^-$ concentration in extraction baths reach a suitably low level, an endpoint determined arbitrarily and dependent upon the treatment practitioner (North and Pearson, 1978b). Though extraction rates vary from sample to sample, alkaline sulfite has been proven effective in reducing corrosion significantly (North and Pearson, 1978b; Rimmer et al., 2012). Despite some $Cl^-$ extractions reaching 99% (Rimmer et al., 2012) alkaline sulfite has never been shown to completely remove $Cl^-$ from objects.

Alkaline desalination can take place at room temperature in a stationary solution, but the system can be altered depending on treatment parameters. Heating solutions to 60°C results in faster, though not necessarily more efficient, treatments (Rimmer et al., 2012). Deoxygenated environments can also be created by substituting $NaSO_3$ by bubbling $N_2$ gas through extraction baths, displacing oxygen (Rimmer et al., 2013). The latter method may be desirable for conservators wishing to reduce the introduction of substances that could potentially remain post-treatment and destabilise objects, though it was shown that $Cl^-$ ions induced corrosion at a much more rapid pace than any post-treatment residues (Rimmer and Watkinson, 2011). The method also produces caustic waste that requires acid neutralisation prior to disposal. However, despite these drawbacks, alkaline sulfite has remained in use for over 40 years due to a combination of its effectiveness, its low-tech approach, and its simplicity. The most complicated equipment required is pH and $Cl^-$ test strips, no thorough understanding of electrochemistry is necessary, it is affordable, does not need constant supervision, and is possible under both controlled and uncontrolled atmospheric conditions.

## 3.3 DEFINING TREATMENT SUCCESS

Nearly all comparative reports examining treatment efficiencies are reliant upon anecdotal evidence (Oddy and Black, 1987), the quantity of chloride extracted (Rinuy and Schweizer, 1982; Watkinson, 1996), visual assessment (Keene and Orton, 1985), or a combination of these, verified by destructive analysis (Rimmer et al., 2013).

However, the successful stabilisation of one heritage artefact does not guarantee the stabilisation of any others that were treated using the same method. As Chapter 2 showed, corrosion mechanisms are extremely subjective to several factors, including metallurgical composition, burial environment, and display/storage conditions. Likewise, the treatment considerations discussed earlier in this chapter allow for a broad definition of ‘success’, especially when considering time, cost, and planned display/storage environments post-treatment. Prior to their corrosion on display, the cannonballs from the *Mary Rose* were determined to have been treated successfully. Therefore, it is important to understand the methods conservators use to determine the relative instability of heritage iron, and how the shortcomings of those methods can lead to unchecked deterioration. This lack of understanding of the effectiveness of treatments is a serious shortcoming within the sector, where there is a perception that treated objects are somehow stable post-treatment.

### 3.3.1 ANECDOTAL AND VISUAL EVIDENCE

Anecdotal and visual checks assume that objects are stable simply by their virtue of showing no physical surface change. Though visual assessment can be quantitative through software-assisted image correlation, it is not an accurate metric of determining the stability of treated objects, as chloride concentrations can remain high where no visual corrosion is occurring (Watkinson et al., 2014). They rely entirely on a specific context, and so are useless both in determining stability if that context changes and in comparing their effectiveness to other methods. However, visual assessment is useful in quickly determining if any of the parameters of that specific context have failed, i.e. visual corrosion growth in a controlled display.

### 3.3.2 CHLORIDE MONITORING

Chapter 2 explained how the amount of chlorides held within objects is highly variable. Unique corrosion profiles create complex pathways for extraction that can result in low $Cl^-$ levels in extraction baths whilst significant quantities can remain in objects (Rimmer et al., 2012). Chloride extraction comparisons do work in showing the inferiority of one method to another (Watkinson, 1982), which is the primary reason that so few treatment methods are still in use. However, the variability of corrosion profiles of objects means $Cl^-$ extraction monitoring is ill-suited for comparing treatment efficacies of objects that have undergone the same treatment. Furthermore, it has been shown that there is no direct correlation between $Cl^-$ content and corrosion rates amongst groups of similar artefacts (Watkinson et al., 2019). Absolute quantification requires destructive analysis, usually by acid dissolution or ion chromatography (Wang et al., 2008)

### 3.3.3 ELECTROCHEMICAL EVALUATION

Electrochemical evaluation measures the current response of a material to an externally applied voltage (potential). Current v. potential measurements are performed by electrochemical polarisation measurements while measurement of resistance to corrosion (impedance) is carried out by electrochemical impedance spectroscopy (EIS). Since the corrosion of a heritage object encased in a thick accretion is often dominated by diffusion of reactants and/or by the electrolyte resistance in the pores of the accretion then smaller currents imply less corrosion from which it may be inferred that more chloride has been removed. Polarisation measurement may also determine whether inhibition or true passivation of the residual conductive core of an artefact has occurred (Scott and Eggert, 2009: 156; Watkinson, 2010). However, due to the complex nature of corrosion layers, the $E$h could be a combination of areas with very high and very low current potentials, meaning that even though the combined $E$h of an object is low, there may be areas of greater instability. Alloying composition of metals can also affect output, which remains a problem as substrates can only be presupposed or determined destructively. X-ray fluorescence (p-XRF) could identify alloying components, though is only capable of surface analysis and cannot determine corrosion products occurring within object interiors. This imprecision means electrochemical evaluation is almost always used in conjunction with $Cl^-$ monitoring.

Electrochemical impedance spectroscopy (EIS) is, in most cases destructive, though conservators have adapted the method to be non-destructive (Angelini et al., 2012). EIS has primarily been used in conservation to evaluate the effectiveness of coatings for metals (Cano et al., 2010). It remains more useful as a means of measuring corrosion rates of large-scale artefacts, objects that cannot be sealed from ingressing oxygen, and those that cannot be moved indoors and must be analysed *in situ* (Ramirez Barat et al., 2019). It is not common to employ EIS to determine post-treatment object stability, as measuring and determining rates in tightly controlled atmospheres would be difficult, if even possible.

### 3.3.4 OXYGEN CONSUMPTION

Recent studies have used alternate methods to determine treatment efficiency. The development of oxygen consumption monitoring has shown that corrosion rates can be determined without knowing residual $Cl^-$ content (Matthiesen, 2007; Thickett et al., 2008; Watkinson and Rimmer, 2013; Matthiesen, 2013; Watkinson et al., 2016; Watkinson et al., 2019). The method involves placing objects in sealed containers conditioned to specific RH values and monitoring the oxygen levels within. As oxygen is used for the cathodic reaction, any reduction in atmospheric oxygen within the sealed vessels is indicative of corrosion. The rate of this depletion corresponds to the corrosion rate of the object under study. The conditioned internal atmosphere allows for the replication of display and storage conditions. If the RH is changed, any difference in rate directly correlates to the stability of an object in that environment. It has been quantitatively shown that a reduction in $Cl^-$ content also corresponds to a reduction in oxygen consumption (Rimmer et al., 2013). Though the use of oxygen consumption monitoring is promising, its relative nascency means that its potential for determining treatment endpoints has yet to be examined.

### 3.3.5 NEUTRON ANALYSIS

Studies have used prompt gamma activation analysis (PGAA) to non-destructively, quantitatively determine remaining chlorides (Selwyn and Argyropoulos, 2006). The method involves monitoring gamma-photons emitted when irradiating objects in a beam of cold neutrons in a nuclear reactor. Bulk $Cl^-$ at the point of analysis are registered, providing a more three-dimensional understanding of $Cl^-$ infestation. Some studies

(Watkinson et al., 2014; Schmutzler et al., 2019) have combined PGAA with oxygen consumption monitoring to link residual $Cl^-$ and its impact on corrosion rates. The authors state that PGAA is not capable of quantitatively determining total $Cl^-$ remaining within objects, as the method is only capable of analysing small areas, resulting in it being a poor determinate of overall stability. Furthermore, the use of a nuclear research reactor is not a luxury most conservators have, and as such, it remains extremely improbable the method will find wider use.

### 3.4 TREATMENT OF THE *MARY ROSE* CANNONBALLS

According to staff in post, their preference for a treatment, resources, priorities for treatment, availability of equipment and the popularity of a treatment at any given point in time resulted in a wide range of treatments being used on the cast iron cannon balls by the MRT (Table 3.2).

| Pretreatment/ storage | Treatment | 2nd Treatment | Coating |
|---|---|---|---|
| **NaOH - 2 weeks** | Hydrogen reduction | N/A | Epoxy resin and microcrystalline wax |
| **Unknown, most likely NaOH** | $NH_3$ Ammonia | N/A | N/A |
| **NaOH; $NaH(CO_3)_2$** | 0.1M Alkaline sulfite at 45°C | N/A | Paraloid B48n |
| **NaOH; $NaH(CO_3)_2$** | 2% Hostacor-IT | N/A | Microcrystalline wax and graphite powder |
| **NaOH; $NaH(CO_3)_2$** | 1% Hostacor-IT | N/A | Microcrystalline wax and graphite powder |
| **NaOH; $NaH(CO_3)_2$** | 2% Hostacor-IT; coated in microcrystalline wax and graphite powder | Wax removed | Paraloid B48N |
| **NaOH; $NaH(CO_3)_2$** | 1% Hostacor-IT; coated in microcrystalline wax and graphite powder | Wax removed; 2% Hostacor-IT | Paraloid B48N |
| **NaOH; $NaH(CO_3)_2$** | 2% Hostacor-IT; coated in microcrystalline wax and graphite powder | Wax removed; 2% Hostacor-IT | Paraloid B48N |
| **NaOH; $NaH(CO_3)_2$** | 2% Hostacor-IT; coated in microcrystalline wax and graphite powder | Wax removed with boiling water; 0.5M alkaline sulfite at 60C | Paraloid B48N |

| | | | |
|---|---|---|---|
| **NaOH; $NaH(CO_3)_2$** | 2% Hostacor-IT | 0.5M alkaline sulfite at 60C | Paraloid B48N |

**Table 3.2:** Treatment combinations employed on the *Mary Rose* cannonballs.

### 3.4.1 HYDROGEN REDUCTION

The decision to use hydrogen reduction to treat many of the iron finds was justified as necessary and cost-effective (Barkman, 1977; Barker et al., 1982; Barker, 2003). The short treatment time offered the advantage of preparing objects for display quickly. The facilities for hydrogen reduction were local and large enough to treat the cannon (Figure 3.11).

**Figure 3.11:** A wrought-iron gun barrel before and immediately after hydrogen reduction. From Kendell (1982: 112)**.**

The theoretical sublimation of most if not all chlorides from within the cannonballs meant atmospheric corrosion would be negligible, regardless of environment (Archer, 1991: 73). The complete reduction of all oxide species meant that HR-treated cannonballs needed to be immediately consolidated with epoxy, as they were far less dense and greatly lacking in cohesion. The method had by that time been employed for many years, most notably on finds from the *Vasa* (Arrhenius et al., 1973), so there was standard protocol in place to follow. Object typology/morphology was also a factor in choosing this treatment, as the number of cannonballs meant that many could remain untreated for future study. This reasoning was used to rationalise the ethical quandary of metallographic structure change caused by the method (Jones, 2020). It was this structural change, alongside the health and safety concerns, that ultimately resulted in the discontinuation of the method at the *Mary Rose* (Jones, 2020). There is no published use of hydrogen reduction being used as a method to treat $Cl^-$-saturated heritage iron after 1982. As the initial need for treated objects to satisfy the public had been fulfilled, there was no longer a need for the MRT to continue this rapid yet controversial treatment (Jones, 2020).

### 3.4.2 AQUEOUS WASHING AND INHIBITION

Following the retirement of hydrogen reduction at the Portsmouth Museum in 1980 (Trust, 2015), the iron cannonballs were placed in an alkaline solution of NaOH, with a change of method in 2007 to immersion in a solution of 0.1M $Na_2CO_3$/ 0.05M $NaHCO_3$. Their placement in NaOH most likely (assuming solution changes) led to bulk removal of chlorides. The use of Hostacor-IT as a desalination treatment beginning in 2010 (Trust, 2015) allowed the cannonballs to be treated in an aqueous environment at a neutral pH, without subjecting them any potential drawbacks from alkaline sulfite (Rimmer and Watkinson, 2011). However, the few published accounts of its suitability as a conservation treatment for marine heritage iron are limited to its use as a corrosion inhibitor in an aqueous solution, not its efficiency as a desalination solution. Several cannonballs treated with this method showed visual signs of corrosion (spot colouration change, cracking) (Jones, 2020). Desalination treatment was then changed to the alkaline sulfite method, with the method also being used to retreat Hostacor-treated cannonballs (Trust, 2015; Jones, 2020).

### 3.4.3 DETERMINING TREATMENT ENDPOINTS

All primary treatments employed on the *Mary Rose* cast iron cannonballs used chloride extraction monitoring to determine endpoints, first by measuring treatment effluent during hydrogen reduction and later using a $Cl^-$ ion meter. Treatment was considered sufficient when $Cl^-$ fell below 0.1M (354 ppm) in hydrogen reduction effluent (Kendell, 1982: 80), or when treatment bath monitoring fell below 100 ppm and ceased to show any further withdrawn $Cl^-$ (Trust, 2015). Those cannonballs that were visually assessed to be in need of retreatment (those that showed rust spots or were cracking) were placed in desalination baths (either Hostacor or alkaline sulfite) until further $Cl^-$ (as determined using a $Cl^-$ ion meter) were no longer removed. In July 2014, most of the treated cast iron cannonballs were removed from display and placed in controlled storage (20% RH) (Trust, 2015).

# 4 EXPERIMENTAL DESIGN

## 4.1 AIMS AND OBJECTIVES

This study aimed to determine the impact of humidity on corrosion rates of cast iron cannonballs at the MRT to inform upon storage and display strategies for the collection. This was achieved by:

- Recording oxygen consumption of the cannonballs at a range of relative humidities as a proxy corrosion rate measure.
- Relating corrosion rates of individual cannonballs to their treatment history.
- Retreating a number of cannonballs by aqueous immersion and correlating chloride ion extraction to changes in oxygen consumption rate post-treatment.
- Producing guidance for the MRT on suitable storage and display environments and retreatment impacts for the cannonballs in relation to their treatment history.

## 4.2 SAMPLE MATERIAL

A total of 56 cannonballs were loaned to Cardiff University by the MRT for this study. Treatment records (Figure 4.1; Appendix A) for the cannonballs were obtained and the samples were selected to encompass both the range of treatments that had been applied and the range of standard sizes of cannonball within the collection. Selected samples had been treated using hydrogen reduction (12 samples), alkaline sulfite (15), and Hostacor-IT (19). The remaining 10 cannonballs had been treated with Hostacor initially followed by a second treatment in either alkaline sulfite (7) or Hostacor (3).

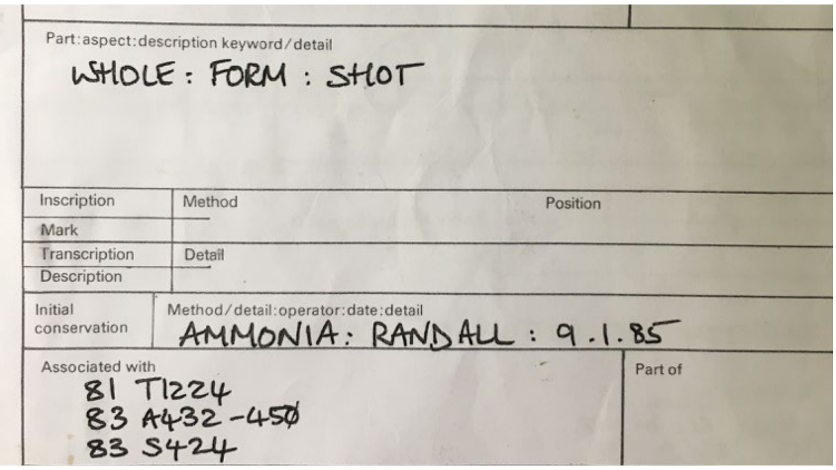

Part:aspect:description keyword/detail
WHOLE : FORM : SHOT

Inscription
Mark
Transcription
Description
Method
Position
Detail

Initial conservation
Method/detail:operator:date:detail
AMMONIA: RANDALL : 9.1.85

Associated with
81 T1224
83 A432-450
83 S424
Part of

**Figure 4.1:** Documentation provided from the MRT for #83A-0449 (iron cannonball) showing AMMONIA as the treatment method.

Table 4.1 lists the diameter, mass, previous treatment method(s) and applied protective coatings for all samples. Each of the four treatment methods employed at the MRT for the cast iron cannonballs are represented by three diameters of cannonball: 6.5cm, 8.5cm, and 9.8-10.5cm. The only size/treatment combination not represented in the sample collection is a retreated cannonball in the 9.8 – 10.5cm range.

| MRT # | Sensor # | Dia. (cm) | Mass (g) | TR.1 | Conc. | TR.2 | Conc. |
|---|---|---|---|---|---|---|---|
| **78A-0604** | HS098 | 8.5 | 1530 | HR-E | | NA | |
| **78A-0605** | RC049 | 8.5 | 1280 | HR-E | | NA | |
| **78A-0606** | RC028 | 8.7 | 1047.50 | HR-E | | | |
| **78A-0608** | RC044 | 8.7 | 1004.23 | HR-E | | | |
| **78A-0610** | RC035 | 8.3 | 2146.04 | HR-E | | | |
| **78A-0703** | HS146 | 8.5 | 1052.28 | HR-E | | | |
| **78A-725x** | HS148 | 6.7 | 825.28 | HR-E | | | |
| **79A-0157** | RC026 | 10.3 | 2940.14 | HR-E | | | |
| **80A-0358** | RC031 | 7.0 | 1141.42 | HR-E | | | |
| **80A-0865** | HS097 | 6.8 | 299.22 | HR-E | | | |
| **80A-1051** | RC041 | 10.6 | 1149.54 | HR-E | | | |
| **80A-1125** | HS100 | 6.4 | 398.98 | HR-E | | | |
| **81A-1106** | RC058 | 8.6 | 1392 | HC-W | 2% | AS-P | 0.5M |
| **81A-2762** | RC051 | 8.5 | 1925.89 | HC-W | 1% | | |
| **81A-3111** | RC023 | 6.4 | 875.65 | HC-W | 2% | NA | |
| **81A-3373** | RC012 | 6.8 | 852.49 | AS-P | 0.1:0.05M | | |
| **81A-3459** | RC002 | 8.5 | 2371 | HC-W | 2% | NA | |
| **81A-3464** | RC021 | 8.5 | 2315.39 | AS-P | 0.1:0.05M | | |
| **81A-3499** | RC048 | 8.8 | 2231.88 | AS-P | 0.1:0.05M | | |
| **81A-3508** | HS149 | 8.4 | 2032.73 | HC-W | 2% | HC-P | 2% |
| **81A-3517** | HS145 | 8.5 | 1688 | HC-W | 2% | AS-P | 0.5M |
| **81A-3527** | RC027 | 8.3 | 1592.73 | HC-W | 1% | HC-P | 2% |
| **81A-3529** | HS125 | 9.5 | 3126.42 | AS-P | 0.1:0.05M | | |
| **81A-3599** | HS141 | 9.9 | 3678 | HC-W | 2% | | |
| **81A-4147** | HS144 | 8.4 | 2145.48 | AS-P | 0.1:0.05M | | |
| **81A-6131** | HS133 | 8.6 | 2392.47 | AS-P | 0.1:0.05M | | |
| **81A-6236** | HS147 | 8.2 | 1840.01 | HC-W | 2% | | |
| **81A-6909** | RC043 | 8.5 | 1254 | HC-W | 2% | NA | |
| **82A-2547** | HS137 | 10.4 | 4081 | HC-W | 2% | | |
| **82A-2615** | RC039 | 8.4 | 1793.87 | HC-W | 2% | | |
| **82A-2624** | HS095 | 10.5 | 3894 | HC-W | 2% | | |
| **82A-3593** | RC030 | 8.6 | 2357.90 | AS-P | 0.1: 0.05M | | |
| **82A-3594** | HS134 | 8.7 | 2041.95 | HC | 2% | AS-P | 0.5M |
| **82A-4113** | RC032 | 8.5 | 2100.91 | AS-P | 0.1: 0.05M | | |
| **82A-4235** | RC046 | 10.6 | 3500 | AS-P | 0.1: 0.05M | | |
| **82A-4362** | HS121 | 8.5 | 2457.64 | AS-P | 0.1: 0.05M | | |
| **82A-4392** | HS122 | 6.0 | 742.02 | AS-P | 0.1: 0.05M | | |
| **82A-4731** | HS143 | 9.8 | 3398.45 | HC-W | 2% | | |
| **82A-4732** | HS140 | 8.5 | 2147.39 | HC-W | 2% | | |

| | | | | | | | |
|---|---|---|---|---|---|---|---|
| **82A-4735** | HS150 | 6.5 | 1031.37 | HC-W | 2% | AS-P | 0.5M |
| **82A-4743** | RC020 | 6.6 | 909.99 | AS-P | 0.1: 0.05M | | |
| **83A-0002** | HS127 | 6.7 | 893.57 | HC-W | 2% | | |
| **83A-0130** | HS138 | 8.6 | 2417.61 | HC-W | 2% | AS-P | 0.5M |
| **83A-0149** | RC042 | 8.4 | 2199.91 | HC-W | 1% | | |
| **83A-0160** | HS099 | 8.7 | 2330.22 | HC-W | 2% | | |
| **83A-0176** | HS136 | 8.7 | 2051.24 | AS-P | 0.1: 0.05M | | |
| **83A-0177** | HS131 | 8.9 | 1996.88 | AS-P | 0.1: 0.05M | | |
| **83A-0180** | HS130 | 6.6 | 878.36 | HC | 2% | AS-P | 0.5M |
| **83A-0201** | HS139 | 6.4 | 959.32 | HC-W | 1% | | |
| **83A-0214** | RC037 | 8.6 | 2261.85 | HC-W | 1% | | |
| **83A-0225** | HS135 | 8.4 | 2232.36 | HC | 2% | AS-P | 0.5M |
| **83A-0233** | RC024 | 8.6 | 2327.49 | AS-P | 0.1: 0.05M | | |
| **83A-0273** | HS142 | 6.5 | 913.73 | HC-W | 2% | NA | |
| **83A-0275** | HS132 | 8.7 | 1971.18 | HC-W | 2% | | |
| **83A-0441** | HS096 | 6.8 | 478.57 | HC-W | 2% | HC-P | 2% |
| **87A-0062** | RC036 | 6.8 | 1033.66 | HC-W | 2% | | |

**Table 4.1:** Iron cannonballs from the *Mary Rose* used for the study. Treatment (TR.) codes: HR = hydrogen reduction; AS = alkaline sulfite; HC = Hostacor IT; W = coated in microcrystalline wax; P = coated in 15% Paraloid B48N; NA = Data for 2nd treatment not available. Concentrations (Conc.) given as percentage or Molar (M).

## 4.3 PHOTOGRAPHY

To relate any physical changes in the cannonballs to corrosion measured by oxygen consumption, the cannonballs were photographed upon their arrival at Cardiff University and at regular intervals throughout the study after exposure to each relative humidity environment. As the objects are spherical, photographs were taken along four axes to ensure every visible surface was captured (Figure 4.2). All photos were taken with a Nikon D7000 DSLR camera, with a Nikon DX 18-105mm lens.

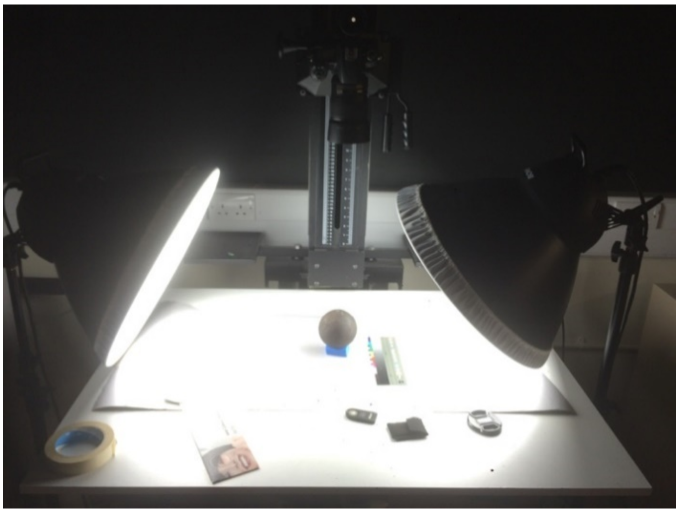

**Figure 4.2:** Photographic setup for imaging of samples. Each sample was photographed on four axes.

## 4.4 OXYGEN CONSUMPTION MEASUREMENT

As the predominant cathodic reaction in atmospheric corrosion of iron is the reduction of oxygen (see 2.3.1), sealing an iron sample in an airtight reaction vessel and measuring the depletion of oxygen within the vessel as corrosion proceeds offers a proxy measure of its corrosion rate (Matthiesen and Wonsyld, 2010). Oxygen levels are measured using sensor spots within the reaction vessels in a process based on luminescence. These spots contain a ruthenium complex (Xu et al., 1994) for measuring oxygen partial pressure. When the LED lights the photoluminescent spot, the sensing compound is excited. The oxygen-saturated, photosensitive polymer then gives a spectral return of that excitation that varies according to oxygen concentration (Amao, 2003) (Figure 4.3). This return is then processed by proprietary software, giving the user a value for the oxygen partial pressure from within the vessel.

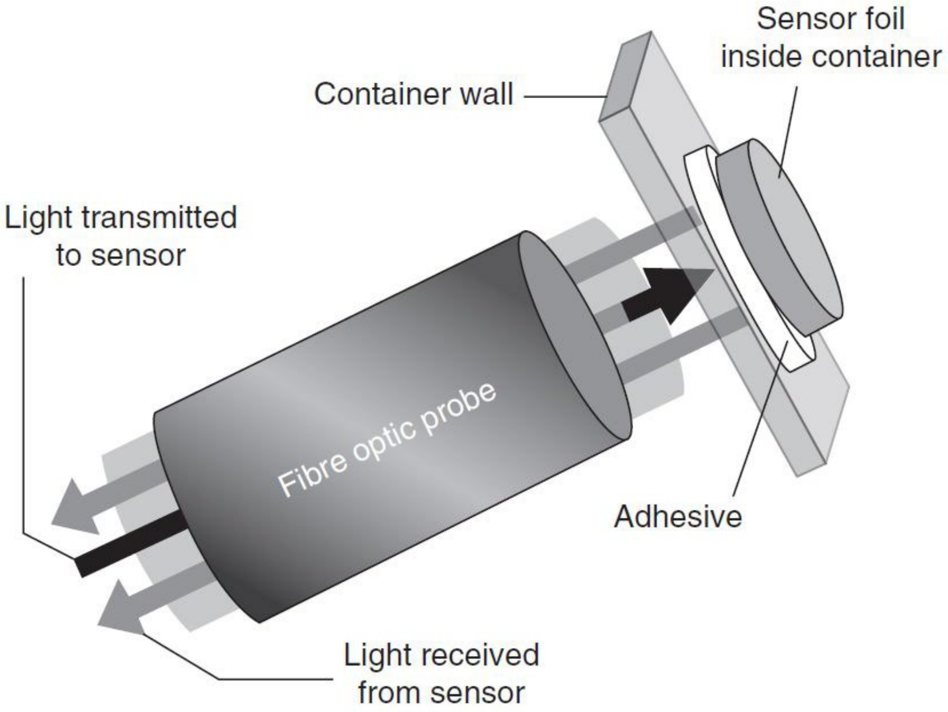

**Figure 4.3:** Diagram of oxygen measuring setup. From Matthiesen (2013).

First proposed for heritage iron by Matthiesen (2007), measuring oxygen consumption to determine corrosion rates has several advantages:

- Affordability and mobility.
- No specialist interpretation.

- Remote measurement through transparent reaction vessels.
- Versatility in reaction vessel dimension.
- Non-destructive.

### 4.4.1 ENVIRONMENTAL REPLICATION

Establishing the corrosion rate of the cannonballs in a range of relative humidity (RH) environments would allow the MRT to make cost-benefit decisions about the storage and display conditions for these artefacts. Silica gel conditioned to specific RH values has been shown to reproduce humidities in sealed reaction vessels (Matthiesen, 2013; Rimmer et al., 2013). As corrosion of chloride-infested iron would not be expected below 12% RH (Watkinson and Lewis, 2005a), 20% RH was chosen as the lowest RH environment. Knowing that the cannonballs had corroded on display at 55% RH and this is likely to be the highest RH to which metal museum artefacts would be subjected, 60% RH was chosen as the highest RH environment in this study. Oxygen consumption of the samples was therefore measured at 20, 30, 40, 50 and 60% RH.

Silica gel (2.0-5.0 mm bead size, supplier Gee Jay Chemicals Ltd) was conditioned to +/- 1% RH using a Binder KBF 720 (E6) climatic chamber at 20°C. The dry mass used was dMadgeTech RHTemp101A dataloggers were used to ensure silica gel reached the appropriate RH. The mass of silica gel contained within each vessel was dependent on the size of the sample. Since cannonball sizes vary between 6.02cm and 10.57cm, the volume of gel used was adjusted accordingly to fill the reaction vessels. Silica gel gains mass as it absorbs water, therefore to maintain the same volume at each humidity, the mass of silica gel was increased (Weintraub, 2002). Table 4.2 displays the mass of silica gel used for each sample size and RH value. However, as the silica gel gains water mass, oxygen is displaced, resulting in less oxygen available within sample jars as humidity is increased. These losses are accounted for in rate calculations (see Section 4.6).

| | **Mass increase from 20% RH (%)** | **Mass of gel by cannonball diameter (g)** | | | |
|---|---|---|---|---|---|
| **RH** | | ~6.5cm | ~8.5cm | ~9.8cm | ~10.5cm |
| **20%** | - | 1450.0 | 1280.0 | 1100.0 | 1000.0 |
| **30%** | 104.4 | 1513.2 | 1335.8 | 1148.0 | 1043.6 |
| **40%** | 109.6 | 1589.3 | 1403 | 1205.7 | 1096.1 |
| **50%** | 115.2 | 1670.4 | 1474.4 | 1267.1 | 1151.9 |
| **60%** | 119.8 | 1737.2 | 1533.5 | 1317.9 | 1198.0 |

**Table 4.2:** Mass of silica gel used for samples, dependent upon size of the sample and RH

### 4.4.2 REACTION VESSELS AND SEALING METHOD

Previous studies (Watkinson and Rimmer, 2013; Emmerson and Watkinson, 2016) using oxygen consumption employed airtight Mason Ball jars equipped with disc lids sealed with threaded rings that deform a silicon seal around the vessel edge under pressure. The diameters of the samples (Table 4.1) are, in most cases, larger than that of available Mason Ball jars. The only reaction vessels of suitable dimensions that could be sourced were not airtight. Other research has used Escal$^{TM}$, a barrier film of double-layer polypropylene/PVA lined with a vacuum-deposited ceramic, to encapsulate samples for oxygen consumption measurements (Matthiesen, 2013) but this was thought impractical for samples of such mass as the cannonballs.

Glass vessels (Clas Ohlson article no. 44-1319) with 2-litre volumetric capacity, 10.8 cm aperture diameter, and mild steel screw top lids were chosen as sample reaction vessels. To form an airtight seal around the lids of the vessels, Mouldlife Platsil Gel 10 silicone was used. Unlike single-part silicones that cure by condensation and off-gas acetic acid (Witucki, 1993), this two-part organofunctional siloxane and platinum complex-setting silicone does not off-gas. The silicone was mixed in a polyethylene bag and piped around the lid/glass interface on the exterior of the vessels. Vessels were placed on a rotating platter to ensure uniform application. Upon drying, seals were inspected for any defects (Figure 4.4) that might compromise airtightness which would otherwise only be detected via the oxygen consumption data.

**Figure 4.4:** A visible defect in the silicone seal. A defect this small is enough to ruin data collection for any given sample.

The use of silicone as a sealant has drawbacks, as it has been shown that oxygen can readily diffuse through it (Matthiesen). However, its use allowed for continual opening and sealing of the reaction vessels, and it met the modest budgetary means of this project. Sealing application with silicone was tested to determine the most effective method (Table 4.3). It was found that freshly applied double seals were more effective in mitigating oxygen ingress than a single application. Old sealings that were left from previous RH threshold tests and covered in new silicone (i.e. 'cut' seals) proved far less effective. All externally-applied seals used a double application.

| | | **N2A** | **N2B** | **N2C** | **N2D** | **N2E** | **N2F** | **N2G** | **N2H** | **HS 125** | **HS 144** | **Ctrl Jar** |
|---|---|---|---|---|---|---|---|---|---|---|---|---|
| **Daily $O_2$ rates (mbar*$e^{-1}$)** | Cut Seal | -3.58 | -5.05 | -3.63 | -2.07 | -5.27 | -5.30 | -5.16 | -4.66 | 1.19 | 0.58 | 0.10 |
| | Fresh Seal | -1.23 | -1.47 | -2.12 | -1.58 | -3.67 | -1.57 | -3.50 | -1.14 | 1.70 | 1.18 | 0.09 |
| | 2x Seal | -1.09 | -1.43 | -1.79 | -1.34 | -3.27 | -1.39 | -2.81 | -1.09 | 1.65 | 1.43 | 0.23 |
| | | | | | | | | | | | | |
| | Fresh % | 65.7 | 70.9 | 41.5 | 23.4 | 30.3 | 70.4 | 32.2 | 75.6 | 42.6 | 104.2 | 14.2 |
| | 2x % | 69.6 | 71.6 | 50.6 | 35.2 | 38.1 | 73.8 | 45.5 | 76.5 | 38.5 | 147.1 | -117.9 |

**Table 4.3:** Results of seal effectiveness testing. Three testing phases (Cut seal, Fresh seal, and 2x seal) are rows 2-4, with % improvement of fresh and 2x seals over cut seals the bottom two rows. Freshly applied double seals are clearly superior to other options tested.

As the lids of the vessels are mild steel, measures were taken to limit their contact with oxygen, which could potentially result in corrosion and consumption of oxygen that may be attributed erroneously to the samples. The silica gel was shown to scratch the lid interior, meaning a robust coating was required. This ruled out the use of a painted coating. The interior surface of each lid was coated with 25g of Mouldlife Platsil Gel 10 silicone (Figure 4.5). Adding a silicone barrier within the lids also led to slight deformation of that barrier during tightening of the lid onto the vessel, improving the seal. Airtightness of the vessels sealed by this method was confirmed by control vessels (see 5.1.1).

**Figure 4.5:** Lid used on reaction vessels, coated with 25g silicone.

### 4.4.3 OXYGEN SENSITIVE SPOTS

PreSens SP-PSt3 glass-mounted oxygen sensor spots were used for this study (precision = +/- .1hPa @ 2hPa, +/- 1hPa @ 207 hPa) (PreSens, 2017). The autoclavable, glass mounted model is more robust and can be reliably removed and re-adhered, a desirable quality given the size and mass of samples and the amount of silica gel used. RS Components RS 692-542 silicone rubber compound was used to adhere a sensor spot to the inside of each reaction vessel. The compound is transparent and resistant to age-induced colour change, meaning the spectral return to the LED will be unencumbered by opacity. It is a single-part, quick setting silicone that off-gases acetic acid during cure, therefore vessels are open for ventilation during curing.

### 4.4.4 PLACEMENT OF COMPONENTS

Each reaction vessel was filled with half the mass of silica gel required. MadgeTech RHTemp 101A dataloggers set to log temperature and humidity (+/- 0.5°C, +/- 3% RH) were placed within 10 of the reaction vessels to ensure the silica gel maintained the target RH within the vessel and the temperature remained constant throughout. Each cannonball was then placed in a polyethylene NetlonTM mesh sleeve (to facilitate placement in and removal from reaction vessels) and lowered into its reaction vessel. The remainder of the silica gel was t then added to each vessel, and the lids were then screwed on and the silicone sealing protocol followed (Figure 4.6).

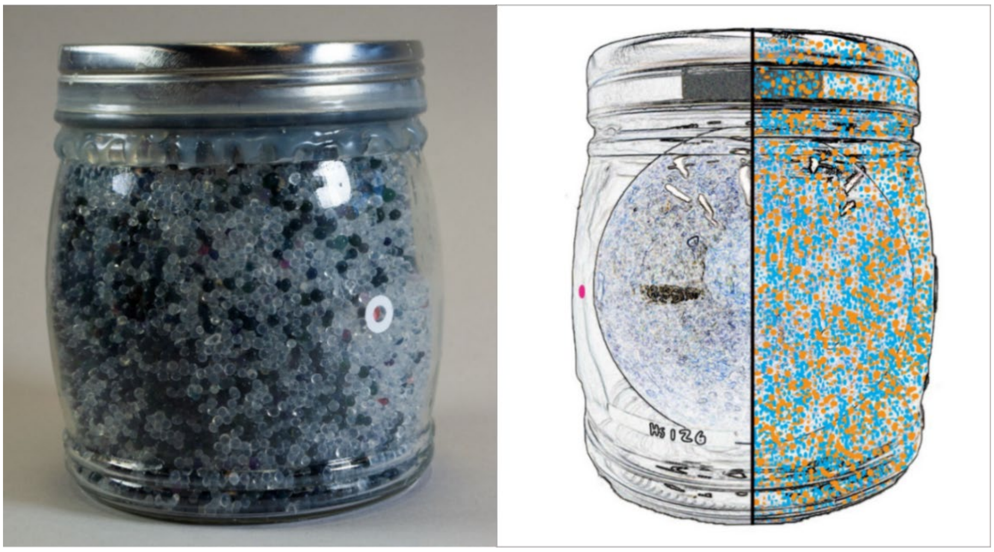

**Figure 4.6:** Left - A sealed reaction vessel containing a cannonball and silica gel conditioned to 50% RH (left); Right - Diagram of a sealed reaction vessel showing the sensor spot (pink dot), datalogger (black bar within lid), cannonball (centre), surrounding silica gel (right hand side).

### 4.4.5 CONTROLS

Any oxygen entering reaction vessels via the seal would influence results by masking consumption by the sample. Recording oxygen ingress into sealed reaction vessels filled with nitrogen gas provides a measure of leakage for the vessels that can be considered in calculations of oxygen consumption (Watkinson and Rimmer, 2013; Emmerson, 2015; Nordgren, 2016).

Eight of the reaction vessels were filled with $N_2$ gas (BOC suppliers, OFN – Oxygen Free Nitrogen, compressed). Lids were quickly screwed onto the vessels, and the silicone seals were immediately applied (see 4.4.2). The oxygen pressure inside these vessels was measured for the duration of the cannonball corrosion rate test at each RH value.

One control vessel was filled with an amount of silica gel equal to those used for samples ~8.5cm diameter and was sealed without any sample placed in it. As the vessel does not have a sample, it should ideally show no consumption; slight gains should appear as oxygen ingresses into the vessel. If the vessel shows losses in oxygen, experimental parameters would have to be re-evaluated. A MadgeTech RHTemp 101A datalogger was placed in the control vessel to measure any variance in the environment compared to sample-containing reaction vessels.

### 4.4.6 DATA COLLECTION OVERVIEW

All 56 cannonballs in vessels with conditioned silica gel, 8 control vessels containing only nitrogen and one control vessel containing silica gel and datalogger but no sample had their oxygen consumption rate measured for each RH (20, 30, 40, 50 and 60%). The following measurement protocol was followed:

1. The vessels were stored in a Binder KBF 720 (E6) climatic chamber at constant 20$^oC$ throughout the measurement period.
2. Oxygen pressure within each reaction vessel was recorded for at least 8 hours or until a linear slope could be defined. A period of 100 minutes was selected from this linear data and averaged to a single oxygen pressure value for that day. This was carried out five times for each humidity value over a period of between 46 and 64 days.

3. After the 5th reading, samples were removed from the climatic chamber. Silicone seals around the reaction vessels were removed and discarded, silica gel was emptied, and samples were placed in storage vessels.
4. Samples were photographed.
5. Samples and controls were then repacked into the same reaction vessels and sealed.
6. Steps 1-4 were repeated for each humidity value.

### 4.4.7 STANDARDISED MEASUREMENT VARIABLES

Two PreSens OXY-1 SMA single-channel meters and a PreSens OXY-4 SMA 4-channel meter were used to measure oxygen consumption of the cannonballs. Data collection was managed via the PreSens Measurement Studio 2 software version 3.0.1.1413.

#### 4.4.7.1 AMPLITUDE

Amplitude is a measure of the intensity of illumination from the meter, transmitted through the fibre optic cable, and is measured in microvolts (µV). A higher amplitude results in higher precision by improving the signal-to-noise ratio whereas a lower amplitude prevents bleaching of the sensor spot, increasing the lifetime of the spot by avoiding photoluminescent degradation (PreSens, 2018). Amplitude must be at least 3000 µV to take a reading. Full diode saturation is possible if the illumination is too high, due to either intensity level or ambient light. As amplitude has an inversely proportional relationship with oxygen partial pressure (Figure 4.7), for each measurement the aim was to meet or exceed the amplitudes of previous readings.

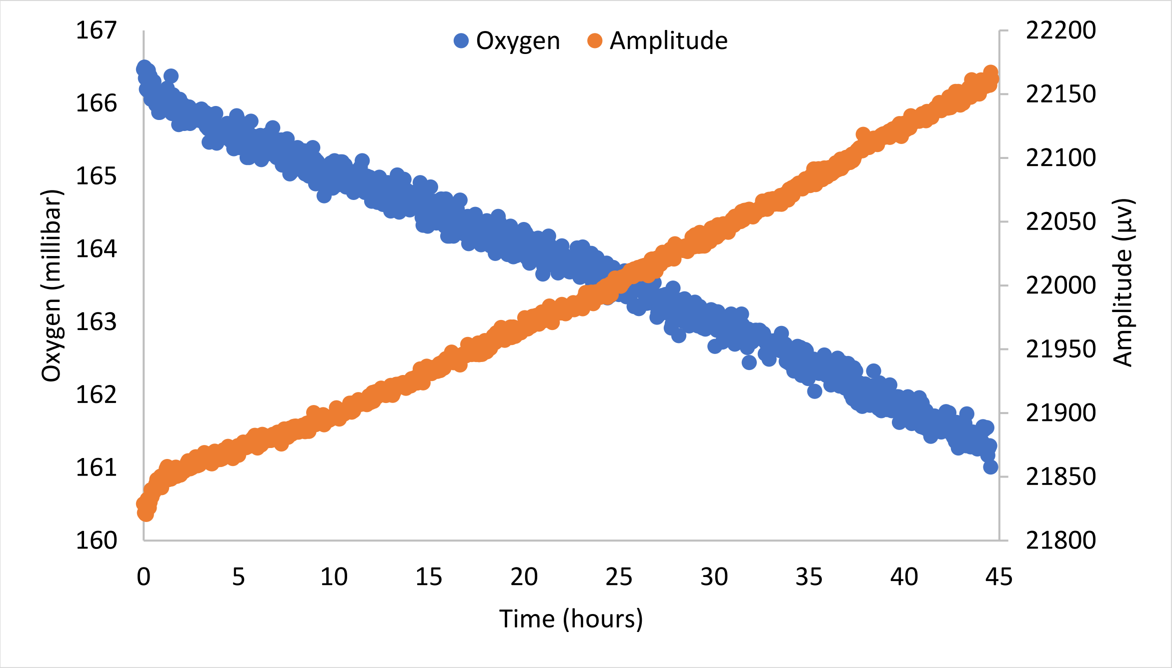

**Figure 4.7:** Graph of oxygen depletion within a reaction vessel due to corrosion showing the inverse relationship between oxygen pressure and amplitude.

### 4.4.7.2 STABILITY OF FIBRE OPTIC CABLE

The condition of fibre optic cables, and the circuitous route they take from meter to sensor spot, can affect oxygen pressure readings (Ghatak and Thyagarajan, 1998). Fibre optic cables between the oxygen meters and reaction vessels were supported on plinths fabricated from aluminium-centred honeycomb glass-reinforced plastic and coated with MouldLife Platsil silicone (Figure 4.8). The silicone reduces vibrations and securing with cable ties diminishes movement of the plinth within the chamber.

**Figure 4.8:** Fabricated plinth custom-made for $O_2$ testing. The silicone enclosure minimises vibrations to the fibre optic cable. The cable is run through an enclosed, silicone-encased channel. Holes in the base allow for cable ties to keep the plinth in place.

## 4.5 SAMPLE RETREATMENT AND OXYGEN MONITORING

Retreating a selection of the samples by aqueous immersion in alkaline sulfite solution, measuring their extracted chlorides, and re-measuring oxygen consumption across the 20-60% RH range would determine if retreatment would be effective in reducing corrosion rate of cannonballs.

### 4.5.1 SAMPLE SELECTION AND PREPARATION

Fifteen samples were chosen for retreatment. They included at least one cannonball of every size and treatment method, with an emphasis on those that consumed more oxygen during the initial oxygen consumption measurements (these results are discussed in Chapter 6) (Table 4.4).

| | Treatment | Coating | Diameter (cm) | Mass (g) | Volume (cm$^3$) |
|---|---|---|---|---|---|
| **78A-0608** | HR | Epoxy | 8.7 | 1004.2 | 340.1 |
| **78A-0703** | HR | Epoxy | 8.5 | 1052.3 | 322.7 |
| **80A-0865** | HR | Epoxy | 6.8 | 299.2 | 163.2 |
| **80A-1051** | HR | Epoxy | 10.6 | 1149.5 | 616.6 |
| **81A-3373** | AS | B48N | 6.8 | 852.5 | 161.7 |
| **81A-3499** | AS | B48N | 8.8 | 2231.9 | 356.8 |
| **81A-3527** | RT-HC | B48N | 8.3 | 1592.7 | 296.2 |
| **81A-6909** | HC | Wax | 8.5 | 1254.0 | 321.6 |
| **82A-2547** | HC | Wax | 10.4 | 4081.0 | 585.6 |
| **82A-3594** | RT-AS | B48N | 8.7 | 2042.0 | 347.2 |
| **82A-4235** | AS | B48N | 10.56 | 3500.0 | 618.3 |
| **83A-0176** | AS | B48N | 8.7 | 2051.2 | 347.2 |
| **83A-0275** | HC | Wax | 8.7 | 1971.2 | 338.9 |
| **83A-0441** | RT-HC | B48N | 6.8 | 478.6 | 164.6 |
| **87A-0062** | HC | Wax | 6.8 | 1033.7 | 163.2 |

**Table 4.4:** Samples chosen for retreatment. HR = hydrogen reduction; AS = alkaline sulfite; HC = Hostacor-IT; RT = retreated; B48N = Paraloid B48N; Wax = Renaissance wax

Protective coatings applied to the cannonballs listed in Table 4.4 could negatively impact chloride extraction. These were removed with solvents (acetone and white spirits) prior to alkaline treatment.

### 4.5.2 ALKALINE SULFITE RETREATMENT OF SAMPLES

Following initial oxygen consumption data acquisition, 15 cannonballs were retreated using the alkaline sulfite desalination method discussed in Chapter 3.2.6.4. Samples were placed in individual desalination vessels containing a solution of 4 litres of 0.1M sodium hydroxide/sodium sulfite (16g NaOH + 25.2g $Na_2SO_3$) and tap water. This concentration kept the pH $\geq$ 13. According to treatment records, a 0.5M alkaline sulfite concentration was used for the treatment of the *Mary Rose* cannonballs (Appendix A). The lower concentration of 0.1M is enough to induce alkaline desalination (Schmidt-Ott and Oswald, 2006).

Four changes of treatment solution were carried out at two monthly intervals with the solution sampled for chloride measurements.

### 4.5.3 CHLORIDE MEASUREMENTS

Chlorides extracted during desalination were measured using a Sherwood 926 Chloride Analyzer. This model of chlorimeter uses a silver electrode placed in an acetic/nitric acid-mixed buffer solution (a variation on traditional silver nitrate testing) that maintains optimal pH for each test. Chloride-containing alkaline solutions can then be directly analysed without the formation of silver hydroxides or oxides that would otherwise corrupt the count of insoluble silver chlorides (Plenderleith and Werner, 1971: 201; Odegaard et al., 2005: 108-109; Sherwood Scientific, 2012). The buffer also contains a colloid, allowing for precipitated, insoluble silver chlorides to hold in suspension. The range of the machine is 1-999 mg (ppm). If readings exceed 999 mg, samples can be diluted with deionised water. 0.5 ml of desalination solution is required to acquire a reading.

Chlorides were measured every two weeks, when possible. Desalination baths were stirred, and 0.5 ml solution was removed and pipetted into the buffer solution cup and analysed. As the solutions contained tap water, tap water samples were also pipetted and measured for chlorides.

### 4.5.4 DRYING AND OXYGEN CONSUMPTION RE-TESTING

Following desalination, samples were dried to remove excess water remaining within the structure. Failure to dry the cannonballs could result in accelerated corrosion. After removal from their alkaline baths, samples were washed in a tap water drip bath for three days to remove any residual treatment solution. The cannonballs were then dried in a SNOL 60/300 LFN GP oven and incubator until their mass stabilised, first at 80˚C and then at 105˚C.

Following drying, samples were packed into reaction vessels with conditioned silica gel and sealed, following protocol laid out in Section **Error! Reference source not found.**. Their rates of oxygen consumption were then measured at the same RH intervals (20-60% RH) following experimental parameters laid out in Section 4.4.6.

## 4.6 CONVERTING CHANGE IN OXYGEN PRESSURE TO MASS OF OXYGEN CONSUMED

Oxygen consumption results are acquired in millibar oxygen remaining within the vessel. However, millibar is not a measure of oxygen quantity, but rather the oxygen partial pressure remaining within a container, regardless of volume. To define corrosion rates, millibar oxygen consumed must be converted into mg oxygen consumed, meaning volume remaining within the reaction vessels after silica gel and sample have been accounted for has to be calculated. Though the samples are of a similar shape, they vary greatly in both mass and volume. For example, converting mbar consumed to mg will allow for corrosion rates of all samples to be directly compared to each other. The ideal gas law can be used to determine the mass of oxygen available (Equ. 4.1) (Woody, 2013):

$$PV = nRT \qquad \textbf{Equ. 4.1}$$

Where P = pressure (in pascals), V = volume (in $m^3$), n = the number of mols of the gas (or the mass), R = the universal gas constant of 8.314 J $mol^{-1}$ $K^{-1}$, and T = temperature (in kelvin). The equation has been used in earlier heritage corrosion studies to determine the oxygen consumed in corrosion reactions and the rate at which they are occurring (Matthiesen, 2007) Applied to this study, the mass of oxygen can be calculated as:

n (mass of oxygen) = (Daily rate of Oxygen consumption * volume of oxygen available in the container)/ (R * 293.15)

The daily consumption rate is converted from hPa (as that is the output of the PreSens software) to Pa by multiplying by 100 (1 hPa = 100 Pa) and 293.15 the temperature in Kelvin that the samples were sealed and monitored at (K = 273.15 + 20°C).

The only other variable to determine is V (in $m^3$). The vessels sourced for this study have an internal volume of 2000 ml. The volume of the cannonball, silica gel, and datalogger (if applicable) placed within them must be subtracted. Additionally, any air displaced with the uptake of water as a result of conditioning silica gel to specific humidities must also be accounted for. One $cm^3$ of air is equal to one $cm^3$ of water, so each gram of water gained results in the loss of one $cm^3$ of air. The density of pure silica gel is 2.2 g/ml (O'Neil et al., 2001: 1523), and the amount of gel used in each reaction vessel is dependent on the size of the corresponding sample. This also means that the amount of air displacement via water uptake by the silica gel will vary by sample size. As previously stated in Section 4.4.1, accounting for mass gain of silica gel with escalating humidity was calculated following Weintraub (Weintraub). To confirm these values and to determine the amount of air displaced by water uptake, silica gel conditioned to 20% RH was measured out for each size category of cannonballs (see Table 4.2) and dried at 105°C for 3 days in a SNOL 60/300 LFN GP Laboratory Oven (+/- 0.2°C). The masses of the gel groups were measured each day using a Kern PCB 3500-2 balance (0.01g resolution) to ensure all moisture was removed. The amount of mass lost during desiccation is equal to the amount of water held by the gel at 20% RH, which in turn is equal (in ml) to the amount of air displaced by it within reaction vessels. The final mass of the gel was then divided by 2.2 to determine dry volume. Once dried, these gel masses were then re-humidified to 20% RH and weighed, with the same pre-drying values attained. The gel was then humidified to 30% and weighed, with masses matching those obtained via Weintraub, confirming rising RH mass gain calculations. Additional mass gained during conditioning to higher RH values can thus be correlated to a loss in air volume. Table 4.5 shows the volume remaining within reaction vessels at each tested RH prior to the placement of samples (and dataloggers, if applicable) within them.

| | **~6.5cm** | | **~8.5cm** | | **~9.8cm** | | **~10.5** | |
|---|---|---|---|---|---|---|---|---|
| | Used cm$^3$ | Avail. cm$^3$ | Used cm$^3$ | Avail. cm$^3$ | Used cm$^3$ | Avail. cm$^3$ | Used cm$^3$ | Avail. cm$^3$ |
| **Dry silica volume** | 597.2 | 1402.8 | 523.7 | 1476.3 | 453.0 | 1547.0 | 411.8 | 1588.2 |
| **20% water volume** | 136.2 | 126.6 | 127.9 | 1348.4 | 103.3 | 1443.6 | 94.0 | 1494.2 |
| **30% water volume** | 199.4 | 1203.4 | 183.7 | 1292.6 | 151.3 | 1395.6 | 137.6 | 1450.6 |
| **40% water volume** | 275.5 | 1127.3 | 250.9 | 1225.4 | 209.0 | 1337.9 | 190.1 | 1398.1 |
| **50% water volume** | 356.6 | 1046.2 | 322.3 | 1154.0 | 270.4 | 1276.5 | 245.9 | 1342.3 |
| **60% water volume** | 423.4 | 979.4 | 381.4 | 1094.9 | 321.2 | 1225.7 | 292.0 | 1296.2 |

**Table 4.5:** The volume of airspace available in sample jars after accounting for silica gel and water. The dry silica volume for each size was confirmed after desiccating 20% RH gel, subtracting the amount of mass lost, and dividing by 2.2.

Now that the volume of oxygen available at 20°C is known for each sample, their rates of consumption as a unit of mass (mg) can be determined. The ideal gas equation can be rewritten to determine mass of oxygen in mol:

$n = PV/RT$

Using an arbitrary daily oxygen consumption value of .3097 hPa at 20% RH for P and a cannonball diameter of 8.5 cm and volume of 321.56 cm$^3$, the conversion to daily mg consumed takes the following steps:

1) Convert hPa to Pa

.3097 hPa*100 = 30.97 Pa

2) Determine volume of oxygen available in cubic meters

   1152.11 g of dry gel required for an 8.5 cm cannonball, divided by 2.2 g/cm$^3$ = 523.69 cm$^3$

   1280 g of 20% RH silica gel – 1152.11 g of dry gel = 127.89 g of water

   2000 ml - 321.56 - 523.69 - 127.89 = 1026.86 cm$^3$ of air space

   1026.86/1000000 = 0.00103 m$^3$

3) Calculate for n

   n = PV/RT = (30.97*0.00103)/(8.314*293.15) = 1.3*10$^{-5}$ mol

4) Convert mol oxygen into mg of oxygen

   1 mol $O_2$ = 32 g

   1.3*10$^{-5}$ mol * 32 g = 4.2*10$^{-4}$ g oxygen

   4.2*10$^{-4}$ g * 1000 = 0.42 mg oxygen consumed daily

This can then be divided by the mass of the sample to determine the mass of oxygen used in the cathodic reaction for each gram of sample, or the amount of oxygen consumed, in milligrams, per day, per gram of sample.

For example, Figure 4.9 shows the acquired oxygen consumption data at 60% RH for samples #81A-3111 and #82A-2547. #81A-3111 is a Hostacor-treated, 6.4 cm diameter shot with a mass of 875.7 g. #82A-2547 is a Hostacor-treated, 10.4 cm diameter shot with a mass of 4081.0 g.

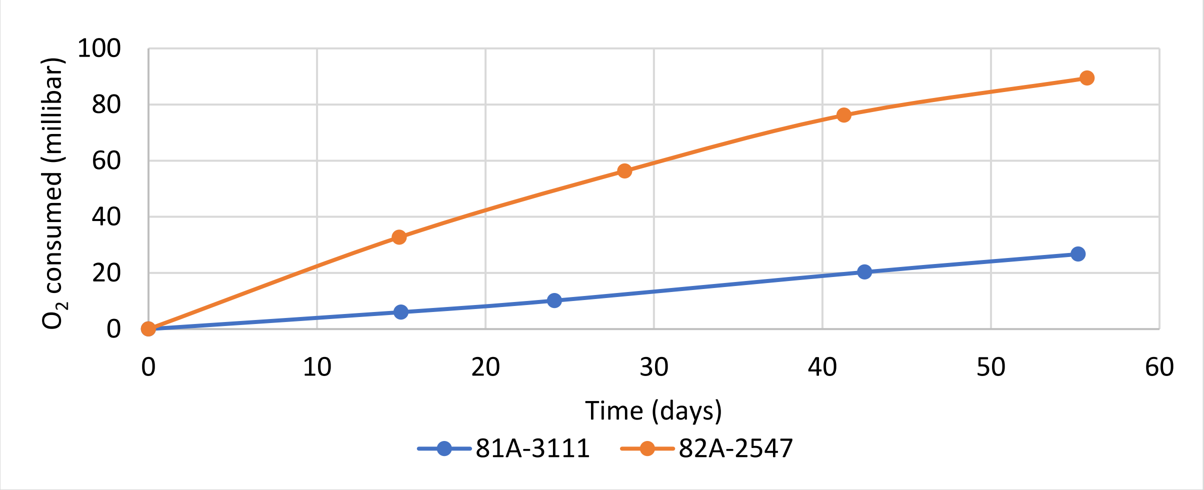

**Figure 4.9:** Millibars of $O_2$ consumed during 60% RH testing phase for samples #81A-3111 and #82A-2547. The consumption ratio is 3.4x.

The data shows the much larger #82A-2547 consuming oxygen at nearly 4x the rate of the smaller #81A-3111, at a daily value of 1.6 mbar to .48 mbar. However, the samples' difference in volume means there is less oxygen available in #82A-2574's reaction vessel, even after accounting for #81A-3111's reaction vessel containing more silica gel. When these volume differences are accounted for and millibars are converted to milligrams following steps 1-4 above, the values become closer to each other (Figure 4.10).

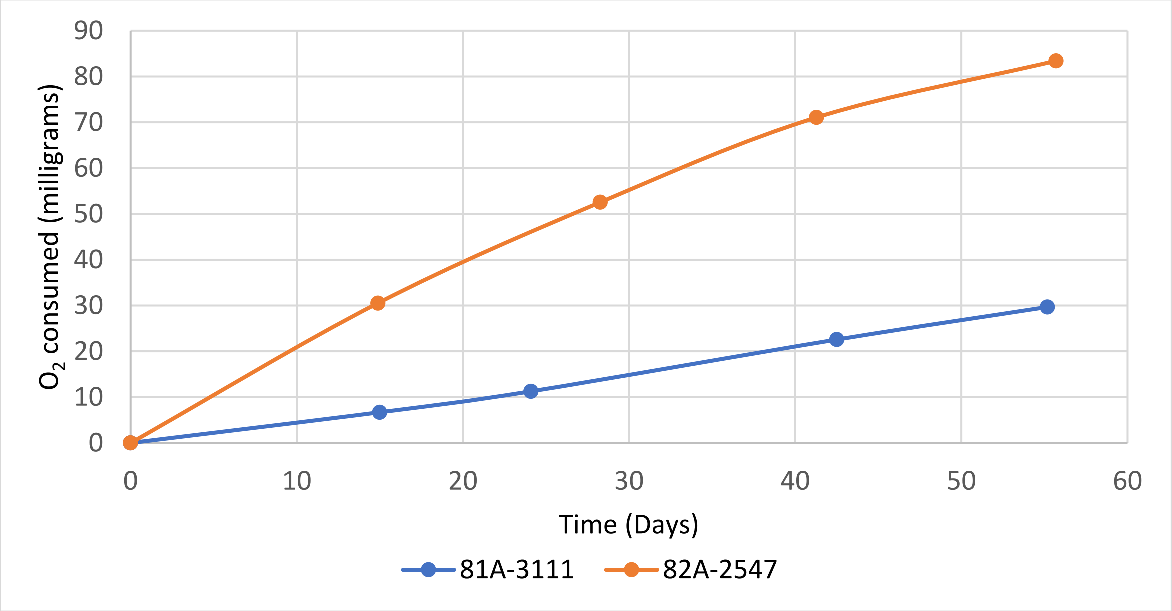

**Figure 4.10:** Milligrams of $O_2$ consumed during 60% RH testing phase for samples #81A-3111 and #82A-2547. The ratio of consumption has been reduced to 2.8x.

One would expect the 10.4 cm #82A-2547 to consume much more oxygen, as it has a larger surface area and is over 4x the mass of #81A-3111. However, to understand the comparable rates at which each is corroding in relation to each other, the oxygen consumed must be considered in terms of the *mass of the sample*. Figure 4.11 accounts for this, showing the samples' corrosion rates to be ratios of oxygen consumed per gram of sample.

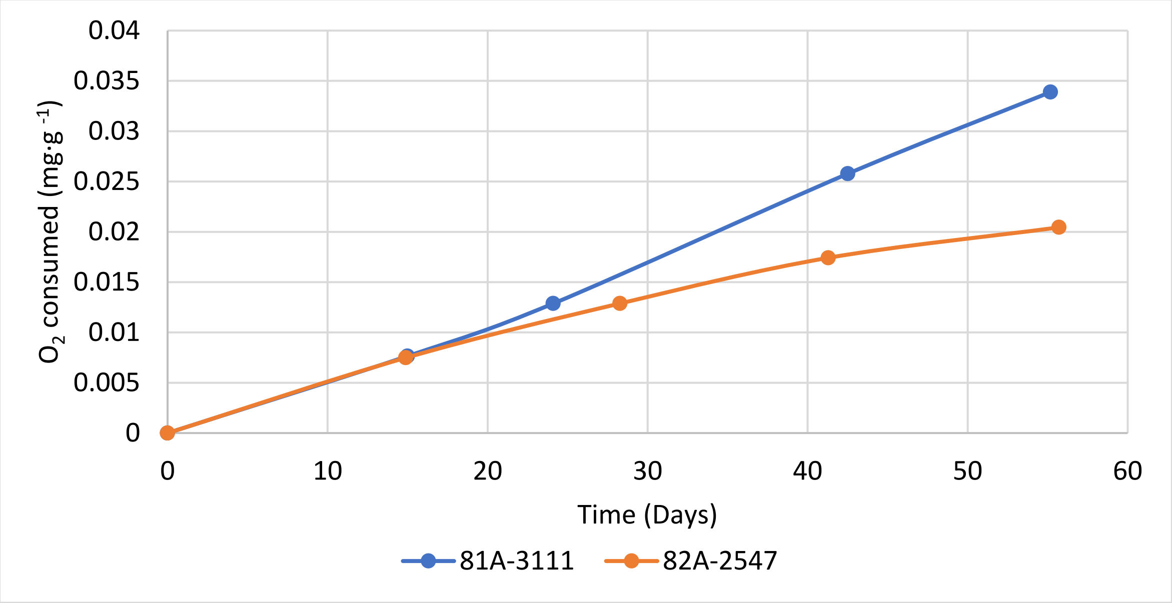

**Figure 4.11:** Oxygen consumed at 60% RH of samples #81A-3111 and #82A-2547 as a function of sample mass. The smaller sample is now shown to be corroding at a faster rate than the 4x larger sample.

Accounting for the sample masses now shows that #81A-3111 is corroding at a faster rate than #82A-2547. The slopes of the lines do not change; only their corrosion rates relative to each other do. Determining oxygen consumed per gram sample allows for a more direct comparison of the variously sized and massed cannonballs. Multiplying this figure by 365 yields milligrams consumed per gram sample per year. Standard conditions are used for all metrics, as all samples were held at 20°C over all testing parameters, and areas of Cardiff are at sea level.

It should be noted that the denser samples have a greater percentage of 'dead weight' iron in them. That is, they have a larger core mass of iron that remains in their centres below the reactive metal interface. Measuring oxygen consumption relative to a sample's mass may underreport corrosion rates for larger samples compared to smaller ones. Reporting consumption as a direct figure per object does not have this issue, though as shown in Figures 4.9 – 4.11 it does not allow for an accurate comparison between size categories.

Matthiesen and Wonsyld (2010) use an equation to measure corrosion rate in terms of depth of iron converted to corrosion product, involving molar mass ratios, metal density, the $i_{\mathrm{corr}}$, and Faraday's constant. To determine the $i_{\mathrm{corr}}$, they first determine the oxygen consumption rate (OCR) as given in mols of oxygen consumed per $\mathrm{cm}^2$ of the object's outer surface per second:

$$i_{\mathrm{corr}} = 4\mathrm{OCR}\cdot\mathrm{F}$$ **Equ. 4.2**

where F is Faraday's constant of 96,485 C $\mathrm{mol}^{-1}$ and 4 represents the number of electrons transferred to one oxygen molecule. Matthiesen and Wonsyld then convert the $i_{\mathrm{corr}}$ to a corrosion rate with the calculation:

$$\frac{\mathrm{d}s}{\mathrm{d}t} = \frac{i_{\mathrm{corr}} M_{\mathrm{Me}} \times 365 \times 24 \times 3600 \times 10000}{z\mathrm{F}\rho}$$ **Equ. 4.3**

In this equation, $M_{\mathrm{Me}}$ is the molar weight of the metal (g $\mathrm{mol}^{-1}$), $\rho$ is the density of that metal (g/$\mathrm{cm}^3$), and F is Faraday's constant (96485 C/mol). $z$ is the oxidation state of the metal, which is assumed to be $\mathrm{Fe}^{3+}$, though if $\mathrm{Fe}^{2+}$ is considered the corrosion rates would be higher. The equation calculates mass loss per unit area of the object's outer surface. However, if the remnant metal core is smaller than the external surface (evidently true for the case of cannonballs) then the equation will underestimate the corrosion rate (because the outer surface area is larger than the reacting area). The equation also assumes that all the oxygen is consumed by metal dissolution, whereas this is also incorrect where quantities of green rust containing ferrous species are present. Nonetheless the equation offers a reasonable comparator for objects of similar dimension. Note that conversion of a mass loss per unit area/time into a thickness loss per unit time would not be valid given the assumptions.

Additionally, that equation does not account for the variability in carbon content and corrosion of cast iron. The density of cast iron depends on amounts of alloying materials, particularly carbon. Grey cast iron varies between 6.8 to 7.5 g/$\mathrm{cm}^3$, and white cast iron has a density range of 7.58 to 7.73 g/$\mathrm{cm}^3$ (Angus, 1976: 113). The *Mary Rose* cannonballs contain both white and grey cast iron, though the original ratio remains unknown. As slower cooling rates favour grey cast iron (Scott, 1992: 39), the density of the shot would *decrease* with depth. When fully corroded, wrought iron contains a void where the metallic core once was, whereas cast iron leaves behind a graphite-heavy product matrix.

The metric of milligrams of oxygen consumed per gram of sample (the cannonball, in this case) per year does not assume that corrosion is simply a matter of depth, but rather a process happening throughout an object at various locations and depths (Neff et al., 2013; Simon et al., 2019).

# 5 RESULTS

## 5.1 CONTROLS

### 5.1.1 $N_2$ VESSELS

Table 5.1 shows the average daily leakage rates in mbar at each RH of the eight $N_2$ control jars used in the study. Internal RH was most likely close to 0% RH due to being filled with $N_2$ and was not conditioned to correspond with cannonball RH trials.

| | 20% | 30% | 40% | 50% | 60% | Std. D |
|---|---|---|---|---|---|---|
| **$N_2$A** | -0.163 | - | -0.111 | -0.117 | -0.120 | 0.021 |
| **$N_2$B** | -0.176 | -0.182 | -0.117 | -0.146 | -0.172 | 0.024 |
| **$N_2$C** | -0.225 | -0.298 | -0.168 | -0.172 | -0.175 | 0.050 |
| **$N_2$D** | -0.135 | -0.172 | -0.121 | -0.135 | -0.117 | 0.019 |
| **$N_2$E** | -0.204 | - | -0.138 | -0.241 | -0.215 | 0.038 |
| **$N_2$F** | - | -0.216 | -0.181 | -0.168 | -0.155 | 0.023 |
| **$N_2$G** | -0.285 | -0.243 | -0.261 | -0.222 | -0.190 | 0.032 |
| **$N_2$H** | -0.101 | -0.133 | -0.183 | -0.105 | -0.094 | 0.033 |
| **Mean** | -0.184 | -0.207 | -0.16 | -0.163 | -0.155 | |
| **Median** | -0.176 | -0.199 | -0.153 | -0.157 | -0.164 | |

**Table 5.1:** Average daily leakage rates (mbar) of $N_2$ control vessels. Mean of all $N_2$ controls = 0.172 mbar with standard deviation = 0.051. Tests with no values indicate the data was unreliable due to a sealing fault.

The results show that not only does silicone application affect ingress rates, but that the reaction vessels affect them as well. For instance, $N_2$G and $N_2$H have nearly identical standard deviations, suggesting uniformity of sealing application. Yet $N_2$G averaged a daily ingress rate of -0.240 mbar across all testing phases, whilst $N_2$H nearly half that at -0.123 mbar. However, the close standard deviation amongst all $N_2$ controls shows that seals were applied consistently, meaning that ingress rates would be approximately the same for each vessel across all RH testing intervals. The mean and median values show that seals became more effective across the course of the trial, most likely due to increased familiarity and efficiency in application.

As expected, leakage rates for the silicone seals are appreciably higher than those reported in other studies (Matthiesen, 2007; Watkinson and Rimmer, 2013; Emmerson, 2015). The figures in Table 5.1 are given in millibar, a measure of partial pressure. Assuming the leakage/ingress rates are roughly the same for the seals of cannonball-containing reaction vessels, each vessel would have different amounts of ingressing oxygen because the volume occupied by the cannonballs is different for every sample. Additionally, Table. 5.1 shows that variability across reaction vessels would be difficult to account for. Converting the mass of oxygen ingressing into the $N_2$ control vessels and applying that figure to the samples could be either a significant over-calculation or under-calculation. There is no way of telling with any certainty. However, it is important to understand the potential impact leakage rates could have on reported data. The ingress rates shown in Table 5.1 are reported in millibar and must first be converted to milligrams. Additionally, as air volume changes with sample size and displacement via conditioned silica gel, ingress rates will change according to the ideal gas law discussed in Section 4.6. For instance, if a vessel has an ingress rate of .2 mbar and the internal volume is reduced from two litres to one litre after the addition of a cannonball and silica gel, the mass of oxygen ingressing into the filled vessel would be considerably less. Knowing this, the potential impact of $O_2$ ingress into the vessels can be shown. Table 5.2 shows the daily $O_2$ ingress rate in mg at each humidity for each size category of cannonball when using the minimum (-.098 mbar) and maximum (-0.298 mbar) daily $N_2$ leakage/$O_2$ ingress rate. The +/- precision of the PreSens sensor has not been accounted for, as this varies depending on oxygen concentration in the vessel.

| | **Cannonball Diameter** | | | | | | | |
|---|---|---|---|---|---|---|---|---|
| | **6.5 $cm^3$** | | **8.5 $cm^3$** | | **9.8 $cm^3$** | | **10.5 $cm^3$** | |
| **20% RH** | 0.145 | 0.440 | 0.132 | 0.384 | 0.128 | 0.390 | 0.115 | 0.350 |
| **30% RH** | 0.137 | 0.415 | 0.125 | 0.380 | 0.122 | 0.371 | 0.110 | 0.333 |
| **40% RH** | 0.127 | 0.385 | 0.116 | 0.354 | 0.115 | 0.348 | 0.103 | 0.313 |
| **50% RH** | 0.116 | 0.354 | 0.107 | 0.326 | 0.107 | 0.324 | 0.096 | 0.291 |
| **60% RH** | 0.126 | 0.327 | 0.100 | 0.303 | 0.100 | 0.305 | 0.090 | 0.273 |

**Table 5.2:** Minimum and maximum observed potential $O_2$ ingress rates (mg/day), as determined by $N_2$ control vessels. As RH of the silica gel is increased, air is displaced by water, resulting in lower volume within reaction vessels. This means ingress rates become less pronounced with increasing RH, according to the ideal gas law.

As Table 5.2 shows, ingress rates may vary greatly as they are dependent upon several variables, and the values are in many cases larger than observed consumption rates discussed further in this chapter. Adding error bars would make readability of plots difficult and would likely not be accurate for most of the results. For this reason, error bars have not been added to any data.

### 5.1.2 SILICA GEL CONTROL

Table 5.3 lists the oxygen consumption results for the silica-filled control vessel, at 20% and 60% RH. The data clarifies that the reaction vessel components (jar, lid, silica gel, data logger) are not impacting observed data as the fluctuations are negligible and within the error of the meter. This confirms that any reduction in oxygen within reaction vessels is due solely to oxidation of the samples held within them.

| | 20% RH | 60% RH |
|---|---|---|
| **Control** | 0.0018 | -0.004 |

**Table 5.3:** Results of $O_2$ consumption monitoring of the silica control vessel. Results given in mbar/day.

### 5.1.3 DATALOGGERS

The five dataloggers recording the internal environment of reaction vessels showed that that the temperature ranged less than 1°C across all loggers and humidity values never varied more than 2.3%, meaning internal atmospheres were stable.

## 5.2 OXYGEN CONSUMPTION RESULTS

**Error! Reference source not found.** plots all oxygen consumption results from all samples. The results are given as the natural logarithms (ln, or $\log_e$) of the consumption results (in mg·year$^{-1}$·g$^{-1}$). This allows for better data readability, as there is a 10000x difference between the fastest consuming sample at 60% RH and the lowest consuming sample at 20% RH. Additionally, ln values of the results are used in Chapter 6 for data normalisation. Any gaps/breaks in trend lines are due to the consumption values being *negative,* meaning they gained oxygen during the trial. Natural logarithms cannot be obtained for negative values. Severe outliers were observed at 40% RH. These values decreased sharply at 50% RH, despite repeated tests. See Appendix A for details and results for all cannonballs used in this trial.

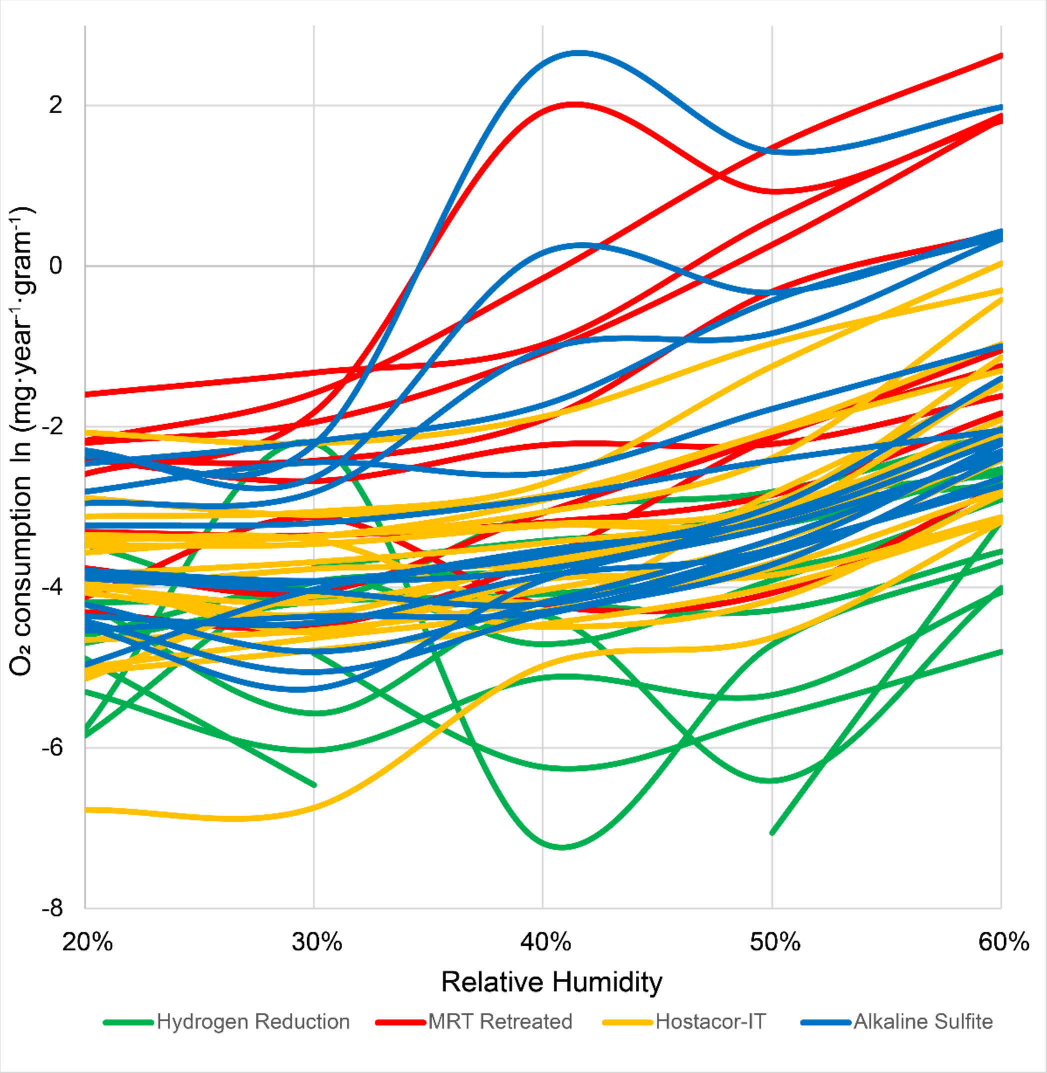

**Figure 5.1:** Results of primary $O_2$ consumption monitoring of 56 treated cast iron cannonballs from the Mary Rose. The results are shown as the natural logarithms (ln) of the yearly rate of consumption per gram of sample ($mg{\cdot}year^{-1}{\cdot}g^{-1}$). Any breaks in consumption lines indicate a sample vessel gained oxygen.

### 5.2.1 CONSUMPTION BY TREATMENT TYPE

#### 5.2.1.1 HYDROGEN REDUCTION

The oxygen consumption rates of 12 hydrogen reduction-treated cannonballs at 20-60% RH are presented in Figure 5.2 and Figure 5.3. Corrosion rates are similar and overlapping from 20% to 40% RH, though at 40%, the upper quartile is markedly higher than at 30% (Figure 5.3). At 50%, a noticeable increase can be seen in the upper two quartiles, and at 60%, every sample is corroding faster than at 50% RH (Figure 5.2). Four negative values, were observed (Table 5.4) and removed from Figure 5.2, meaning that oxygen ingressed into the vessels faster than the samples inside consumed it. This is due to either the leakage rates discussed in Section 4.4.2 and 5.1.1, those samples not consuming oxygen, or a combination of both.

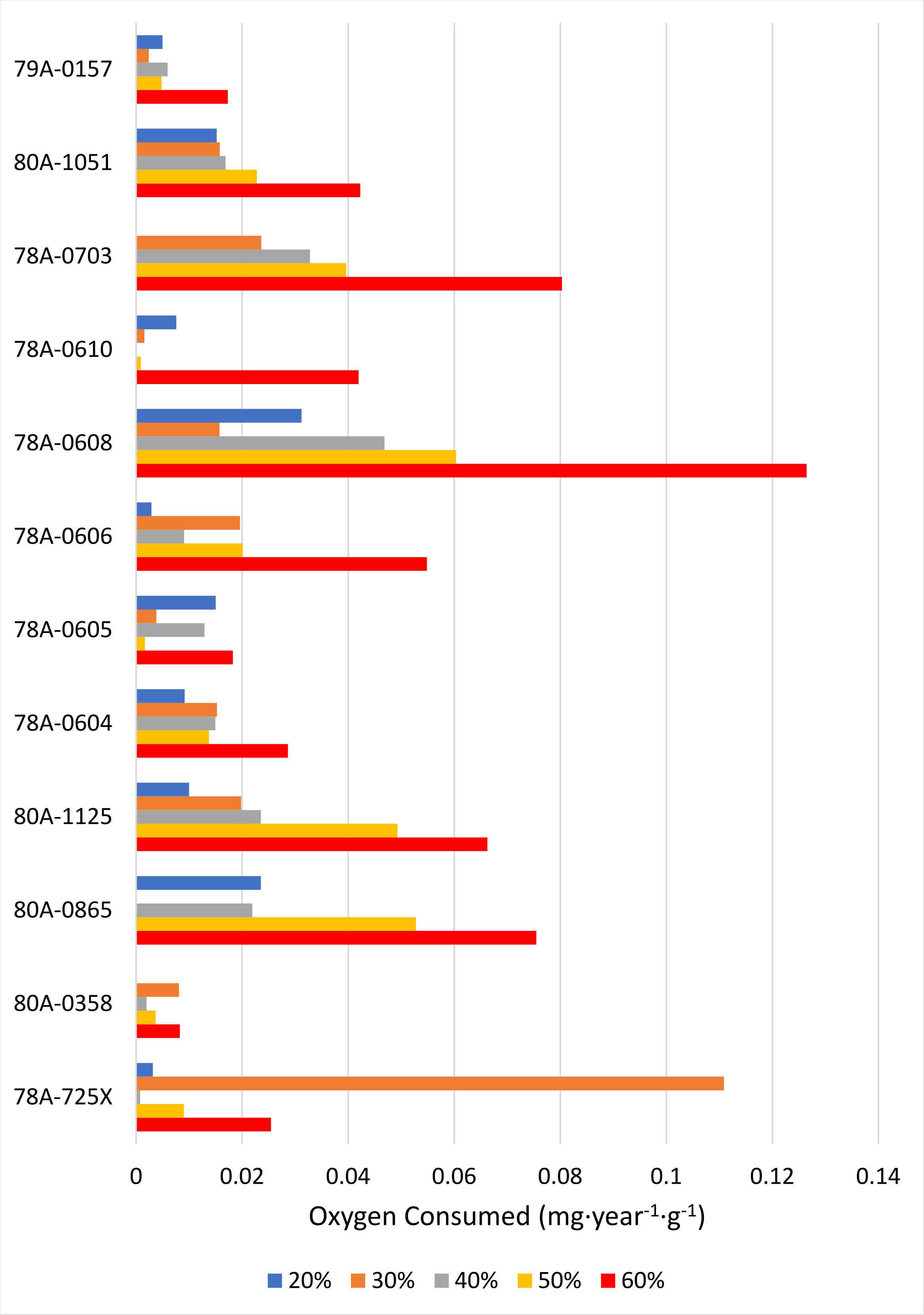

**Figure 5.2:** $O_2$ consumption rates of hydrogen-reduced samples**.** Negative values have been removed to increase readability.

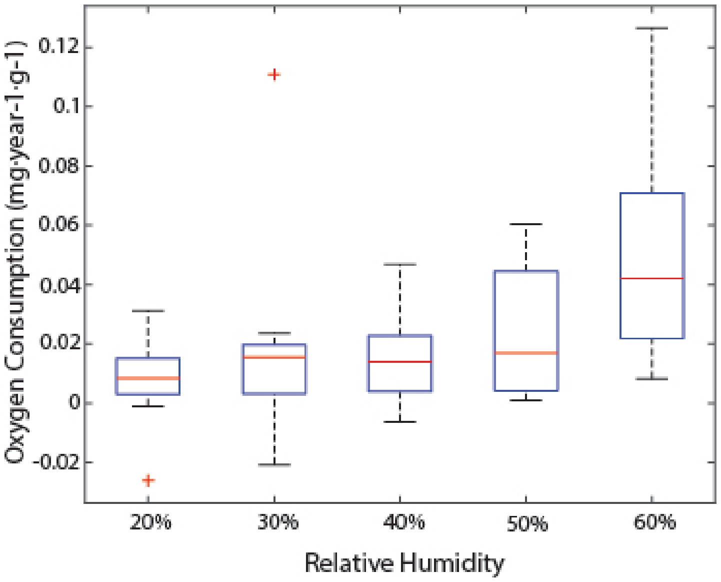

**Figure 5.3:** Hydrogen reduction $O_2$ consumption data arranged as boxplots. Note the negligible increase in the median from 20-40% RH.

| Sample# | 20% | 30% | 40% |
|---|---|---|---|
| **80A-0358** | -0.0010 | | |
| **78A-0703** | -0.0261 | | |
| **80A-0865** | | -0.0208 | |
| **78A-0610** | | | -0.0062 |

**Table 5.4:** Negative consumption values (mg·year$^{-1}$·g$^{-1}$) removed from Figure 5.2.

### 5.2.1.2 ALKALINE SULFITE

The oxygen consumption rates of 14 alkaline sulfite-treated cannonballs at 20-60% RH are presented in Figure 5.4 and Figure 5.5. Results of alkaline sulfite-treated cannonballs show near uniformity in increasing oxygen consumption as RH increases. There is negligible change between 20% and 30% RH of alkaline-treated shot. The range of oxygen consumption rates at 40% RH increases in comparison to 20% and 30% RH despite the similarity in median consumption rate (Figure 5.5). This trend continues up to 60% RH with an substantial increase in the oxygen consumption rates of the same outlying samples. One additional alkaline sulfite-treated sample was tested, though this extreme outlier was corroding at such a rate that it skewed all consumption trends significantly higher (**Error! Reference source not found.**).

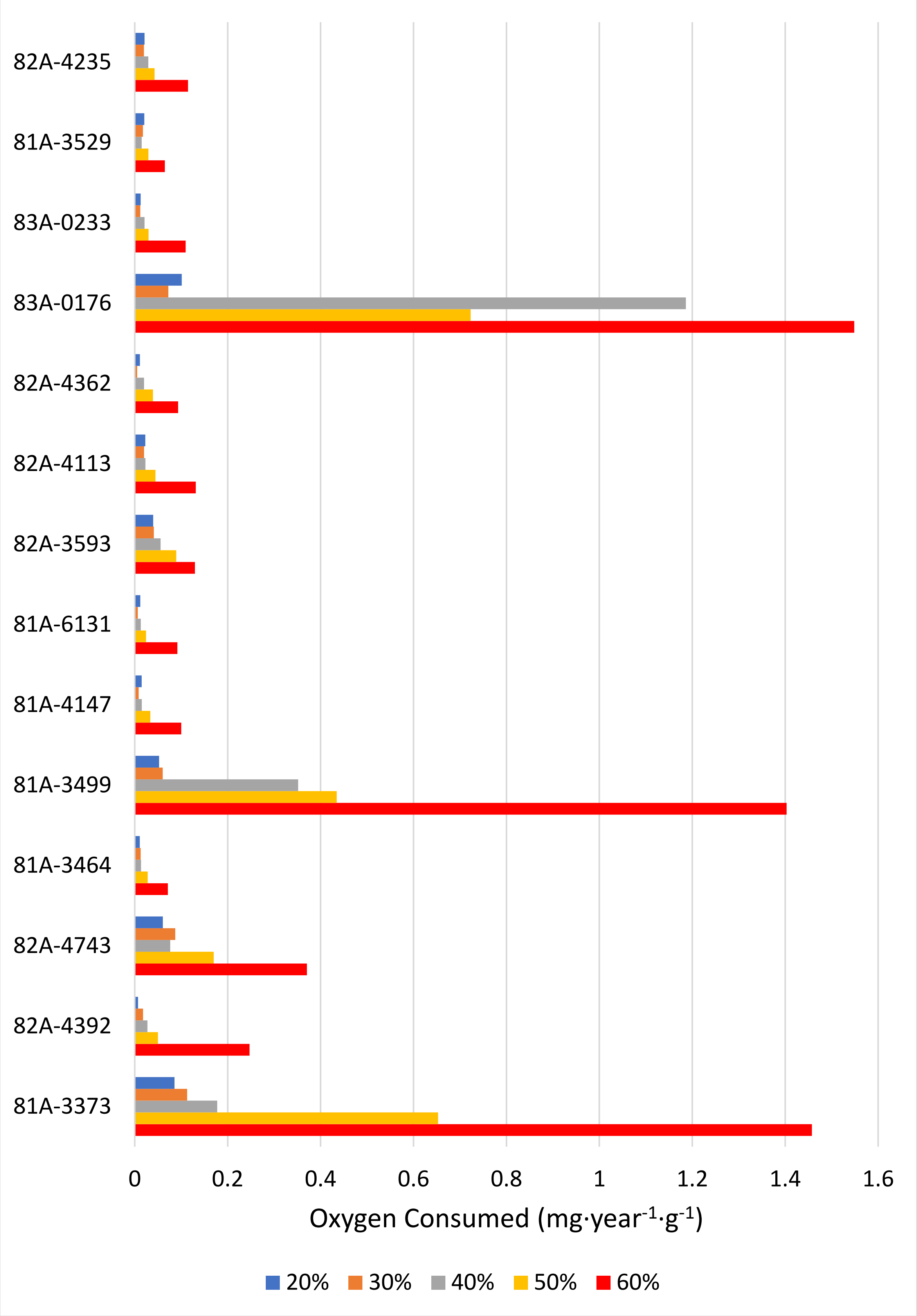

**Figure 5.4:** Oxygen consumption results of alkaline sulfite-treated samples. Sample #83A-0177 has been omitted to improve readability.

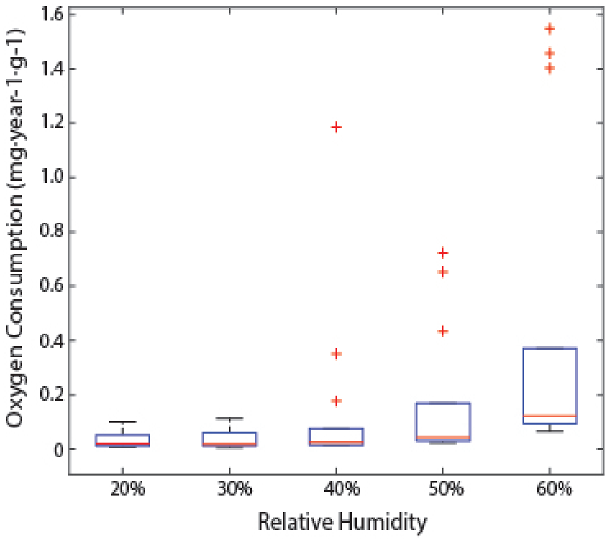

**Figure 5.5:** Boxplots of alkaline sulfite $O_2$ consumption data. Median consumption values are nearly equal from 20% - 40%, whilst rising substantially after.

| Sample # | Dia. (cm) | Mass (g) | Density (g/cm$^3$) | 20% RH | 30% RH | 40% RH | 50% RH | 60% RH |
|---|---|---|---|---|---|---|---|---|
| **83A-0177** | 8.9 | 1996.9 | 5.47 | 0.0941 | 0.1089 | 12.42 | 4.173 | 7.246 |

**Table 5.5:** $O_2$ consumption results (mg·year$^{-1}$·g$^{-1}$) for #83A-0177. The data shows the sample to be an extreme outlier when compared to other samples.

### 5.2.1.3 HOSTACOR-IT

The oxygen consumption rates of the 19 Hostacor-IT-treated cannonballs at 20-60% RH are presented in Figure 5.6 and Figure 5.7. The range, median and outlying oxygen consumption rates are similar at 20% and 30% RH, increasing slightly at 40% RH and substantially between 40% and 60% RH with values at 60% showing a 3.2x increase over 50% RH (Figure 5.7).

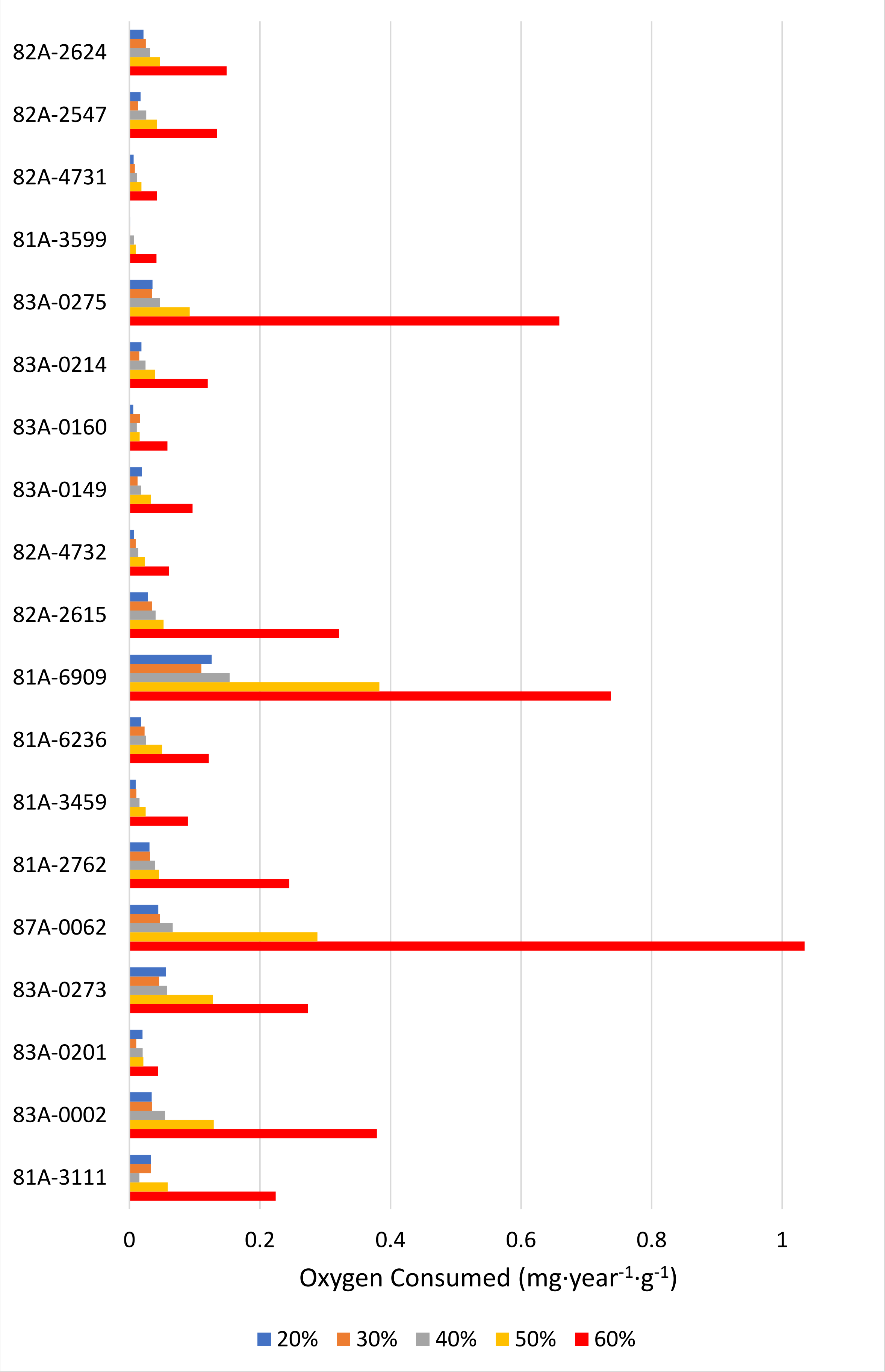

**Figure 5.6:** $O_2$ consumption results for Hostacor-IT treated samples.

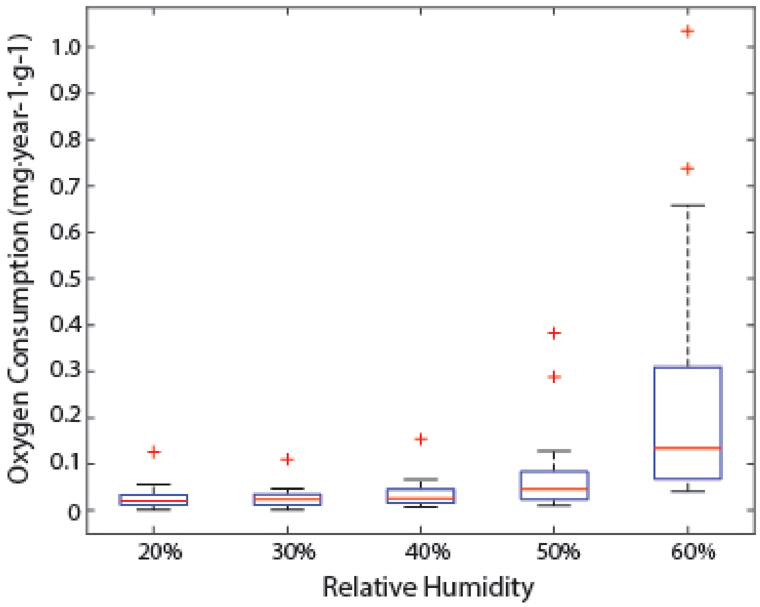

**Figure 5.7:** Boxplots of Hostacor-IT $O_2$ consumption data. Consumption ranges vary little from 20% to 40%, with substantial gains after this point.

### 5.2.1.4 MARY ROSE RETREATED

Oxygen consumption rates of 10 cannonballs that underwent multiple treatments at the Mary Rose are given in Figure 5.8, Figure 5.9, and Figure 5.10. Apart from one outlier (#82A-3594 at 40% RH), rate increases were small between 20% and 40% RH and substantially between 40% and 60% RH. There is a large range between the fastest and slowest consuming cannonballs in this group of samples with the fastest consuming cannonball at 60% RH (#83A-0180) consuming oxygen at a rate 216x that of the slowest consuming (#82A-4735).

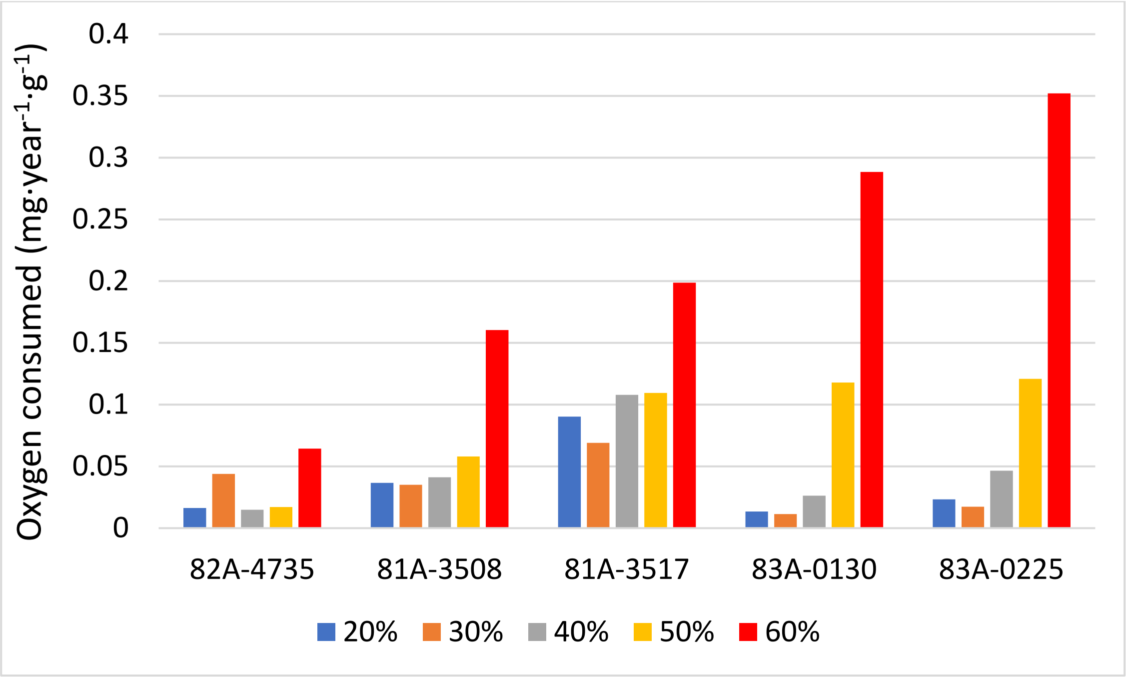

**Figure 5.8:** $O_2$ consumption results for MRT retreated samples that feature slower rates.

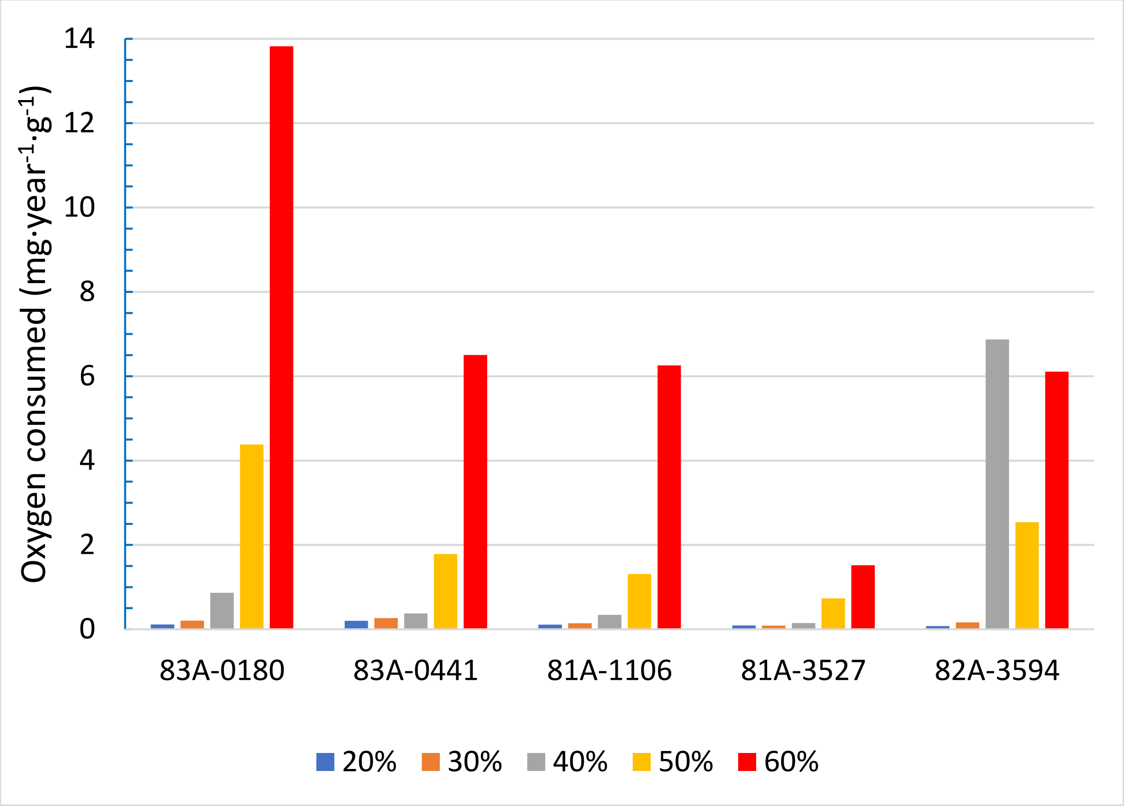

**Figure 5.9:** $O_2$ consumption results for MRT retreated samples that feature faster rates.

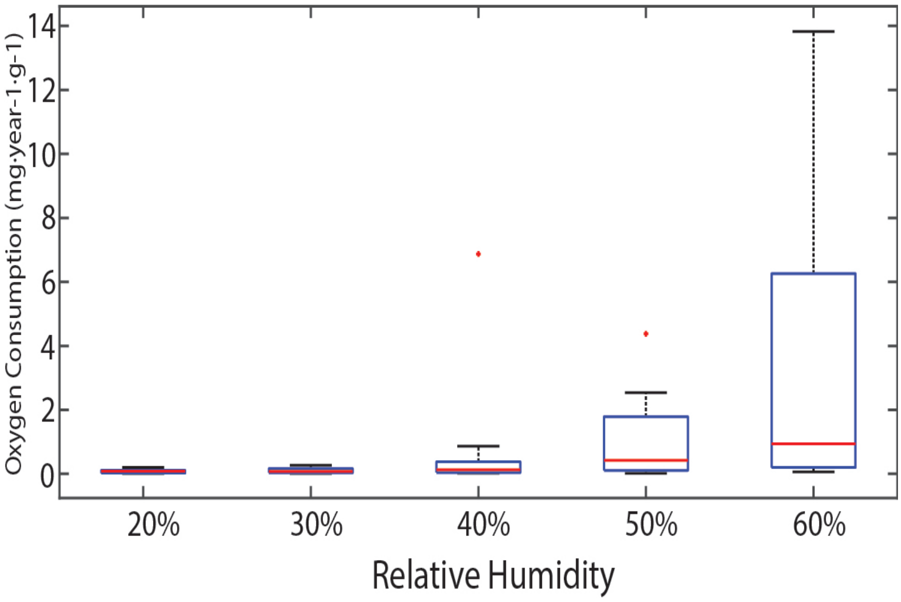

**Figure 5.10:** Boxplots of $O_2$ consumption data of MRT retreated samples. Ranges vary little from 20% RH to 30% in relation to humidities above this.

### 5.2.2 VISUAL OBSERVATIONS

The results of visual observation of change in cannonball condition following oxygen consumption rate testing are given in Table 5.6 and Figure 5.11 - Figure 5.15. Only those 12 cannonballs for which visible change was identified are included here. Damage manifested as either a widening and lengthening of pre-existing cracks, or as spalling around them, resulting in material loss.

| Sample | Dia. | 60% $O_2$ | Assessment - Arrival | Assessment – End of study |
|---|---|---|---|---|
| **83A-0180** | **6.6** | 13.82 | Object was cracked and spalling upon arrival | Spalling continued throughout; object suffered material loss (Figure 5.12) |
| **83A-0177** | **8.9** | 7.25 | Large though thin crack across its surface upon arrival | Crack widened during the trial; area around crack now out of alignment |
| **81A-1106** | **~8.5** | 6.26 | Pilot study sample; featured large cracks throughout its façade | Object suffered heavy spalling and fragmentation (Figure 5.14) |
| **83A-0441** | **6.8** | 6.51 | Deep fissures running across and through the sample upon arrival | No change during primary trial; sample cleaved in 2 following retreatment (Figure 5.15) |
| **82A-3594** | **8.7** | 6.11 | Large fissures running through the object | Object suffered spalling during the trial (Figure 5.11) and further damage during retreatment (Figure 5.22) |
| **81A-3527** | **8.3** | 1.52 | Arrived with large cracks, with areas that were beginning to spall | Cracks widened and grew in length |
| **83A-0176** | **8.7** | 1.55 | Arrived with a hairline crack running across it | Crack had grown considerably over the course of the trial and retreatment (Figure 5.21) |
| **81A-3499** | **8.8** | 1.40 | Arrived cracked | Areas are now being pushed out of plain |
| **81A-3373** | **6.8** | 1.46 | A nearly 8cm fissure was visible upon arrival | Slight growth during the course of the trial |
| **87A-0062** | **6.8** | 1.03 | Cracking visible in several areas | Cracks had widened |
| **81A-6909** | **~8.5** | 0.74 | Arrived with a hairline crack, though MRT treatment records do not say this | Crack is more noticeable following retreatment |
| **82A-2615** | **8.4** | 0.32 | Crack and potential spalling visible in one area upon arrival | No change over the course of the trial |

**Table 5.6:** Results of visual assessment of the cannonballs, upon arrival at Cardiff and at the end of the study (including retreatment). The samples listed here were the only ones that showed damage over the course of the initial trial. All of them arrived at Cardiff with at least hairline fractures, and many much more severe than that. Red = MRT RT; Orange = HC; Blue = AS. Consumption values = mg·year$^{-1}$·g$^{-1}$

**Figure 5.11:** Cannonball #82A-3594 at the start of the project (left), after the 30% RH trial (middle), and after completion of the 60% RH trial (right). All spalling sections were kept and tested with the larger whole to ensure experimental consistency.

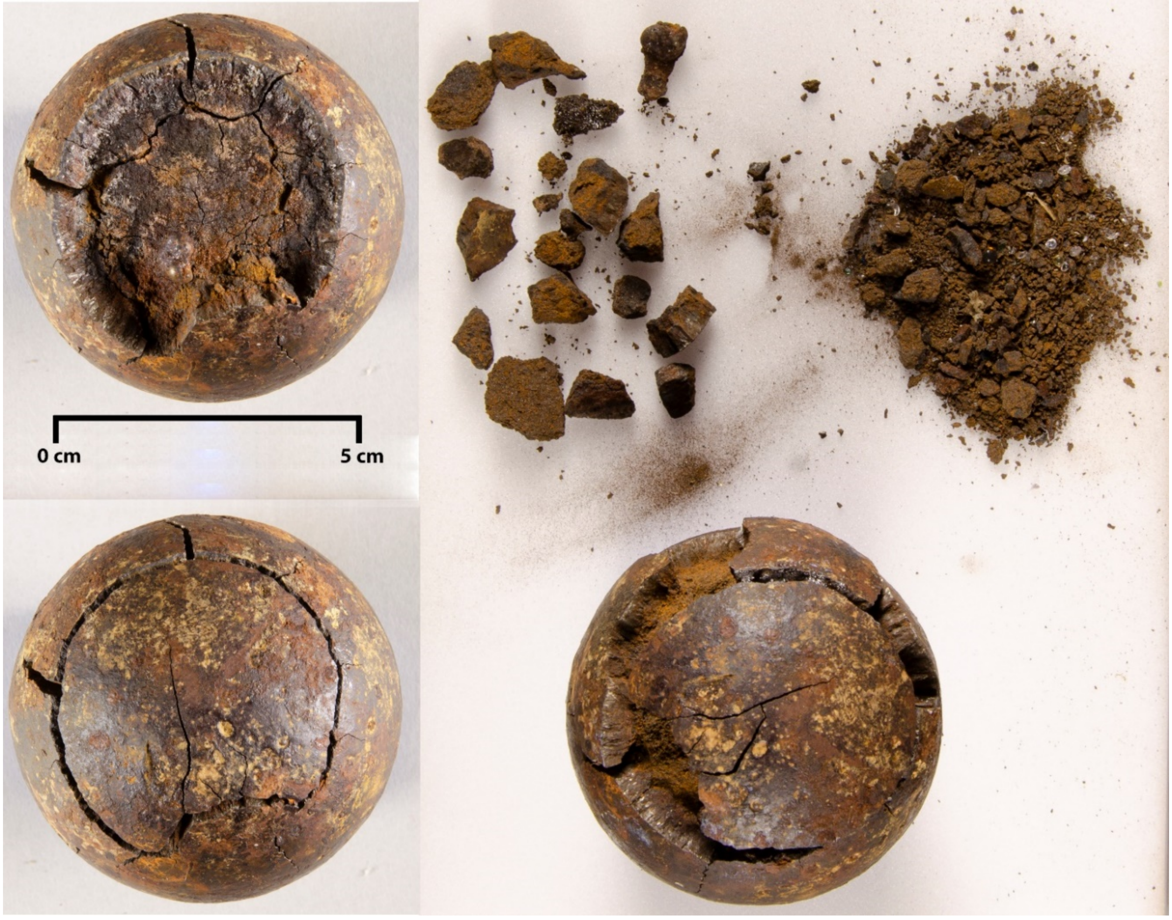

**Figure 5.12:** MRT #83A-0180 as it arrived at Cardiff University (top and bottom left) and after the 50% RH trial (right). The spalling section lifted off the shot to reveal the graphitised zone underneath. At 50% RH, the areas adjacent to this spalling also began to cleave.

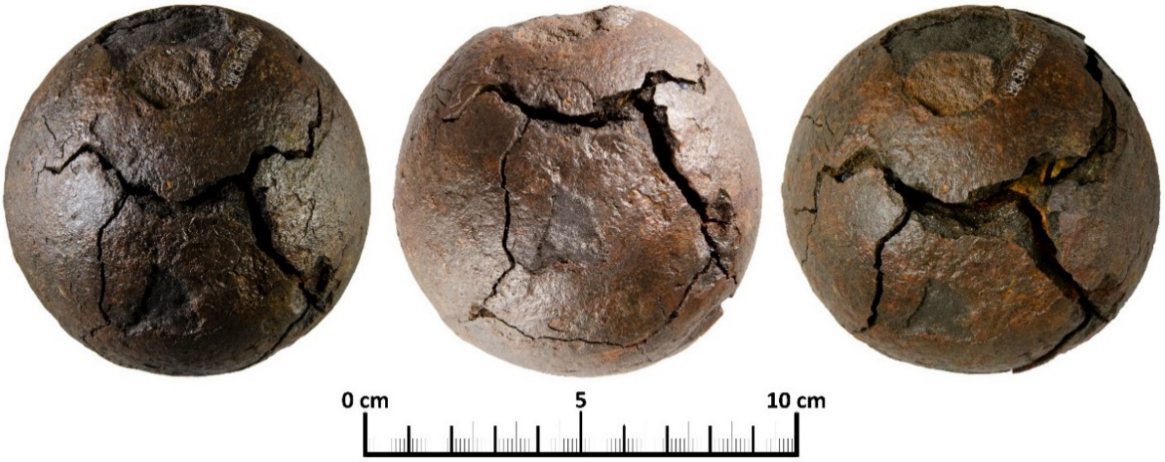

**Figure 5.13:** MRT #81A-1106 as it arrived at Cardiff in 2015 (left) at the beginning of the larger study in November 2016 (middle) and after completion of the 60% RH trial (right). The cracking has spread and significantly widened, indicating that spalling is imminent.

**Figure 5.14:** MRT #81A-1106, at the completion of the project. The cannonball began spalling along its fissures, revealing visible graphite flakes, salt efflorescence, and a powdery, voluminous orange corrosion (most likely akaganeite) underneath.

**Figure 5.15:** MRT #83A-0441, pretrial (left), after 30% (middle), and after 60% (right) RH consumption trials. Though deeply cracked, it did not show any further observable damage. #83A-0441 also consumed the 4th most $O_2$ by mass of any of the samples tested.

## 5.3 CARDIFF RETREATED CANNONBALLS

### 5.3.1 CHLORIDE EXTRACTION

The amount of chloride removed from each cannonball during Cardiff retreatment is recorded in Figure 5.16. Table 5.7 and Chloride readings of the tap water the cannonballs were placed in were taken. These ranged from 16-22 ppm, an average of 18.6 ppm which has been subtracted from the results in Table 5.7. The $Cl^-$ extraction values for the final treatment baths at the MRT, which determined when treatments had reached their end points, are also given. All cannonballs retreated at Cardiff recorded $Cl^-$ extraction values higher than those in the final treatment baths at the MRT.

| | **Sample mass (g)** | **MRT $Cl^-$ (ppm)** | **Bath 1 (mg)** | **Bath 2 (mg)** | **Bath 3 (mg)** | **Bath 4 (mg)** | **Sum (mg)** | **mg Cl/ gram** |
|---|---|---|---|---|---|---|---|---|
| **78A-0608** | **1004.2** | - | 106 | 90 | 122 | 26 | 344 | 0.343 |
| **78A-0703** | **1052.3** | - | 142 | 182 | 98 | 98 | 520 | 0.494 |
| **80A-0865** | **299.2** | - | 62 | 14 | 270 | 18 | 364 | 1.216 |
| **80A-1051** | **1149.5** | - | 242 | 162 | 170 | 46 | 620 | 0.539 |
| **81A-3373** | **852.5** | 3 | 442 | 326 | 190 | 26 | 984 | 1.154 |
| **81A-3499** | **2231.9** | - | 246 | 350 | 198 | 34 | 828 | 0.371 |

| | | | | | | | | |
|---|---|---|---|---|---|---|---|---|
| **81A-3527** | **1592.7** | 4 | 906 | 398 | 370 | 86 | 1760 | 1.105 |
| **81A-6909** | **1254.0** | - | 214 | 146 | 302 | 54 | 716 | 0.571 |
| **82A-2547** | **4081.0** | 44 | 38 | 78 | 102 | 106 | 324 | 0.079 |
| **82A-3594** | **2042.0** | 2 | 3142 | 1698 | 1782 | 214 | 6836 | 3.348 |
| **82A-4235** | **3500.0** | 2 | 38 | 78 | 82 | 18 | 216 | 0.062 |
| **83A-0176** | **2051.2** | 5 | 390 | 454 | 554 | 90 | 1488 | 0.725 |
| **83A-0275** | **1971.2** | 77 | 58 | 14 | 110 | 14 | 196 | 0.099 |
| **83A-0441** | **478.6** | 41 | 934 | 822 | 694 | 66 | 2516 | 5.257 |
| **87A-0062** | **1033.7** | 20 | 842 | 578 | 1242 | 170 | 2832 | 2.740 |

**Table 5.7:** Results of alkaline sulfite retreatment of 15 cannonballs from the *Mary Rose*. $Cl^-$ extraction figures have been multiplied 4x, since the chlorimeter gives output in ppm and the shot were desalinated in four litres of solution. The final column shows the extraction figures as a ratio of mg $Cl^-$ to sample mass (g). The final MRT $Cl^-$ readings are listed as a reference. Red = MRT RT; Orange = HC; Blue = AS; Green = HR

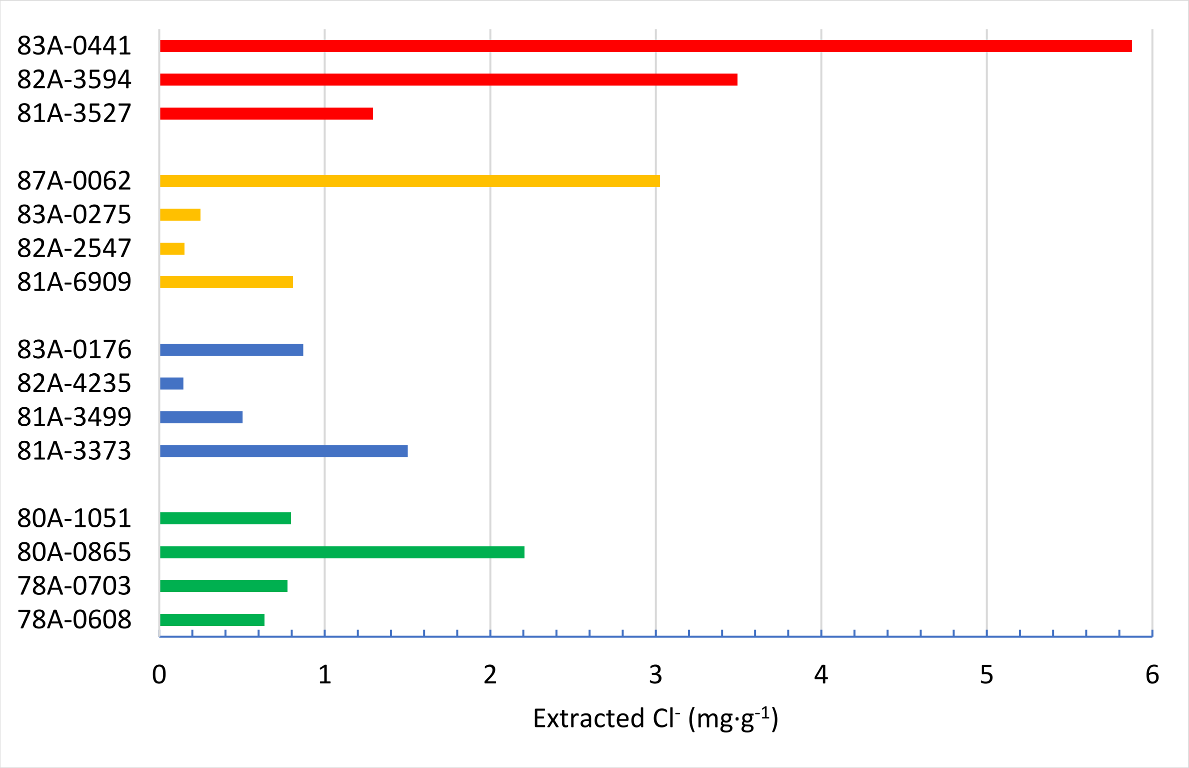

**Figure 5.16:** Chlorides extracted during retreatment of selected cannonballs. Red = MRT RT; Orange = HC; Blue = AS; Green = HR. The lower masses of the hydrogen reduced samples impacted their Cl-extraction values, as values given are a function of mass.

### 5.3.2 POST-TREATMENT DRYING

The mass loss of the cannonballs on drying at 80°C followed by 105°C is recorded in Table 5.8. Water remained in all cannonballs after their masses stabilised at 80°C which was subsequently driven off at 105°C.

| | Starting mass (g) | Mass after 80 °C (g) | Mass after 105°C (g) | Mass loss at 80 °C (g) | Mass loss at 105 °C (g) | Total loss (g) |
|---|---|---|---|---|---|---|
| **78A-0608** | 914.94 | 913.86 | 913.37 | 1.08 | 0.49 | 1.57 |
| **78A-0703** | 981.98 | 980.95 | 980.06 | 1.92 | 0.89 | 2.81 |
| **80A-0865** | 261.32 | 259.70 | 259.5 | 1.62 | 0.2 | 1.82 |
| **80A-1051** | 1119.77 | 1114.74 | 1112.9 | 6.87 | 1.84 | 8.71 |
| **81A-3373** | 850.56 | 849.50 | 848.67 | 1.06 | 0.83 | 1.89 |
| **81A-3499** | 2239.46 | 2237.34 | 2235.3 | 4.16 | 2.04 | 6.20 |
| **81A-3527** | 1595.93 | 1593.95 | 1592.35 | 1.98 | 1.6 | 3.58 |
| **81A-6909** | 1181.73 | 1177.72 | 1172.92 | 8.81 | 4.8 | 13.61 |
| **82A-2547** | - | - | - | - | - | - |
| **82A-3594** | 2039.48 | 2036.51 | 2035.04 | 4.44 | 1.47 | 5.91 |
| **82A-4235** | - | - | - | - | - | - |
| **83A-0176** | 2060.68 | 2057.64 | 2054.98 | 5.7 | 2.66 | 8.36 |
| **83A-0275** | 1973.78 | 1971.05 | 1969.09 | 2.73 | 1.96 | 4.69 |
| **83A-0441** | 463.63 | 461.08 | 459.42 | 4.21 | 1.66 | 5.87 |
| **87A-0062** | 1029.75 | 1029.55 | 1029.35 | 0.20 | 0.20 | 0.40 |

**Table 5.8:** Mass loss (in grams) of retreated shot due to oven drying, prior to $O_2$ consumption reacquisition. An appropriate balance that could accommodate the mass of #82A-2547 and #82A-4235 could not be sourced during this period of experimentation.

### 5.3.3 OXYGEN CONSUMPTION RATES POST-CARDIFF RETREATMENT

The oxygen consumption rates of Cardiff re-treated cannonballs at 20-60% RH are given in Figure 5.17 – Figure 5.20 and Appendix B. Individual rates at 60% (Figure 5.17 – Figure 5.18) are greater after retreatment for all but two samples. Hydrogen-reduced samples saw their oxygen consumption increase on average 96% over their pre-retreatment rate (Figure 5.19). Hostacor (68%) and alkaline sulfite (36%) also saw large increases in consumption values post-retreatment. MRT-retreated samples saw a decline; however, this is due to both #82A-3594 (-26%) and #83A-0441 (-31.6%) seeing their oxygen consumption greatly reduced. The boxplot distribution (Figure 5.20) show ratio increases at 50% and 60% RH far exceeding those observed during the primary data.

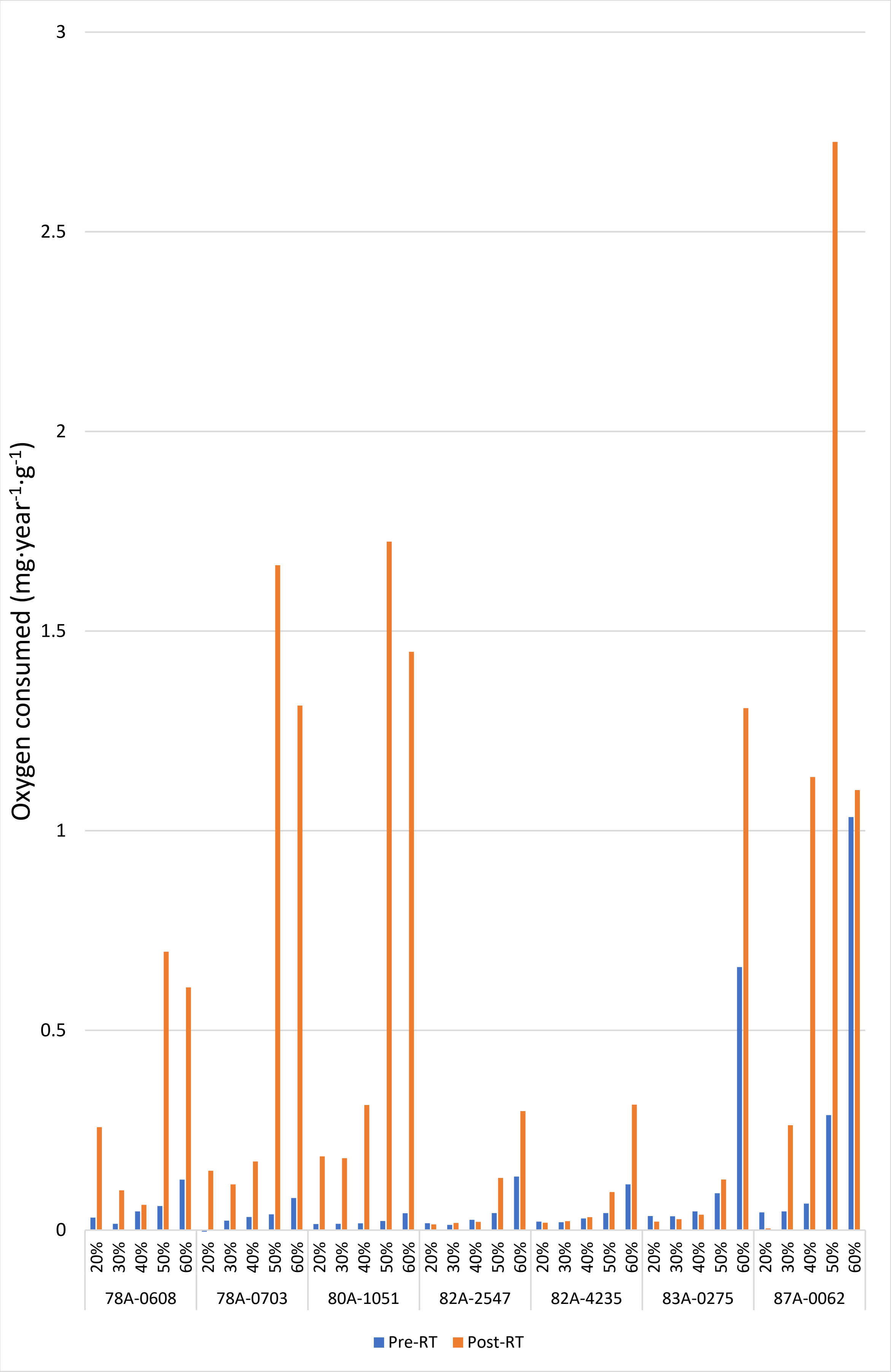

**Figure 5.17:** Pre- and post-Cardiff retreatment O2 consumption data for the seven slower $O_2$ consuming cannonballs.

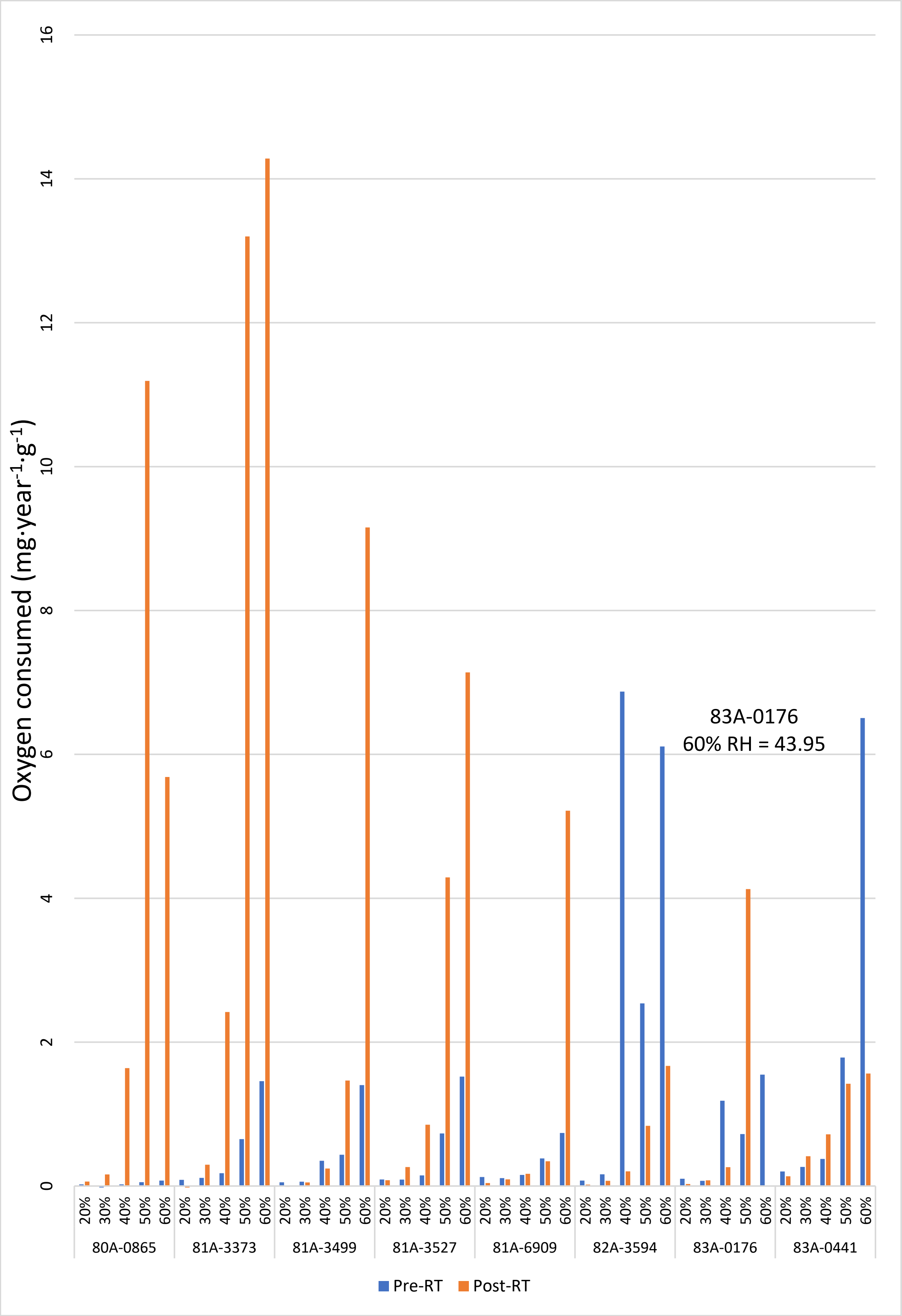

**Figure 5.18:** Pre- and post-CU retreatment O2 consumption data for the eight faster $O_2$ consuming cannonballs. The 60% RH column for #83A-0176 has been removed to improve readability.

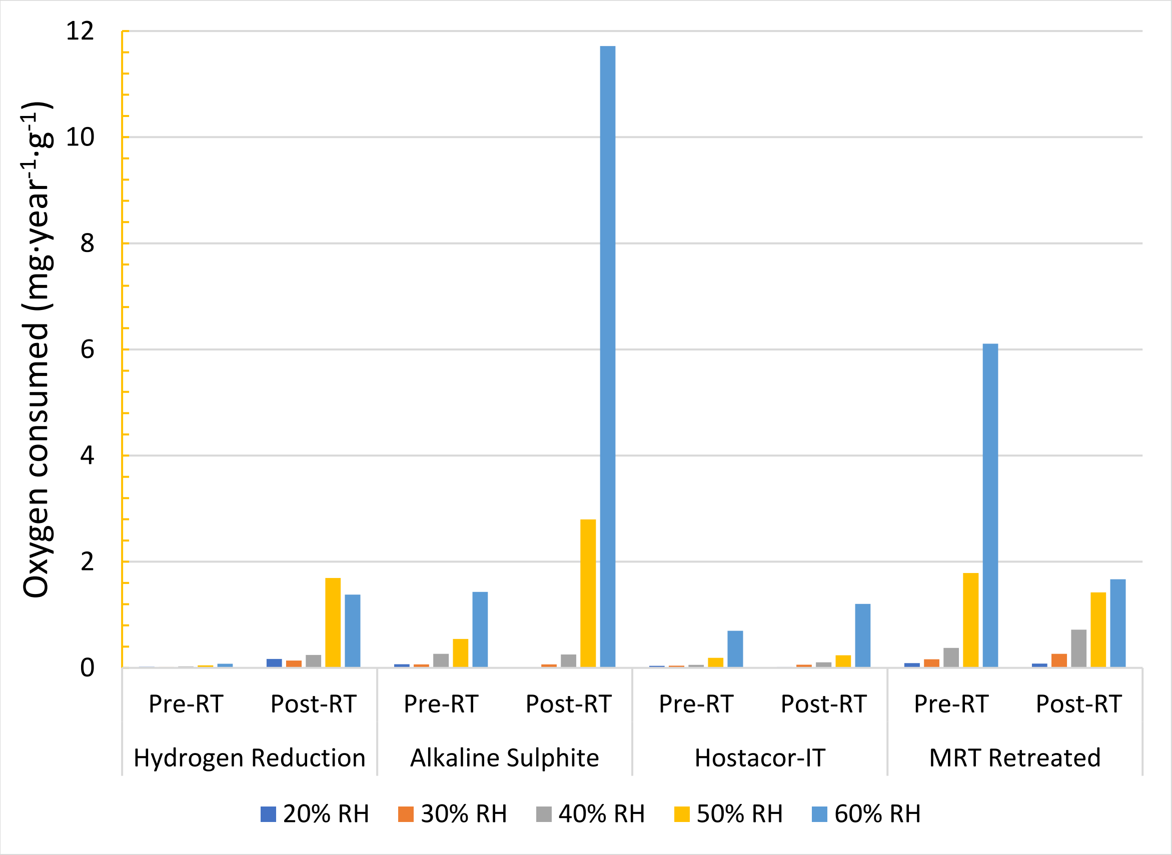

**Figure 5.19:** Pre- and post-retreatment median $O_2$ consumption rates (mg·year$^{-1}$·g$^{-1}$) by treatment type of CU-retreated cannonballs.

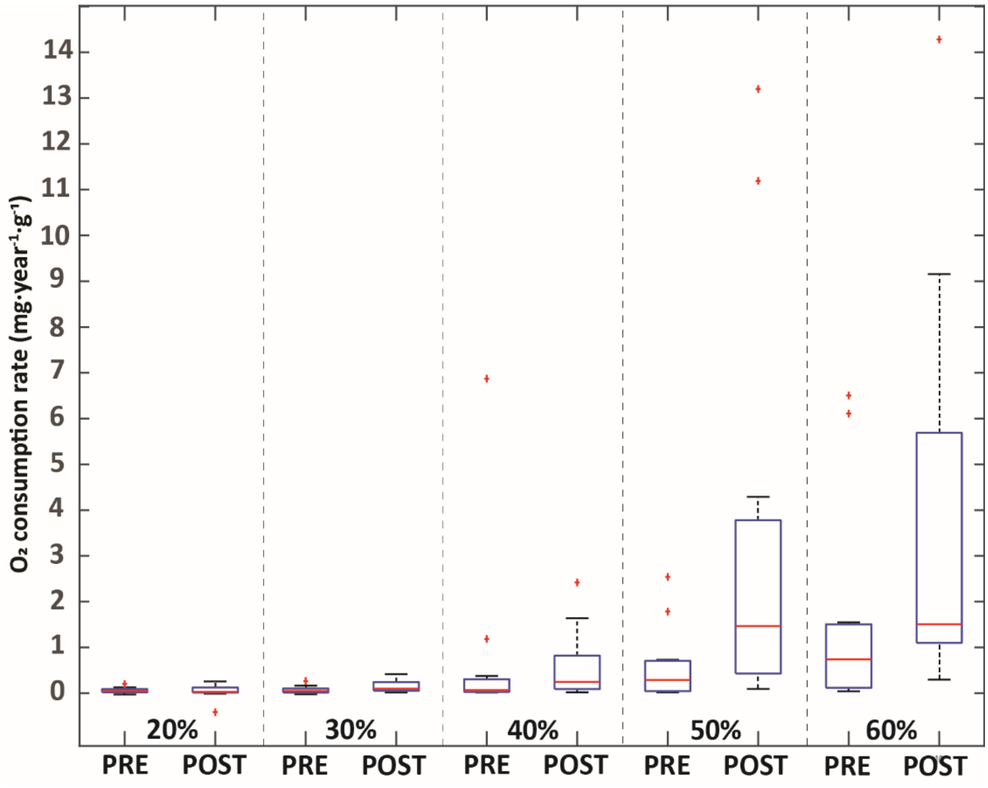

**Figure 5.20:** Boxplots of $O_2$ consumption figures pre/post-retreatment. Consumption - both overall values and medians - greatly increased following retreatment. Data for #83A-0176 at 60% RH has been removed to improve readability.

### 5.3.4 VISUAL OBSERVATIONS

The results of visual observation of change in cannonball condition following oxygen consumption rate testing post-retreatment are shown in Figure 5.21 – Figure 5.26 and Appendix B. Damage manifested as either a widening and lengthening of pre-existing cracks, or as spalling around them, and detachment of previously adhered fragments.

**Figure 5.21:** #83A-0176 upon arrival at Cardiff (left) and after retreatment (right). The thin fracture across the centre has now widened and become easily visible.

**Figure 5.22:** #82A-3594 as it arrived in Cardiff (left), after completion of the primary $O_2$ study (centre), and after retreatment (right).

**Figure 5.23:** #83A-0441 after the initial 60% RH trial (left) and after retreatment separated it into two halves (centre and right). The cannonball had previously been conserved with adhesive to hold the two halves together.

Hydrogen reduction samples underwent significant visual change including colour change. Sample #80A-0865 suffered damage almost immediately after placement in alkaline sulfite (Figure 5.24). Sample #78A-0608 exfoliated what appeared to be a concretion layer that was never removed during primary treatment (Figure 5.25). Retreatment of #78A-0703 caused its exterior to become so soft and powdery that any pressure now applied to it causes an impression and material loss (Figure 5.26).

**Figure 5.24:** #80-0865 after primary 60% RH $O_2$ consumption trial (left), and after retreatment in alkaline sulfite (right). Not only are there fissures running through the object after retreatment, it has also undergone a dramatic change in appearance.

**Figure 5.25:** #78A-0608 after primary 60% RH $O_2$ monitoring (left), and after retreatment (right). Note the loss of concretions that were not removed during initial treatment.

**Figure 5.26:** #78A-0703 after primary 60% RH $O_2$ monitoring (left), and after retreatment (right). Following retreatment, the centre area displayed is now powdery and soft to the touch.

Excluding hydrogen-reduced shot, no samples that had not already showed cracking prior to retreatment (those listed in Table 5.6) suffered any visible damage.

# 6 DISCUSSION

A rigorous discussion of the results reported in Chapter 5 addresses options for the preservation, storage and display of the *Mary Rose* cannonballs. Relating their consumption rates, retreatment efficacy, and accrued damage to best care practices to ensure their continued survival requires understanding how their treatments, post-treatment environments, and morphology (density, volume) impact their corrosion.

## 6.1 THE IMPACT OF RELATIVE HUMIDITY

### 6.1.1 RESULTS OF COMBINED TREATMENTS AND DATA INTERPRETATION

The results show oxygen consumption rates of the cannonballs escalate very little from 20%-40% RH, with rates then increasing considerably at 50% and again at 60% RH (Figure 6.1). Adjusting for mg·year-1·g-1 indicates that cannonballs treated by alkaline sulfite and Hostacor-IT have nearly identical corrosion rates. Retreated cannonballs are on average the fastest corroding objects in this study, consuming at least 7x more oxygen annually at 60% RH than those that underwent a single treatment. Though actual mg oxygen consumed by cannonballs differs by treatment type, the rate escalations at each humidity are similar. For example, hydrogen reduction treated cannonballs have the lowest median corrosion rate, yet similar rate escalation factors are observed; though consuming significantly less oxygen than other treatments, consumption rates of hydrogen-reduced cannonballs more than double from 50% to 60% RH.

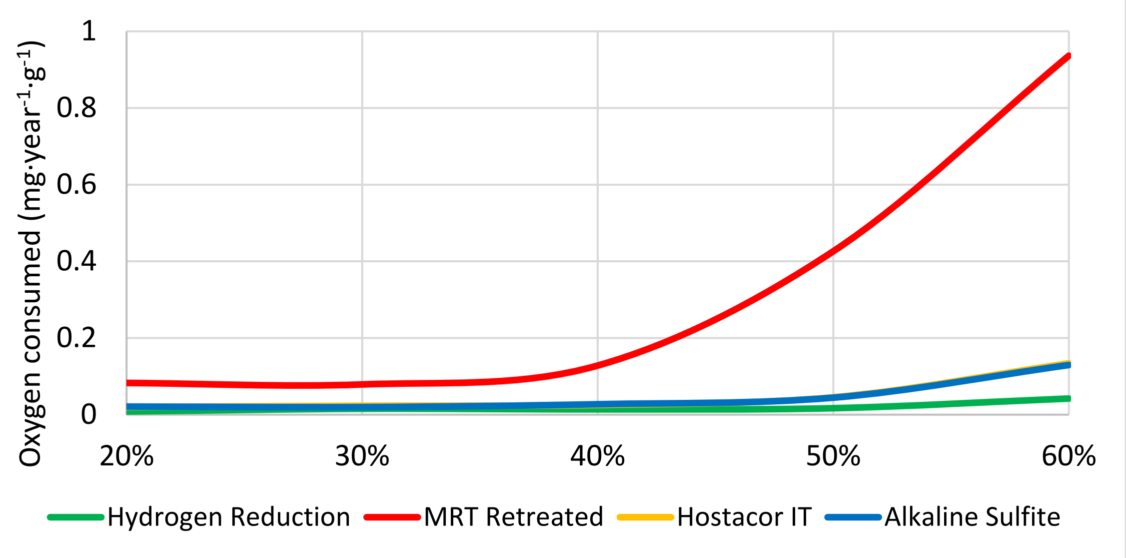

**Figure 6.1:** Median $O_2$ consumption values from 20 - 60% RH, by treatment type. Note that alkaline sulfite overplots Hostacor, as both consume nearly identical median values.

Though the impact of humidities above 40% on heritage cast iron corrosion rates is clear, it should note that corrosion rates across all treatment types follow a multiplicative scale regardless of RH, with consumption ratio values increasing multiplicatively with increasing humidity (Figure 6.2).

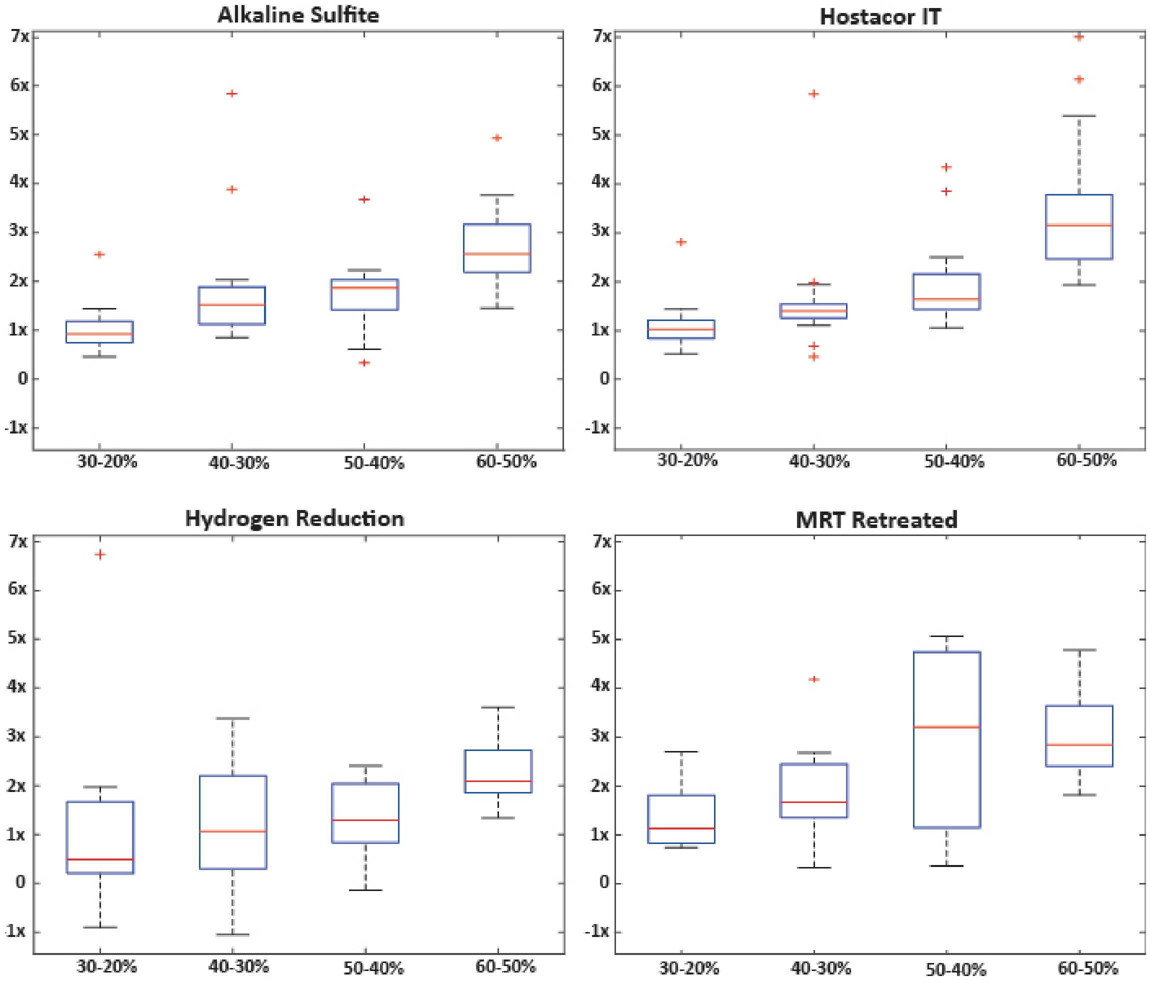

**Figure 6.2:** Boxplots of ratio increases (X-multipliers) at tested RHs over the previously tested RH value, by treatment type. Alkaline sulfite, Hostacor, and hydrogen-reduced samples show multiplicative gains with each rise in humidity. MRT retreated samples nearly follow suit, with the 50-40% plot greatly showing the largest median increase.

This escalation follows earlier research on archaeological wrought iron nails from two archaeological sites (Watkinson et al., 2019). In that instance, the authors showed that higher $Cl^-$ content could be related to higher consumption rates broadly on a site-by-site comparison; however, no correlation was found between $Cl^-$ content and oxygen consumption from nails from the same sites. Despite this, consumption escalations of both sites in that study (Figure 6.3) broadly followed the same pattern seen in Figure 6.1.

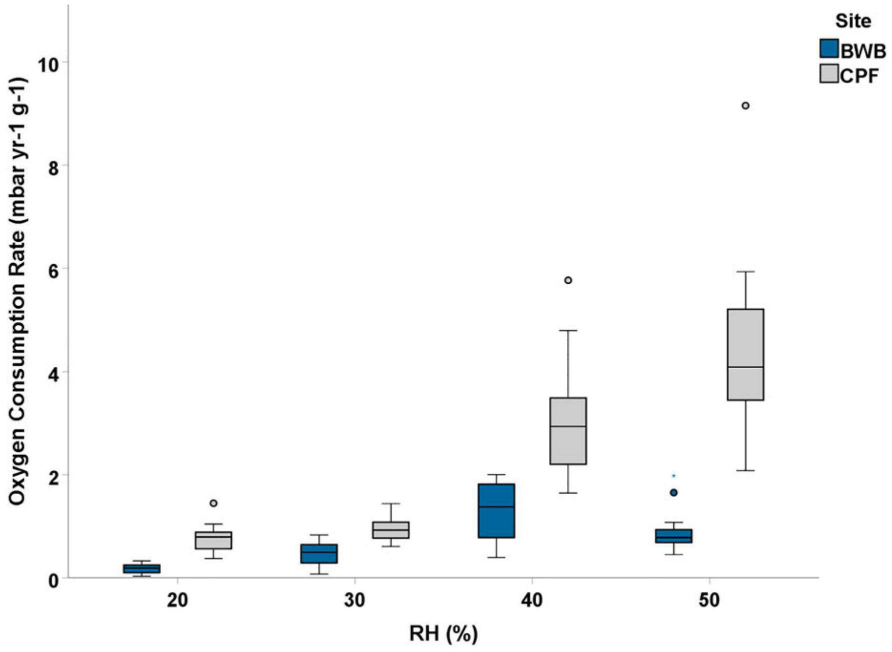

**Figure 6.3:** Oxygen consumption rates of excavated archaeological nails from two different sites. With the exception of BWB 50% data, consumption gains are shown to be multiplicative. From Watkinson et al. (2019).

Whilst Figure 6.1 shows how the median consumption values of treatments compare to each other, it does not show the relationship between individual cannonballs. Figure 6.4 is a scatter plot of the consumption test results with a regression line of best fit, as determined by linear regression analysis (Chatterjee and Simonoff, 2013: 4) and modelled using R-Studio statistical software package (R Team, 2021).

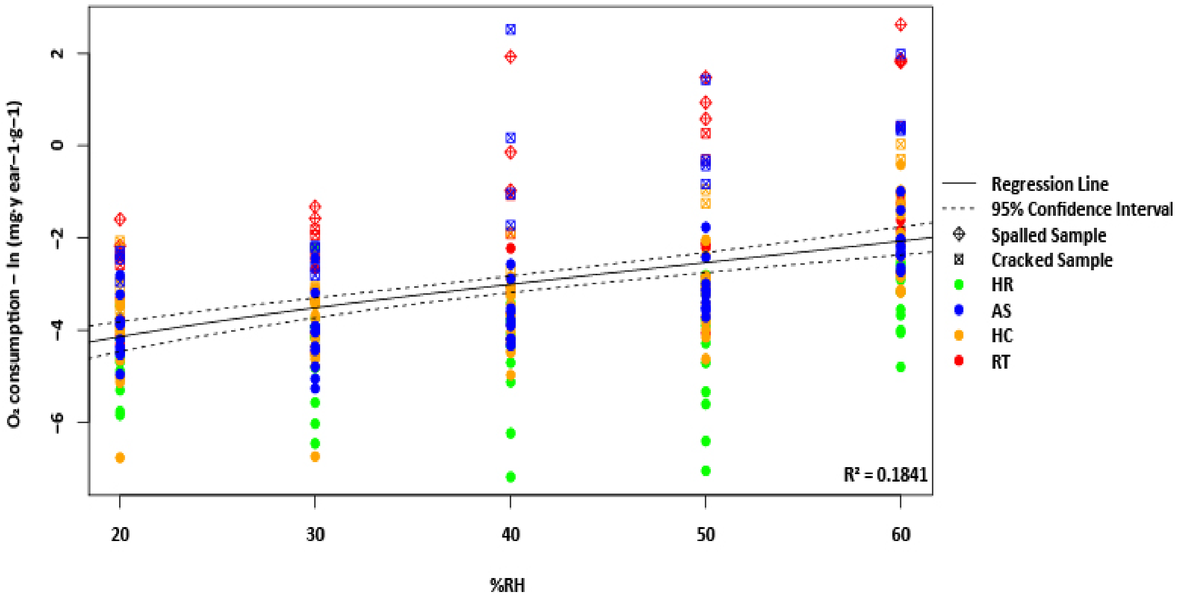

**Figure 6.4:** X/Y scatterplot of oxygen consumption values of all samples at tested RH. The data has been natural log-transformed. A linear regression line shows the median regression trend. Cracked and spalled samples have been demarcated.

Figure 6.4 is a redraw of Figure 5.1 using a different graphical format to show oxygen consumption. To prevent overplotting obscuring datapoints in Figure 6.4 these points have been adjusted along the X-axis.

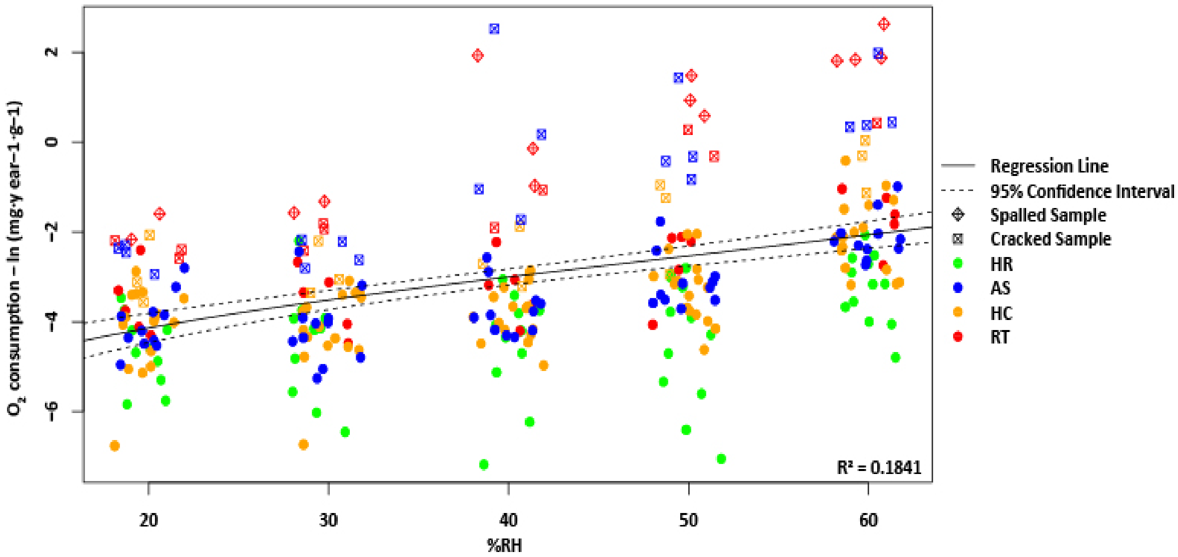

**Figure 6.5:** Linear regression model for the impact of RH on oxygen consumption values when considering all samples. The X-axis positions have been jittered to increase readability. This has not impacted the regression line.

The X-axis in Figure 6.5 does not have minor demarcations between given humidities. Data points have been 'jittered' horizontally to increase visibility, and so their exact horizontal positions are not indicative of specific RHs. All points that fall within a general RH grouping have been tested at that RH. For instance, every data point in the vertical column moving up from 40% RH was tested at 40%, rather than where their horizontal positions relative to 40% may indicate. The regression line is not impacted by their jittered positions. The data has been natural log (ln, or $\log_e$) transformed, a method used to normalise the data and change the multiplicative scale shown in Figures 6.1 – 6.2 into an additive scale. This allows for better linear regression analyses and readability (Feng et al., 2014). Even after normalising the data, humidity increases clearly impact corrosion rates, regardless of treatment type.

The mean regression line is bounded on either side by a 95% confidence interval, indicating the uncertainty about the location of the regression line. The $R^2$ value – a measure of how well the data points correlate to the regression line, on a 0 (no correlation) to 1 (perfect correlation) scale – is low, though is most likely influenced by aggressively consuming cannonballs on one end, and slowly consuming hydrogen-reduced cannonballs on the other.

Figure 6.5 demarcates cracked and spalled cannonballs, as discussed in Chapter 5.2.2, Table 5.6. Unsurprisingly, those featuring cracks or spalling are consuming the most oxygen at every humidity threshold, which results in their consumption increases with escalating humidity being greater than nearly all samples not featuring fractures.

Understanding the regression coefficients of the plot, or how rises in RH (the predictor, or independent variable) affect consumption (the response, or dependent variable), can inform on the relative impact a treatment or treatments have on oxygen consumption with escalating humidity (Darlington and Hayes, 2017). Table 6.1 shows the regression coefficients for the model shown in Figure 6.5.

| **Coefficient** | **Estimate** | **Std. Error** | **t value** | **p-value** |
|---|---|---|---|---|
| **(Intercept)** | -2.54 | 0.1115 | -22.745 | $<_{e}^{-16}$ |
| **RH (logit)** | 1.158 | 0.1458 | 7.941 | $5.21_{e}^{-14}$ |
| | | | | |
| **Multiple $R^2$:** | 0.1871 | **Adjusted $R^2$:** | 0.1841 | |
| **F-statistic:** | 63.05 on 1 and 274 DF | | | |

**Table 6.1:** Coefficients for the linear regression model when combining the results of all samples. The RH estimate is the slope of the regression line, whilst the standard error reflects the value of uncertainty (+/-). The standard error here is relatively low compared to the RH estimate, with a p-value inferring RH has a significant effect on consumption values.

The (Intercept) is the y-intercept of the regression line. The RH coefficient is the slope of the regression line, or the predicted rise in $\log_{e}$ consumption with increasing RH unit, which is described in a logit scale. Logit is used in log distributions to expand the probability of the dependent variable to obtain values from the independent variables, from negative infinity to infinity, on a straight line (Ciaburro, 2018). A logit scale goes from 0 (negative infinity) to 1 (infinity), with logit 0.5 having a value of 0. Equal values on either side of 0.5 are reciprocals of each other. For instance, a logit value of 0.6 is equivalent to 0.405, whilst 0.4 has a value of -0.405. Logits are used for better linear fitting and is advantageous to this specific discussion as the RH values (20%, 30%, 40%, 50%, 60%) can be easily translated to logit values (0.2, 0.3, 0.4, 0.5, 0.6) that can then be transformed into consumption rates (Chatterjee and Simonoff, 2013: 152). Table 6.2 shows the value of each logit number used in this analysis.

| RH VALUE | 20% | 30% | 40% | 50% | 60% |
|---|---|---|---|---|---|
| **LOGIT NUMBER** | 0.2 | 0.3 | 0.4 | 0.5 | 0.6 |
| **LOGIT VALUE** | -1.386 | -0.847 | -0.405 | 0 | 0.405 |

**Table 6.2:** Logit numbers and values used in linear regression analysis. Logit numbers represent an infinity of values on a 0 – 1 scale.

The equation for plotting basic linear regression can be used to turn logit RH coefficients into actual consumption values:

$Y = a + bX$ **Equ. 6.1**

where Y = the dependent variable ($\log_e$ of consumption), a = the intercept, b is the slope (RH coefficient) and X is the independent variable (logit RH). Plotting this equation for 20% RH gives the following value:

$\log_e$ of consumption $= -2.54 + (1.158 * -1.386) = -4.145$

This is the value of the regression line at 20% RH shown in Figure 6.5. Converting it from its natural log gives an oxygen consumption value of 0.0158 $\text{mg·year}^{-1}\text{·g}^{-1}$. Consumption variations between RH values can be determined by calculating the regression points for different RH values and determining the difference.

The standard error reflects the uncertainty (+/-) of the estimate. The standard error reflects the uncertainty (+/-) of the estimate. For the regression model of all samples, a deviation of up to 0.1458 logit RH from the coefficient can be anticipated. The t-value is the number of standard deviations away from zero the coefficient estimate is, and the further away from zero, the better the relationship between the variables (in this case, $O_2$ and RH). The t-value is the result of a t-test (a method used to compare the means of two groups to determine if one influences the data set in relation to the other) on the estimate, its standard error, and the number of samples used in the model minus one (or 56 – 1). The t-value is then used to calculate the p-value. A p-value is the probability of seeing a statistic (the t-value) as (or more) extreme as the observed value under the null hypothesis, which in this case is that the coefficient value = 0. The p-value then assumes that, if the coefficient value were to be 0, then the outcome would be the t-value or a more extreme value p% of the time. As the p-value in Table 6.1 is lower than the threshold, the hypothesis that the coefficient value = 0 can be rejected. A p-value < 0.05 is considered significant (Chatterjee and Simonoff, 2013: 5), though a p-value should also be considered in relation to whether it is meaningful in terms of what it is being applied to (in this case, the relationship between

RH and oxygen consumption). The F-statistic is an indicator of a relationship between RH and $O_2$ consumption, with the further away from zero, the higher the likelihood that the result is statistically significant. However, the test is binary (yes/no) and cannot be used to infer strength of the relationship (Chatterjee and Simonoff, 2013: 12). The results in Table 6.3 infer a significant relationship between both oxygen consumption and escalating RH when considering all samples and the value of (1.158) of that relationship.

### 6.1.2 HYDROGEN-REDUCED CANNONBALLS

Of all treatment types tested, hydrogen reduction as a group showed the slowest rates of oxygen consumption. Figure 6.6 displays consumption values for hydrogen-reduced cannonballs.

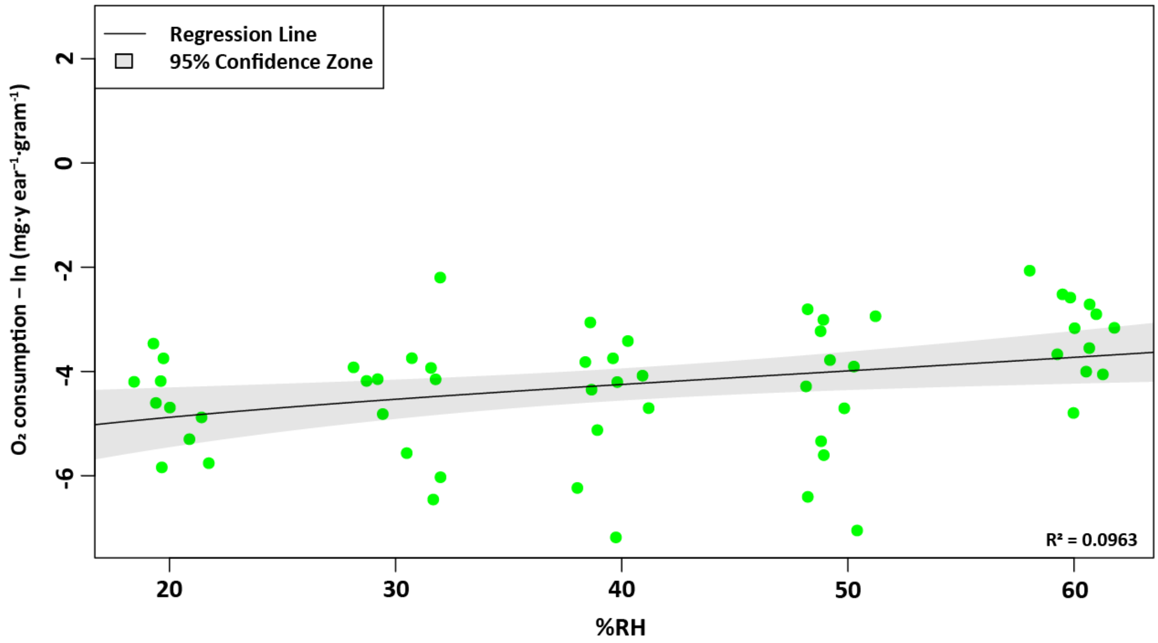

**Figure 6.6:** Oxygen consumption linear regression model for hydrogen-reduced cannonballs, with regression line and confidence zone. The X-axis positions have been jittered to increase readability.

The adjusted $R^2$ value for the regression line is low, showing the data is not explained well by a single line. However, this is most likely due to the larger variances and low consumption rates at 40% and 50%. At 60%, consumption rates have escalated and there is less variance amongst results. Table 6.3 shows the regression coefficients for Figure 6.6.

| **Coefficient** | **Estimate** | **Std. Error** | **t value** | **p-value** |
|---|---|---|---|---|
| **(Intercept)** | -3.99 | 0.1821 | -21.912 | $<2_{e}^{-16}$ |
| **RH (logit)** | 0.642 | 0.2451 | 2.619 | 0.0114 |
| | | | | |
| **Multiple $R^2$:** | 0.1127 | **Adjusted $R^2$:** | 0.09626 | |
| **F-statistic:** | 6.858 on 1 and 54 DF | | | |

**Table 6.3:** Coefficients for the linear regression model of hydrogen-reduced samples. The standard error is higher in relation to other treatment methods, most likely as a result of larger variability at 40% an 50%. The p-value and F-statistic confirm the significance of the relationship, and that the estimate is not 0.

The RH coefficient estimate shown in Table 6.3 is the lowest of any of the treatment methods tested, though its standard error is high relative to the estimate. The p-value of the relationship falls well below the 0.05 threshold, and the F-statistic confirms the coefficients are not zero.

As shown in Figure 6.5, consumption of oxygen relative to sample mass (as opposed to just mass of oxygen consumed) shows corrosion of HR-treated samples occurring at rates more comparable (yet still well below) alkaline sulfite and Hostacor, with several aqueous desalination samples consuming oxygen at a slower rate than their HR-treated counterparts. According to Kendall (1982: 80), hydrogen reduction treatment was stopped when monitored chlorides fell below 0.01M, or 354 ppm. This level of chloride in the effluent gas indicates that chloride was still being volatilised when the treatment was stopped. Therefore, chlorides are likely to remain within these cannonballs to support corrosion.

### 6.1.3 ALKALINE SULFITE AND HOSTACOR-IT

Figure 6.1 shows cannonballs treated in aqueous solutions of alkaline sulfite and Hostacor-IT display comparable rates of corrosion across all tested humidities. Figure 6.7 shows consumption results for both alkaline sulfite and Hostacor-IT, with Table 6.4 showing the coefficients when considering the results of both together.

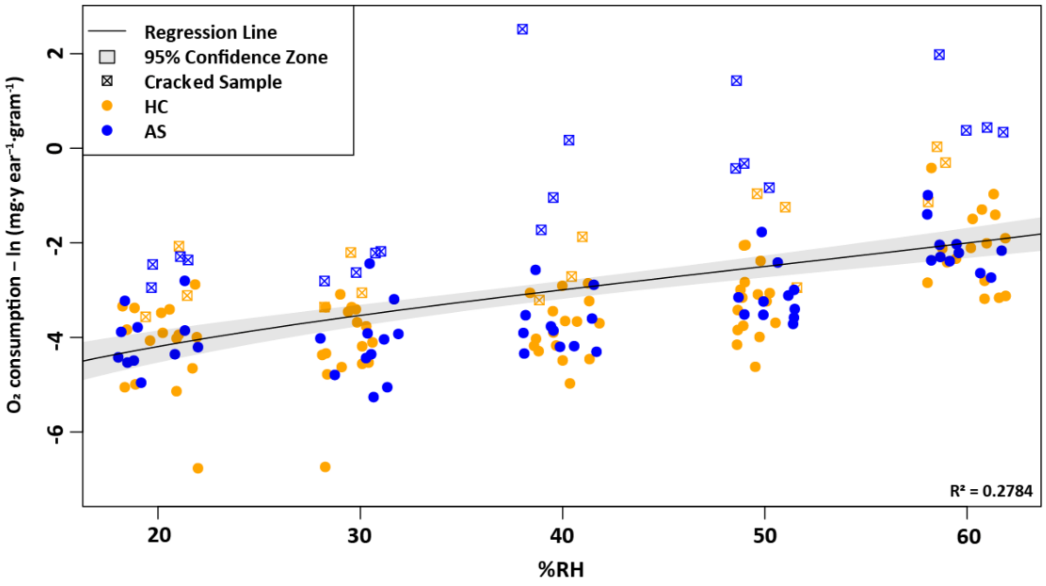

**Figure 6.7:** Combined oxygen consumption linear regression model for Hostacor-IT and alkaline sulfite, with the regression line taking into account the results of both. Data points have been jittered along the X-axis to improve readability. Note the overlapping results of the aqueous treatments.

| Coefficient | Estimate | Std. Error | t value | p-value |
|---|---|---|---|---|
| **(Intercept)** | -2.5001 | 0.1157 | -21.608 | $<2_{e}^{-16}$ |
| **RH (logit)** | 1.2217 | 0.1502 | 8.136 | $8.677_{e}^{-14}$ |
| | | | | |
| **Multiple R$^2$:** | 0.2826 | **Adjusted R$^2$:** | 0.2784 | |
| **F-statistic:** | 66.19 on 1 and 168 DF | | | |

**Table 6.4:** Coefficients for the combined linear regression model of Hostacor-IT and alkaline sulfite samples. The RH estimate and standard error are likely affected by outlier alkaline sulfite data at 40% RH. However, the impact of RH on consumption values is shown to be significant and not 0.

The results confirm the impact of escalating humidity on corrosion rates. The RH estimate coefficient is nearly double that of hydrogen-reduced samples, and the standard error is smaller both as a value and in relation to the estimate. The p-value and F-statistic confirm the significance of the results and the relationship between the consumption rates of aqueously-treated samples and rising RH. In relation to hydrogen-reduced samples, single aqueous treatments on the cannonballs were less effective by a wide margin.

The data presented in Figure 6.7 and Table 6.4 shows the performance of alkaline sulfite and Hostacor treatments when considered together. Their individual regression results show differences in their respective treatment efficacies. Figure 6.8 and Figure 6.9 show the individual consumption plots and regression lines of alkaline sulfite and Hostacor-IT respectively, with Table 6.5 showing the coefficients of the regression models. The plots and coefficients suggest Hostacor to be a more effective treatment, as both its estimate and standard error are lower than those of alkaline sulfite. However, the plots and R$^2$ values show alkaline sulfite's model is more influenced by a handful of aggressively corroding samples, as its regression line is above the bulk of results from 30% to 60% RH. Looking at Figure 6.7 suggests a parity between the efficacies of the two aqueous treatments. The RH coefficient of the combined treatments splits their individual results and features a lower standard error than both. Their individual rates feature enough error where both fall within their combined regression model, further reducing an argument for one treatment being more effective than the other.

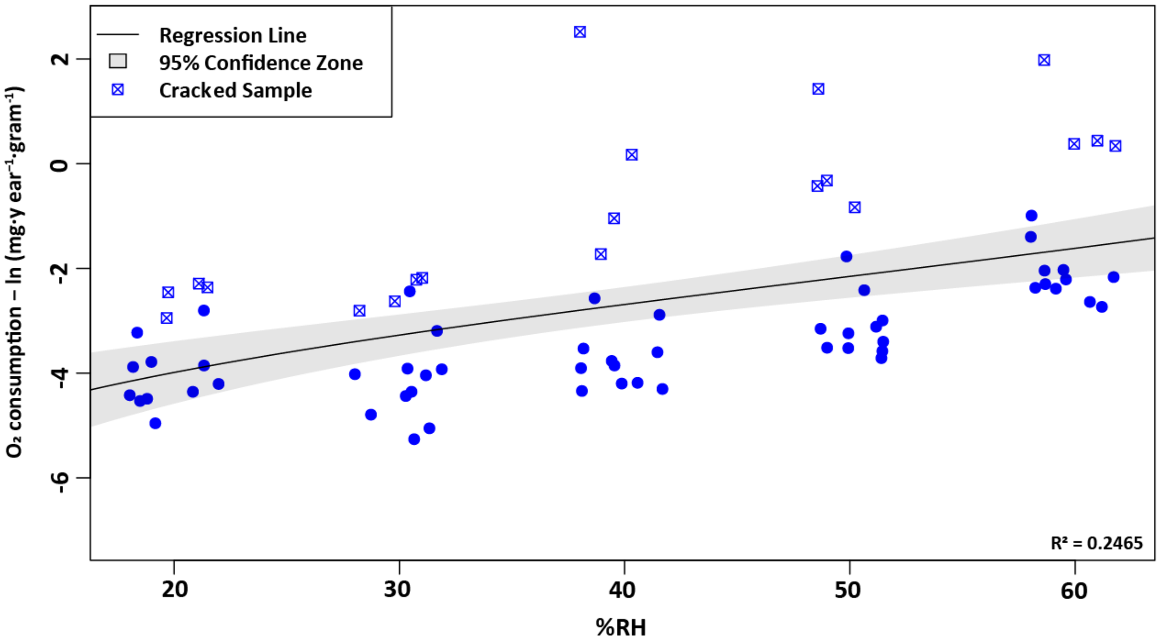

**Figure 6.8:** Oxygen consumption linear regression model for alkaline sulfite-treated cannonballs, with regression line and confidence zone. The X-axis positions have been jittered to increase readability. High consumption rates of damaged samples have influenced the regression line.

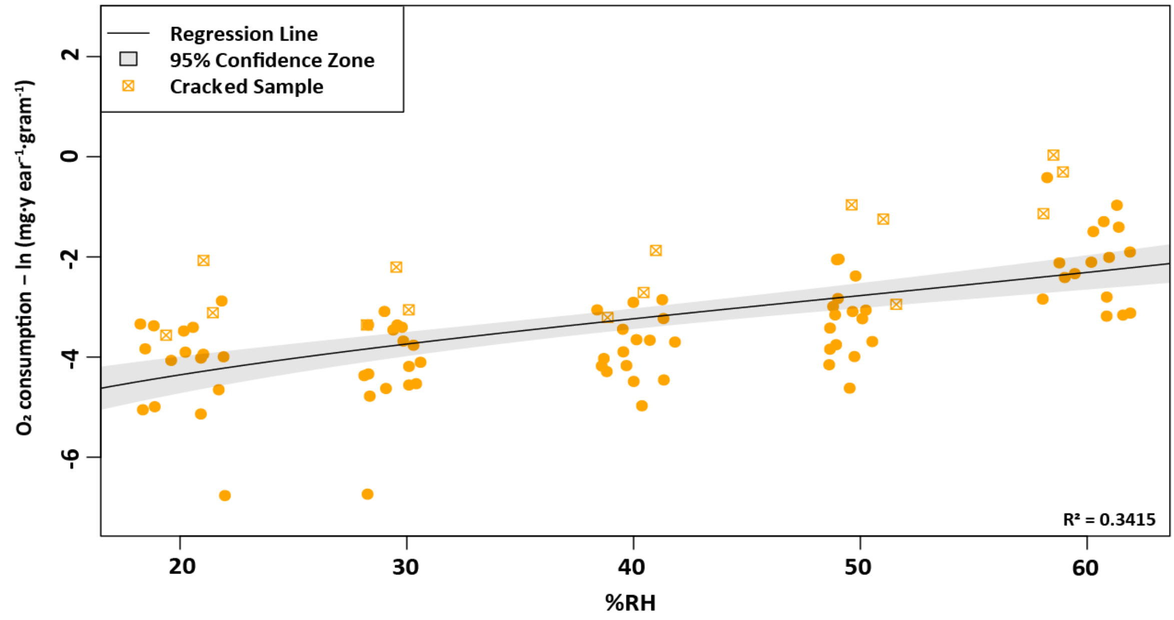

**Figure 6.9:** Oxygen consumption linear regression model for Hostacor IT-treated cannonballs, with regression line and confidence zone. The X-axis positions have been jittered to increase readability.

| | Coefficient | Estimate | Std. Error | t value | p-value |
|---|---|---|---|---|---|
| **AS** | (Intercept) | -2.1535 | 0.2031 | -10.605 | $<2_{e}^{-16}$ |
| | RH (logit) | 1.3232 | 0.2635 | 5.021 | $3.52_{e}^{-06}$ |
| **HC** | (Intercept) | -2.7736 | 0.1247 | -22.240 | $<2_{e}^{-16}$ |
| | RH (logit) | 1.1415 | 0.1619 | 7.053 | $3.05_{e}^{-10}$ |
| | | | | | |
| **AS** | **Multiple $R^2$:** | 0.2567 | **Adjusted $R^2$:** | 0.2465 | |
| | **F-statistic:** | 25.21 on 1 and 73 DF | | | |
| **HC** | **Multiple $R^2$:** | 0.3485 | **Adjusted $R^2$:** | 0.3415 | |
| | **F-statistic:** | 49.74 on 1 and 93 DF | | | |

**Table 6.5:** Individual coefficients for the linear regression models of alkaline sulfite and Hostacor IT-treated samples. Alkaline sulfite is shown to have a higher RH coefficient, as well as a larger standard error, compared to Hostacor.

### 6.1.4 MARY ROSE TRUST RETREATED CANNONBALLS

Treatment records show that all retreated cannonballs used in this study were first treated in Hostacor baths. Seven were then retreated in 0.5M alkaline sulfite baths, and three others retreated in Hostacor. Plotting these retreatments against each other shows some difference at 50%-60% RHs but is almost entirely due to #83A-0180 skewing the average curve. Removing this data point swaps the outcomes, with Hostacor consuming more than alkaline sulfite (Figure 6.10). As their consumption rates are comparable and depend on the inclusion of one sample, no distinction in treatment efficacy between the two retreatments can be made.

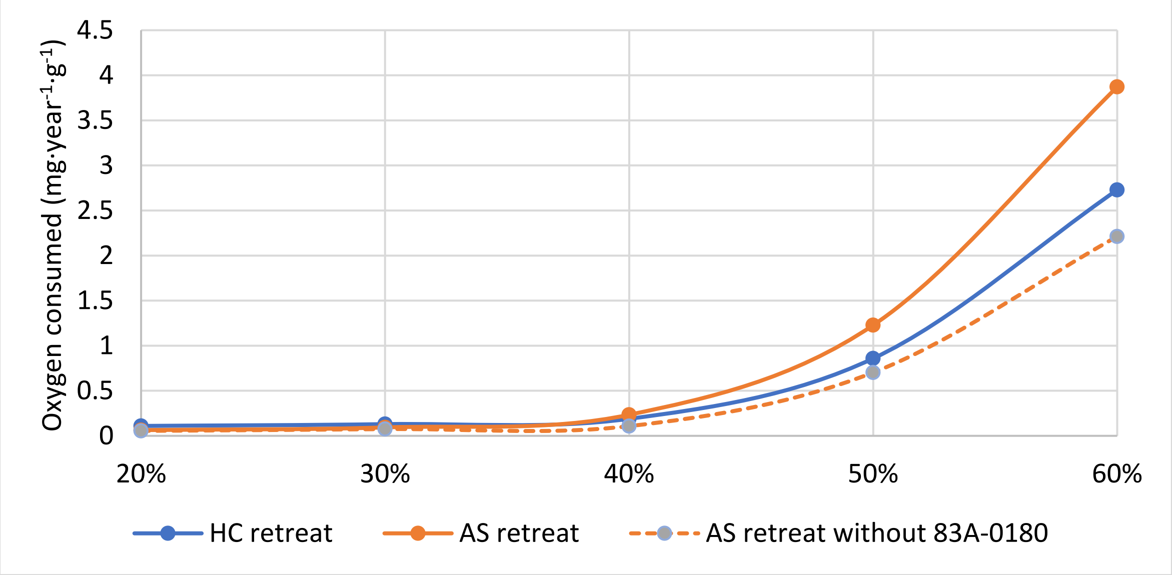

**Figure 6.10:** Mary Rose retreated samples separated by retreatment method. The results are dependent on inclusion of #83A-0180, the fastest $O_2$ consuming sample tested. Sample #82A-3594 data at 40%RH has been removed to improve readability.

The consumption model for MRT-retreated cannonballs is shown in Figure 6.11, with its coefficients presented in Table 6.6: Coefficients for the linear regression model of MRT-retreated samples. As already shown earlier, the retreated cannonballs are consuming oxygen at a rate far exceeding those that underwent single treatments. There is a wide divide between samples showing visible damage and those that do not. The large standard error and confidence zone confirm this, with the latter covering a larger range of values than the other tested treatments. This is unsurprising, as one would assume damaged cannonballs that continue to visibly deteriorate would be the highest oxygen consumers. The individual nature of each cannonball and its chloride content and the fact that these were selected for retreatment due to visible corrosion makes it difficult to attribute the faster oxygen consumption rate of these cannonballs directly to their treatment regime being less effective. However, when considering the consumption values from the Cardiff retreated shot, it is likely retreated shot are more vulnerable in higher humidities than those treated using other methods.

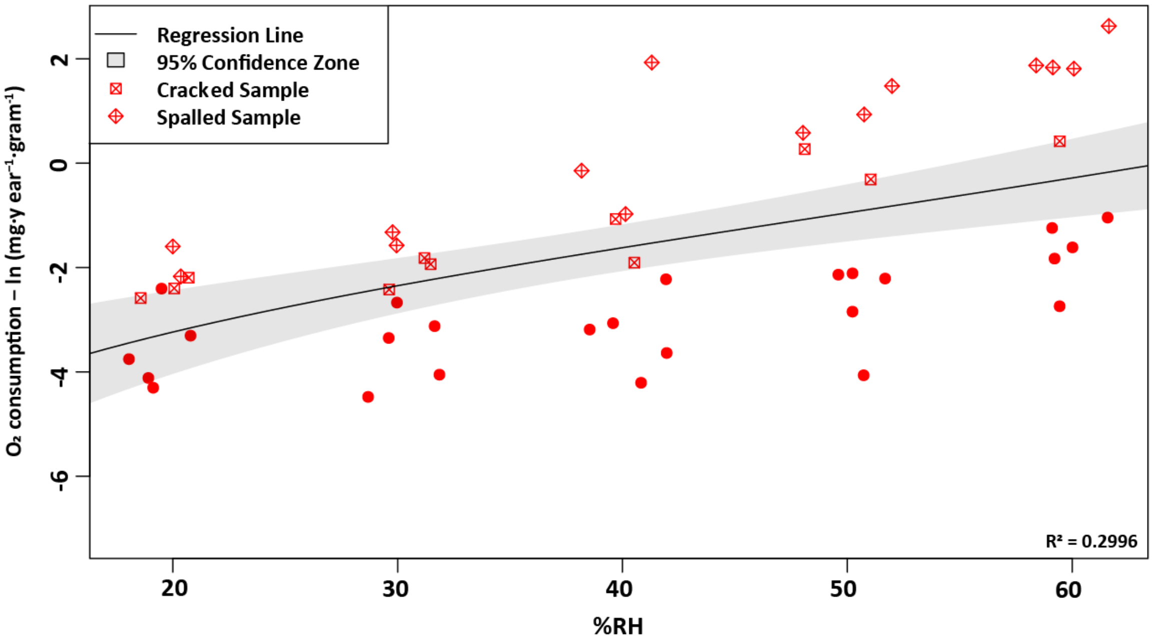

**Figure 6.11:** Oxygen consumption linear regression model for MRT-retreated cannonballs, with regression line and confidence zone. The X-axis positions have been jittered to increase readability. The regression line splits the damaged and undamaged samples.

| Coefficient | Estimate | Std. Error | t value | p-value |
|---|---|---|---|---|
| **(Intercept)** | -0.9531 | 0.2709 | -3.518 | 0.000963 |
| **RH (logit)** | 1.6477 | 0.3516 | 4.686 | $2.33_{e}^{-05}$ |
| | | | | |
| **Multiple R²:** | 0.3139 | **Adjusted R²:** | 0.2996 | |
| **F-statistic:** | 21.96 on 1 and 48 DF | | | |

**Table 6.6:** Coefficients for the linear regression model of MRT-retreated samples. Both the RH coefficient and standard error are the highest of any treatment tested.

## 6.2 IMPACT OF SAMPLE MORPHOLOGY

### 6.2.1 ALL SAMPLES

#### 6.2.1.1 DENSITY

Section 6.1 outlines how humidity impacts the corrosion rates of the cannonballs under study. However, their rates may also be impacted by their specific morphologies (volume, density). A linear regression analysis like those shown in the previous section can be used to determine whether or not morphology has an effect on corrosion rates and the consumption coefficients discussed in the previous section.

Determining the impact of morphology requires an understanding of interaction effects amongst variables. Figure 6.12 shows the consumption results for all samples, as natural log values of their yearly consumption rate (mg·year$^{-1}$), as opposed to consumption in relation to sample mass (mg·year$^{-1}$·g$^{-1}$). Earlier discussions used the mg·year$^{-1}$·g$^{-1}$ metric as a means of better comparing corrosion rates of the cannonballs to each other regardless of morphological differences. As this discussion is centred on how morphology impacts rates, discussing consumption in mg·year$^{-1}$ is more suitable. There are three separate regression lines associated with the plot: The regression line for cannonballs at average density, and the regression lines if the density of the samples plotted were increased and decreased by one standard deviation, respectively. Any deviations in slope of the +/- regression lines relative to the mean show the effect density may have. Density values are not visible in the plot but are instead factored into the regression equation.

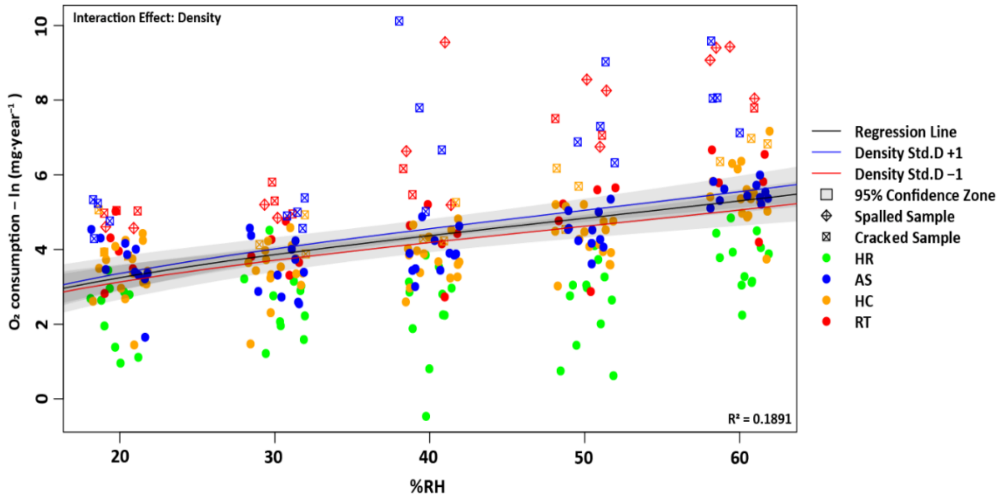

**Figure 6.12:** Density/RH regression plot for all MRT-retreated cannonballs. The X-axis positions have been jittered to increase readability. The deviations in slope as RH progresses suggest density slightly interacts with RH to affect consumption rates, though the coefficients (Table 6.7) do not bear this out.

Looking at Figure 6.12, the regression lines show that denser cannonballs will consume more oxygen than less dense cannonballs. The changes in slopes also suggest denser samples will consume oxygen in a higher ratio as humidity increases, and consumption values for lower density cannonballs will increase at a lower ratio with escalating humidity. However, the confidence zones of each regression line overplot each other, meaning any impact suggested by density may be in error. Examining the coefficients of the model (Table 6.7) will assist with interpretation.

| Coefficient | Estimate | Std. Error | t value | p-value |
|---|---|---|---|---|
| **(Intercept)** | 3.6969 | 0.5869 | 6.299 | $1.2_e^{-09}$ |
| **RH (logit)** | 0.7652 | 0.7758 | 0.986 | 0.3248 |
| **Density (log)** | 0.6620 | 0.3357 | 1.972 | 0.0496 |
| **Interaction Coefficient** | 0.2231 | 0.4426 | 0.504 | 0.6147 |

| **Multiple $R^2$:** | 0.1979 | **Adjusted $R^2$:** | 0.1891 |
|---|---|---|---|
| **F-statistic:** | 22.37 on 1 and 272 DF | **Model p-value:** | $5.61_e^{-13}$ |

**Table 6.7:** Coefficients of density/RH interaction regression model for all samples.

Table 6.7 features additional coefficients, as the regression model is now multilinear and has an additional variable. Accommodating the new variable changes the regression equation accordingly (Chatterjee and Simonoff, 2013: 38):

$$Y\ (\text{Log}_e \text{ of consumption}) = a + (b_1 * X_1) + (b_2 * X_2) + (b_3 * (X_1 * X_2)) \qquad \textbf{Equ. 6.2}$$

where a = y-intercept, $X_1$ = independent variable #1 (logit RH), $X_2$ = independent variable #2 (the log densities of the cannonballs), $b_1$ and $b_2$ are the slopes of $X_1$ and $X_2$, respectively, and $b_3$ is the interaction coefficient between the two variables (RH:Density). The value for $X_2$ changes based on the cannonball. The effect of density on the regression lines seen in Figure 6.12 is the difference in values when calculating for Equation 6.1 (coefficients without interaction effect) and Equation 6.2. For example, the model says that when plotting all results together, the effect that the density of sample #81A-3373 (5.27 g/cm$^3$, or a $\log_e$ value of 1.66) has on its consumption at 40% RH assumes the difference between:

$\text{Log}_e$ of consumption (interaction) = 3.6969 + (0.7652 * -0.405) + (0.662 * 1.66) + (0.2231 * (-0.405 * 1.66)) = $\log_e$(4.336) mg/year

and

$\text{Log}_e$ of consumption (no interaction) = 3.6969 + (0.7652 * -0.405) = $\log_e$(3.387) mg/year

for an impact of 4.336 – 3.6969 = $\log_e$ of 0.949 = 2.583 mg/year. However, that number is highly suspect, as the standard error of the RH coefficient is larger than the coefficient itself, with a t-value under one standard deviation and p-value that cannot exclude the possibility that RH has no impact on consumption rate. As evidenced by Section 6.1, this is not the case. Though the p-value of the density coefficient suggests a significant interaction, its standard error is half that of its coefficient. The interaction coefficient also features a standard error double that of its estimate and a very high p-value, indicating density does not interact with RH to affect consumption. These values are influenced by the variations amongst the sample densities, as the means by treatment range from 4.25 g/cm$^3$ (hydrogen reduction) to 6.50 g/cm$^3$ (alkaline sulfite). Any influence density may have on consumption values cannot be determined by considering all samples together.

### 6.2.1.2 VOLUME

Figure 6.13 shows the regression plots for the influence of volume when considering all samples. The coefficients are listed in Table 6.8.

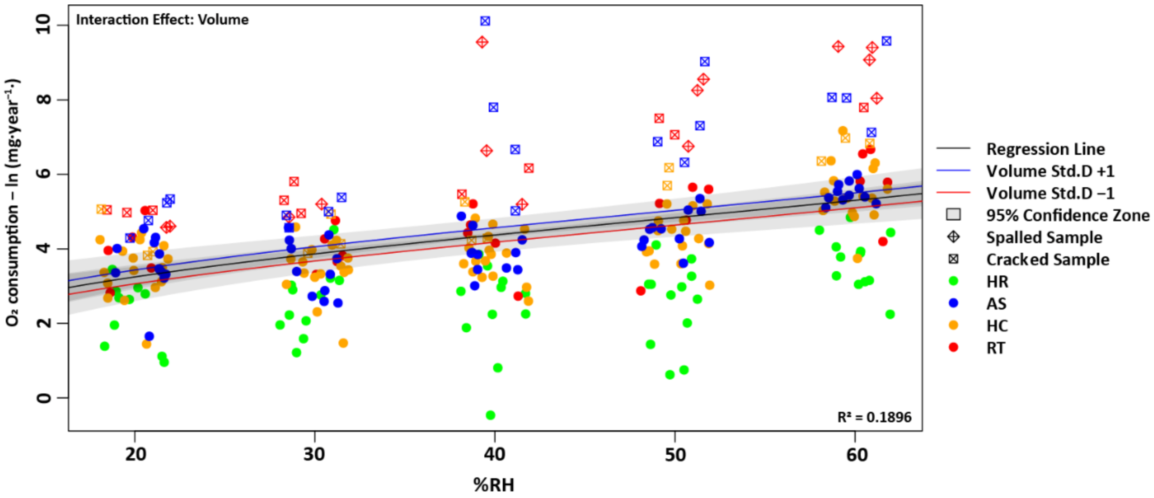

**Figure 6.13:** Volume/RH regression plot for all MRT-retreated cannonballs. The X-axis positions have been jittered to increase readability. The lack of deviations in slope as RH progresses suggest volume does not interact with RH to influence consumption values.

| Coefficient | Estimate | Std. Error | t value | p-value |
|---|---|---|---|---|
| **(Intercept)** | 2.2772 | 1.43874 | 1.583 | 0.1146 |
| **RH (logit)** | 1.0373 | 1.8788 | 0.552 | 0.5813 |
| **Volume (log)** | 0.4523 | 0.2538 | 1.782 | 0.0758 |
| **Interaction Coefficient** | 0.0194 | 0.3312 | 0.059 | 0.9533 |
| | | | | |
| **Multiple R$^2$:** | 0.1984 | **Adjusted R$^2$:** | 0.1896 | |
| **F-statistic:** | 22.45 on 3 and 272 DF | **Model p-value:** | 5.14$_{e-}^{13}$ | |

**Table 6.8:** Coefficients of Volume/RH interaction regression model for all samples.

Viewing the plot, the slopes of the regression lines are functionally identical, showing that volume does not interact with RH to impact consumption values. The coefficients confirm this, as all feature very high standard errors in relation to their estimates and corresponding p-values fail to show significant impacts on these variables. Larger samples will consume more in relation to smaller samples, though this is to be expected given that the larger the sample, the larger the reactive surface for corrosion to occur. Like density, modelling the interaction of the volume of all samples fails to show any influence on consumption rates with escalating RH.

### 6.2.2 HYDROGEN REDUCTION

#### 6.2.2.1 DENSITY

The average density of hydrogen reduction samples is 4.25 g/cm$^3$, well below any other tested groups, probably due to transformation and volatilisation of corrosion products. Conversely, the standard deviation of their log$_e$ density is the highest (0.43) out of the tested treatments. Figure 6.14 shows the density interaction regression model for hydrogen-reduced samples.

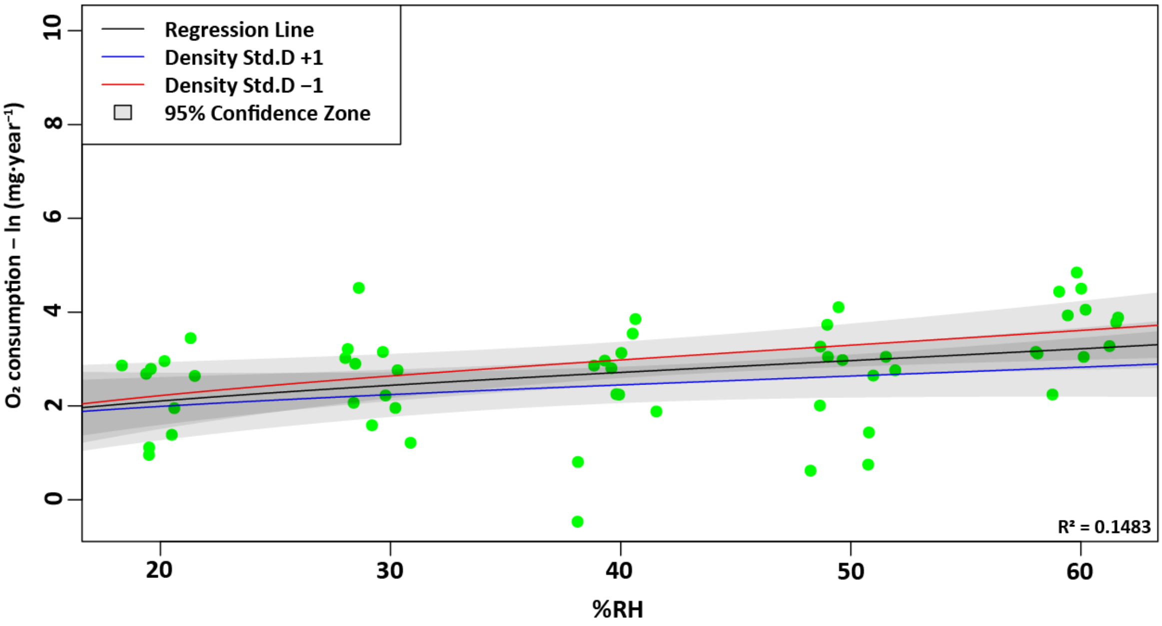

**Figure 6.14:** Density/RH regression plot for hydrogen-reduced cannonballs. The X-axis positions have been jittered to increase readability. In contrast to the all-sample model, less dense samples are shown to likely consume more oxygen rather than less.

Compared to Figure 6.12, the standard deviation regression lines are swapped, indicating that the consumption values of less dense samples increase more with rising humidity than denser samples. Overlap of the confidence zones suggests this may not be the case, though this overlap does decrease as the model progresses. Table 6.9 lists the coefficients for the regression model.

| **Coefficient** | **Estimate** | **Std. Error** | **t value** | **p-value** |
|---|---|---|---|---|
| **(Intercept)** | 3.9930 | 0.5260 | 7.592 | $5.65_{e}^{-10}$ |
| **RH (logit)** | 1.1027 | 0.6976 | 1.581 | 0.120 |
| **Density (log)** | -0.7877 | 0.3835 | -2.054 | 0.045 |
| **Interaction Coefficient** | -0.3691 | 0.102 | -0.723 | 0.473 |
| | | | | |
| **Multiple $R^2$:** | 0.1948 | **Adjusted $R^2$:** | 0.1483 | |
| **F-statistic:** | 4.192 on 3 and 52 DF | **Model p-value:** | 0.0099 | |

**Table 6.9:** Coefficients of density/RH interaction regression model for hydrogen-reduced samples. Though the density coefficient suggests a possible impact on consumption rates, the interaction coefficient t-value is too low and p-value too high to say that density interacts with RH to impact consumption values with any certainty.

The RH coefficient estimate is nearly double that of the non-interaction hydrogen reduction model, though the standard error is large, and the associated p-value shows little faith in that value. There appears to be a mild association between density and consumption values, but the standard error is again so large in relation to the estimate that it would be difficult to confirm this with the current sample size. The interaction coefficient estimate is high, though its t-value is less than one standard deviation, and its p-value suggests this value occurs by chance. Considering the samples underwent a treatment that fundamentally altered their metallography, feature low densities with a high standard deviation of that density, and their model coefficients lack significance, it is unlikely that any relationship between density and RH exists that affects the outcome of hydrogen-reduced cannonballs, as suggested by this model.

### 6.2.2.2 VOLUME

Figure 6.15 is the volume/RH interaction model for hydrogen reduced cannonballs. The model coefficients are listed in Table 6.10.

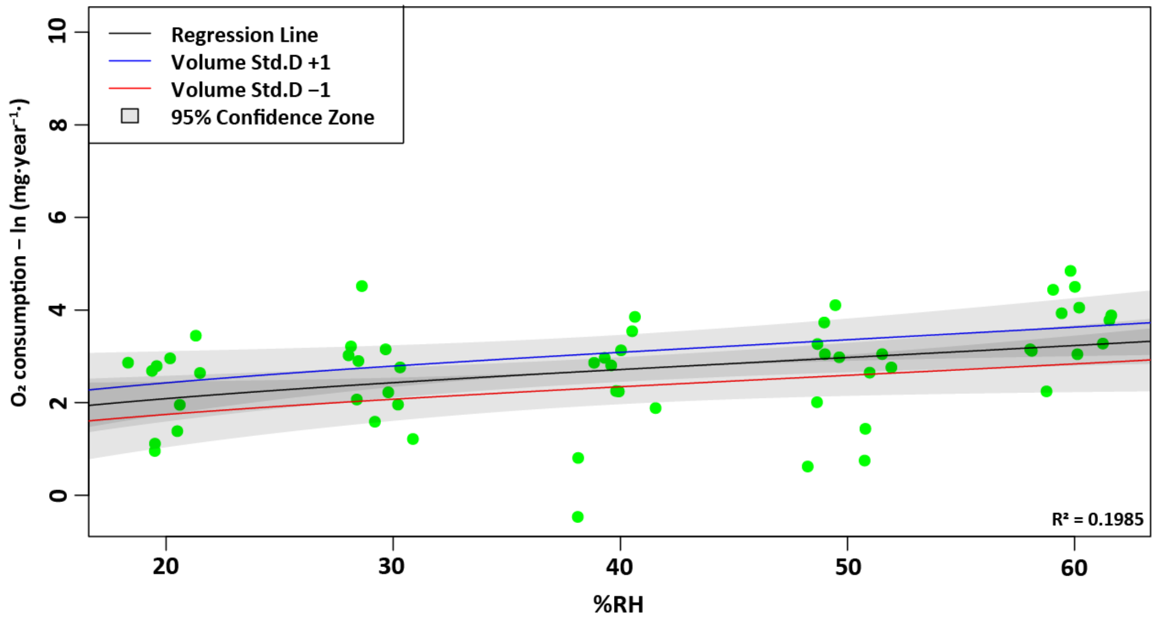

**Figure 6.15:** Volume/RH regression plot for hydrogen-reduced cannonballs. The X-axis positions have been jittered to increase readability. The parallel regression lines indicate that volume does not interact with RH to affect consumption rates.

| **Coefficient** | **Estimate** | **Std. Error** | **t value** | **p-value** |
|---|---|---|---|---|
| **(Intercept)** | -1.6625 | 1.9172 | -0.867 | 0.390 |
| **RH (logit)** | 0.2644 | 2.5593 | 0.103 | 0.918 |
| **Volume (log)** | 0.8192 | 0.3385 | 2.420 | 0.019 |
| **Interaction Coefficient** | 0.0665 | 0.4504 | 0.148 | 0.883 |
| | | | | |
| **Multiple $R^2$:** | 0.2422 | **Adjusted $R^2$:** | 0.1985 | |
| **F-statistic:** | 5.541 on 3 and 52 DF | **Model p-value:** | 0.0022 | |

**Table 6.10:** Coefficients of volume/RH interaction regression model for hydrogen-reduced samples. Though volume is shown to affect consumption values, the interaction coefficient shows that there is no interaction between volume and RH.

The standard deviation regression lines shown in Figure 6.15 are nearly identical, again showing that, though larger cannonballs will consume more oxygen, volume does not interact with RH to influence corrosion rates of hydrogen-reduced cannonballs. Though the coefficients confirm volume does affect corrosion (almost certainly due to a surface area effect), it does not interact with RH to influence corrosion rate escalations in hydrogen-reduced cannonballs.

### 6.2.3 ALKALINE SULFITE AND HOSTACOR-IT

#### 6.2.3.1 DENSITY

The average density of samples used for this study treated with Hostacor is 6.4 g/cm$^3$ (log$_e$ standard deviation of 0.13), which comparable to the 6.5 g/cm$^3$ for alkaline sulfite-treated samples (log$_e$ standard deviation of 0.11). Figure 6.16 shows the density/RH regression model when considering both aqueous treatments together, with Table 6.11 displaying the model coefficients.

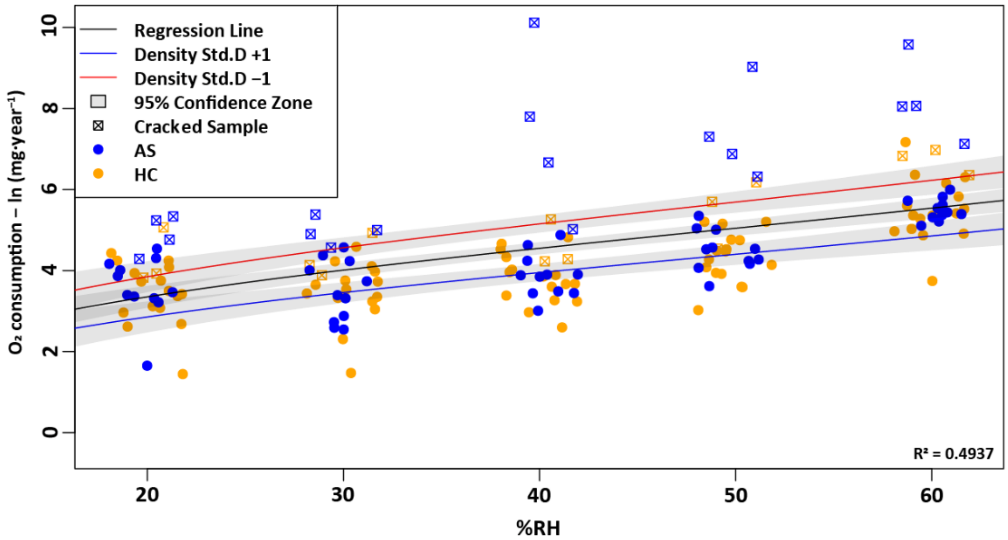

**Figure 6.16:** Combined density/RH regression plot for Hostacor and alkaline sulfite samples. The X-axis positions have been jittered to increase readability. Though less dense samples consume more oxygen, the parallel regression lines suggest density and RH do not interact to impact consumption values.

| Coefficient | Estimate | Std. Error | t value | p-value |
|---|---|---|---|---|
| **(Intercept)** | 14.529 | 1.3647 | 10.647 | $< 2_e^{-16}$ |
| **RH (logit)** | 2.7819 | 1.7711 | 1.571 | 0.118 |
| **Density (log)** | -5.1016 | 0.7323 | -6.966 | $7.26_e^{-11}$ |
| **Interaction Coefficient** | -0.8392 | 0.9504 | -0.883 | 0.379 |
| | | | | |
| **Multiple R$^2$:** | 0.5027 | **Adjusted R$^2$:** | 0.4937 | |
| **F-statistic:** | 55.94 on 3 and 166 DF | **Model p-value:** | $< 2_e^{-16}$ | |

**Table 6.11:** Coefficients of combined density/RH interaction regression model for alkaline sulfite and Hostacor-IT treated samples. Though the density coefficient confirms the effect of density on consumption values, the interaction coefficient shows that density does not interact with RH to affect consumption values.

As with hydrogen reduction, Figure 6.16 shows a slight change in the slopes of the regression lines as they progress from 20% to 60% RH, with denser samples showing smaller rises in consumption compared to less dense samples. As is the case with other density interaction models, the RH coefficient estimate lacks significance and features a large standard error. The density coefficients confirm there is a relation between the density of the aqueously-treated samples and obtained consumption results. However, the density:RH interaction coefficients show there is most likely not an interaction between the two that affects consumption rates. The visible slope differences in the regression lines could be influenced by the fact that three of the four fastest corroding alkaline sulfite-treated samples are also the least dense of those treated with alkaline sulfite. Likewise, the two fastest corroding Hostacor samples are the least dense of those treated with Hostacor.

When examining the individual density models of alkaline sulfite and Hostacor (Figure 6.17 and Figure 6.18, Table 6.12), the former distinctly shows less dense samples consuming oxygen in greater ratios as humidity rises. Hostacor, however, shows no change in regression slopes with escalating RH.

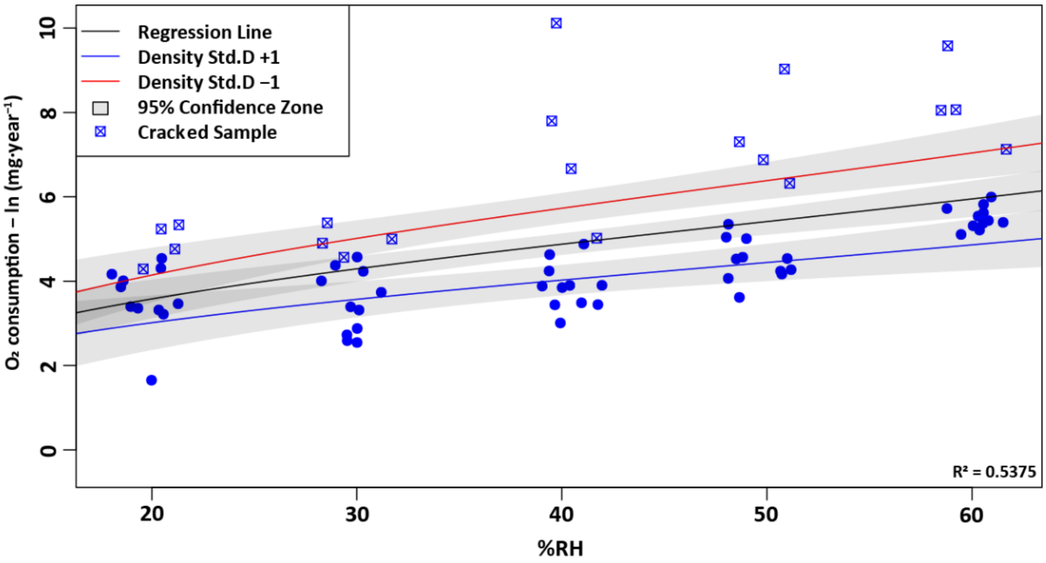

**Figure 6.17:** Density/RH regression plot alkaline sulfite samples. The X-axis positions have been jittered to increase readability. Though the deviations in slopes of the regression lines suggest an interaction between density and RH, they are affected by the extreme outlier occurring at 40% RH.

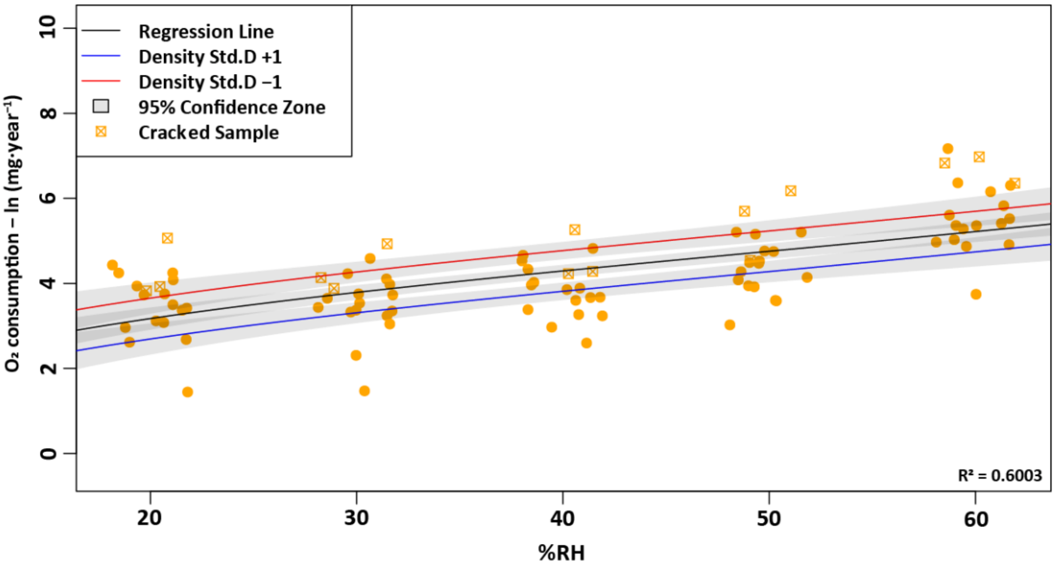

**Figure 6.18:** Density/RH regression plot for Hostacor-IT samples. The X-axis positions have been jittered to increase readability. Though they suggest density affects consumption rates, the parallel regression lines show that there is unlikely to be an interaction between density and RH.

|  | **Coefficient** | **Estimate** | **Std. Error** | **t value** | **p-value** |
|---|---|---|---|---|---|
| **AS** | **(Intercept)** | 21.879 | 2.65 | 8.251 | $5.72_{e}^{-12}$ |
|  | **RH (logit)** | 6.288 | 3.44 | 1.827 | 0.0719 |
|  | **Density (log)** | -8.821 | 1.418 | -6.221 | $3.05_{e}^{-08}$ |
|  | **Interaction Coefficient** | -2.660 | 1.840 | -1.445 | 0.1528 |
| **HC** | **(Intercept)** | 11.175 | 1.191 | 9.384 | $4.95_{e}^{-15}$ |
|  | **RH (logit)** | 1.119 | 1.545 | 0.724 | 0.471 |
|  | **Density (log)** | -3.464 | 0.641 | -5.407 | $5.13_{e}^{-07}$ |
|  | **Interaction Coefficient** | 0.01243 | 0.832 | 0.015 | 0.988 |
|  |  |  |  |  |  |
| **AS** | **Multiple $R^2$:** | 0.5562 | **Adjusted $R^2$:** | 0.5375 |  |
|  | **F-statistic:** | 29.66 on 3 and 71 DF | **Model p-value:** | $1.53_{e}^{-12}$ |  |
| **HC** | **Multiple $R^2$:** | 0.6131 | **Adjusted $R^2$:** | 0.6003 |  |
|  | **F-statistic:** | 48.06 on 3 and 91 DF | **Model p-value:** | $< 2_{e}^{-16}$ |  |

**Table 6.12:** Coefficients of individual density/RH interaction regression models for alkaline sulfite and Hostacor-IT treated samples. Both confirm lower densities are more likely to consume more oxygen, though also do not suggest an interaction between RH and density for either treatment.

Looking at the coefficients table, both treatments feature significant density coefficients, which are most likely reflected in the higher initial consumption rates of lower density samples. The high standard errors for all other alkaline sulfite coefficients and associated p-values give little confidence that density and RH interact in any meaningful way. The regression lines in Figure 6.17 show slight deviation in slope but are broadly parallel, a sign that there is no interaction. The same can be said of Hostacor, as its plot features parallel regression lines, an interaction coefficient standard error 67x higher than its estimate, and a p-value that is nearly 1.

#### 6.2.3.2 VOLUME

The combined volume/RH interaction plot for alkaline sulfite and Hostacor is shown in Figure 6.19, with coefficients listed in Table 6.13.

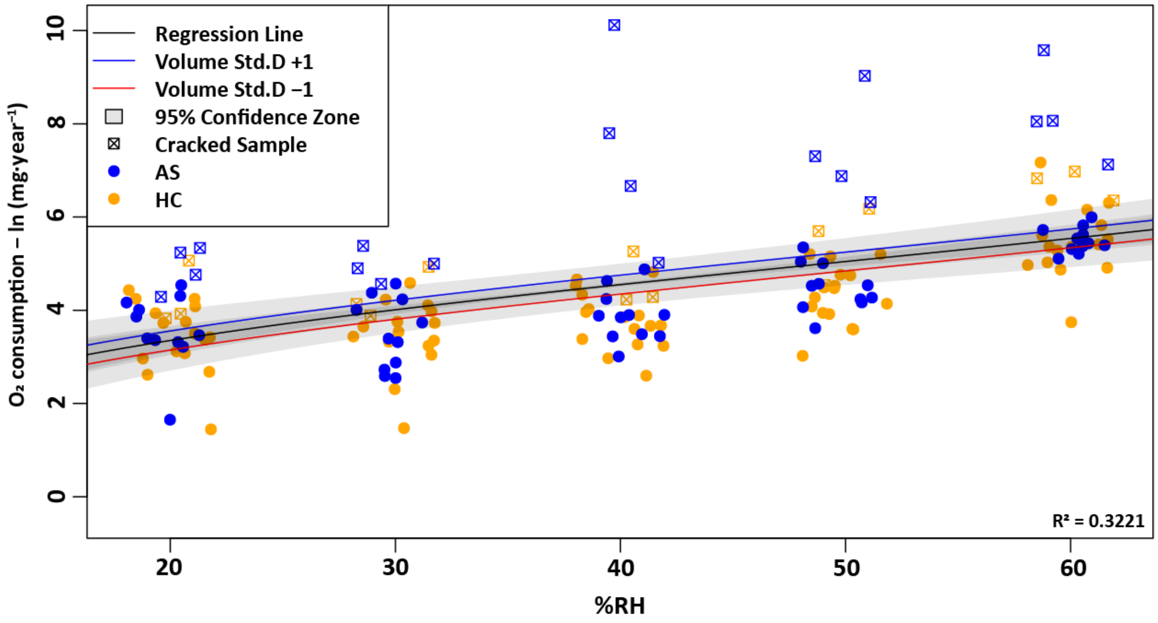

**Figure 6.19:** Combined volume/RH regression plot for Hostacor and alkaline sulfite samples. The X-axis positions have been jittered to increase readability. More voluminous samples are likely to consume more oxygen, though the parallel regression lines suggest this is not due to any interaction between volume and RH.

| Coefficient | Estimate | Std. Error | t value | p-value |
|---|---|---|---|---|
| **(Intercept)** | 2.4645 | 1.3706 | 1.798 | 0.0739 |
| **RH (logit)** | 1.2411 | 1.7788 | 0.698 | 0.4863 |
| **Volume (log)** | 0.4537 | 0.2403 | 1.888 | 0.0608 |
| **Interaction Coefficient** | -0.0034 | 0.3119 | -0.011 | 0.9913 |
| | | | | |
| **Multiple $R^2$:** | 0.3341 | **Adjusted $R^2$:** | 0.3221 | |
| **F-statistic:** | 27.76 on 3 and 166 DF | **Model p-value:** | $1.33_e{}^{-14}$ | |

**Table 6.13:** Coefficients of combined volume/RH interaction regression model for alkaline sulfite and Hostacor-IT treated samples. The interaction estimate, standard error, t value, and p-value all show an interaction between volume and RH to be extremely unlikely.

The combined aqueous treatment model follows that of hydrogen-reduced samples, with larger cannonballs consuming more oxygen relative to smaller ones. However, the standard deviation regression lines show little to no slope change with escalating RH, suggesting oxygen consumption is not influenced by an interaction between volume and humidity. The coefficients confirm volume has a relationship with consumption values, but there is no interaction effect with humidity. Individual volume/RH regression models are shown in Figure 6.20 and Figure 6.21, with coefficients listed in Table 6.14.

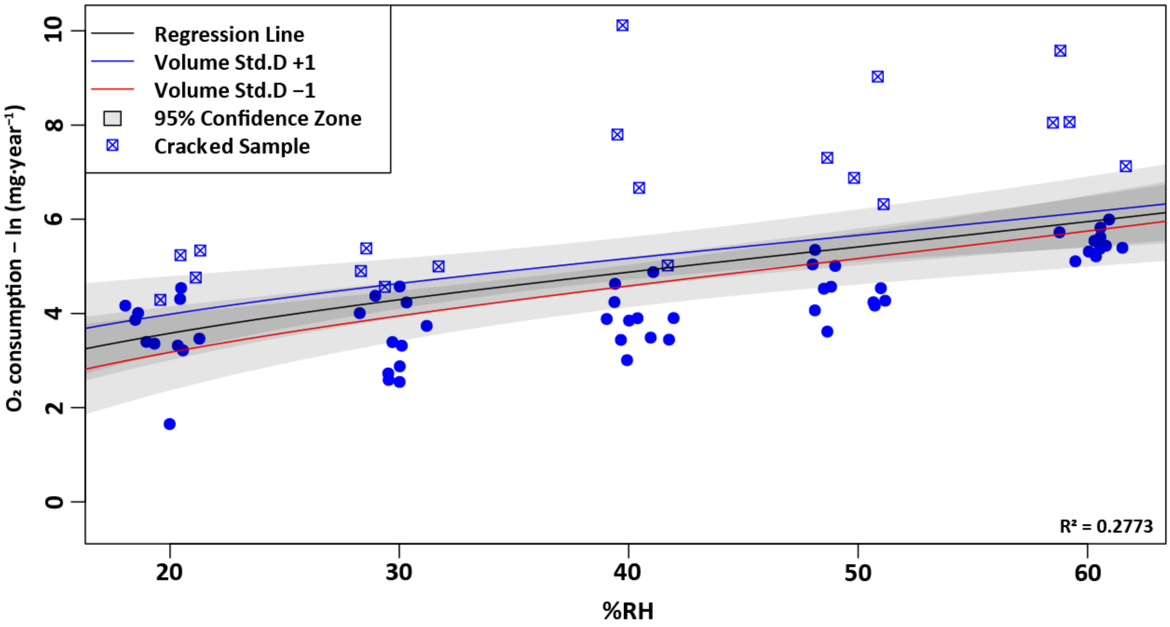

**Figure 6.20:** Volume/RH regression plot for alkaline sulfite samples. The X-axis positions have been jittered to increase readability. The regression lines show that, though volume affects consumption values, its effect lessens in escalating RH. The lines, however, are broadly parallel, so this remains unlikely.

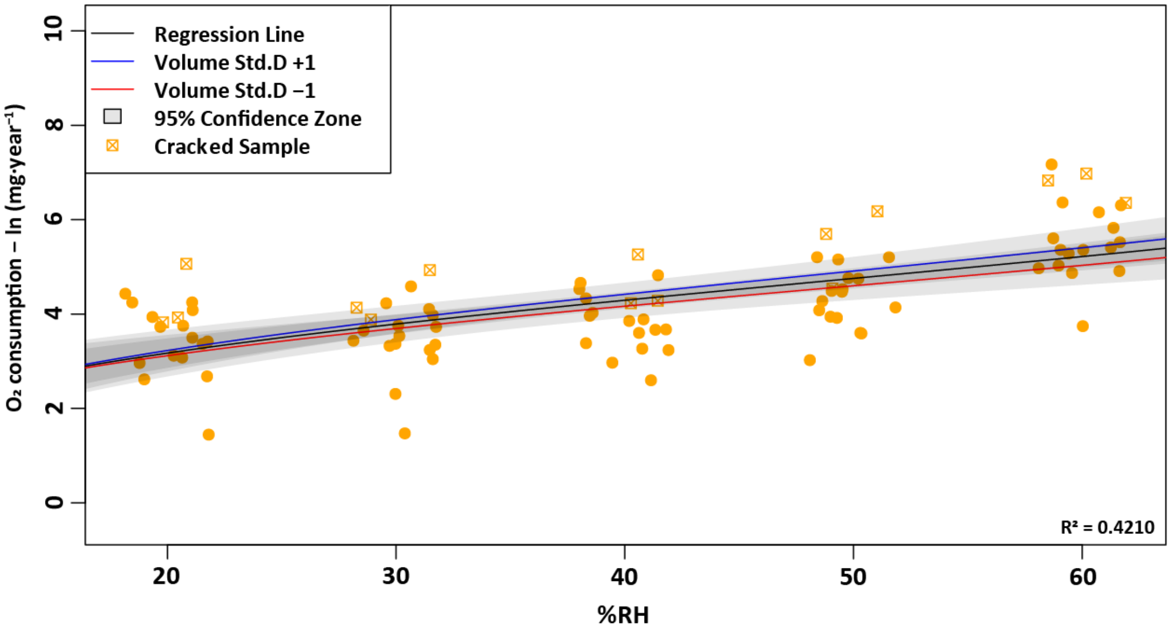

**Figure 6.21:** Volume/RH regression plot for Hostacor-IT samples. The X-axis positions have been jittered to increase readability. The regression lines show that there is unlikely to be an interaction between RH and volume, and that volume may not affect consumption values at all.

| | Coefficient | Estimate | Std. Error | t value | p-value |
|---|---|---|---|---|---|
| **AS** | **(Intercept)** | 2.0481 | 2.666 | 0.768 | 0.445 |
| | **RH (logit)** | 2.8763 | 3.460 | 0.831 | 0.409 |
| | **Volume (log)** | 0.5903 | 0.466 | 1.265 | 0.210 |
| | **Interaction Coefficient** | -0.2725 | 0.606 | -0.405 | 0.654 |
| **HC** | **(Intercept)** | 2.8549 | 1.297 | 2.202 | 0.0302 |
| | **RH (logit)** | 0.2508 | 1.683 | 0.149 | 0.8819 |

| | | | | | |
|---|---|---|---|---|---|
| | **Volume (log)** | 0.3347 | 0.228 | 1.470 | 0.1451 |
| | **Interaction Coefficient** | 0.1570 | 0.296 | 0.531 | 0.5967 |
| | | | | | |
| **AS** | **Multiple R$^2$:** | 0.3066 | **Adjusted R$^2$:** | 0.2773 | |
| | **F-statistic:** | 10.47 on 3 and 71 DF | **Model p-value:** | $8.76_{e}^{-06}$ | |
| **HC** | **Multiple R$^2$:** | 0.4395 | **Adjusted R$^2$:** | 0.421 | |
| | **F-statistic:** | 23.79 on 3 and 91 DF | **Model p-value:** | $1.87_{e}^{-11}$ | |

**Table 6.14:** Coefficients of individual volume/RH interaction regression models for alkaline sulfite and Hostacor-IT treated samples. Unlike their combined model, the coefficients of the individual treatments show a link between their volumes and consumption values may not exist.

Like their combined model, both alkaline sulfite and Hostacor show larger samples consume more oxygen. Though their individual models both show slope changes in their standard deviation regression lines, these are largely parallel and not reliable. It is unsurprising, then, that the interaction coefficients for both have very large standard errors relative to their estimates, and that there is a high probability those estimates appear by chance. As is the case with hydrogen reduction, Hostacor-IT and alkaline sulfite treatments show no apparent interaction between their volumes and RH that influences their oxygen consumption rates.

### 6.2.4 MARY ROSE TRUST RETREATED CANNONBALLS

#### 6.2.4.1 DENSITY

The average density of retreated samples under study is 5.8 g/cm3, over 0.5 g/cm3 less than the examined alkaline sulfite and Hostacor single-treated samples. That the retreated samples are much less dense than their single-treatment Hostacor and alkaline counterparts indicates that they may have undergone more corrosion post-deposition.

The density/RH interaction regression model is shown in Figure 6.22, with coefficients listed in Table 6.15. The model follows other treatments, with less dense samples consuming more oxygen. However, the apparent impact of density to adjust consumption rates with escalating humidity is not supported by the coefficients. The model is influenced by cracked and spalling samples that feature high consumption rates and low densities, and it is unlikely that these low densities are fuelling consumption rate ratio increases. Whilst Table 6.15 again confirms a relationship between density and consumption, the interaction coefficient standard error and p-value are large. As evidenced by the Cardiff-retreated samples, consumption rates post-retreatment may be due to other factors.

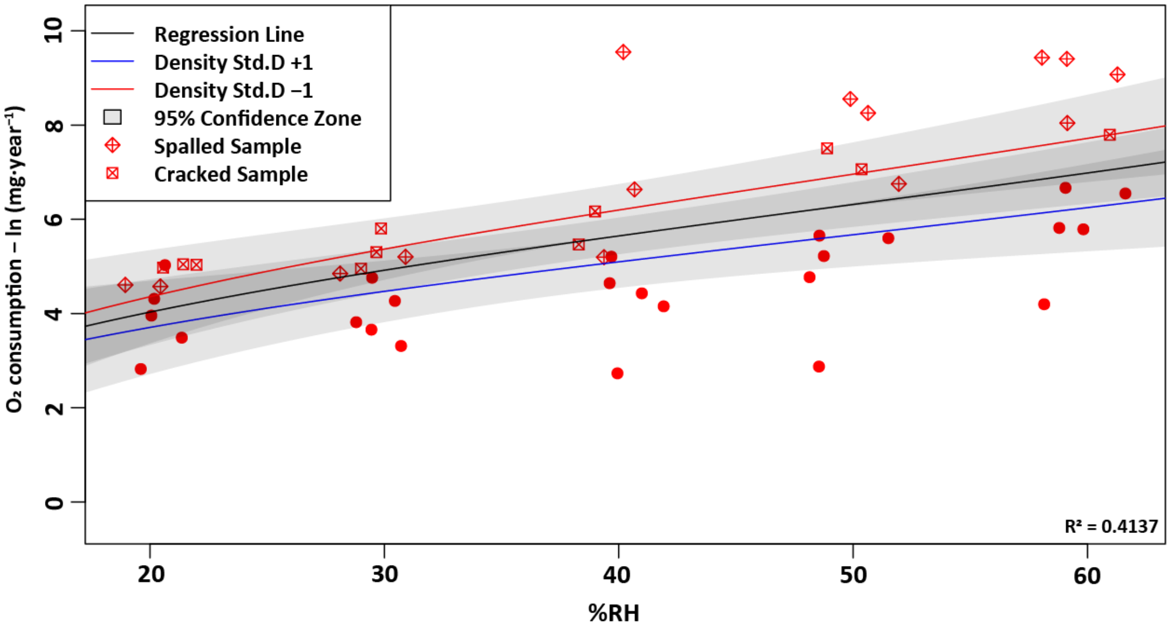

**Figure 6.22:** Density/RH regression plot for MRT-retreated samples. The X-axis positions have been jittered to increase readability. Density is once again shown to impact consumption values. However, the regression lines are broadly parallel and are influenced by aggressively corroding samples at 40 – 605 RH, and so an interaction between density and RH seems unlikely.

| Coefficient | Estimate | Std. Error | t value | p-value |
|---|---|---|---|---|
| **(Intercept)** | 10.332 | 1.5024 | 6.878 | $1.39_{e}^{-08}$ |
| **RH (logit)** | 3.0777 | 1.9498 | 1.578 | 0.12131 |
| **Density (log)** | -2.3365 | 0.8628 | -2.708 | 0.00095 |
| **Interaction Coefficient** | -0.8314 | 1.1197 | -0.743 | 0.46153 |
| | | | | |
| **Multiple $R^2$:** | 0.4496 | **Adjusted $R^2$:** | 04137 | |
| **F-statistic:** | 12.52 on 3 and 46 DF | **Model p-value:** | $4.11_{e}^{-06}$ | |

**Table 6.15:** Coefficients of density/RH interaction regression model for MRT retreated samples. Though it remains likely density affects oxygen consumption values, a large standard error low p-value and high p-value suggest any interaction between density and RH that affects consumption values is not probable.

### 6.2.4.2 VOLUME

The volume/RH interaction regression model for the Mary Rose Trust retreated samples is shown in Figure 6.23, with coefficients listed in Table 6.16. Like the other tested treatments, larger cannonballs are shown to consume more relative to smaller cannonballs, though the lack of any change in the slope of the regression lines indicates that the effect sample volume has on consumption rates does not change with humidity. The regression confidence zones overplot one another at all RH thresholds, suggesting that volume has even less impact. The coefficients confirm this, with all featuring large standard errors and p-values.

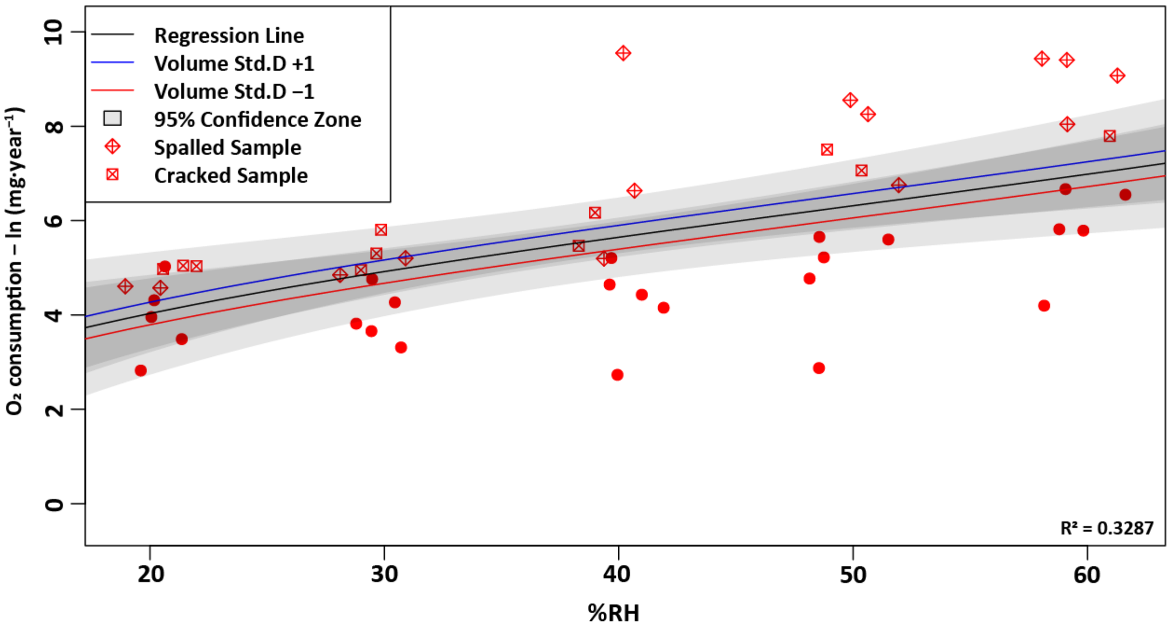

**Figure 6.23:** Volume/RH regression plot for MRT-retreated samples. The X-axis positions have been jittered to increase readability. The parallel regression lines show volume is unlikely to interact with RH to influence consumption rates.

| Coefficient | Estimate | Std. Error | t value | p-value |
|---|---|---|---|---|
| **(Intercept)** | 2.2609 | 3.9946 | 0.566 | 0.574 |
| **RH (logit)** | 1.4326 | 5.1842 | 0.276 | 0.784 |
| **Volume (log)** | 0.7307 | 0.7187 | 1.017 | 0.315 |
| **Interaction Coefficient** | 0.0388 | 0.9327 | 0.042 | 0.967 |
| | | | | |
| **Multiple $R^2$:** | 0.3698 | **Adjusted $R^2$:** | 0.3287 | |
| **F-statistic:** | 8.999 on 3 and 46 DF | **Model p-value:** | $8.44_{e}^{-05}$ | |

**Table 6.16:** Coefficients of volume/RH interaction regression model for MRT retreated samples. The large standard error and p-value of the volume coefficient suggest that volume may not impact consumption values of MRT-retreated samples. The interaction coefficient values do, however, confirm any interaction between volume and RH that might impact consumption rates is unlikely.

## 6.3 CARDIFF RETREATED CANNONBALLS

Chlorides were successfully removed from all 15 cannonballs that underwent retreatment at Cardiff. Retreatment was only effective in reducing the oxygen consumption rates of two samples. However, their coatings were removed prior to retreatment and not reapplied before rate reacquisition, so it remains difficult to say if the rates of the other 13 would be lower than observed values. The two samples that had their rates reduced (#82A-3594 and #83A-0441) had both the highest pre-retreatment 60% RH consumption rates (of Cardiff retreated samples) and the most chlorides extracted. The oxygen consumption rates of the other 13 cannonballs do not correlate to the amount of $Cl^-$ extracted from them (Table 6.17). This confirms research by Watkinson et al. (2019) where the authors show corrosion rate (as determined by oxygen consumption) cannot be used to predict $Cl^-$ content, stating other factors besides $Cl^-$ concentration must influence corrosion rate escalations with escalating RH.

| 20% | **30%** | **40%** | **50%** | **60%** |
|---|---|---|---|---|
| 0.033275 | 0.728101 | 0.344735 | 0.133315 | -0.12155 |

**Table 6.17:** Correlation coefficients between extracted Cl- (mg·gram$^{-1}$) and post-retreatment oxygen consumption rates (mg·year$^{-1}$·g$^{-1}$)

The extraction of $Cl^-$ (in large quantities, in some cases) from all samples *after* the MRT treatments met widely accepted endpoint values (as measured by concentration of $Cl^-$ in treatment baths/gaseous effluent) confirms that this measure is not an indicator of all chloride having been removed from an object. Chloride, for instance, is part of the lattice structure of akaganeite and is difficult to remove, remaining trapped within objects and capable of facilitating corrosion. Chloride extraction, may, however, indicate that no further chloride can be extracted by that treatment at that point in time.

There is also a possibility that residual alkaline sulfite remaining within the cannonballs post-retreatment is inducing corrosion. As explained in Section 2.3.3.5, GR($SO_4^{2-}$) can form in deoxygenated environments and will quickly oxidise into FeOOH upon contact with atmosphere. It is probable that the placement of the cannonballs into a deoxygenated, aqueous environment caused the formation of GR($SO_4^{2-}$) that, once dried, formed FeOOH polymorphs. As aqueous treatments solvate and mobilise $Cl^-$, it is possible they were available in higher concentrations in areas of GR($SO_4^{2-}$) oxidation, forming akaganeite.

Sodium sulfate has been observed upon drying of aqueous solutions containing $Na_2SO_3$, $Na_2SO_3$ and $FeCl_3{\cdot}4H_2O$, and the latter with additional NaOH (Rimmer and Watkinson). These $SO_4^{2-}$ ions can be present in different hydrated forms, depending on $Cl^-$ and $OH^-$ concentration. Iron sulfate is hydroscopic and can induce corrosion, which could account for some of the oxygen consumption.

### 6.3.1 RETREATMENT OF HYDROGEN REDUCTION CANNONBALLS

Retreatment of hydrogen-reduction treated cannonballs increased their oxygen consumption rates, with some samples consuming oxygen over 27x faster at 60% RH than prior to CU retreatment. This may result from a combination of factors.

Barkman (1977) and O'Shea et al. (1982) noted that application of an epoxy resin was necessary soon after treatment, as a pyrophoric reaction between the newly reduced iron, remaining sulfur, and atmospheric oxygen occurred. In other words, the reduction process eliminated any oxygen or oxides from the structure and caused the formation of iron sulfide. When the reduced iron and FeS once again came into contact with atmospheric oxygen, it would cause rapid oxidation. The initial reduction reactions are:

$$\mathrm{Fe_2O_3} + 3\mathrm{H_2S} \rightarrow 2\mathrm{FeS} + \mathrm{S} + 3\mathrm{H_2O} \qquad \textbf{Equ. 6.3}$$

and

$$3\mathrm{H_2S} + 2\mathrm{FeO(OH)} \rightarrow \mathrm{S}^{\circ} + 2\mathrm{FeS} + 4\mathrm{H_2O} \qquad \textbf{Equ. 2.16}$$

These leave increased quantities of FeS within an object (Walker et al., 1996). When exposed to an oxygenated environment at ambient conditions, the following reaction occurs:

$$4\mathrm{FeS} + 7\mathrm{O_2} \rightarrow 2\mathrm{Fe_2O_3} + 4\mathrm{SO_2} \qquad \textbf{Equ. 6.4}$$

Hydrogen sulfide was present in treatment effluents, so would have been available during ferrous reduction, though it should be noted that hydrogen reduction would also remove sulfur as $H_2S$. Any metallic iron present (i.e. ferrite) would also oxidise with atmospheric oxygen. Epoxy impregnation may have reduced the rate of oxidation reactions, by limiting oxygen permeation to the cannonball interior.

The elevated consumption rates may also be due to chlorides. The primary oxygen results show ratio escalations at RH thresholds similar to other treatments. This similarity would indicate that corrosion is being facilitated in some manner. O'Shea et al. (1982) state that treatment usually proceeded until the effluent had a neutral pH. However, this did not guarantee the removal of all chlorides. A neutral pH meant no more $Cl^-$ was being withdrawn in the form of $HCl_{(g)}$, but $HCl_{(g)}$ no longer evolves after 500°C (North and Pearson, 1977). Also pH does not inform on sodium chloride remaining in the cannonballs, as hydrogen does not reduce sodium chloride and therefore would not affect acquired pH (O'Shea et al., 1982).

Ten months of immersion in alkaline sulfite appears to have resulted in the degradation of the epoxy resin from these cannonballs. It is clear that consolidant removal is the reason for the visual and physical changes observed in the cannonballs. O'Shea et al. (1982) state that they found a low-viscosity epoxide resin the best performing post-HR consolidate, and the treatment records provided by the MRT state that a thermosetting resin was used. Epoxies are fairly resistant to reactions with alkaline compounds, including NaOH (Cooke et al., 1964). Barker et al. (1982) say the process of determining optimal consolidation was one of trial-and-error, though. Barkman (1977) states that HR-treated finds from the *Vasa* were consolidated by vacuum-treating with paraffin wax and the addition of a corrosion inhibitor, though there is no evidence provided by the MRT that this was carried out on their assemblage. It is also possible that the epoxy failed due to an impact retreatment had on the hydrogen-reduced cannonballs, resulting in the breakdown of the epoxy's adhering structure.

In any case, the removal of the consolidant during retreatment is likely to be the main contributor to increased oxygen consumption and physical change in the hydrogen-reduced samples.

### 6.3.2 DRYING OF MARY ROSE TRUST AND CARDIFF RETREATED SAMPLES

Both MRT and Cardiff retreated cannonballs indicate that retreatment may increase instability rather than mitigate it. Results show that the oxygen consumption of most of the Cardiff retreated cannonballs increased following retreatment, despite the removal of chlorides. It has been shown that drying prior to treatment can impact the dechlorination efficiency of heritage marine iron. Though the cannonballs had previously undergone desalination treatment, their drying and storage/display in atmosphere prior to re-immersion may have induced more akaganeite formation than if they had only undergone a single treatment (Guilminot et al., 2012). Unfortunately, time constraints meant determining with any clarity why retreatment at Cardiff University led to faster corrosion rates remains unexamined.

### 6.3.3 THE ROLE OF COATINGS

As discussed in Section 4.5.1, coatings were removed from the cannonballs prior to retreatment. The coatings of microcrystalline wax (Hostacor-IT samples) and Paraloid B48N (alkaline sulfite and retreated samples) are most likely influencing observed corrosion rates. Investigating the role coatings play in the post-treatment corrosion of the *Mary Rose* cannonballs was not an objective at the outset of this project, and so was not investigated with the rigour required to quantitatively state their effectiveness in the corrosion mitigation of the cannonballs. However, a review of the consumption data shows that coatings may be limiting the supply of corrosion-inducing oxygen.

Shashoua and Matthiesen (2010) analysed the effectiveness of coatings to limit corrosion (as determined by oxygen consumption) on rolled steel panels that were subjected to salt sprays and left outdoors in Danish weather. Included in their assessment were Paraloid B72, an ethyl methacrylate/methyl acrylate copolymer, and Renaissance wax, a microcrystalline wax. Though Paraloid B72 is a different formula than B48N (the latter is a methyl methacrylate/butyl acrylate copolymer), both are thermoplastic acrylic resins that are used in the conservation field and have similar properties (Down, 2015). It was found that both reduced corrosion of an uncoated panel from 130 µm/year to 1 µm/year (Paraloid) and 1.9 µm/year (Renaissance wax). The porous yet smooth morphology of the cannonballs is the ideal surface for coating application, as it creates a penetrating yet even, homogenous barrier layer (Otieno-Alego et al., 2001), all of which would optimise the effectiveness of an applied coating. (Matthiesen and Stemann-Petersen, 2013) reported reduction in oxygen consumption rates over 10x after applying coatings. In this instance, the wax Mobilkote M420 was applied to both a cast-iron artillery shell and a wrought iron rivet plate, showing further evidence of the effectiveness of coatings to reduce oxygen consumption.

The protective Paraloid B48N coating was removed prior to Cardiff retreatment in order to facilitate $Cl^-$ diffusion and was not reapplied before acquisition of oxygen consumption rates post-retreatment. This undoubtedly contributed to the escalation of their observed consumption rates, even with the removal of more $Cl^-$.

## 6.4 ASSESSING RISK TO THE MARY ROSE CANNONBALLS

The evidence presented earlier in this chapter shows the escalating risk the *Mary Rose* cannonballs face with increasing humidity. The closeness of rates at 20% and 30% RH show that there is little difference in risk to objects stored in either environment. The data also shows that 20% RH may not be low enough to prevent aggressive corrosion in some artefacts. For example, #83A-0441 consumed more at 20% RH than all but 10 other cannonballs did at 50%. As β-FeOOH (15%), and $FeCl_2{\cdot}H_20$ (19%) all actively corrode metal at low RH, desiccated storage should aim for below 20% RH rather than for it, if possible, to best mitigate damage. This confirms evidence discussed in earlier reports (Watkinson and Lewis, 2005a; 2005b; Watkinson et al., 2019).

As the corrosion rate of each cannonball is different, the risk to each is different. Treatment has been shown to have an impact on these rates. Samples treated with hydrogen reduction have noticeably lower consumption rates than either Hostacor-IT or alkaline sulfite, though their rate escalations are, like these other treatments, multiplicative with rising humidity, showing that risk even to them becomes appreciably greater in higher RH environments.

Density and volume have been shown to influence consumption rates, though not as a function of humidity. Cannonballs that are larger in volume or less dense consume more oxygen, indicating that they corrode faster than other cannonballs. It is likely that the effect of volume is due to larger samples featuring larger reactive surfaces relative to smaller samples. However, the apparent trend of less dense samples to consume more oxygen relative to denser cannonballs is less easily explained from this dataset. One possibility relates to chloride content; less dense samples have undergone more corrosion, and so may contain a higher ratio of chlorides to iron surface area than denser cannonballs at the time of excavation. Without measuring the chloride content of the cannonballs, which would require destructive analysis, it is not possible to verify this theory.

Though the number of unknown factors makes determining the exact risk to each specific cannonball impossible, an attempt can be made to estimate risk based on the data from this study. For instance, considering volume, density and oxygen consumption alongside observed damage may allow for the creation of risk models. Figure 6.24 is a logistic regression model showing the probability of cracked cannonballs to spall as a function of their consumption values. Consumption values are considered in mg·year$^{-1}$·gram$^{-1}$, as it remains the best comparator to use when considering objects of different morphologies.

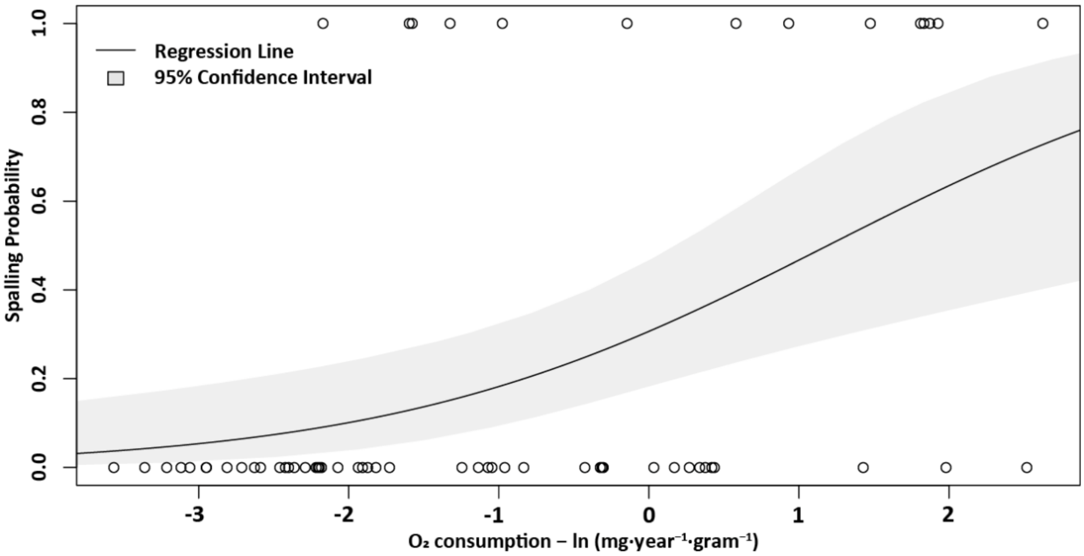

**Figure 6.24:** Spalling probability model for cracked samples. The regression line shows the probability of a cracked cannonball to spall at a given consumption rate, regardless of RH, with the confidence interval showing the uncertainty in the regression.

The model shows that cracked cannonballs are unlikely to spall if their consumption values are kept appreciably low, though spalling is the likely outcome if consumption is left unchecked. Logistic regression is more appropriate when attempting to model the probability of a binary outcome (Chatterjee and Simonoff, 2013: 150), in this case those cannonballs that are spalled (1) and those that have yet to spall (0). This determines the Y-axis. The likelihood is founded upon the assumption that the cannonballs must first be cracked prior to spalling, and so the model is determined by data only from cracked and spalled samples. The cracked-to-spalling outcome is based on the visual observations discussed in Chapter 5.2.2. Most damaged samples saw their damage increase during specific RH trials. Two of these spalled (#82A-3594 and #81A-1106) during monitoring. These observations were then given a binary response at the consumption rate they happened at and were then used to calculate Figure 6.24. Two others (#83A-0180 and #83A-0441) had spalled prior to consumption monitoring, with their condition worsening throughout the course of the trial. These cannonballs were assigned their 20% RH rate as their spall point. Though they most likely spalled at a higher rate, the use of these two cannonballs in the model increases the probability of spalling with less consumption, and so Figure 6.24 can be seen as a conservative model. Consumption values are normalised using natural log (ln, $\log_e$) transformations. The distinctive S-curve shown is produced by plotting the inverse logit values of the model as it moves from 0 to 1, as logit values are reciprocals of each other (producing an 'S' around 0, or logit 0.5) and place infinite numbers and negative numbers on a binary 0 to 1 scale. Confidence zones are applied to show the uncertainty in the regression.

The model can be adjusted to consider the impact sample volume and density have on risk. Figure 6.25 is a logistic regression model showing probability of spalling when considering a cannonball's density. Consumption values are considered in mg·year$^{-1}$.

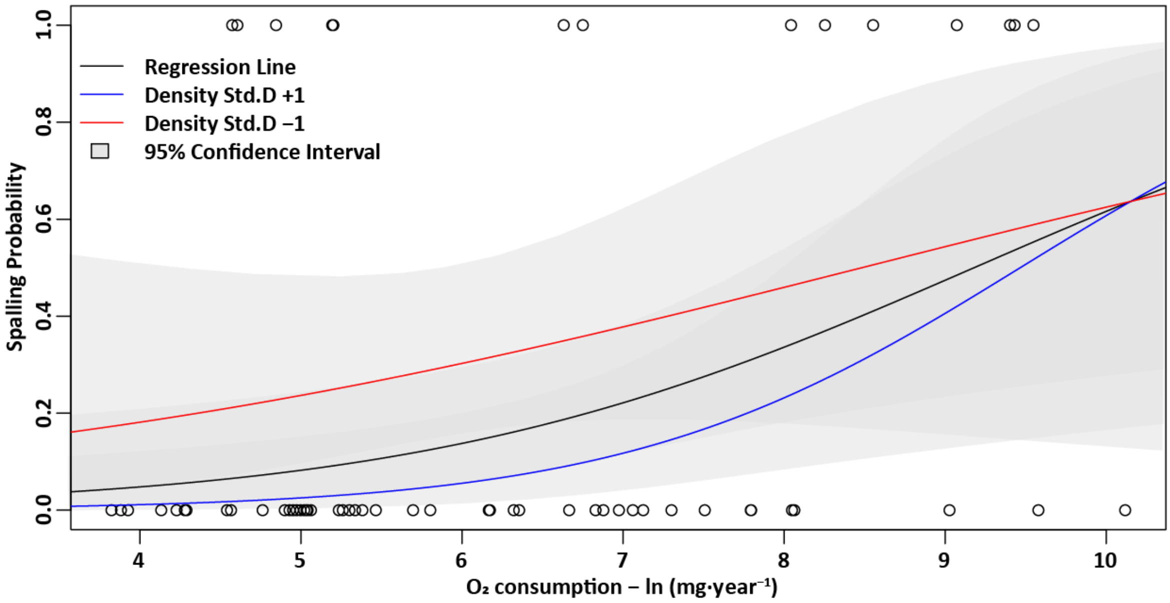

**Figure 6.25:** Spalling probability model for cracked cannonballs when considering sample density. The regression line considers mean density, whilst the others consider the impact a higher (+1 standard deviation) or lower (-1 standard deviation) density may have on the probability of a cracked cannonball to spall. All 12 cracked samples were used to make the model.

The plot shows that less dense cracked cannonballs are at a higher risk of spalling at lower consumption values, until consumption values are so high that density no longer makes a difference. The central regression line is the spalling probability as a function of the mean density of the samples. The others consider the probability of spalling if the density were increased or decreased one standard deviation. The same model can be applied to sample volume (Figure 6.26).

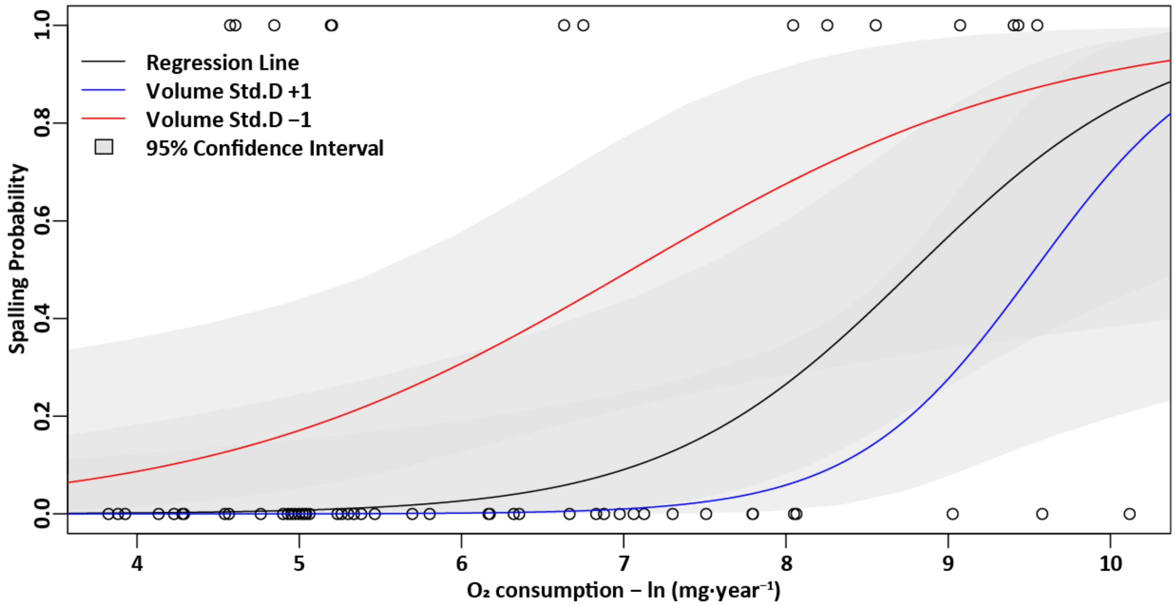

**Figure 6.26:** Spalling probability model for cracked cannonballs when considering sample volume. The regression line considers mean volume, whilst the others consider the impact a higher (+1 standard deviation) or lower (-1 standard deviation) volume may have on the probability of a cracked cannonball to spall. All 12 cracked samples were used to make the model and is independent of RH and density.

The volume model shows smaller samples are at a greater risk of spalling than larger ones, until consumption is so large as to negate any differentiation amongst volumes. Whereas the density model mirrored the density/RH interaction plots (less density = more consumption and more risk), volume shows that, though they contribute less to oxygen consumption, smaller samples are more at risk of spalling.

Though Figures 6.24 – 6.26 show probable risk to already cracked cannonballs, they make statistical assumptions and should not be relied upon to inform on the risk of damage to specific cannonballs. One significant factor that is impacting their accuracy and reliability is the number of samples included. Only twelve samples feature cracking, with only four of those spalling. Though additional damaged samples would improve the accuracy and most likely reduce the confidence zones, a risk model showing the probability of uncracked samples to crack would be of more value. As no cracks formed over the course of this study in samples that did not already feature cracks, a more complete 0-1 damage probability model featuring all samples cannot be drawn.

## 6.5 ADVICE TO THE MARY ROSE TRUST ON THE CARE OF THEIR CAST IRON CANNONBALLS

Based on the above discussion of the data acquired from oxygen consumption monitoring of 56 treated cast iron cannonballs from the *Mary Rose* (and the retreatment of 15 of those), the following recommendations are made with regard to their storage and possible display in a range of environments.

### 6.5.1 USE OF OXYGEN CONSUMPTION MONITORING TO DETERMINE RISK TO CANNONBALLS ON AND INTENDED FOR DISPLAY

To ascertain the instability of their cast iron cannonballs and their fitness for display, the MRT could implement the use of oxygen consumption monitoring. Measuring oxygen consumption is an effective method of ascertaining corrosion rates of these artefacts in given environments, whereas it has been shown that $Cl^-$ monitoring during treatment and low $Cl^-$ levels in effluents at the end of treatment do not necessarily translate to an efficacious treatment and low corrosion rates.

Following the methodology laid out in Chapter 4.4.6 should allow their results to be directly compared to those shown in Chapter 5 and discussed in Chapter 6. Table 6.18 shows the components and associated capital necessary for incorporation.

| Component | Cost |
|---|---|
| **PreSens OXY-1 SMA Single Channel Fiber Optic Oxygen Transmitter** | £760 |
| **Polymer Optical Fiber Cable** | £46 |
| **PreSens Oxygen Sensor Spot SP-PSt3-NAU** | £18 - £36/each |
| | |
| **Total** | £842 |

**Table 6.18:** Cost of component required for an oxygen consumption monitoring system. Other consumables (silicone, reaction vessel, silica gel, etc.) are not considered.

### 6.5.2 RETREATMENT VIABILITY

At this time, aqueous retreatment of cannonballs from the *Mary Rose* cannot be recommended. Both MRT and Cardiff retreated cannonballs were consistently the worst performing (i.e. fastest corroding) samples across all tested humidities. Even though thousands of mg of $Cl^-$ were extracted during Cardiff retreatment, most samples' oxygen consumption rates increased post-retreatment. Whether this increase, despite further $Cl^-$ reduction, is due to the loss of any coatings or consolidants remains unexplored, though presumably their removal played a part in higher oxygen consumption values. However, practitioners and researchers can use the consumption methodology discussed in Chapter 4 to examine whether under certain conditions retreatment becomes a viable option.

Though retreatment is not recommended, hydrogen-reduced samples are of special note. Their placement in alkaline sulfite baths not only increased their instability but caused irreparable physical damage once their binding epoxy dissolved. Given their increased corrosion rate following removal of their epoxy, hydrogen-reduced cannonballs should never be considered for retreatment.

### 6.5.3 STORAGE AND DISPLAY

Once treatment is completed, objects should be stored and displayed in the lowest RH environment possible (ideally < 20% RH), regardless of their post-treatment oxygen consumption. Consumption monitoring should then be carried out again prior to their display. Sample volume and density should be considered when weighing associated display risks, as they may be an indicator of both higher consumption rates and future damage. The cannonballs should never be displayed at or above 60% RH, regardless of treatment type, with even 50% RH posing significant unknown risk. If the Mary Rose Trust desires to place cannonballs in the 55% RH context galleries, they should anticipate damage.

# 7 CONCLUSION

## 7.1 OUTCOMES

The research presented in this thesis has given a better understanding of the stability, corrosion, and storage and display parameters of the cast iron cannonballs from the *Mary Rose.* Non-invasive oxygen consumption monitoring successfully determined their corrosion rates across a range of humidities. The study reinforced the risk that escalating humidity poses to treated heritage marine iron, particularly above 40% RH. The results of the primary consumption and subsequent retreatment studies show escalating oxygen consumption with escalating relative humidity, confirming results from early work on this material (Watkinson et al., 2016) and those carried out on wrought iron (Watkinson and Rimmer, 2013; Watkinson et al., 2019). It was also shown that morphological differences may impact consumption values, if not necessarily rates as a factor of humidity.

Examining regression plots of the data shows that hydrogen reduction is the most efficacious treatment that has been applied to the cannonballs. However, their low consumption rates may rely as much on their consolidating resin as the effectiveness of the treatment. Aqueous desalination treatments carried out by the MRT are similar in effectiveness and consistency, though feature regression slopes double that of hydrogen reduction. Post-treatment oxygen-barring coatings are likely effective in slowing the corrosion rates of the cannonballs. Aqueous desalination retreatments carried out by the Mary Rose Trust and Cardiff University to mitigate corrosion rates of select cannonballs proved ineffective. In some instances, the Cardiff retreatment increased instability, though this may be due to lack of any protecting coating applied post-reatreatment. Cardiff University retreatment did confirm that large quantities of chlorides likely remain with treated cannonballs, though there is no way to be certain of how many. This shows chloride monitoring on its own to be an ineffective method of treatment endpoint determination.

Mary Rose Trust conservation practitioners now have a method for non-invasively assessing their cannonball assemblage and can reference their acquired data against the data analysed in this thesis. They also have a more nuanced understanding of the risk posed to their collection from display and storage environments and can make choices about the amount of risk they are prepared to accept in order to create contextual displays for visitors.

## 7.2 CONTINUING RESEARCH

The data and methodology shown in the preceding chapters have raised several intriguing avenues for continuing research. Further work is required to determine why retreatment increased the instability of the cannonballs, and whether this was due to coating application or other reason(s). If successful, a method to retreat objects with elevated corrosion rates (and not just those from the *Mary Rose*) could be developed based on this understanding and prove invaluable in mitigating destruction of ferrous cultural heritage.

The results of retreatment raise an exciting prospect. Practitioners have attempted to determine at what point alkaline sulfite solutions no longer provide deoxygenated environments. The practice of leaving objects in solution until $Cl^-$ values have levelled off may be causing incalculable harm if treatment baths are no longer anoxic. Oxygen consumption sensor spots function in pH 14 environments, so consumption monitoring could be used to determine when treatment baths become hostile to the objects in them.

The methodology of oxygen consumption monitoring presented in Chapter 4 allows it to be reproduced by practitioners throughout the sector. However, several factors that may influence data output remain unexplored. The influence of temperature and RH fluctuations on oxygen consumption is currently being examined at Cardiff University. It has been observed that barometric pressure affects recorded oxygen pressure values with consequences for quantifying oxygen consumption rates. Cardiff University researchers are in the primary stages of planning this study.

Consumption rates can be acquired for cannonballs from different marine wreck sites. This data can then be combined with the data presented here to potentially build a corrosion rate model, which would ideally show expected consumption rates in higher humidities (when considering known variables) after acquiring sample consumption rates at lower humidities. Consumption rates of cannonballs from terrestrial sites could be examined and incorporated to determine differences between and effects of different burial environments. Such a model would be invaluable to heritage professionals.

# 8 REFERENCES

ALBINI, M., COMENSOLI, L., BRAMBILLA, L., DOMON BEURET, E., KOOLI, W., MATHYS, L., LETARDI, P. & JOSEPH, E. 2016. Innovative biological approaches for metal conservation. *Materials and Corrosion,* 67**,** 200-206.

AMAO, Y. 2003. Probes and Polymers for Optical Sensing of Oxygen. *Microchimica Acta,* 143**,** 1-12.

ANGELINI, E., GRASSINI, S., PARVIS, M. & ZUCCHI, F. 2012. An in situ investigation of the corrosion behaviour of a weathering steel work of art. *Surface and Interface Analysis,* 44**,** 942-946.

ANGELINI, E., GRASSINI, S. & TUSA, S. 2013. Underwater corrosion of metallic heritage artefacts. *Corrosion and Conservation of Cultural Heritage Metallic Artefacts***,** 236.

ANGUS, H. T. 1976. *Cast iron : physical and engineering properties*, London, Boston : Butterworths.

ANTONY, H., LEGRAND, L. & CHAUSSÉ, A. 2008. Carbonate and sulphate green rusts—Mechanisms of oxidation and reduction. *Electrochimica Acta,* 53**,** 7146-7156.

ARCHER, J. 1991. *Conservation of archaeological artefacts by thermal methods.* PhD, Portsmouth Polytechnic.

ARGO, J. 1982. The treatment of corrosion with amines. *Conservation news***,** 7-9.

ARGYROPOULOS, V., DEGRIGNY, C. & GUILMINOT, E. 2000. Monitoring Treatments of Waterlogged Iron-Wood Composite Artifacts Using Hostacor IT-PEG 400 Solutions. *Studies in Conservation,* 45**,** 253-264.

ARGYROPOULOS, V., RAMEAU, J. J., DALARD, F. & DEGRIGNY, C. 1999. Testing Hostacor It as a Corrosion Inhibitor for Iron in Polyethylene Glycol Solutions. *Studies in Conservation,* 44**,** 49-57.

ARRHENIUS, O., BARKMAN, L. & SJÖSTRAND, E. 1973. *Conservation of old rusty iron objects: reduction of rust with hydrogen gas*, National Swedish Maritime Museum and Swedish Corrosion Institute.

ASHKENAZI, D., ARONSON, A., CVIKEL, D., MENTOVICH, E., BARKAI, O. & KAHANOV, Y. 2012. *Archaeometallurgical Investigation of Iron Artifacts from Shipwrecks-A Review*, INTECH Open Access Publisher.

AVRAMI, E. 2009. Heritage, values, and sustainability. *Conservation: principles, dilemmas and uncomfortable truths***,** 177-183.

BARKER, B., KENDELL, K. & O'SHEA, C. The hydrogen reduction process for the conservation of ferrous objects. Conservation of iron. Proceedings of a symposium held at Greenwich on July 4th 1980, 1982. National Maritime Museum, 23-27.

BARKER, D. 2003. Conservation of metals. *In:* JONES, M. & MARY ROSE, T. (eds.) *For future generations : conservation of a Tudor maritime collection.* Portsmouth : Mary Rose Trust.

BARKMAN, L. 1977. Conservation of Rusty Iron Objects By Hydrogen Reduction. *Corrosion and Metal Artifacts: A Dialogue Between Conservators and Archaeologists and Corrosion Scientists,* 479**,** 155.

BARRIO, J., CHAMÓN, J., PARDO, A. I. & ARROYO, M. 2009. Electrochemical techniques applied to the conservation of archaeological metals from Spain: a historical review. *Journal of Solid State Electrochemistry,* 13**,** 1767-1776.

BAYLE, M., DE VIVIÉS, P., MEMET, J.-B., FOY, E., DILLMANN, P. & NEFF, D. 2016a. Corrosion product transformations in alkaline baths under pressure and high temperature: The sub-critical stabilisation of marine iron artefacts stored under atmospheric conditions. *Materials and Corrosion,* 67**,** 190-199.

BAYLE, M., MEMET, J.-B., DILLMANN, P., NEFF, D. & DE VIVIÉS, P. 2016b. Impact of the subcritical stabilisation process on corrosion layers of iron artefacts from different archaeological corrosion contexts. *In:* MENON, R., CHEMELLO, C., PANDYA, A. & GROUP, I. C. F. C. M. W. (eds.) *Metal 2016: proceedings of the interim meeting of the ICOM-CC Metals Working Group, September 26-30, 2016, New Delhi, India.* Paris: ICOM Committee for Conservation. Metals Working Group, Paris, France.

BELL, L. S., LEE THORP, J. A. & ELKERTON, A. 2009. The sinking of the Mary Rose warship: a medieval mystery solved? *Journal of Archaeological Science,* 36**,** 166-173.

BERKO, A., SMITH, A., JONES, A., SCHOFIELD, E., MOSSELMANS, J. & CHADWICK, A. XAS studies of the effectiveness of iron chelating treatments of Mary Rose timbers. Journal of Physics: Conference Series, 2009. IOP Publishing, 012147.

BHADESHIA, H. 2020. Cementite. *International Materials Reviews,* 65**,** 1-27.

BJÖRDAL, C. & NILSSON, T. 2001. Observations on microbial growth during conservation treatment of waterlogged archaeological wood. *Studies in conservation,* 46**,** 211-220.

BLADES, N., CASSAR, M., ORESZCZYN, T. & CROXFORD, B. 2000a. Preventive conservation strategies for sustainable urban pollution control in museums. *Studies in Conservation,* 45**,** 24-28.

BLADES, N., ORESZCZYN, T., BORDASS, B. & CASSAR, M. 2000b. Guidelines on pollution control in heritage buildings.

BLECK, R.-D. 1978. On the desalting or archaeological iron finds from the earth in anhydrous medium. *In:* ORGAN, R. M. (ed.) *Conservation of iron objects found in a salty environments.*

BRESLE, Å. 1974. *Jern-kontorets annaler,* 158**,** 33-36.

BRESLE, A. R. A. 1976. Method for inhibiting rust formation on iron-containing articles. Google Patents.

BUCK, R. D. 1974. On conservation: what is a regional conservation center and why? *Museum news (American Association of Museums), v.52, no.8,* 52**,** pp.10-11.

BUSSE, E. The Manitoba north cannon stabilization project. METAL 95: proceedings of the international conference on metals conservation (Semur en Auxois, 25-28 September 1995), 1997. 263-268.

CANO, E., LAFUENTE, D. & BASTIDAS, D. M. 2010. Use of EIS for the evaluation of the protective properties of coatings for metallic cultural heritage: a review. *Journal of Solid State Electrochemistry,* 14**,** 381-391.

CHADWICK, A. V., BERKO, A., SCHOFIELD, E. J., JONES, A. M., MOSSELMANS, J. F. W. & SMITH, A. D. 2012a. Application of microfocus x-ray beams from synchrotrons in heritage conservation. *International journal of architectural heritage: conservation, analysis, and restoration,* 6**,** 228-258.

CHADWICK, A. V., BERKO, A., SCHOFIELD, E. J., SMITH, A. D., MOSSELMANS, J. F. W., JONES, A. M. & CIBIN, G. 2016. The application of X-ray absorption spectroscopy in archaeological conservation: Example of an artefact from Henry VIII warship, the Mary Rose. *Journal of Non-Crystalline Solids,* 451**,** 49-55.

CHADWICK, A. V., SCHOFIELD, E. J., JONES, A. M., CIBIN, G. & MOSSELMANS, J. F. W. 2012b. Ionic nanoparticles in heritage conservation; treatments for the Mary Rose timbers. *Solid State Ionics,* 225**,** 742-746.

CHATTERJEE, S. & SIMONOFF, J. S. 2013. *Handbook of regression analysis*, Wiley Online Library.

CHESTER, R. 2009. *Marine geochemistry*, John Wiley & Sons.

CHILDS, C., GOODMAN, B., PATERSON, E. & WOODHAMS, F. 1980. The nature of iron in akaganéite (β-FeOOH). *Australian Journal of Chemistry,* 33**,** 15-26.

CIABURRO, G. 2018. *Regression analysis with R: Design and develop statistical nodes to identify unique relationships within data at scale*, Packt Publishing Ltd.

COLE, I. S. 2010. 2.16 - Atmospheric Corrosion. *In:* COTTIS, B., GRAHAM, M., LINDSAY, R., LYON, S., RICHARDSON, T., SCANTLEBURY, D. & STOTT, H. (eds.) *Shreir's Corrosion.* Oxford: Elsevier.

COMENSOLI, L., MAILLARD, J., ALBINI, M., SANDOZ, F., JUNIER, P. & JOSEPH, E. 2017. Use of Bacteria To Stabilize Archaeological Iron. *Applied and Environmental Microbiology,* 83**,** e03478-16.

COMMISSION, M. G. 1992. Standards in the museum care of archaeological collections. London: United Kingdom: Museums & Galleries Commission.

CONSERVATION, I. O. 2016. Professional Standards. Online: Institute of Conservation.

CONSERVATION, I. O. 2020. Ethical Guidance. Online: Institute of Conservation.

COOKE, H., STROHSCHER, A. & MCWHORTER, W. 1964. Chemical resistance of epoxy resins. *Industrial & Engineering Chemistry,* 56**,** 38-41.

CORFIELD, M. 1982. Radiography of archaeological ironwork. *In:* CLARKE, R. W. & BLACKSHAW, S. M. (eds.) *Conservation of iron.* Greenwich: National Maritime Museum (Great Britain), Greenwich, United Kingdom.

CORNELL, R. & GIOVANOLI, R. 1990. Transformation of akaganeite into goethite and hematite in alkaline media. *Clays and Clay minerals,* 38**,** 469-476.

CORNELL, R. M. & SCHWERTMANN, U. 2003. *The iron oxides: structure, properties, reactions, occurrences and uses,* John Wiley & Sons.

CORNWELL, J. C. & MORSE, J. W. 1987. The characterization of iron sulfide minerals in anoxic marine sediments. *Marine Chemistry,* 22**,** 193-206.

CORPORATION, B. B. 2013. *Mary Rose mueum opens in Portsmouth at cost of £35m* [Online]. Onlline: British Broadcasting Corporation. Available: https://www.bbc.co.uk/news/uk-england-hampshire-22691645 [Accessed 5 August 2020].

DANIELS, V. 1981. Plasma reduction of silver tarnish on daguerreotypes. *Studies in Conservation,* 26**,** 45-49.

DANIELS, V. D., HOLLAND, L. & PASCOE, M. 1979. Gas plasma reactions for the conservation of antiquities. *Studies in Conservation,* 24**,** 85-92.

DARLINGTON, R. B. & HAYES, A. F. 2017. Regression analysis and linear models. *New York, NY: Guilford*.

DEAN, S. W. & REISER, D. B. 1995. Time of wetness and dew formation: a model of atmospheric heat transfer. *Atmospheric Corrosion.* ASTM International.

DEVAUD, C., GUILMINOT, E., LABROCHE, S. & BARON, G. 2016. Stabilization of iron copper composites: an overview of treatment difficulties. *In:* MENON, R., CHEMELLO, C., PANDYA, A. & GROUP, I. C. F. C. M. W. (eds.) *Metal 2016: proceedings of the interim meeting of the ICOM-CC Metals Working Group, September 26-30, 2016, New Delhi, India.* Paris: ICOM Committee for Conservation. Metals Working Group, Paris, France.

DILLMANN, P., MAZAUDIER, F. & HOERLE, S. 2004. Advances in understanding atmospheric corrosion of iron. I. Rust characterisation of ancient ferrous artefacts exposed to indoor atmospheric corrosion. *Corrosion Science,* 46**,** 1401-1429.

DOWN, J. L. 2015. The evaluation of selected poly (vinyl acetate) and acrylic adhesives: A final research update. *Studies in conservation,* 60**,** 33-54.

DREWS, M. J., DE VIVIÉS, P., GONZÁLEZ, N. G. & MARDIKIAN, P. 2004. A study of the analysis and removal of chloride in iron samples from the <i>Hunley</i>. *In:* ASHTON, J. & HALLAM, D. (eds.) *Metal 04: proceedings of the International Conference on Metals Conservation = actes de la conférence internationale sur la conservation des métaux, Canberra, Australia, 4-8 October 2004.* Canberra: National Museum of Australia, Canberra, Australia.

DUNCAN, S. 1986. Chloride removal from iron-new techniques. *Newsletter/icom committee for conservation metals working group***,** 7-7.

EMMERSON, N. 2015. *Heritage wrought iron: towards the development of evidence based standards for coating.* Cardiff University.

EMMERSON, N. J. & WATKINSON, D. E. 2016. Surface preparation of historic wrought iron: Evidencing the requirement for standardisation. *Materials and Corrosion,* 67**,** 176-189.

ENNING, D. & GARRELFS, J. 2014. Corrosion of Iron by Sulfate-Reducing Bacteria: New Views of an Old Problem. *Applied and Environmental Microbiology,* 80**,** 1226-1236.

ERIKSEN, E. & THEGEL, S. 1966. Conservation of iron recovered from the sea.

FABECH, E. & TRIER, J. Notes on the conservation of iron, especially the heating to redness and the lithium hydroxide methods. ICOM Committee for Conservation. 5th Triennial Meeting, Zagreb, 1-8 Oct. 1978. Preprints, 1978. 78/23/13/1-6.

FENG, C., WANG, H., LU, N., CHEN, T., HE, H., LU, Y. & TU, X. M. 2014. Log-transformation and its implications for data analysis. *Shanghai archives of psychiatry,* 26**,** 105-109.

FENN, J. D. & FOLEY, K. 1975. PASSIVATION OF IRON. *Studies in Conservation,* 20**,** 195-198.

FLORIAN, M. 1987. The underwater environment. *Conservation of marine archaeological objects,* 15.

GABE, D. R., WILCOX, G. D. & CARTER, V. E. 2010. 4.04 - General Principles of Protection by Coatings*. *In:* COTTIS, B., GRAHAM, M., LINDSAY, R., LYON, S., RICHARDSON, T., SCANTLEBURY, D. & STOTT, H. (eds.) *Shreir's Corrosion.* Oxford: Elsevier.

GARDNER, L. R. 1973. Chemical models for sulfate reduction in closed anaerobic marine environments. *Geochimica et Cosmochimica Acta,* 37**,** 53-68.

GARVERICK, L. 1994. *Corrosion in the petrochemical industry*, ASM international.

GERRISH, S. & MCDONALD, S. 2004. The conservation of the Millennium Clock Tower. *SSCR journal: the quarterly news magazine of the Scottish Society for Conservation and Restoration, v.15, no.1,* 15**,** pp.13-15, bibliog.

GHATAK, A. & THYAGARAJAN, K. 1998. *An introduction to fiber optics*, Cambridge university press.

GILBERG, M. R. & SEELEY, N. J. 1982. Liquid ammonia as a solvent and reagent in conservation. *Studies in conservation,* 27**,** 38-44.

GONZÁLEZ, N., MARDIKIAN, P., NÄSÄNEN, L. & DREWS, M. 2013. The use of subcritical fluids for the stabilisation of archaeological iron: an overview. *Corrosion and conservation of cultural heritage metallic artefacts.* Elsevier.

GREENFIELD, D. & SCANTLEBURY, D. 2000. The protective action of organic coatings on steel: a review. *Journal of Corrosion Science & Engineering,* 3.

GUILMINOT, E., NEFF, D., RÉMAZEILLES, C., REGUER, S., KERGOURLAY, F., PELÉ, C., DILLMANN, P., REFAIT, P., NICOT, F., MIELCAREK, F., HUET, N. & REBIÈRE, J. 2012. Influence of crucial parameters on the dechlorination treatments of ferrous objects from seawater. *Studies in Conservation,* 57**,** 227-236.

HACK, H. P. 2010. 2.07 - Galvanic Corrosion. *In:* COTTIS, B., GRAHAM, M., LINDSAY, R., LYON, S., RICHARDSON, T., SCANTLEBURY, D. & STOTT, H. (eds.) *Shreir's Corrosion.* Oxford: Elsevier.

HEALTH & EXECUTIVE, S. 2018. EH40/2005 Workplace exposure limits.

HILDRED, A. 2011. *Weapons of warre : the armaments of the Mary Rose,* Portsmouth, Portsmouth : Mary Rose Trust.

HŒRLÉ, S., MAZAUDIER, F., DILLMANN, P. & SANTARINI, G. 2004. Advances in understanding atmospheric corrosion of iron. II. Mechanistic modelling of wet–dry cycles. *Corrosion science,* 46**,** 1431-1465.

HOFFMAN, W. & KING, L. 2019. Equipment Identification and the Development of Dry-Ice Blasting Parameters for Cleaning Archaeological Wrought Iron, Copper Alloys, and Gray Cast Iron. *In:* CHEMELLO, C., BRAMBILLA, L. & JOSEPH, E. (eds.) *Metal 2019 Neuchâtel, Switzerland. Interim meeting of the International Council of Museums Committee for Conservation Metal Working Group.* Neuchâtel, Switzerland: Haute Ecole Arc Conservation-restauration (HE-Arc CR) & International Council of Museums - Committee for Conservation (ICOM-CC).

JAKOBSEN, T. Iron conservation at the National Museum of Copenhagen-past and present. Icom 7th triennial meeting. Copenhagen, 10-14 September 1984. Preprints, 1984. 84.22. 8-84.22. 10.

JOHNSON, D., TYLDESLEY, J., LOWE, T., WITHERS, P. J. & GRADY, M. M. 2013. Analysis of a prehistoric Egyptian iron bead with implications for the use and perception of meteorite iron in ancient Egypt. *Meteoritics & Planetary Science,* 48**,** 997-1006.

JOHNSON, S. 2020. *Functional Fires in Historic Houses: The Impact on the Internal Environment and the Response of Timber Objects.* PhD, Cardiff University.

JONES, A. & JONES, E. 1993. Observations on the marine gasteromycete Nia vibrissa. *Mycological research,* 97**,** 1-6.

JONES, M. (ed.) 2003. *For future generations : conservation of a Tudor maritime collection*: Portsmouth : Mary Rose Trust.

JONES, M. 2020. *RE: Personal communication.*

JONES, S. P., SLATER, N. K., JONES, M., WARD, K. & SMITH, A. D. 2009. Investigating the processes necessary for satisfactory freeze-drying of waterlogged archaeological wood. *Journal of Archaeological Science,* 36**,** 2177-2183.

JØRGENSEN, B. B. & NELSON, D. C. 2004. Sulfide oxidation in marine sediments: geochemistry meets microbiology. *Geological Society of America Special Papers,* 379**,** 63-81.

KEENE, S. 2012. *Managing conservation in museums*, Routledge.

KEENE, S. & ORTON, C. 1985. Stability of Treated Archaeological Iron: An Assessment. *Studies in Conservation,* 30**,** 136-142.

KENDELL, K. 1982. *The Gaseous Reduction of Archaeological Ironwork.* PhD, Portsmouth Polytechnic.

KOLMAN, A., CHOVANEC, M. & OSTERMAN-GOLKAR, S. 2002. Genotoxic effects of ethylene oxide, propylene oxide and epichlorohydrin in humans: update review (1990–2001). *Mutation Research/Reviews in Mutation Research,* 512**,** 173-194.

KOOLI, W. M., COMENSOLI, L., MAILLARD, J., ALBINI, M., GELB, A., JUNIER, P. & JOSEPH, E. 2018. Bacterial iron reduction and biogenic mineral formation for the stabilisation of corroded iron objects. *Scientific Reports,* 8**,** 764.

KRAUSKOPF, K. B. 1995. *Introduction to geochemistry*, New York : McGraw-Hill.

LADEBURG, H. 1973. Konservierung der Eisenteile der Bremer Kogge. *Der Präparator,* 19**,** 11-20.

LANGUMIER, M., SABOT, R., OBAME-NDONG, R., JEANNIN, M., SABLÉ, S. & REFAIT, P. 2009. Formation of Fe(III)-containing mackinawite from hydroxysulphate green rust by sulphate reducing bacteria. *Corrosion Science,* 51**,** 2694-2702.

LAWSON, A. 2016. *Assessment of the performance of three clear coatings for use in heritage conservation by an oxygen consumption technique.* PhD Thesis, Cardiff University.

LEYGRAF, C., WALLINDER, I. O., TIDBLAD, J. & GRAEDEL, T. 2016. *Atmospheric corrosion*, John Wiley & Sons.

LEYSSENS, K., ADRIAENS, A. & DEGRIGNY, C. 2005. Electrochemical monitoring of the storage or stabilization of archaeological copper-based artifacts in sodium sesquicarbonate solutions. *In:* VERGER, I. (ed.) *14th triennial meeting, The Hague, 12-16 September 2005: preprints (ICOM Committee for Conservation).* London: Earthscan Ltd., London, United Kingdom.

LIN, C.-C. 2014. *Chloride Form and the Response of Archaeological Iron to Humidity.* MSc thesis, Cardiff University.

LINGLE, A. 2019. *Application of aqueous polymers on earthen substrates.* PhD, Cardiff University.

LITTLE, B. J., RAY, R. I. & POPE, R. K. 2000. Relationship Between Corrosion and the Biological Sulfur Cycle: A Review. *Corrosion,* 56**,** 433-443.

MACLEOD, I. D. 1981. Shipwrecks and applied electrochemistry. *Journal of Electroanalytical Chemistry and Interfacial Electrochemistry,* 118**,** 291-303.

MACLEOD, I. D. 1986. CONSERVATION OF THE STEAM SHIP XANTHO. *AICCM Bulletin,* 12**,** 67-94.

MACLEOD, I. D. 1989. The electrochemistry and conservation of iron in sea water. *Chemistry in Australia,* 56**,** 227-229.

MACLEOD, I. D. 1990. Conservation management of iron steamships: the S.S. Xantho (1872). *In:* MOULDS, A., JAMES, B. W. S., MOYNIHAN, J. F. & KEITH, C. (eds.) *Fifth National Conference on Engineering Heritage 1990, Perth 3-5 December 1990: interpreting engineering heritage.* Perth, Western Australia, Australia: Institution of Engineers, Australia. Western Australia Division.

MACLEOD, I. D. 1996. In situ conservation of cannon and anchors on shipwreck sites. *Studies in Conservation,* 41**,** 111-115.

MACLEOD, I. D. 1998. In situ corrosion studies on iron shipwrecks and cannon: the impact of water depth and archaeological activities on corrosion rates. *In:* MOUREY, W. & ROBBIOLA, L. (eds.) *Metal 98: proceedings of the International Conference on Metals Conservation = Actes de la conférence internationale sur la conservation des métaux: Draguignan-Figanières, France, 27-29 May 1998.* London, United Kingdom: Earthscan Ltd.

MACLEOD, I. D. 2006. Corrosion and conservation management of iron shipwrecks in Chuuk Lagoon, Federated States of Micronesia. *Conservation and Management of Archaeological Sites,* 7**,** 203-223.

MACLEOD, I. D. 2011. Corrosion and conservation management of the HMAS AE2 submarine (1915) in the Sea of Marmara Turkey. *In:* MARDIKIAN, P., CHEMELLO, C., WATTERS, C. & HULL, P. (eds.) *Metal 2010: proceedings of the interim meeting of the ICOM-CC Metal Working Group, October 11-15, 2010, Charleston, South Carolina, USA.* Clemson, South Carolina, United States: Clemson University.

MACLEOD, I. D. 2016. In-situ corrosion measurements of WWII shipwrecks in Chuuk Lagoon, quantification of decay mechanisms and rates of deterioration. *Frontiers in Marine Science,* 3**,** 38.

MACLEOD, I. D., COOK, D. & SCHINDELHOLZ, E. Corrosion and conservation of three elements of the American Civil War ironclad USS Monitor (1862). ICOM Committee for Conservation, ICOM-CC, 15th Triennial Conference New Delhi, 22-26 September 2008: preprints, 2008. Allied Publishers Pvt., 427-433.

MACLEOD, I. D., NORTH, N. A. & BEEGLE, C. J. 1986. The excavation, analysis and conservation of shipwreck sites. *In:* INTERNATIONAL CENTRE FOR THE STUDY OF THE, P., THE RESTORATION OF CULTURAL, P. & RIJKSUNIVERSITEIT TE, G. (eds.) *Preventive measures during excavation and site protection: conference Ghent, 6-8 November 1985 = Mesures préventives en cours de fouilles et protection du site: conférence, Gand, 6-8 novembre 1985.* Rome, Italy: ICCROM.

MARDIKIAN, P. 2004. Conservation and Management Strategies Applied to Post-Recovery Analysis of the American Civil War Submarine HL Hunley (1864). *International Journal of Nautical Archaeology,* 33**,** 137-148.

MATTHIESEN, H. 2007. A novel method to determine oxidation rates of heritage materials in vitro and in situ. *Studies in Conservation,* 52**,** 271-280.

MATTHIESEN, H. 2013. Oxygen monitoring in the corrosion and preservation of metallic heritage artefacts. *Corrosion and conservation of cultural heritage artefacts***,** 368-391.

MATTHIESEN, H., HILBERT, L. R. & GREGORY, D. J. 2003. Siderite as a Corrosion Product on Archaeological Iron from a Waterlogged Environment. *Studies in Conservation,* 48**,** 183-194.

MATTHIESEN, H. & STEMANN-PETERSEN, K. A fast and non-destructive method to document and quantify the efficiency of metals conservation. Metal 2013: Interim Meeting of the ICOM-CC Metal Working Group. Edinburgh, 2013. 16-20.

MATTHIESEN, H. & WONSYLD, K. 2010. In situ measurement of oxygen consumption to estimate corrosion rates. *Corrosion Engineering, Science and Technology,* 45**,** 350-356.

MCNEIL, I. 2002. *An encyclopedia of the history of technology*, Routledge.

MEEKS, N. D. 1987. Artefacts, surfaces and the SEM. *In:* BLACK, J. (ed.) *Recent advances in the conservation and analysis of artifacts: jubilee conservation conference papers, London 6-10 July 1987.* London: Summer Schools Press, London, United Kingdom.

MEMET, J. 2007a. The corrosion of metallic artefacts in seawater: descriptive analysis. *EUROPEAN FEDERATION OF CORROSION PUBLICATIONS,* 48**,** 152.

MEMET, J. B. 2007b. 9 - The corrosion of metallic artefacts in seawater: descriptive analysis. *In:* DILLMANN, P., BÉRANGER, G., PICCARDO, P. & MATTHIESEN, H. (eds.) *Corrosion of Metallic Heritage Artefacts.* Woodhead Publishing.

MENTOVICH, E., SCHREIBER, D., GOREN, Y., KAHANOV, Y., GOREN, H., CVIKEL, D. & ASHKENAZI, D. 2010. New insights regarding the Akko 1 shipwreck: a metallurgic and petrographic investigation of the cannonballs. *Journal of Archaeological Science,* 37**,** 2520-2528.

MERCER, A. D. 1979. Inhibition of the Corrosion of Grey Cast Iron in Ethanediol/Water Solutions by Benzoate/Benzotriazole Mixture: A Synergistic Effect. *British Corrosion Journal,* 14**,** 179-182.

NEFF, D., REGUER, S. & DILLMANN, P. 2013. Analytical techniques for the study of corrosion of metallic heritage artefacts: from micrometer to nanometer scales. *In:* DILLMANN, P., WATKINSON, D., ANGELINI, E. & ADRIAENS, A. (eds.) *Corrosion and Conservation of Cultural Heritage Metallic Artefacts. European Federation of Corrosion (EFC) Series.* Woodhead.

NEFF, D., VEGA, E., DILLMANN, P., DESCOSTES, M., BELLOT-GURLET, L. & BÉRANGER, G. 2007. 4 - Contribution of iron archaeological artefacts to the estimation of average corrosion rates and the long-term corrosion mechanisms of low-carbon steel buried in soil. *In:* DILLMANN, P., BÉRANGER, G., PICCARDO, P. & MATTHIESEN, H. (eds.) *Corrosion of Metallic Heritage Artefacts.* Woodhead Publishing.

NEUHAUS, E. 2013. A critical look at the use of HVAC systems in the museum environment. *In:* ASHLEY-SMITH, J., BURMESTER, A. & EIBL, M. (eds.) *Climate for collections: standards and uncertainties.* London, Munich: Archetype Publications Ltd., London, United Kingdom; Bayerische Staatsgemäldesammlungen. Doerner-Institut, Munich, Germany.

NORDGREN, E. 2016. *The effect of metallurgical structure on the chloride-induced corroion of archaeological wrought iron.* PhD, Cardiff University.

NORDGREN, E., GONCALVES, P., SCHINDELHOLZ, E., YUNOVICH, M. & BROSSIA, S. 2007. Corrosion Assessment and Implementations of Techniques to Mitigate Corrosion of Large Artifacts from the USS Monitor (1862). *Metal,* 7**,** 55-61.

NORTH, N. A. 1976. Formation of coral concretions on marine iron. *International Journal of Nautical Archaeology,* 5**,** 253-258.

NORTH, N. A. 1982. Corrosion Products on Marine Iron. *Studies in Conservation,* 27**,** 75-83.

NORTH, N. A. 1987. Conservation of metals. *Conservation of marine archaeological objects.* Butterworths.

NORTH, N. A. & MACLEOD, I. D. 1987. Corrosion of metals. *In:* PEARSON, C. (ed.) *Conservation of marine archaeological objects.* London, United Kingdom: Butterworth & Co. (Publishers) Ltd.

NORTH, N. A., OWENS, M. & PEARSON, C. 1976. Thermal stability of cast and wrought marine iron. *Studies in conservation,* 21**,** 192-197 205-206.

NORTH, N. A. & PEARSON, C. 1975a. Alkaline sulfite reduction treatment of marine iron. *In:* CONSERVATION, I. C. F. (ed.) *ICOM Committee for Conservation 4th triennial meeting, Venice, 13-18 October 1975: preprints.* Paris, France: International Council of Museums.

NORTH, N. A. & PEARSON, C. 1975b. Investigations into methods for conserving iron relics recovered from the sea. *Conservation in archaeology and the applied arts: preprints of the contributions to the Stockholm Congress, 2-6 June 1975.* London, United Kingdom: International Institute for Conservation of Historic and Artistic Works.

NORTH, N. A. & PEARSON, C. 1977. Thermal Decomposition of FeOCl and Marine Cast Iron Corrosion Products. *Studies in Conservation,* 22**,** 146-157.

NORTH, N. A. & PEARSON, C. Methods for treating marine iron. ICOM Committee for Conservation. 5th Triennial Meeting, Zagreb, 1-8 Oct. 1978. Preprints, 1978a. 10-10.

NORTH, N. A. & PEARSON, C. 1978b. Washing Methods for Chloride Removal from Marine Iron Artifacts. *Studies in Conservation,* 23**,** 174-186.

O'NEIL, M. J., SMITH, A., HECKELMAN, P. E. & BUDAVARI, S. 2001. The merck index-An encyclopedia of chemicals, drugs, and biologicals. whitehouse station, NJ: Merck and Co. *Inc,* 767**,** 4342.

O'SHEA, C., DAVIES, B., KENDELL, K. & AKED, S. 1982. The use of hydrogen reduction in stabilizing large items of iron recovered from the sea. *Studies in Conservation,* 27**,** 126-129.

ODDY, W. & HUGHES, M. 1970. The stabilization of 'Active'bronze and iron antiquities by the use of sodium sesquicarbonate. *Studies in conservation,* 15**,** 183-189.

ODDY, W. A. & BLACK, J. A new method for the conservation of iron: ionophoresis in a non-aqueous electrolyte. Recent advances in the conservation and analysis of artifacts. Jubilee Conservation Conference, London 6-10 July 1987, 1987. 155-158.

ODEGAARD, N., CARROLL, S. & ZIMMT, W. S. 2005. *Material characterization tests for objects of art and archaeology,* London, London : Archetype.

ORGAN, R. M. 1955. The washing of treated bronzes. *The museums journal,* 55**,** 112-119.

ORGAN, R. M. 1961. The examination and treatment of bronze antiquities. *Studies in Conservation,* 6**,** 104-110.

OTIENO-ALEGO, V., CREAGH, D., HALLAM, D., VIDUKA, A. & HEATH, G. 2001. In situ and laboratory studies of the ageing of protective wax coatings on metal surfaces of museum objects and outdoor statues. *Ageing Studies and Lifetime Extension of Materials.* Springer.

PATOHARJU, O. 1975. Conservation of Cannon Recovered from the Brackish Sea. *Studies in Conservation,* 20**,** 183-187.

PATOHARJU, O. 1978. Conservation of cast-iron objects recovered from Brackish Sea. *In:* ORGAN, R. M. (ed.) *Conservation of iron objects found in a salty environments.*

PATSCHEIDER, J. & VEPŘEK, S. 1986. Application of low-pressure hydrogen plasma to the conservation of ancient iron artifacts. *Studies in conservation,* 31**,** 29-37.

PEARSON, C. 1972. The Preservation of Iron Cannon after 200 Years under the Sea. *Studies in Conservation,* 17**,** 91-110.

PEARSON, D. 2020. *RE: Personal communication.*

PELIKÁN, J. B. 1966. Conservation of Iron with Tannin. *Studies in Conservation,* 11**,** 109-116.

PHULL, B. 2010. 2.18 - Marine Corrosion. *In:* COTTIS, B., GRAHAM, M., LINDSAY, R., LYON, S., RICHARDSON, T., SCANTLEBURY, D. & STOTT, H. (eds.) *Shreir's Corrosion.* Oxford: Elsevier.

PINDER, L. W., DAWSON, K. & TATLOCK, G. J. 2010. 1.22 - High Temperature Corrosion of Low Alloy Steels. *In:* COTTIS, B., GRAHAM, M., LINDSAY, R., LYON, S., RICHARDSON, T., SCANTLEBURY, D. & STOTT, H. (eds.) *Shreir's Corrosion.* Oxford: Elsevier.

PLENDERLEITH, H. J. & WERNER, A. E. 1971. *The conservation of antiquities and works of art: treatment, repair and restoration*.

POINTING, S., JONES, E. B. G. & JONES, M. 1996. Radiosensitivity of fungi isolated from waterlogged archaeological wood. *Mycoscience,* 37**,** 455-458.

POURBAIX, M. 1974. Applications of electrochemistry in corrosion science and in practice. *Corrosion Science,* 14**,** 25-82.

POURBAIX, M. 1977. Electrochemcial corrosion and reduction. *Corrosion and Metal Artifacts: A Dialogue Between Conservators and Archaeologists and Corrosion Scientists,* 479**,** 1.

POURNOU, A., JONES, A. M. & MOSS, S. 2001. Biodeterioration dynamics of marine wreck-sites determine the need for their in situ protection. *International Journal of Nautical Archaeology,* 30**,** 299-305.

PRESENS 2017. Oxygen Sensor Spots PSTt3/PSt6 Instruction Manual. Regensburg, Germany: Precision Sensing GmbH.

PRESENS 2018. PreSens Measurement Studio 2 for O2 Instruction Manual. Regensburg, Germany: Precision Sensing GmbH.

PRESTON, J., SMITH, A. D., SCHOFIELD, E. J., CHADWICK, A. V., JONES, M. A. & WATTS, J. E. 2014. The effects of Mary Rose conservation treatment on iron oxidation processes and microbial communities contributing to acid production in marine archaeological timbers. *PloS one,* 9**,** e84169.

PRESTON, J., WATTS, J. E. & JONES, M. 2012. Novel bacterial community associated with 500-year-old unpreserved archaeological wood from King Henry VIII's Tudor warship the Mary Rose. *Applied and environmental microbiology,* 78**,** 8822-8828.

RAMIREZ BARAT, B., LETARDI, P. & CANO, E. 2019. An Overview of the Use of EIS Measurements for the Assessment of Patinas and Coatings in the Conservation of Metallic Cultural Heritage. *In:* CHEMELLO, C., BRAMBILLA, L. & JOSEPH, E. (eds.) *Metal 2019 Neuchâtel, Switzerland. Interim meeting of the International Council of Museums Committee for Conservation Metal Working Group.* Neuchâtel, Switzerland: Haute Ecole Arc Conservation-restauration (HE-Arc CR) & International Council of Museums - Committee for Conservation (ICOM-CC).

RATHGEN, F. 1898. *Die Konservierung von Alterthumsfunden*, W. Spemann.

RATHGEN, F. 1905. *The preservation of antiquities: a handbook for curators,* University Press.

REES-JONES, S. G. 1972. Some Aspects of Conservation of Iron Objects from the Sea. *Studies in Conservation,* 17**,** 39-43.

REFAIT, P., BENALI, O., ABDELMOULA, M. & GÉNIN, J.-M. 2003a. Formation of 'ferric green rust'and/or ferrihydrite by fast oxidation of iron (II–III) hydroxychloride green rust. *Corrosion science,* 45**,** 2435-2449.

REFAIT, P. & GÉNIN, J. M. R. 1997. The mechanisms of oxidation of ferrous hydroxychloride β-Fe2(OH)3Cl in aqueous solution: The formation of akaganeite vs goethite. *Corrosion Science,* 39**,** 539-553.

REFAIT, P., MEMET, J.-B., BON, C., SABOT, R. & GÉNIN, J.-M. 2003b. Formation of the Fe (II)–Fe (III) hydroxysulphate green rust during marine corrosion of steel. *Corrosion Science,* 45**,** 833-845.

REFAIT, P. H., ABDELMOULA, M. & GÉNIN, J. M. R. 1998. Mechanisms of formation and structure of green rust one in aqueous corrosion of iron in the presence of chloride ions. *Corrosion Science,* 40**,** 1547-1560.

RÉGUER, S., NEFF, D., BELLOT-GURLET, L. & DILLMANN, P. 2007. Deterioration of iron archaeological artefacts: micro-Raman investigation on Cl-containing corrosion products. *Journal of Raman Spectroscopy,* 38**,** 389-397.

REHREN, T., BELGYA, T., JAMBON, A., KÁLI, G., KASZTOVSZKY, Z., KIS, Z., KOVÁCS, I., MARÓTI, B., MARTINÓN-TORRES, M., MINIACI, G., PIGOTT, V. C., RADIVOJEVIĆ, M., ROSTA, L., SZENTMIKLÓSI, L. & SZŐKEFALVI-NAGY, Z. 2013. 5,000 years old Egyptian iron beads made from hammered meteoritic iron. *Journal of Archaeological Science,* 40**,** 4785-4792.

RÉMAZEILLES, C., NEFF, D., KERGOURLAY, F., FOY, E., CONFORTO, E., GUILMINOT, E., REGUER, S., REFAIT, P. & DILLMANN, P. 2009. Mechanisms of long-term anaerobic corrosion of iron archaeological artefacts in seawater. *Corrosion Science,* 51**,** 2932-2941.

RÉMAZEILLES, C. & REFAIT, P. 2007. On the formation of β-FeOOH (akaganéite) in chloride-containing environments. *Corrosion Science,* 49**,** 844-857.

RÉMAZEILLES, C. & REFAIT, P. 2009. Fe(II) hydroxycarbonate Fe2(OH)2CO3 (chukanovite) as iron corrosion product: Synthesis and study by Fourier Transform Infrared Spectroscopy. *Polyhedron,* 28**,** 749-756.

REYNAUD, A. 2010. 3.02 - Corrosion of Cast Irons. *In:* COTTIS, B., GRAHAM, M., LINDSAY, R., LYON, S., RICHARDSON, T., SCANTLEBURY, D. & STOTT, H. (eds.) *Shreir's Corrosion.* Oxford: Elsevier.

RIMMER, M. & WATKINSON, D. 2011. Residues of alkaline sulphite treatment and their effects on the corrosion of archaeological iron objects. *In:* MARDIKIAN, P., CHEMELLO, C., WATTERS, C. & HULL, P. (eds.) *Metal 2010: proceedings of the interim meeting of the ICOM-CC Metal Working Group, October 11-15, 2010, Charleston, South Carolina, USA.* Clemson, South Carolina, United States: Clemson University.

RIMMER, M., WATKINSON, D. & WANG, Q. 2012. The efficiency of chloride extraction from archaeological iron objects using deoxygenated alkaline solutions. *Studies in conservation,* 57**,** 29-41.

RIMMER, M., WATKINSON, D. & WANG, Q. 2013. The impact of chloride desalination on the corrosion rate of archaeological iron. *Studies in conservation,* 58**,** 326-337.

RINUY, A. & SCHWEIZER, F. Application of the alkaline sulphite treatment to archaeological iron: a comparative study of different desalination methods. Conservation of iron. Proceedings of a symposium held at greenwich on july 4th 1980, 1982. National maritime museum, 44-49.

RODGERS, S. J. 1960. THE REACTION RATE OF SODIUM SULFITE WITH DISSOLVED OXYGEN. Technical Report No. 73. ; MSA Research Corp., Callery, Penna.

ROSENBERG, G. A. T. 1917. *Antiquités en fer et en bronze: leur transformation dans la terre contenant de l'acide carbonique et des chlorures et leur conservation*, Gyldendal.

RULE, M. 1982. *The Mary Rose: the excavation and raising of Henry VIII's flagship*, US Naval Institute Press.

SALOMONSEN, E. 1977. Fjernelse af klorider fra forhistorisk jern. *Afangsopgave fra Konservatorskolen*.

SCHMIDT-OTT, K. 1997. Applications of low pressure plasma treatment at the Swiss National Museum and assessment of the results. *Zeitschrift für schweizerische Archäologie und Kunstgeschichte,* 54**,** 45-50.

SCHMIDT-OTT, K. & BOISSONNAS, V. 2002. Low-Pressure Hydrogen Plasma: An Assessment of Its Application on Archaeological Iron. *Studies in Conservation,* 47**,** 81-87.

SCHMIDT-OTT, K. & OSWALD, N. Alkaline sulfite desalination: tips and tricks. VDR Conference Handbook “Archaeological Metal Finds–From Excavation to Exhibition”, Manheim, 11–13 October, 2006. 17.

SCHMUTZLER, B., REVAY, Z. & STIEGHORST, C. 2019. Desalination of Archaeological Iron Objects: Comparing the Effectiveness of Sodium Hydroxide Treatments. *In:* CHEMELLO, C., BRAMBILLA, L. & JOSEPH, E. (eds.) *Metal 2019 Neuchâtel, Switzerland. Interim meeting of* *the International Council of Museums Committee for Conservation Metal Working Group.* Neuchâtel, Swizterland: Haute Ecole Arc Conservation-restauration (HE-Arc CR) & International Council of Museums - Committee for Conservation (ICOM-CC).

SCHOFIELD, E. J., SARANGI, R., MEHTA, A., JONES, A. M., MOSSELMANS, F. J. & CHADWICK, A. V. 2011. Nanoparticle de-acidification of the Mary Rose. *Materials Today,* 14**,** 354-358.

SCHOFIELD, E. J., SARANGI, R., MEHTA, A., JONES, A. M., SMITH, A., MOSSELMANS, J. F. W. & CHADWICK, A. V. 2016. Strontium carbonate nanoparticles for the surface treatment of problematic sulfur and iron in waterlogged archaeological wood. *Journal of Cultural Heritage,* 18**,** 306-312.

SCHUBERT, H. R. 1957. History of the British iron & steel industry.

SCHWERTMANN, U. & CORNELL, R. M. 2008. *Iron oxides in the laboratory: preparation and characterization*, John Wiley & Sons.

SCIENTIFIC, S. 2012. Model 926S Chloride Analyser Operator's Manual. Sherwod Scientific Ltd.

SCOTT, A. 1922. THE RESTORATION AND PRESERVATION OF OBJECTS AT THE BRITISH MUSEUM. *Journal of the Royal Society of Arts,* 70**,** 327-338.

SCOTT, D. A. 1992. *Metallography and Microstructure in Ancient and Historic Metals*, Getty Publications.

SCOTT, D. A. & EGGERT, G. 2009. Iron and steel in art. *Corrosion, Colorants, Conservation*.

SEIFERT, J. 2015. *Oxygen consumption as an indicator of corrosion rates of cast iron shot from The Mary Rose, in relation to treatment method and relative hummidity.* Disseration for the requirement of Master of Science, Cardiff University.

SELWYN, L. & ARGYROPOULOS, V. 2006. Chlorine determination in archaeological wrought iron by instrumental neutron activation analysis. *Journal of the Canadian Association for Conservation,* 31**,** 3-12.

SELWYN, L. S. & ARGYROPOULOS, V. 2005. Removal of Chloride and Iron Ions from Archaeological Wrought Iron with Sodium Hydroxide and Ethylenediamine Solutions. *Studies in Conservation,* 50**,** 81-100.

SELWYN, L. S. & MCKINNON, W. R. 2006. Removing charged species from porous archaeological material: diffusion, electromigration, electrophoresis and electro-osmosis in fully immersed objects. *Studies in Conservation,* 51**,** 83-93.

SHARMA, M. K. 2016. Uses and problems of arsenic in taxidermy. *Conservation of cultural property in India, v.41,* 41**,** pp.133-134, bibliog.

SHASHOUA, Y. & MATTHIESEN, H. 2010. Protection of iron and steel in large outdoor industrial heritage objects. *Corrosion Engineering, Science and Technology,* 45**,** 357-361.

SHIMURA, S. 1930. A study on the structure of cementite. *Proceedings of the Imperial Academy,* 6**,** 269-271.

SHREIR, L. L. 2010. 1.05 - Basic Concepts of Corrosion*. *In:* COTTIS, B., GRAHAM, M., LINDSAY, R., LYON, S., RICHARDSON, T., SCANTLEBURY, D. & STOTT, H. (eds.) *Shreir's Corrosion.* Oxford: Elsevier.

SIMON, H. J., CIBIN, G., REINHARD, C., LIU, Y., SCHOFIELD, E. & FREESTONE, I. C. 2019. Influence of microstructure on the corrosion of archaeological iron observed using 3D synchrotron micro-tomography. *Corrosion Science,* 159**,** 108132.

SIMON, H. J., CIBIN, G., ROBBINS, P., DAY, S., TANG, C., FREESTONE, I. & SCHOFIELD, E. 2018. A Synchrotron-Based Study of the Mary Rose Iron Cannonballs. *Angewandte Chemie International Edition,* 0.

SINGH, M. M. & GUPTA, A. 1996. Corrosion behaviour of mild steel in formic acid solutions. *Materials Chemistry and Physics,* 46**,** 15-22.

SINGH, S. K. & MUKHERJEE, A. K. 2010. Kinetics of Mild Steel Corrosion in Aqueous Acetic Acid Solutions. *Journal of Materials Science & Technology,* 26**,** 264-269.

SNOW, R. F. 1984. The 'Holland' Surfaces. *American Heritage.*

SONG, X. 2013. *Surface and Bulk Reactivity of Iron Oxyhydroxides: A Molecular Perspective.* PhD Thesis, Umea University.

STÅHL, K., NIELSEN, K., JIANG, J., LEBECH, B., HANSON, J. C., NORBY, P. & VAN LANSCHOT, J. 2003. On the akaganéite crystal structure, phase transformations and possible role in post-excavational corrosion of iron artifacts. *Corrosion Science,* 45**,** 2563-2575.

STARLEY, D. & HILDRED, A. 2002. Technological examination of a Mary Rose Hailshot piece. New evidence for early iron gun casting. *Royal Armouries Yearbook,* 7**,** 139-146.

STEFANESCU, D. 2017. A history of cast iron. *ASM Handbook,* 1**,** 3-11.

TEAM, R. C. 2021. R: A Language and Environment for Statistical Computing. *In:* TEAM, R. C. (ed.). Vienna, Austria.

TEESDALE, E. B. 1991. *Gunfounding in the Weald in the Sixteenth Century*, Trustees of the Royal Armouries.

TERRAGLIO, F. P. & MANGANELLI, R. M. 1967. The absorption of atmospheric sulfur dioxide by water solutions. *Journal of the Air Pollution Control Association,* 17**,** 403-406.

THICKETT, D., LAMBARTH, S. & WYETH, P. Determining the stability and durability of archaeological materials. 9th International Conference on NDT of Art, Jerusalem, Israel, 2008. 1-10.

THICKETT, D. & ODLYHA, M. 2013. The formation and transformation of akaganeite. *In:* HISLOP, E., GONZALEZ, VANESA, TROALEN, LORE AND WILSON, LYN (ed.) *Metal 2013 Edinburgh, Scotland. Interim meeting of the international Council of Museums Committee for Conservation Metal Working Group.* Edinburgh, UK: Historic Scotland.

THUNBERG, J. C., WATKINSON, D. E. & EMMERSON, N. J. 2020. Desiccated Microclimates for Heritage Metals: Creation and Management. *Studies in Conservation***,** 1-27.

TIDBLAD, J. 2013. 3 - Atmospheric corrosion of heritage metallic artefacts: processes and prevention. *In:* DILLMANN, P., WATKINSON, D., ANGELINI, E. & ADRIAENS, A. (eds.) *Corrosion and Conservation of Cultural Heritage Metallic Artefacts.* Woodhead Publishing.

TIKKANEN, A. 2020. The Mary Rose. *Encyclopaedia Britannica.* Online: Encyclopaedia Britannica.

TRETHEWEY, K. R. & CHAMBERLAIN, J. 1995. Corrosion for science and engineering.

TRUST, M. R. 2015. Selected object conservation records from the Mary Rose. The Mary Rose Trust.

TURGOOSE, S. 1982a. The nature of surviving iron objects. *Conservation of Iron (Maritime Monographs and Reports No. 53).*

TURGOOSE, S. 1982b. Post-Excavation Changes in Iron Antiquities. *Studies in Conservation,* 27**,** 97-101.

TURGOOSE, S. 1985. The Corrosion of Archaeological Iron during Burial and Treatment. *Studies in Conservation,* 30**,** 13-18.

TURGOOSE, S. 1993. Structure, composition and deterioration of unearthed iron objects. *Current problems in the conservation of metal antiquities: thirteenth international symposium on the the conservation and restoration of cultural property, 4-6 October 1989, Tokyo, Japan.* Bunka-cho Tokyo Kokuritsu Bunkazai Kenkyujo Hozon Kagakubu.

TYLECOTE, R. & BLACK, J. 1980. The effect of hydrogen reduction on the properties of ferrous materials. *Studies in Conservation,* 25**,** 87-96.

TYLECOTE, R. F. 1976. *A history of metallurgy*, The Metals Society.

VERNON, W. H. J. 1935. A laboratory study of the atmospheric corrosion of metals. Part II.—Iron: the primary oxide film. Part III.—The secondary product or rust (influence of sulphur dioxide, carbon dioxide, and suspended particles on the rusting of iron). *Transactions of the Faraday Society,* 31**,** 1668-1700.

VILHAR, B. Reduction thermique des objets confectionnés en fer entierement corrodés ou presque. ICOM Committee for Conservation. 5th Triennial Meeting, Zagreb, 1-8 Oct. 1978. Preprints, 1978. 78/23/7/1-3.

WALKER, R. 2001. Instability of Iron Sulfides on Recently Excavated Artifacts. *Studies in Conservation,* 46**,** 141-152.

WALKER, R. & HILDRED, A. 2000. Quantitative non-destructive analysis of metals in artefacts. *International Journal of Nautical Archaeology,* 29**,** 163-166.

WALKER, R., STEELE, A. D. & MORGAN, D. T. B. 1996. Pyrophoric Nature of Iron Sulfides. *Industrial & Engineering Chemistry Research,* 35**,** 1747-1752.

WANG, Q., DOVE, S., SHEARMAN, F. & SMIRNIOU, M. 2008. Evaluation of methods of chloride ion concentration determination and effectiveness of desalination treatments using sodium hydroxide and alkaline sulphite solutions. *The Conservator,* 31**,** 67-74.

WATKINSON, D. 1982. An assessment of lithium hydroxide and sodium hydroxide treatments for archaeological ironwork. *Conservation of Iron (Maritime Monographs and Reports No. 53).*

WATKINSON, D. 1996. Chloride extraction from archaeological iron: comparative treatment efficiencies. *Studies in Conservation,* 41**,** 208-212.

WATKINSON, D. 2010. Measuring effectiveness of washing methods for corrosion control of archaeological iron: problems and challenges. *Corrosion Engineering, Science and Technology,* 45**,** 400-406.

WATKINSON, D., EMMERSON, N. & SEIFERT, J. 2016. Matching Display Relative Humidity to Corrosion Rate: Quantitative Evidence for Marine Cast Iron Cannon Balls. *Metal 2016 New Delhi, India. Interim meeting of the international Council of Museums Committee for Conservation Metal Working Group.* New Delhi, India.

WATKINSON, D. & LEWIS, M. 2004. ss Great Britain iron hull: modelling corrosion to define storage relative humidity. *Metal,* 4**,** 88-103.

WATKINSON, D. & LEWIS, M. ss Great Britain: Science and Technology Underpin Enclosure Design. Conservation Matters in Wales. On Display: Showcases and Enclosures. Post prints of a one day conference held on, 2007. 13-17.

WATKINSON, D. & LEWIS, M. 2008. Dessicated storage of chloride contaminated iron: a study of the effects of loss of environmental control.

WATKINSON, D. & LEWIS, M. R. T. 2005a. Desiccated storage of chloride-contaminated archaeological iron objects. *Studies in conservation,* 50**,** 241-252.

WATKINSON, D. & LEWIS, M. R. T. 2005b. The role of ßFeOOH in the corrosion of archaeological iron. *In:* VANDIVER, P. B., MASS, J. L. & MURRAY, A. (eds.) *Materials issues in art and archaeology VII: symposium held November 30-December 3, 2004, Boston, Massachusetts, U.S.A.* Warrendale, Pennsylvania, United States: Materials Research Society.

WATKINSON, D. & RIMMER, M. 2013. Quantifying Effectiveness of chloride desalination treatments for archaeological iron using oxygen measurement. *In:* HISLOP, E., GONZALEZ, VANESA, TROALEN, LORE AND WILSON, LYN (ed.) *Metal 2013 Edinburgh, Scotland. Interim meeting of the international Council of Museums Committee for Conservation Metal Working Group.* Edinburgh, UK: Historic Scotland.

WATKINSON, D., RIMMER, M., KASZTOVSZKY, Z., KIS, Z., MARÓTI, B. & SZENTMIKLÓSI, L. 2014. The Use of Neutron Analysis Techniques for Detecting The Concentration And Distribution of Chloride Ions in Archaeological Iron. *Archaeometry,* 56**,** 841-859.

WATKINSON, D., RIMMER, M. & KERGOURLAY, F. 2013a. Alkaline desalination techniques for archaeological iron. *Corrosion and Conservation of Cultural Heritage Metallic Artefacts***,** 407.

WATKINSON, D., RIMMER, M. B. & KERGOURLAY, F. 2013b. Alkaline desalination techniques for archaeological iron. *In:* DILLMANN, P., WATKINSON, D., ANGELINI, E. & ADRIAENS, A. (eds.) *Corrosion and Conservation of Cultural Heritage Metallic Artefacts.* Woodhead Publishing.

WATKINSON, D. & TANNER, M. 2008. ss Great Britain: conservation and access–synergy and cost. *Studies in Conservation,* 53**,** 109-114.

WATKINSON, D., TANNER, M., TURNER, R. & LEWIS, M. 2005. ss Great Britain: teamwork as a platform for innovative conservation. *The conservator,* 29**,** 73-86.

WATKINSON, D. E., RIMMER, M. B. & EMMERSON, N. J. 2019. The Influence of Relative Humidity and Intrinsic Chloride on Post-excavation Corrosion Rates of Archaeological Wrought Iron. *Studies in Conservation***,** 1-16.

WEAVER, M. 1987. Fighting Rust. *APT bulletin,* 19**,** 16-18.

WEAVER, M. E. 2004. The conservation of heritage submarines. *APT Bulletin: The Journal of Preservation Technology,* 35**,** 51-59.

WEINTRAUB, S. 2002. Demystifying silica gel. *Object Specialty Group*.

WETHERALL, K. M., MOSS, R. M., JONES, A. M., SMITH, A. D., SKINNER, T., PICKUP, D. M., GOATHAM, S. W., CHADWICK, A. V. & NEWPORT, R. J. 2008. Sulfur and iron speciation in recently recovered timbers of the Mary Rose revealed via X-ray absorption spectroscopy. *Journal of Archaeological Science,* 35**,** 1317-1328.

WIHR, R. 1975. Electrolytic desalination of archaeological iron. *Studies in Conservation,* 20**,** 189-193.

WILLIAMS, D. & JOHNSON, W. 2000. A note on casting iron cannon balls: ideality and porosity. *International journal of impact engineering,* 24**,** 429-433.

WITUCKI, G. L. 1993. A silane primer: chemistry and applications of alkoxy silanes. *Journal of coatings technology,* 65**,** 57-57.

WOODY, A. I. 2013. How is the Ideal Gas Law Explanatory? *Science & Education,* 22**,** 1563-1580.

XIA, C. & CHUNCHUN, X. 2006. Effect of chloride on the atmospheric corrosion of cast iron in sulphur-bearing pollutant environments. *Anti-Corrosion Methods and Materials,* 53**,** 161-168.

XU, W., MCDONOUGH III, R. C., LANGSDORF, B., DEMAS, J. & DEGRAFF, B. 1994. Oxygen sensors based on luminescence quenching: interactions of metal complexes with the polymer supports. *Analytical Chemistry,* 66**,** 4133-4141.

ZIMMERMAN, D. G. & EPPELSHEIMER, D. S. 1963. Comparative Microstructure Manual - Cast Irons. Chicago: Precision Scientific Co.

# 9 APPENDICES

## 9.1 APPENDIX A – DETAILED SAMPLE INFORMATION AND CORROSION RATES

Detailed information and photos of each cannonball under study are shown, as well as their treatment records provided by the MRT.

<table>
<tr><td rowspan="10"> </td><td colspan="10"><b>MRT #78A-0604</b></td><td colspan="10"><b>Sensor HS 098</b></td></tr>
<tr><td colspan="20"><b>$O_2$ Consumption Rates (mg·year$^{-1}$·g$^{-1}$ )</b></td></tr>
<tr><td colspan="4"><b>20% RH</b></td><td colspan="4"><b>30% RH</b></td><td colspan="4"><b>40% RH</b></td><td colspan="4"><b>50% RH</b></td><td colspan="4"><b>60% RH</b></td></tr>
<tr><td colspan="4">0.0092</td><td colspan="4">0.0153</td><td colspan="4">0.0149</td><td colspan="4">0.0137</td><td colspan="4">0.0286</td></tr>
<tr><td colspan="5"><b>Dia. (cm)</b></td><td colspan="5"><b>Mass (g)</b></td><td colspan="5"><b>Vol. (cm$^3$)</b></td><td colspan="5"><b>Dens. (g/cm$^3$)</b></td></tr>
<tr><td colspan="5">8.5</td><td colspan="5">1530.0</td><td colspan="5">321.6</td><td colspan="5">4.76</td></tr>
<tr><td colspan="20"><b>Primary Treatment</b></td></tr>
<tr><td colspan="20">Concretion Removed, Soaked in dilute NaOH for 2 weeks, Hydrogen Reduction, consolidated with Thermosetting resin and coated with Microcrystalline Wax.</td></tr>
<tr><td colspan="5"><b>Cl$^-$ Count:</b></td><td colspan="5">N/A</td><td colspan="5"><b>Year:</b></td><td colspan="5">1980s</td></tr>
<tr><td colspan="20"><b>Secondary Treatment</b></td></tr>
<tr><td><b>Date In Museum:</b></td><td colspan="20" rowspan="2">N/A</td></tr>
<tr><td><b>26/04/2013</b></td></tr>
<tr><td><b>Date Out of Museum:</b></td><td colspan="5"><b>Cl$^-$ Count:</b></td><td colspan="5">N/A</td><td colspan="5"><b>Year:</b></td><td colspan="5">N/A</td></tr>
<tr><td><b>22/07/2014</b></td><td colspan="10"><b>Condition When Leaving:</b></td><td colspan="10">Good</td></tr>
</table>

<table>
<tr><td rowspan="10"> </td><td colspan="10"><b>MRT #78A-0605</b></td><td colspan="10"><b>Sensor RC 049</b></td></tr>
<tr><td colspan="20"><b>$O_2$ Consumption Rates (mg·year$^{-1}$·g$^{-1}$ )</b></td></tr>
<tr><td colspan="4"><b>20% RH</b></td><td colspan="4"><b>30% RH</b></td><td colspan="4"><b>40% RH</b></td><td colspan="4"><b>50% RH</b></td><td colspan="4"><b>60% RH</b></td></tr>
<tr><td colspan="4">0.0150</td><td colspan="4">0.0038</td><td colspan="4">0.0129</td><td colspan="4">0.0017</td><td colspan="4">0.0182</td></tr>
<tr><td colspan="5"><b>Dia. (cm)</b></td><td colspan="5"><b>Mass (g)</b></td><td colspan="5"><b>Vol. (cm$^3$)</b></td><td colspan="5"><b>Dens. (g/cm$^3$)</b></td></tr>
<tr><td colspan="5">~8.5</td><td colspan="5">1280.0</td><td colspan="5">321.6</td><td colspan="5">3.98</td></tr>
<tr><td colspan="20"><b>Primary Treatment</b></td></tr>
<tr><td colspan="20">Concretion Removed, Soaked in dilute NaOH for 2 weeks, Hydrogen Reduction, consolidated with Thermosetting resin and coated with Microcrystalline Wax.</td></tr>
<tr><td colspan="5"><b>Cl$^-$ Count:</b></td><td colspan="5">N/A</td><td colspan="5"><b>Year:</b></td><td colspan="5">1980s</td></tr>
<tr><td colspan="20"><b>Secondary Treatment</b></td></tr>
<tr><td><b>Date In Museum:</b></td><td colspan="20" rowspan="2">N/A</td></tr>
<tr><td><b>26/04/2013</b></td></tr>
<tr><td><b>Date Out of Museum:</b></td><td colspan="5"><b>Cl$^-$ Count:</b></td><td colspan="5">N/A</td><td colspan="5"><b>Year:</b></td><td colspan="5">N/A</td></tr>
<tr><td><b>22/07/2014</b></td><td colspan="10"><b>Condition When Leaving:</b></td><td colspan="10">Good</td></tr>
</table>

|  | MRT #78A-0606 | | | Sensor RC 028 | |
|---|---|---|---|---|---|
| | O$_2$ Consumption Rates (mg·year$^{-1}$·g$^{-1}$ ) | | | | |
| | 20% RH | 30% RH | 40% RH | 50% RH | 60% RH |
| | 0.0029 | 0.0196 | 0.0091 | 0.0201 | 0.0548 |
| | Dia. (cm) | Mass (g) | Vol. (cm$^3$) | Dens. (g/cm$^3$) | |
| | 8.7 | 1047.5 | 338.9 | 3.09 | |
| | Primary Treatment | | | | |
| | Concretion Removed, Soaked in dilute NaOH for 2 weeks, Hydrogen Reduction, consolidated with Thermosetting resin and coated with Microcrystalline Wax. | | | | |
| | Cl$^-$ Count: | N/A | Year: | 1980s | |
| | Secondary Treatment | | | | |
| Date In Museum: | N/A | | | | |
| 22/07/2014 | | | | | |
| Date Out of Museum: | Cl$^-$ Count: | N/A | Year: | N/A | |
| 02/12/2015 | Condition When Leaving: | N/A | | | |

|  | MRT #78A-0608 | | | Sensor RC 044 | |
|---|---|---|---|---|---|
| | O$_2$ Consumption Rates (mg·year$^{-1}$·g$^{-1}$ ) | | | | |
| | 20% RH | 30% RH | 40% RH | 50% RH | 60% RH |
| | 0.0312 | 0.0157 | 0.0468 | 0.0603 | 0.1265 |
| | Dia. (cm) | Mass (g) | Vol. (cm$^3$) | Dens. (g/cm$^3$) | |
| | 8.7 | 1004.2 | 340.1 | 2.95 | |
| | Primary Treatment | | | | |
| | Concretion Removed, Soaked in dilute NaOH for 2 weeks, Hydrogen Reduction, consolidated with Thermosetting resin and coated with Microcrystalline Wax. | | | | |
| | Cl$^-$ Count: | N/A | Year: | 1980s | |
| | Secondary Treatment | | | | |
| Date In Museum: | N/A | | | | |
| 22/07/2014 | | | | | |
| Date Out of Museum: | Cl$^-$ Count: | N/A | Year: | N/A | |
| 02/12/2015 | Condition When Leaving: | N/A | | | |

|  | MRT #78A-0610 | | | Sensor RC 035 | |
|---|---|---|---|---|---|
| | O$_2$ Consumption Rates (mg·year$^{-1}$·g$^{-1}$ ) | | | | |
| | 20% RH | 30% RH | 40% RH | 50% RH | 60% RH |
| | 0.0076 | 0.0016 | -0.0062 | 0.0009 | 0.0420 |
| | Dia. (cm) | Mass (g) | Vol. (cm$^3$) | Dens. (g/cm$^3$) | |
| | 8.3 | 2146.0 | 294.0 | 7.30 | |
| | Primary Treatment | | | | |
| | Concretion Removed, Soaked in dilute NaOH for 2 weeks, Hydrogen Reduction, consolidated with Thermosetting resin and coated with Microcrystalline Wax. | | | | |
| | Cl$^-$ Count: | N/A | Year: | 1980s | |
| | Secondary Treatment | | | | |
| Date In Museum: | N/A | | | | |
| 22/07/2014 | | | | | |
| Date Out of Museum: | Cl$^-$ Count: | N/A | Year: | N/A | |
| 02/12/2015 | Condition When Leaving: | N/A | | | |

| | | | | |
|---|---|---|---|---|
| **MRT #78A-0703** | | | **Sensor HS 146** | |
| **O$_2$ Consumption Rates (mg·year$^{-1}$·g$^{-1}$ )** | | | | |
| **20% RH** | **30% RH** | **40% RH** | **50% RH** | **60% RH** |
| -0.0261 | 0.0236 | 0.0328 | 0.0396 | 0.0803 |
| **Dia. (cm)** | **Mass (g)** | **Vol. (cm$^3$)** | **Dens. (g/cm$^3$)** | |
| 8.5 | 1052.3 | 322.7 | 3.26 | |
| **Primary Treatment** | | | | |
| Concretion Removed, Soaked in dilute NaOH for 2 weeks, Hydrogen Reduction, consolidated with Thermosetting resin and coated with Microcrystalline Wax. | | | | |
| **Cl$^-$ Count:** | N/A | **Year:** | 1980s | |
| **Secondary Treatment** | | | | |
| N/A | | | | |
| **Cl$^-$ Count:** | N/A | **Year:** | N/A | |
| **Condition When Leaving:** | | N/A | | |
| **Date In Museum:** | 22/07/2014 | | | |
| **Date Out of Museum:** | 02/12/2015 | | | |

| | | | | |
|---|---|---|---|---|
| **MRT #78A-725X** | | | **Sensor HS 148** | |
| **O$_2$ Consumption Rates (mg·year$^{-1}$·g$^{-1}$ )** | | | | |
| **20% RH** | **30% RH** | **40% RH** | **50% RH** | **60% RH** |
| 0.0032 | 0.1109 | 0.0008 | 0.0090 | 0.0254 |
| **Dia. (cm)** | **Mass (g)** | **Vol. (cm$^3$)** | **Dens. (g/cm$^3$)** | |
| 6.7 | 825.3 | 160.3 | 5.15 | |
| **Primary Treatment** | | | | |
| Concretion Removed, Soaked in dilute NaOH for 2 weeks, Hydrogen Reduction, consolidated with Thermosetting resin and coated with Microcrystalline Wax. | | | | |
| **Cl$^-$ Count:** | N/A | **Year:** | 1980s | |
| **Secondary Treatment** | | | | |
| N/A | | | | |
| **Cl$^-$ Count:** | N/A | **Year:** | N/A | |
| **Condition When Leaving:** | | N/A | | |
| **Date In Museum:** | 22/07/2014 | | | |
| **Date Out of Museum:** | 02/12/2015 | | | |

| | | | | |
|---|---|---|---|---|
| **MRT #79A-0157** | | | **Sensor RC 026** | |
| **O$_2$ Consumption Rates (mg·year$^{-1}$·g$^{-1}$ )** | | | | |
| **20% RH** | **30% RH** | **40% RH** | **50% RH** | **60% RH** |
| 0.0050 | 0.0024 | 0.0059 | 0.0048 | 0.0173 |
| **Dia. (cm)** | **Mass (g)** | **Vol. (cm$^3$)** | **Dens. (g/cm$^3$)** | |
| 10.3 | 2940.1 | 565.5 | 5.20 | |
| **Primary Treatment** | | | | |
| Concretion Removed, Soaked in dilute NaOH for 2 weeks, Hydrogen Reduction, consolidated with Thermosetting resin and coated with Microcrystalline Wax. | | | | |
| **Cl$^-$ Count:** | N/A | **Year:** | 1980s | |
| **Secondary Treatment** | | | | |
| N/A | | | | |
| **Cl$^-$ Count:** | N/A | **Year:** | N/A | |
| **Condition When Leaving:** | | N/A | | |
| **Date In Museum:** | 22/07/2014 | | | |
| **Date Out of Museum:** | 02/12/2015 | | | |

| | | | | |
|---|---|---|---|---|
| **MRT #80A-0358** | | | **Sensor RC 031** | |
| **O$_2$ Consumption Rates (mg·year$^{-1}$·g$^{-1}$ )** | | | | |
| **20% RH** | **30% RH** | **40% RH** | **50% RH** | **60% RH** |
| -0.0010 | 0.0081 | 0.0020 | 0.0037 | 0.0082 |
| **Dia. (cm)** | **Mass (g)** | **Vol. (cm$^3$)** | **Dens. (g/cm$^3$)** | |
| 7 | 1141.4 | 179.6 | 6.36 | |
| **Primary Treatment** | | | | |
| Concretion Removed, Soaked in dilute NaOH for 2 weeks, Hydrogen Reduction, consolidated with Thermosetting resin and coated with Microcrystalline Wax. | | | | |
| **Cl$^-$ Count:** | N/A | **Year:** | 1980s | |
| **Secondary Treatment** | | | | |
| N/A | | | | |
| **Cl$^-$ Count:** | N/A | **Year:** | N/A | |
| **Condition When Leaving:** | N/A | | | |

| | |
|---|---|
| **Date In Museum:** | |
| **Date Out of Museum:** | |

| | | | | |
|---|---|---|---|---|
| **MRT #80A-0865** | | | **Sensor HS 097** | |
| **O$_2$ Consumption Rates (mg·year$^{-1}$·g$^{-1}$ )** | | | | |
| **20% RH** | **30% RH** | **40% RH** | **50% RH** | **60% RH** |
| 0.0235 | -0.0208 | 0.0219 | 0.0528 | 0.0755 |
| **Dia. (cm)** | **Mass (g)** | **Vol. (cm$^3$)** | **Dens. (g/cm$^3$)** | |
| 6.8 | 299.2 | 163.2 | 1.83 | |
| **Primary Treatment** | | | | |
| Concretion Removed, Soaked in dilute NaOH for 2 weeks, Hydrogen Reduction, consolidated with Thermosetting resin and coated with Microcrystalline Wax. | | | | |
| **Cl$^-$ Count:** | N/A | **Year:** | 1980s | |
| **Secondary Treatment** | | | | |
| N/A | | | | |
| **Cl$^-$ Count:** | N/A | **Year:** | N/A | |
| **Condition When Leaving:** | N/A | | | |

| | |
|---|---|
| **Date In Museum:** | **22/07/2014** |
| **Date Out of Museum:** | **02/12/2015** |

*** Cannonball is missing ~ 1/3 its volume**

| | | | | |
|---|---|---|---|---|
| **MRT #80A-1051** | | | **Sensor RC 041** | |
| **O$_2$ Consumption Rates (mg·year$^{-1}$·g$^{-1}$ )** | | | | |
| **20% RH** | **30% RH** | **40% RH** | **50% RH** | **60% RH** |
| 0.0152 | 0.0158 | 0.0169 | 0.0228 | 0.0423 |
| **Dia. (cm)** | **Mass (g)** | **Vol. (cm$^3$)** | **Dens. (g/cm$^3$)** | |
| 10.6 | 1149.5 | 616.6* | 1.86* | |
| **Primary Treatment** | | | | |
| Concretion Removed, Soaked in dilute NaOH for 2 weeks, Hydrogen Reduction, consolidated with Thermosetting resin and coated with Microcrystalline Wax. | | | | |
| **Cl$^-$ Count:** | N/A | **Year:** | 1980s | |
| **Secondary Treatment** | | | | |
| N/A | | | | |
| **Cl$^-$ Count:** | N/A | **Year:** | N/A | |
| **Condition When Leaving:** | N/A | | | |

| | |
|---|---|
| **Date In Museum:** | **22/07/2014** |
| **Date Out of Museum:** | **02/12/2015** |

|  |  |  |  |  |
|---|---|---|---|---|
| MRT #80A-1125 |  | Sensor HS 100 |  |  |
| $O_2$ Consumption Rates (mg·year$^{-1}$·g$^{-1}$ ) |  |  |  |  |
| 20% RH | 30% RH | 40% RH | 50% RH | 60% RH |
| 0.0100 | 0.0198 | 0.0235 | 0.0493 | 0.0663 |
| Dia. (cm) | Mass (g) | Vol. (cm$^3$) | Dens. (g/cm$^3$) |  |
| 6.4 | 399.0 | 139.8 | 2.85 |  |
| Primary Treatment |  |  |  |  |
| Concretion Removed, Soaked in dilute NaOH for 2 weeks, Hydrogen Reduction, consolidated with Thermosetting resin and coated with Microcrystalline Wax. |  |  |  |  |
| Cl$^-$ Count: | N/A | Year: | 1980s |  |
| Secondary Treatment |  |  |  |  |
| N/A |  |  |  |  |
| Cl$^-$ Count: | N/A | Year: | N/A |  |
| Condition When Leaving: | N/A |  |  |  |

|  |
|---|
| Date In Museum: |
| 22/07/2014 |
| Date Out of Museum: |
| 02/12/2015 |

|  |  |  |  |  |
|---|---|---|---|---|
| MRT #81A-1106 |  | Sensor RC 058 |  |  |
| $O_2$ Consumption Rates (mg·year$^{-1}$·g$^{-1}$ ) |  |  |  |  |
| 20% RH | 30% RH | 40% RH | 50% RH | 60% RH |
| 0.1112 | 0.1442 | 0.3425 | 1.3094 | 6.2577 |
| Dia. (cm) | Mass (g) | Vol. (cm$^3$) | Dens. (g/cm$^3$) |  |
| ~8.5 | 1392 | 333.0 | 4.18 |  |
| Primary Treatment |  |  |  |  |
| Washed in 2% Hostacor in water solution, dried using 50% Acetone:50%Water then 100% Acetone and finally coated with microcrystalline wax with a small amount of graphite powder. |  |  |  |  |
| Cl$^-$ Count: | 35ppm, 26ppm | Year: | 2011 |  |
| Secondary Treatment |  |  |  |  |
| Wax removed with boiling water and placed in a 0.5M Alkaline Sulfite solution at 60oC. Finally it was dried at 50oC and coated with 15% Paraloid B48 w/v in Acetone. |  |  |  |  |
| Cl$^-$ Count: | 1; 46; 10ppm | Year: | 2011 |  |
| Condition When Leaving: | Poor (cracked) |  |  |  |

|  |
|---|
| Date In Museum: |
| 26/04/2013 |
| Date Out of Museum: |
| 28/03/2014 |

|  |  |  |  |  |
|---|---|---|---|---|
| MRT #81A-2762 |  | Sensor RC 051 |  |  |
| $O_2$ Consumption Rates (mg·year$^{-1}$·g$^{-1}$ ) |  |  |  |  |
| 20% RH | 30% RH | 40% RH | 50% RH | 60% RH |
| 0.0308 | 0.0314 | 0.0395 | 0.0454 | 0.2448 |
| Dia. (cm) | Mass (g) | Vol. (cm$^3$) | Dens. (g/cm$^3$) |  |
| 8.5 | 1925.9 | 318.2 | 6.05 |  |
| Primary Treatment |  |  |  |  |
| Washed in 1% Hostacor in water solution, dried using 50% Acetone:50%Water then 100% Acetone and finally coated with microcrystalline wax with a small amount of graphite powder. |  |  |  |  |
| Cl$^-$ Count: | 13ppm | Year: | 2010 |  |
| Secondary Treatment |  |  |  |  |
| N/A |  |  |  |  |
| Cl$^-$ Count: | N/A | Year: | N/A |  |
| Condition When Leaving: | N/A |  |  |  |

|  |
|---|
| Date In Museum: |
| 26/04/2013 |
| Date Out of Museum: |
| 22/07/2014 |

| **MRT #81A-3111** | **Sensor RC 023** |
|---|---|

**$O_2$ Consumption Rates ($mg \cdot year^{-1} \cdot g^{-1}$)**

| 20% RH | 30% RH | 40% RH | 50% RH | 60% RH |
|---|---|---|---|---|
| 0.0331 | 0.0332 | 0.0153 | 0.0589 | 0.2241 |

| Dia. (cm) | Mass (g) | Vol. ($cm^3$) | Dens. ($g/cm^3$) |
|---|---|---|---|
| 6.4 | 875.7 | 137.3 | 6.38 |

**Primary Treatment**

Washed in 2% Hostacor in water solution, dried using 50% Acetone:50%Water then 100% Acetone and finally coated with microcrystalline wax with a small amount of graphite powder.

| **$Cl^-$ Count:** | 98; 9; 74; 46ppm | **Year:** | 2010 |
|---|---|---|---|

**Secondary Treatment**

Wax removed with acetone and coated with 15% Paraloid B48 w/v in Acetone.

| **$Cl^-$ Count:** | N/A | **Year:** | 2011 |
|---|---|---|---|
| **Condition When Leaving:** | N/A | | |

| **Date In Museum:** |
|---|
| **26/04/2013** |
| **Date Out of Museum:** |
| **22/07/2014** |

| **MRT #81A-3373** | **Sensor RC 012** |
|---|---|

**$O_2$ Consumption Rates ($mg \cdot year^{-1} \cdot g^{-1}$)**

| 20% RH | 30% RH | 40% RH | 50% RH | 60% RH |
|---|---|---|---|---|
| 0.0855 | 0.1128 | 0.1776 | 0.6527 | 1.4575 |

| Dia. (cm) | Mass (g) | Vol. ($cm^3$) | Dens. ($g/cm^3$) |
|---|---|---|---|
| 6.8 | 852.5 | 161.7 | 5.27 |

**Primary Treatment**

Placed in a 0.1:0.05M Solution of Alkaline Sulfite and heated to 45°C. Rinsed in deionised water and dried at 50°C then coated with 15% Paraloid B48 w/v Acetone.

| **$Cl^-$ Count:** | 3ppm | **Year:** | 2011 |
|---|---|---|---|

**Secondary Treatment**

N/A

| **$Cl^-$ Count:** | N/A | **Year:** | N/A |
|---|---|---|---|
| **Condition When Leaving:** | Cracked | | |

| **Date In Museum:** |
|---|
| **26/04/2013** |
| **Date Out of Museum:** |
| **22/07/2014** |

| **MRT #81A-3459** | **Sensor RC 002** |
|---|---|

**$O_2$ Consumption Rates ($mg \cdot year^{-1} \cdot g^{-1}$)**

| 20% RH | 30% RH | 40% RH | 50% RH | 60% RH |
|---|---|---|---|---|
| 0.0095 | 0.0207 | 0.0154 | 0.0249 | 0.0896 |

| Dia. (cm) | Mass (g) | Vol. ($cm^3$) | Dens. ($g/cm^3$) |
|---|---|---|---|
| 8.5 | 2371.0 | 321.6 | 7.37 |

**Primary Treatment**

Washed in 2% Hostacor in water solution, dried using 50% Acetone:50%Water then 100% Acetone and finally coated with microcrystalline wax with a small amount of graphite powder.

| **$Cl^-$ Count:** | 75; 191ppm | **Year:** | 2010 |
|---|---|---|---|

**Secondary Treatment**

N/A

| **$Cl^-$ Count:** | N/A | **Year:** | N/A |
|---|---|---|---|
| **Condition When Leaving:** | Good | | |

| **Date In Museum:** |
|---|
| **26/04/2013** |
| **Date Out of Museum:** |
| **22/07/2014** |

| | | | | |
|---|---|---|---|---|
| **MRT #81A-3464** | | | **Sensor RC 021** | |
| **$O_2$ Consumption Rates (mg·year$^{-1}$·g$^{-1}$ )** | | | | |
| **20% RH** | **30% RH** | **40% RH** | **20% RH** | **30% RH** |
| 0.0108 | 0.0128 | 0.0135 | 0.0278 | 0.0713 |
| **Dia. (cm)** | **Mass (g)** | **Vol. (cm$^3$)** | **Dia. (cm)** | |
| 8.5 | 2315.4 | 320.4 | 8.5 | |
| **Primary Treatment** | | | | |
| Placed in a 0.1:0.05M Solution of Alkaline Sulfite and heated to 45°C. Rinsed in Deionised water and dried at 50°C then coated with 15% Paraloid B48 w/v acetone. | | | | |
| **$Cl^-$ Count:** | 2ppm | **Year:** | **$Cl^-$ Count:** | |
| **Secondary Treatment** | | | | |
| N/A | | | | |
| **$Cl^-$ Count:** | N/A | **Year:** | N/A | |
| **Condition When Leaving:** | N/A | | | |
| **Date In Museum:** | **26/04/2013** | | | |
| **Date Out of Museum:** | **22/07/2014** | | | |

| | | | | |
|---|---|---|---|---|
| **MRT #81A-3499** | | | **Sensor RC 048** | |
| **$O_2$ Consumption Rates (mg·year$^{-1}$·g$^{-1}$ )** | | | | |
| **20% RH** | **30% RH** | **40% RH** | **50% RH** | **60% RH** |
| 0.0524 | 0.0602 | 0.3517 | 0.4347 | 1.4031 |
| **Dia. (cm)** | **Mass (g)** | **Vol. (cm$^3$)** | **Dens. (g/cm$^3$)** | |
| 8.8 | 2231.9 | 356.8 | 6.25 | |
| **Primary Treatment** | | | | |
| Placed in a 0.1:0.05M Solution of Alkaline Sulfite and heated to 45°C. Rinsed in deionised water and dried at 50°C then coated with 15% Paraloid B48 w/v acetone. | | | | |
| **$Cl^-$ Count:** | N/A | **Year:** | N/A | |
| **Secondary Treatment** | | | | |
| N/A | | | | |
| **$Cl^-$ Count:** | N/A | **Year:** | N/A | |
| **Condition When Leaving:** | Cracked | | | |
| **Date In Museum:** | **26/04/2013** | | | |
| **Date Out of Museum:** | **22/07/2014** | | | |

| | | | | |
|---|---|---|---|---|
| **MRT #3508** | | | **Sensor HS 149** | |
| **$O_2$ Consumption Rates (mg·year$^{-1}$·g$^{-1}$ )** | | | | |
| **20% RH** | **30% RH** | **40% RH** | **50% RH** | **60% RH** |
| 0.0366 | 0.0350 | 0.0412 | 0.0580 | 0.1604 |
| **Dia. (cm)** | **Mass (g)** | **Vol. (cm$^3$)** | **Dens. (g/cm$^3$)** | |
| 8.4 | 2032.7 | 304.8 | 6.67 | |
| **Primary Treatment** | | | | |
| Washed in 2% Hostacor in water solution, dried using 50% Acetone:50%Water then 100% Acetone and finally coated with microcrystalline wax with a small amount of graphite powder. | | | | |
| **$Cl^-$ Count:** | 69ppm, 150ppm | **Year:** | 2010 | |
| **Secondary Treatment** | | | | |
| Wax removed with acetone and placed back in a wash of 2% Hostacor then coated with 15% Paraloid B48 w/v in Acetone. | | | | |
| **$Cl^-$ Count:** | 20; 16; 3; 12; 2ppm | **Year:** | 2011-2012 | |
| **Condition When Leaving:** | N/A | | | |
| **Date In Museum:** | **26/04/2013** | | | |
| **Date Out of Museum:** | **22/07/2014** | | | |

| | | | | |
|---|---|---|---|---|
| **MRT #81A-3517** | | **Sensor HS 145** | | |
| **$O_2$ Consumption Rates (mg·year$^{-1}$·g$^{-1}$ )** | | | | |
| **20% RH** | **30% RH** | **40% RH** | **50% RH** | **60% RH** |
| 0.0903 | 0.0691 | 0.1079 | 0.1094 | 0.1988 |
| **Dia. (cm)** | **Mass (g)** | **Vol. (cm$^3$)** | **Dens. (g/cm$^3$)** | |
| 8.5 | 1688.0 | 321.6 | 5.25 | |
| **Primary Treatment** | | | | |
| Washed in 2% Hostacor in water solution, dried using 50% Acetone:50%Water then 100% Acetone and finally coated with microcrystalline wax with a small amount of graphite powder. | | | | |
| **Cl$^-$ Count:** | 23ppm | **Year:** | 2010 | |
| **Secondary Treatment** | | | | |
| Wax removed with boiling water and placed in a 0.5M Alkaline Sulfite solution at 60°C. Finally it was dried at 50°C and coated with 15% Paraloid B48 w/v in acetone. | | | | |
| **Cl$^-$ Count:** | 78; 88; 53; 100; 16; 6ppm | **Year:** | 2011-2012 | |
| **Condition When Leaving:** | Good | | | |
| **Date In Museum:** | 26/04/2013 | | | |
| **Date Out of Museum:** | 22/07/2014 | | | |

| | | | | |
|---|---|---|---|---|
| **MRT #81A-3527** | | **Sensor RC 027** | | |
| **$O_2$ Consumption Rates (mg·year$^{-1}$·g$^{-1}$ )** | | | | |
| **20% RH** | **30% RH** | **40% RH** | **50% RH** | **60% RH** |
| 0.0907 | 0.0888 | 0.1484 | 0.7315 | 1.5207 |
| **Dia. (cm)** | **Mass (g)** | **Vol. (cm$^3$)** | **Dens. (g/cm$^3$)** | |
| 8.3 | 1592.7 | 296.2 | 5.38 | |
| **Primary Treatment** | | | | |
| Washed in 1% Hostacor in water solution, dried using 50% Acetone:50%Water then 100% Acetone and finally coated with microcrystalline wax with a small amount of graphite powder. | | | | |
| **Cl$^-$ Count:** | 58; 48ppm | **Year:** | 2010 | |
| **Secondary Treatment** | | | | |
| Wax removed with acetone and placed back in a wash of 2% Hostacor then coated with 15% Paraloid B48 w/v in Acetone. | | | | |
| **Cl$^-$ Count:** | 36; 64; 106; 17; 20; 16; 23; 4ppm | **Year:** | 2011-2012 | |
| **Condition When Leaving:** | Cracked | | | |
| **Date In Museum:** | 26/04/2013 | | | |
| **Date Out of Museum:** | 22/07/2014 | | | |

| | | | | |
|---|---|---|---|---|
| **MRT #81A-3529** | | **Sensor HS 125** | | |
| **$O_2$ Consumption Rates (mg·year$^{-1}$·g$^{-1}$ )** | | | | |
| **20% RH** | **30% RH** | **40% RH** | **50% RH** | **60% RH** |
| 0.0206 | 0.0176 | 0.0150 | 0.0295 | 0.0649 |
| **Dia. (cm)** | **Mass (g)** | **Vol. (cm$^3$)** | **Dens. (g/cm$^3$)** | |
| 9.5 | 3126.4 | 447.5 | 6.99 | |
| **Primary Treatment** | | | | |
| Placed in a 0.1:0.05M Solution of Alkaline Sulfite and heated to 45°C. Rinsed in Deionised water and dried at 50°C then coated with 15% Paraloid B48 w/v acetone. | | | | |
| **Cl$^-$ Count:** | 15; 6; 2; 2ppm | **Year:** | 2011-2012 | |
| **Secondary Treatment** | | | | |
| N/A | | | | |
| **Cl$^-$ Count:** | N/A | **Year:** | N/A | |
| **Condition When Leaving:** | N/A | | | |
| **Date In Museum:** | 26/04/2013 | | | |
| **Date Out of Museum:** | 22/07/2014 | | | |

| **MRT #81A-3599** | | **Sensor HS 141** | | |
|---|---|---|---|---|
| **$O_2$ Consumption Rates (mg·year$^{-1}$·g$^{-1}$ )** | | | | |
| **20% RH** | **30% RH** | **40% RH** | **50% RH** | **60% RH** |
| 0.0012 | 0.0012 | 0.0069 | 0.0098 | 0.0414 |
| **Dia. (cm)** | **Mass (g)** | **Vol. (cm$^3$)** | **Dens. (g/cm$^3$)** | |
| 9.9 | 3678.0 | 506.5 | 7.26 | |
| **Primary Treatment** | | | | |
| Washed in 2% Hostacor in water solution, dried using 50% Acetone:50%Water then 100% Acetone and finally coated with microcrystalline wax with a small amount of graphite powder. | | | | |
| **Cl$^-$ Count:** | 21ppm | **Year:** | 2010 | |
| **Secondary Treatment** | | | | |
| N/A | | | | |
| **Cl$^-$ Count:** | N/A | **Year:** | N/A | |
| **Condition When Leaving:** | N/A | | | |

| **Date In Museum:** |
|---|
| **26/04/2013** |
| **Date Out of Museum:** |
| **22/07/2014** |

| **MRT #81A-4147** | | **Sensor HS144** | | |
|---|---|---|---|---|
| **$O_2$ Consumption Rates (mg·year$^{-1}$·g$^{-1}$ )** | | | | |
| **20% RH** | **30% RH** | **40% RH** | **50% RH** | **60% RH** |
| 0.0149 | 0.0083 | 0.0152 | 0.0333 | 0.1002 |
| **Dia. (cm)** | **Mass (g)** | **Vol. (cm$^3$)** | **Dens. (g/cm$^3$)** | |
| 8.4 | 2145.5 | 304.8 | 7.04 | |
| **Primary Treatment** | | | | |
| Placed in a 0.1:0.05M Solution of Alkaline Sulfite and heated to 45°C. Rinsed in deionised water and dried at 50°C then coated with 15% Paraloid B48 w/v Acetone. | | | | |
| **Cl$^-$ Count:** | 1ppm | **Year:** | 2011 | |
| **Secondary Treatment** | | | | |
| N/A | | | | |
| **Cl$^-$ Count:** | N/A | **Year:** | N/A | |
| **Condition When Leaving:** | N/A | | | |

| **Date In Museum:** |
|---|
| **26/04/2013** |
| **Date Out of Museum:** |
| **22/07/2014** |

| **MRT #81A-6131** | | **Sensor HS 133** | | |
|---|---|---|---|---|
| **$O_2$ Consumption Rates (mg·year$^{-1}$·g$^{-1}$ )** | | | | |
| **20% RH** | **30% RH** | **40% RH** | **50% RH** | **60% RH** |
| 0.0120 | 0.0064 | 0.0130 | 0.0244 | 0.0918 |
| **Dia. (cm)** | **Mass (g)** | **Vol. (cm$^3$)** | **Dens. (g/cm$^3$)** | |
| 8.6 | 2392.5 | 329.6 | 7.26 | |
| **Primary Treatment** | | | | |
| Placed in a 0.1:0.05M Solution of Alkaline Sulfite and heated to 45°C. Rinsed in deionised water and dried at 50°C then coated with 15% Paraloid B48 w/v Acetone. | | | | |
| **Cl$^-$ Count:** | 379; 5; 0ppm | **Year:** | 2011 | |
| **Secondary Treatment** | | | | |
| N/A | | | | |
| **Cl$^-$ Count:** | N/A | **Year:** | N/A | |
| **Condition When Leaving:** | N/A | | | |

| **Date In Museum:** |
|---|
| **26/04/2013** |
| **Date Out of Museum:** |
| **22/07/2014** |

| | | | | |
|---|---|---|---|---|
| **MRT #81A-6236** | | **Sensor HS 147** | | |
| **$O_2$ Consumption Rates ($mg \cdot year^{-1} \cdot g^{-1}$ )** | | | | |
| **20% RH** | **30% RH** | **40% RH** | **50% RH** | **60% RH** |
| 0.0179 | 0.0232 | 0.0256 | 0.0502 | 0.1216 |
| **Dia. (cm)** | **Mass (g)** | **Vol. ($cm^3$)** | **Dens. ($g/cm^3$)** | |
| 8.2 | 1840.0 | 287.6 | 6.40 | |
| **Primary Treatment** | | | | |
| Washed in 2% Hostacor in water solution, dried using 50% Acetone:50%Water then 100% Acetone and finally coated with microcrystalline wax with a small amount of graphite powder. | | | | |
| **$Cl^-$ Count:** | 32ppm | **Year:** | 2010-2011 | |
| **Secondary Treatment** | | | | |
| N/A | | | | |
| **$Cl^-$ Count:** | N/A | **Year:** | N/A | |
| **Condition When Leaving:** | N/A | | | |
| **Date In Museum:** | **26/04/2013** | | | |
| **Date Out of Museum:** | **22/07/2014** | | | |

| | | | | |
|---|---|---|---|---|
| **MRT #81A-6909** | | **Sensor RC 043** | | |
| **$O_2$ Consumption Rates ($mg \cdot year^{-1} \cdot g^{-1}$ )** | | | | |
| **20% RH** | **30% RH** | **40% RH** | **50% RH** | **60% RH** |
| 0.1260 | 0.1102 | 0.1536 | 0.3829 | 0.7377 |
| **Dia. (cm)** | **Mass (g)** | **Vol. ($cm^3$)** | **Dens. ($g/cm^3$)** | |
| 8.5 | 1254.0 | 321.6 | 3.90 | |
| **Primary Treatment** | | | | |
| Washed in 2% Hostacor in water solution, dried using 50% Acetone:50%Water then 100% Acetone and finally coated with microcrystalline wax with a small amount of graphite powder. | | | | |
| **$Cl^-$ Count:** | N/A | **Year:** | 2011 | |
| **Secondary Treatment** | | | | |
| N/A | | | | |
| **$Cl^-$ Count:** | N/A | **Year:** | N/A | |
| **Condition When Leaving:** | Good | | | |
| **Date In Museum:** | **26/04/2013** | | | |
| **Date Out of Museum:** | **22/07/2014** | | | |

| | | | | |
|---|---|---|---|---|
| **MRT #82A-2547** | | **Sensor HS 137** | | |
| **$O_2$ Consumption Rates ($mg \cdot year^{-1} \cdot g^{-1}$ )** | | | | |
| **20% RH** | **30% RH** | **40% RH** | **50% RH** | **60% RH** |
| 0.0171 | 0.0130 | 0.0259 | 0.0425 | 0.1339 |
| **Dia. (cm)** | **Mass (g)** | **Vol. ($cm^3$)** | **Dens. ($g/cm^3$)** | |
| 10.4 | 4081.0 | 585.6 | 6.97 | |
| **Primary Treatment** | | | | |
| Washed in 2% Hostacor in water solution, dried using 50% Acetone:50%Water then 100% Acetone and finally coated with microcrystalline wax with a small amount of graphite powder. | | | | |
| **$Cl^-$ Count:** | 44ppm | **Year:** | 2010 | |
| **Secondary Treatment** | | | | |
| N/A | | | | |
| **$Cl^-$ Count:** | N/A | **Year:** | N/A | |
| **Condition When Leaving:** | N/A | | | |
| **Date In Museum:** | **26/04/2013** | | | |
| **Date Out of Museum:** | **22/07/2014** | | | |

| | |
|---|---|
| Date In Museum: | 26/04/2013 |
| Date Out of Museum: | 22/07/2014 |

| | | | | |
|---|---|---|---|---|
| MRT #82A-2615 | Sensor RC 039 | | | |
| $O_2$ Consumption Rates (mg·year$^{-1}$·g$^{-1}$ ) | | | | |
| 20% RH | 30% RH | 40% RH | 50% RH | 60% RH |
| 0.0283 | 0.0348 | 0.0403 | 0.0523 | 0.3210 |
| Dia. (cm) | Mass (g) | Vol. (cm$^3$) | Dens. (g/cm$^3$) | |
| 8.4 | 1793.9 | 313.7 | 5.72 | |
| Primary Treatment | | | | |
| Washed in 2% Hostacor in water solution, dried using 50% Acetone:50%Water then 100% Acetone and finally coated with microcrystalline wax with a small amount of graphite powder. | | | | |
| Cl$^-$ Count: | 40ppm | Year: | 2010 | |
| Secondary Treatment | | | | |
| N/A | | | | |
| Cl$^-$ Count: | N/A | Year: | N/A | |
| Condition When Leaving: | N/A | | | |

| | |
|---|---|
| Date In Museum: | 26/04/2013 |
| Date Out of Museum: | 22/07/2014 |

| | | | | |
|---|---|---|---|---|
| MRT #82A-2624 | Sensor HS 095 | | | |
| $O_2$ Consumption Rates (mg·year$^{-1}$·g$^{-1}$ ) | | | | |
| 20% RH | 30% RH | 40% RH | 50% RH | 60% RH |
| 0.0215 | 0.0252 | 0.0319 | 0.0467 | 0.1490 |
| Dia. (cm) | Mass (g) | Vol. (cm$^3$) | Dens. (g/cm$^3$) | |
| 10.5 | 3894.0 | 599.2 | 6.50 | |
| Primary Treatment | | | | |
| Washed in 2% Hostacor in water solution, dried using 50% Acetone:50%Water then 100% Acetone and finally coated with microcrystalline wax with a small amount of graphite powder. | | | | |
| Cl$^-$ Count: | 25ppm | Year: | 2010 | |
| Secondary Treatment | | | | |
| N/A | | | | |
| Cl$^-$ Count: | N/A | Year: | N/A | |
| Condition When Leaving: | N/A | | | |

| | |
|---|---|
| Date In Museum: | 26/04/2013 |
| Date Out of Museum: | 22/07/2014 |

| | | | | |
|---|---|---|---|---|
| MRT #82A-3593 | Sensor RC 030 | | | |
| $O_2$ Consumption Rates (mg·year$^{-1}$·g$^{-1}$ ) | | | | |
| 20% RH | 30% RH | 40% RH | 50% RH | 60% RH |
| 0.0396 | 0.0410 | 0.0557 | 0.0892 | 0.1295 |
| Dia. (cm) | Mass (g) | Vol. (cm$^3$) | Dens. (g/cm$^3$) | |
| 8.6 | 2357.9 | 333.0 | 7.08 | |
| Primary Treatment | | | | |
| Placed in a 0.1:0.05M Solution of Alkaline Sulfite and heated to 45°C. Rinsed in deionised water and dried at 50°C then coated with 15% Paraloid B48N w/v Acetone. | | | | |
| Cl$^-$ Count: | 9; 2ppm | Year: | 2011-2012 | |
| Secondary Treatment | | | | |
| N/A | | | | |
| Cl$^-$ Count: | N/A | Year: | N/A | |
| Condition When Leaving: | N/A | | | |

| | | | | | |
|---|---|---|---|---|---|
|  | **MRT #82A-3594** | | **Sensor HS 134** | | |
| | **$O_2$ Consumption Rates (mg·year$^{-1}$·g$^{-1}$ )** | | | | |
| | **20% RH** | **30% RH** | **40% RH** | **50% RH** | **60% RH** |
| | 0.0752 | 0.1623 | 6.8720 | 2.5389 | 6.1091 |
| | **Dia. (cm)** | **Mass (g)** | **Vol. (cm$^3$)** | **Dens. (g/cm$^3$)** | |
| | 8.7 | 2042.0 | 347.2 | 5.88 | |
| | **Primary Treatment** | | | | |
| | Washed in 2% Hostacor in water solution. | | | | |
| | **Cl$^-$ Count:** | 46; 32ppm | **Year:** | 2011 | |
| | **Secondary Treatment** | | | | |
| **Date In Museum:** | Placed in a 0.5M Alkaline Sulfite solution at 60°C. Finally it was dried at 50°C and coated with 15% Paraloid B48 w/v in Acetone. | | | | |
| **26/04/2013** | | | | | |
| **Date Out of Museum:** | **Cl$^-$ Count:** | 9; 2ppm | **Year:** | 2011 | |
| **01/08/2013** | **Condition When Leaving:** | Cracked | | | |

| | | | | | |
|---|---|---|---|---|---|
|  | **MRT #82A-4113** | | **Sensor RC 032** | | |
| | **$O_2$ Consumption Rates (mg·year$^{-1}$·g$^{-1}$ )** | | | | |
| | **20% RH** | **30% RH** | **40% RH** | **50% RH** | **60% RH** |
| | 0.227 | 0.0199 | 0.0231 | 0.0444 | 0.1313 |
| | **Dia. (cm)** | **Mass (g)** | **Vol. (cm$^3$)** | **Dens. (g/cm$^3$)** | |
| | 8.5 | 2100.9 | 320.4 | 6.56 | |
| | **Primary Treatment** | | | | |
| | Placed in a 0.1:0.05M Solution of Alkaline Sulfite and heated to 45°C. Rinsed in deionised water and dried at 50°C then coated with 15% Paraloid B48 w/v Acetone. | | | | |
| | **Cl$^-$ Count:** | 21; 74; 20; 34; 98; 130; 24ppm | **Year:** | 2011-2012 | |
| | **Secondary Treatment** | | | | |
| **Date In Museum:** | N/A | | | | |
| **26/04/2013** | | | | | |
| **Date Out of Museum:** | **Cl$^-$ Count:** | N/A | **Year:** | N/A | |
| **22/07/2014** | **Condition When Leaving:** | N/A | | | |

| | | | | | |
|---|---|---|---|---|---|
|  | **MRT #82A-4235** | | **Sensor RC 046** | | |
| | **$O_2$ Consumption Rates (mg·year$^{-1}$·g$^{-1}$ )** | | | | |
| | **20% RH** | **30% RH** | **40% RH** | **50% RH** | **60% RH** |
| | 0.0212 | 0.0197 | 0.0292 | 0.0427 | 0.1146 |
| | **Dia. (cm)** | **Mass (g)** | **Vol. (cm$^3$)** | **Dens. (g/cm$^3$)** | |
| | 10.6 | 3500.0 | 618.3 | 5.66 | |
| | **Primary Treatment** | | | | |
| | Placed in a 0.1:0.05M Solution of Alkaline Sulfite and heated to 45°C. Rinsed in deionised water and dried at 50°C then coated with 15% Paraloid B48 w/v Acetone. | | | | |
| | **Cl$^-$ Count:** | 12; 1; < 2ppm | **Year:** | 2011 | |
| | **Secondary Treatment** | | | | |
| **Date In Museum:** | N/A | | | | |
| **26/04/2013** | | | | | |
| **Date Out of Museum:** | **Cl$^-$ Count:** | N/A | **Year:** | N/A | |
| **22/07/2014** | **Condition When Leaving:** | N/A | | | |

| | | | | |
|---|---|---|---|---|
| **MRT #82A-4362** | | | **Sensor HS 121** | |
| **$O_2$ Consumption Rates (mg·year$^{-1}$·g$^{-1}$ )** | | | | |
| **20% RH** | **30% RH** | **40% RH** | **50% RH** | **60% RH** |
| 0.0112 | 0.0052 | 0.0201 | 0.0391 | 0.0934 |
| **Dia. (cm)** | **Mass (g)** | **Vol. (cm$^3$)** | **Dens. (g/cm$^3$)** | |
| 8.5 | 2457.6 | 326.1 | 7.54 | |
| **Primary Treatment** | | | | |
| Placed in a 0.1:0.05M Solution of Alkaline Sulfite and heated to 45°C. Rinsed in deionised water and dried at 50°C then coated with 15% Paraloid B48 w/v Acetone. | | | | |
| **Cl$^-$ Count:** | 2ppm | **Year:** | 2011 | |
| **Secondary Treatment** | | | | |
| N/A | | | | |
| **Cl$^-$ Count:** | N/A | **Year:** | N/A | |
| **Condition When Leaving:** | N/A | | | |

| | |
|---|---|
| **Date In Museum:** | **26/04/2013** |
| **Date Out of Museum:** | **22/07/2014** |

| | | | | |
|---|---|---|---|---|
| **MRT #82A-4392** | | | **Sensor HS 122** | |
| **$O_2$ Consumption Rates (mg·year$^{-1}$·g$^{-1}$ )** | | | | |
| **20% RH** | **30% RH** | **40% RH** | **50% RH** | **60% RH** |
| 0.0070 | 0.0179 | 0.0273 | 0.0500 | 0.2470 |
| **Dia. (cm)** | **Mass (g)** | **Vol. (cm$^3$)** | **Dens. (g/cm$^3$)** | |
| 6 | 742.0 | 114.2 | 6.50 | |
| **Primary Treatment** | | | | |
| Placed in a 0.1:0.05M Solution of Alkaline Sulfite and heated to 45°C. Rinsed in Deionised water and dried at 50°C then coated with 15% Paraloid B48 w/v Acetone. | | | | |
| **Cl$^-$ Count:** | 2; 1ppm | **Year:** | 2011 | |
| **Secondary Treatment** | | | | |
| N/A | | | | |
| **Cl$^-$ Count:** | N/A | **Year:** | N/A | |
| **Condition When Leaving:** | N/A | | | |

| | |
|---|---|
| **Date In Museum:** | **26/04/2013** |
| **Date Out of Museum:** | **22/07/2014** |

| | | | | |
|---|---|---|---|---|
| **MRT #82A-4731** | | | **Sensor HS 143** | |
| **$O_2$ Consumption Rates (mg·year$^{-1}$·g$^{-1}$ )** | | | | |
| **20% RH** | **30% RH** | **40% RH** | **50% RH** | **60% RH** |
| 0.0064 | 0.0084 | 0.0116 | 0.0185 | 0.0423 |
| **Dia. (cm)** | **Mass (g)** | **Vol. (cm$^3$)** | **Dens. (g/cm$^3$)** | |
| 9.8 | 3398.5 | 494.3 | 6.88 | |
| **Primary Treatment** | | | | |
| Washed in 2% Hostacor in water solution, dried using 50% Acetone:50%Water then 100% Acetone and finally coated with microcrystalline wax with a small amount of graphite powder. | | | | |
| **Cl$^-$ Count:** | 24ppm | **Year:** | 2010 | |
| **Secondary Treatment** | | | | |
| N/A | | | | |
| **Cl$^-$ Count:** | N/A | **Year:** | N/A | |
| **Condition When Leaving:** | N/A | | | |

| | |
|---|---|
| **Date In Museum:** | **26/04/2013** |
| **Date Out of Museum:** | **22/07/2014** |

<table>
<tr><td rowspan="10"> </td><td colspan="2">MRT #82A-4732</td><td colspan="3">Sensor HS 140</td></tr>
<tr><td colspan="5">$O_2$ Consumption Rates ($mg·year^{-1}·g^{-1}$ )</td></tr>
<tr><td>20% RH</td><td>30% RH</td><td>40% RH</td><td>50% RH</td><td>60% RH</td></tr>
<tr><td>0.0068</td><td>0.0098</td><td>0.0137</td><td>0.0234</td><td>0.606</td></tr>
<tr><td>Dia. (cm)</td><td>Mass (g)</td><td>Vol. ($cm^3$)</td><td colspan="2">Dens. ($g/cm^3$)</td></tr>
<tr><td>8.5</td><td>2147.4</td><td>318.2</td><td colspan="2">6.75</td></tr>
<tr><td colspan="5">Primary Treatment</td></tr>
<tr><td colspan="5">Washed in 2% Hostacor in water solution, dried using 50% Acetone:50%Water then 100% Acetone and finally coated with microcrystalline wax with a small amount of graphite powder.</td></tr>
<tr><td>$Cl^-$ Count:</td><td>21ppm</td><td>Year:</td><td colspan="2">2010</td></tr>
<tr><td colspan="5">Secondary Treatment</td></tr>
<tr><td>Date In Museum:</td><td colspan="5" rowspan="2">N/A</td></tr>
<tr><td>26/04/2013</td></tr>
<tr><td>Date Out of Museum:</td><td>$Cl^-$ Count:</td><td>N/A</td><td>Year:</td><td colspan="2">N/A</td></tr>
<tr><td>22/07/2014</td><td colspan="2">Condition When Leaving:</td><td colspan="3">N/A</td></tr>
</table>

<table>
<tr><td rowspan="10"> </td><td colspan="2">MRT #82A-4735</td><td colspan="3">Sensor HS 150</td></tr>
<tr><td colspan="5">$O_2$ Consumption Rates ($mg·year^{-1}·g^{-1}$ )</td></tr>
<tr><td>20% RH</td><td>30% RH</td><td>40% RH</td><td>50% RH</td><td>60% RH</td></tr>
<tr><td>0.0163</td><td>0.0440</td><td>0.0149</td><td>0.0171</td><td>0.0644</td></tr>
<tr><td>Dia. (cm)</td><td>Mass (g)</td><td>Vol. ($cm^3$)</td><td colspan="2">Dens. ($g/cm^3$)</td></tr>
<tr><td>6.5</td><td>1031.4</td><td>142.5</td><td colspan="2">7.24</td></tr>
<tr><td colspan="5">Primary Treatment</td></tr>
<tr><td colspan="5">Washed in 2% Hostacor in water solution, dried using 50% Acetone:50%Water then 100% Acetone and finally coated with microcrystalline wax with a small amount of graphite powder.</td></tr>
<tr><td>$Cl^-$ Count:</td><td colspan="2">26ppm</td><td>Year:</td><td>2010</td></tr>
<tr><td colspan="5">Secondary Treatment</td></tr>
<tr><td>Date In Museum:</td><td colspan="5" rowspan="2">Wax removed with boiling water and placed in a 0.5M Alkaline Sulfite solution at 60°C. Finally it was dried at 50°C and coated with 15% Paraloid B48 w/v in Acetone.</td></tr>
<tr><td>26/04/2013</td></tr>
<tr><td>Date Out of Museum:</td><td>$Cl^-$ Count:</td><td colspan="2">338; 51; 22; 0ppm</td><td>Year:</td><td>2011</td></tr>
<tr><td>22/07/2014</td><td colspan="3">Condition When Leaving:</td><td colspan="2">N/A</td></tr>
</table>

<table>
<tr><td rowspan="10"> </td><td colspan="2">MRT #82A-4743</td><td colspan="3">Sensor RC 020</td></tr>
<tr><td colspan="5">$O_2$ Consumption Rates ($mg·year^{-1}·g^{-1}$ )</td></tr>
<tr><td>20% RH</td><td>30% RH</td><td>40% RH</td><td>50% RH</td><td>60% RH</td></tr>
<tr><td>0.0605</td><td>00872</td><td>0.0763</td><td>0.1698</td><td>0.3705</td></tr>
<tr><td>Dia. (cm)</td><td>Mass (g)</td><td>Vol. ($cm^3$)</td><td colspan="2">Dens. ($g/cm^3$)</td></tr>
<tr><td>6.6</td><td>910.0</td><td>153.3</td><td colspan="2">5.94</td></tr>
<tr><td colspan="5">Primary Treatment</td></tr>
<tr><td colspan="5">Placed in a 0.1:0.05M Solution of Alkaline Sulfite and heated to 45°C. Rinsedin Deionised water and dried at 50°C then coated with 15% Parloid B48 w/v Acetone.</td></tr>
<tr><td>$Cl^-$ Count:</td><td>5; 2ppm</td><td>Year:</td><td colspan="2">2011</td></tr>
<tr><td colspan="5">Secondary Treatment</td></tr>
<tr><td>Date In Museum:</td><td colspan="5" rowspan="2">N/A</td></tr>
<tr><td>26/04/2013</td></tr>
<tr><td>Date Out of Museum:</td><td>$Cl^-$ Count:</td><td>N/A</td><td>Year:</td><td colspan="2">N/A</td></tr>
<tr><td>22/07/2014</td><td colspan="2">Condition When Leaving:</td><td colspan="3">N/A</td></tr>
</table>

| | | | | |
|---|---|---|---|---|
| **MRT #83A-0002** | | | **Sensor HS 127** | |
| **$O_2$ Consumption Rates (mg·year$^{-1}$·g$^{-1}$ )** | | | | |
| **20% RH** | **30% RH** | **40% RH** | **50% RH** | **60% RH** |
| 0.0341 | 0.0347 | 0.0545 | 0.1292 | 0.3791 |
| **Dia. (cm)** | **Mass (g)** | **Vol. (cm$^3$)** | **Dens. (g/cm$^3$)** | |
| **6.7** | **893.6** | 154.0 | 5.80 | |
| **Primary Treatment** | | | | |
| Washed in 2% Hostacor in water solution, dried using 50% Acetone:50%Water then 100% Acetone and finally coated with microcrystalline wax with a small amount of graphite powder. | | | | |
| **$Cl^-$ Count:** | 27ppm | **Year:** | 2010 | |
| **Secondary Treatment** | | | | |
| N/A | | | | |
| **$Cl^-$ Count:** | N/A | **Year:** | N/A | |
| **Condition When Leaving:** | N/A | | | |

| | |
|---|---|
| **Date In Museum:** | **26/04/2013** |
| **Date Out of Museum:** | **22/07/2014** |

| | | | | |
|---|---|---|---|---|
| **MRT #83A-0130** | | | **Sensor HS 138** | |
| **$O_2$ Consumption Rates (mg·year$^{-1}$·g$^{-1}$ )** | | | | |
| **20% RH** | **30% RH** | **40% RH** | **50% RH** | **60% RH** |
| 0.0135 | 0.0113 | 0.0263 | 0.1179 | 0.2884 |
| **Dia. (cm)** | **Mass (g)** | **Vol. (cm$^3$)** | **Dens. (g/cm$^3$)** | |
| **8.6** | **2417.6** | 336.5 | 7.18 | |
| **Primary Treatment** | | | | |
| Washed in 2% Hostacor in water solution, dried using 50% Acetone:50%Water then 100% Acetone and finally coated with microcrystalline wax with a small amount of graphite powder. | | | | |
| **$Cl^-$ Count:** | 30ppm | **Year:** | 2010 | |
| **Secondary Treatment** | | | | |
| Wax removed with boiling water and placed in a 0.5M Alkaline Sulfite solution at 60°C. Finally it was dried at 50°C and coated with 15% Paraloid B48 w/v in Acetone. | | | | |
| **$Cl^-$ Count:** | 162; 151, 106, 121, 67, 5, 14, 1ppm | **Year:** | 2011-2012 | |
| **Condition When Leaving:** | N/A | | | |

| | |
|---|---|
| **Date In Museum:** | **26/04/2013** |
| **Date Out of Museum:** | **22/07/2014** |

| | | | | |
|---|---|---|---|---|
| **MRT #83A-0149** | | | **Sensor RC 042** | |
| **$O_2$ Consumption Rates (mg·year$^{-1}$·g$^{-1}$ )** | | | | |
| **20% RH** | **30% RH** | **40% RH** | **50% RH** | **60% RH** |
| 0.0193 | 0.0126 | 0.0178 | 0.0326 | 0.0968 |
| **Dia. (cm)** | **Mass (g)** | **Vol. (cm$^3$)** | **Dens. (g/cm$^3$)** | |
| 8.4 | 2199.9 | 312.6 | 7.04 | |
| **Primary Treatment** | | | | |
| Washed in 1% Hostacor in water solution, dried using 50% Acetone:50%Water then 100% Acetone and finally coated with microcrystalline wax with a small amount of graphite powder. | | | | |
| **$Cl^-$ Count:** | 47ppm | **Year:** | 2010 | |
| **Secondary Treatment** | | | | |
| N/A | | | | |
| **$Cl^-$ Count:** | N/A | **Year:** | N/A | |
| **Condition When Leaving:** | N/A | | | |

| | |
|---|---|
| **Date In Museum:** | **26/04/2013** |
| **Date Out of Museum:** | **22/07/2014** |

<table>
<tr><td rowspan="10"></td><td colspan="2"><b>MRT #83A-0160</b></td><td colspan="3"><b>Sensor HS 099</b></td></tr>
<tr><td colspan="5"><b>$O_2$ Consumption Rates (mg·year$^{-1}$·g$^{-1}$ )</b></td></tr>
<tr><td><b>20% RH</b></td><td><b>30% RH</b></td><td><b>40% RH</b></td><td><b>50% RH</b></td><td><b>60% RH</b></td></tr>
<tr><td>0.0059</td><td>0.0165</td><td>0.0112</td><td>0.0157</td><td>0.0582</td></tr>
<tr><td><b>Dia. (cm)</b></td><td><b>Mass (g)</b></td><td><b>Vol. (cm$^3$)</b></td><td colspan="2"><b>Dens. (g/cm$^3$)</b></td></tr>
<tr><td>8.7</td><td>2330.2</td><td>340.1</td><td colspan="2">6.85</td></tr>
<tr><td colspan="5"><b>Primary Treatment</b></td></tr>
<tr><td colspan="5">Washed in 2% Hostacor in water solution, dried using 50% Acetone:50%Water then 100% Acetone and finally coated with microcrystalline wax with a small amount of graphite powder.</td></tr>
<tr><td><b>$Cl^-$ Count:</b></td><td>110; 29ppm</td><td><b>Year:</b></td><td colspan="2">2010</td></tr>
<tr><td colspan="5"><b>Secondary Treatment</b></td></tr>
<tr><td><b>Date In Museum:</b></td><td colspan="5" rowspan="2">N/A</td></tr>
<tr><td><b>26/04/2013</b></td></tr>
<tr><td><b>Date Out of Museum:</b></td><td><b>$Cl^-$ Count:</b></td><td>N/A</td><td><b>Year:</b></td><td colspan="2">N/A</td></tr>
<tr><td><b>22/07/2014</b></td><td colspan="2"><b>Condition When Leaving:</b></td><td colspan="3">N/A</td></tr>
</table>

<table>
<tr><td rowspan="10"></td><td colspan="2"><b>MRT #83A-0176</b></td><td colspan="3"><b>Sensor HS 136</b></td></tr>
<tr><td colspan="5"><b>$O_2$ Consumption Rates (mg·year$^{-1}$·g$^{-1}$ )</b></td></tr>
<tr><td><b>20% RH</b></td><td><b>30% RH</b></td><td><b>40% RH</b></td><td><b>50% RH</b></td><td><b>60% RH</b></td></tr>
<tr><td>0.1013</td><td>0.0722</td><td>1.1861</td><td>0.7230</td><td>1.5486</td></tr>
<tr><td><b>Dia. (cm)</b></td><td><b>Mass (g)</b></td><td><b>Vol. (cm$^3$)</b></td><td colspan="2"><b>Dens. (g/cm$^3$)</b></td></tr>
<tr><td>8.7</td><td>2051.2</td><td>347.2</td><td colspan="2">5.91</td></tr>
<tr><td colspan="5"><b>Primary Treatment</b></td></tr>
<tr><td colspan="5">Placed in a 0.1:0.05M Solution of Alkaline Sulfite and heated to 45°C. Rinsed in deionised water and dried at 50°C then coated with 15% Paraloid B48 w/v Acetone.</td></tr>
<tr><td><b>$Cl^-$ Count:</b></td><td>5; 0ppm</td><td><b>Year:</b></td><td colspan="2">2011</td></tr>
<tr><td colspan="5"><b>Secondary Treatment</b></td></tr>
<tr><td><b>Date In Museum:</b></td><td colspan="5" rowspan="2">N/A</td></tr>
<tr><td><b>26/04/2013</b></td></tr>
<tr><td><b>Date Out of Museum:</b></td><td><b>$Cl^-$ Count:</b></td><td>N/A</td><td><b>Year:</b></td><td colspan="2">N/A</td></tr>
<tr><td><b>22/07/2014</b></td><td colspan="2"><b>Condition When Leaving:</b></td><td colspan="3">N/A</td></tr>
</table>

<table>
<tr><td rowspan="10"></td><td colspan="2"><b>MRT #83-0177</b></td><td colspan="3"><b>Sensor</b></td></tr>
<tr><td colspan="5"><b>$O_2$ Consumption Rates (mg·year$^{-1}$·g$^{-1}$ )</b></td></tr>
<tr><td><b>20% RH</b></td><td><b>30% RH</b></td><td><b>40% RH</b></td><td><b>50% RH</b></td><td><b>60% RH</b></td></tr>
<tr><td>0.0941</td><td>0.1089</td><td>12.43232</td><td>4.1728</td><td>7.2456</td></tr>
<tr><td><b>Dia. (cm)</b></td><td><b>Mass (g)</b></td><td><b>Vol. (cm$^3$)</b></td><td colspan="2"><b>Dens. (g/cm$^3$)</b></td></tr>
<tr><td>8.9</td><td>1996.9</td><td>365.4</td><td colspan="2">5.46</td></tr>
<tr><td colspan="5"><b>Primary Treatment</b></td></tr>
<tr><td colspan="5">Placed in a 0.1:0.05M Solution of Alkaline Sulfite and heated to 45°C. Rinsed in deionised water and dried at 50°C then coated with 15% Paraloid B48 w/v Acetone.</td></tr>
<tr><td><b>$Cl^-$ Count:</b></td><td>3; 4; 0ppm</td><td><b>Year:</b></td><td colspan="2">2011</td></tr>
<tr><td colspan="5"><b>Secondary Treatment</b></td></tr>
<tr><td><b>Date In Museum:</b></td><td colspan="5" rowspan="2">N/A</td></tr>
<tr><td><b>26/04/2013</b></td></tr>
<tr><td><b>Date Out of Museum:</b></td><td><b>$Cl^-$ Count:</b></td><td>N/A</td><td><b>Year:</b></td><td colspan="2">N/A</td></tr>
<tr><td><b>12/08/2013</b></td><td colspan="2"><b>Condition When Leaving:</b></td><td colspan="3">Cracked</td></tr>
</table>

| | | | | |
|---|---|---|---|---|
| **MRT #** | | **Sensor** | | |
| **$O_2$ Consumption Rates (mg·year$^{-1}$·g$^{-1}$ )** | | | | |
| **20% RH** | **30% RH** | **40% RH** | **50% RH** | **60% RH** |
| 0.1140 | 0.2066 | 0.8648 | 4.3799 | 13.8231 |
| **Dia. (cm)** | **Mass (g)** | **Vol. (cm$^3$)** | **Dens. (g/cm$^3$)** | |
| 6.6 | 878.4 | 147.8 | 5.94 | |
| **Primary Treatment** | | | | |
| Washed in 2% Hostacor in water solution. | | | | |
| **Cl$^-$ Count:** | 35ppm | **Year:** | 2011 | |
| **Secondary Treatment** | | | | |
| Placed in a 0.5M Alkaline Sulfite solution at 60°C. Finally it was dried at 50°C and coated with 15% Paraloid B48 w/v in Acetone. | | | | |
| **Cl$^-$ Count:** | 208; 31; 0ppm | **Year:** | 2011 | |
| **Condition When Leaving:** | | Cracked | | |

**Date In Museum:** 26/04/2013

**Date Out of Museum:** 01/08/2013

| | | | | |
|---|---|---|---|---|
| **MRT #83A-0201** | | **Sensor HS 139** | | |
| **$O_2$ Consumption Rates (mg·year$^{-1}$·g$^{-1}$ )** | | | | |
| **20% RH** | **30% RH** | **40% RH** | **50% RH** | **60% RH** |
| 0.0202 | 0.0105 | 0.0203 | 0.0214 | 0.0440 |
| **Dia. (cm)** | **Mass (g)** | **Vol. (cm$^3$)** | **Dens. (g/cm$^3$)** | |
| 6.4 | 959.3 | 136.0 | 7.06 | |
| **Primary Treatment** | | | | |
| Washed in 1% Hostacor in water solution, dried using 50% Acetone:50%Water then 100% Acetone and finally coated with microcrystalline wax with a small amount of graphite powder. | | | | |
| **Cl$^-$ Count:** | 68; 50ppm | **Year:** | 2010 | |
| **Secondary Treatment** | | | | |
| N/A | | | | |
| **Cl$^-$ Count:** | N/A | **Year:** | N/A | |
| **Condition When Leaving:** | | N/A | | |

**Date In Museum:** 26/04/2013

**Date Out of Museum:** 22/07/2014

| | | | | |
|---|---|---|---|---|
| **MRT #83A-0214** | | **Sensor RC 037** | | |
| **$O_2$ Consumption Rates (mg·year$^{-1}$·g$^{-1}$ )** | | | | |
| **20% RH** | **30% RH** | **40% RH** | **50% RH** | **60% RH** |
| 0.0184 | 0.0152 | 0.0247 | 0.0393 | 0.1200 |
| **Dia. (cm)** | **Mass (g)** | **Vol. (cm$^3$)** | **Dens. (g/cm$^3$)** | |
| 6.4 | 959.3 | 136.0 | 7.06 | |
| **Primary Treatment** | | | | |
| Washed in 1% Hostacor in water solution, dried using 50% Acetone:50%Water then 100% Acetone and finally coated with microcrystalline wax with a small amount of graphite powder. | | | | |
| **Cl$^-$ Count:** | 68; 50ppm | **Year:** | 2010 | |
| **Secondary Treatment** | | | | |
| N/A | | | | |
| **Cl$^-$ Count:** | N/A | **Year:** | N/A | |
| **Condition When Leaving:** | | N/A | | |

**Date In Museum:** 26/04/2013

**Date Out of Museum:** 22/07/2014

| MRT #83A-0225 | | | Sensor HS 135 | |
|---|---|---|---|---|
| $O_2$ Consumption Rates (mg·year$^{-1}$·g$^{-1}$ ) | | | | |
| 20% RH | 30% RH | 40% RH | 50% RH | 60% RH |
| 0.0234 | 0.0173 | 0.0465 | 0.1209 | 0.3521 |
| Dia. (cm) | Mass (g) | Vol. (cm$^3$) | Dens. (g/cm$^3$) | |
| 8.4 | 2232.4 | 314.8 | 7.09 | |
| Primary Treatment | | | | |
| Washed in 2% Hostacor in water solution. | | | | |
| Cl$^-$ Count: | 31; 35ppm | Year: | 2011 | |
| Secondary Treatment | | | | |
| Placed in a 0.5M Alkaline Sulfite solution at 60oC. Finally it was dried at 50oC and coated with 15% Paraloid B48 w/v in Acetone. | | | | |
| Cl$^-$ Count: | 10; 4; 0ppm | Year: | 2011 | |
| Condition When Leaving: | N/A | | | |

| Date In Museum: | Date Out of Museum: |
|---|---|
| 26/04/2013 | 22/07/2014 |

| MRT #83A-0233 | | | Sensor RC 024 | |
|---|---|---|---|---|
| $O_2$ Consumption Rates (mg·year$^{-1}$·g$^{-1}$ ) | | | | |
| 20% RH | 30% RH | 40% RH | 50% RH | 60% RH |
| 0.0128 | 0.0118 | 0.0212 | 0.0297 | 0.1095 |
| Dia. (cm) | Mass (g) | Vol. (cm$^3$) | Dens. (g/cm$^3$) | |
| 8.6 | 2327.5 | 337.7 | 6.89 | |
| Primary Treatment | | | | |
| Placed in a 0.1:0.05M Solution of Alkaline Sulfite and heated to 45°C. Rinsed in deionised water and dried at 50°C then coated with 15% Paraloid B48 w/v Acetone. | | | | |
| Cl$^-$ Count: | 62; 2; 790; 2ppm | Year: | 2011-2012 | |
| Secondary Treatment | | | | |
| N/A | | | | |
| Cl$^-$ Count: | N/A | Year: | N/A | |
| Condition When Leaving: | N/A | | | |

| Date In Museum: | Date Out of Museum: |
|---|---|
| 26/04/2013 | 22/07/2014 |

| MRT #83-0273 | | | Sensor HS 142 | |
|---|---|---|---|---|
| $O_2$ Consumption Rates (mg·year$^{-1}$·g$^{-1}$ ) | | | | |
| 20% RH | 30% RH | 40% RH | 50% RH | 60% RH |
| 00561 | 0.0455 | 00575 | 0.1278 | 0.2734 |
| Dia. (cm) | Mass (g) | Vol. (cm$^3$) | Dens. (g/cm$^3$) | |
| 6.5 | 913.7 | 142.5 | 6.41 | |
| Primary Treatment | | | | |
| Washed in 2% Hostacor in water solution, dried using 50% Acetone:50%Water then 100% Acetone and finally coated with microcrystalline wax with a small amount of graphite powder. | | | | |
| Cl$^-$ Count: | N/A | Year: | 2010 | |
| Secondary Treatment | | | | |
| Wax removed with acetone and coated with 15% Paraloid B48 w/v in Acetone. | | | | |
| Cl$^-$ Count: | N/A | Year: | 2011 | |
| Condition When Leaving: | N/A | | | |

| Date In Museum: | Date Out of Museum: |
|---|---|
| 26/04/2013 | 22/07/2014 |

| | | | | |
|---|---|---|---|---|
| **MRT #83-0275** | | | **Sensor HS 132** | |
| **$O_2$ Consumption Rates (mg·year$^{-1}$·g$^{-1}$ )** | | | | |
| **20% RH** | **30% RH** | **40% RH** | **50% RH** | **60% RH** |
| 0.0354 | 0.0348 | 0.0469 | 0.0923 | 0.6585 |
| **Dia. (cm)** | **Mass (g)** | **Vol. (cm$^3$)** | **Dens. (g/cm$^3$)** | |
| 8.7 | 1971.2 | 338.9 | 5.82 | |
| **Primary Treatment** | | | | |
| Washed in 2% Hostacor in water solution, dried using 50% Acetone:50%Water then 100% Acetone and finally coated with microcrystalline wax with a small amount of graphite powder. | | | | |
| **Cl$^-$ Count:** | 77; 188ppm | **Year:** | 2010 | |
| **Secondary Treatment** | | | | |
| N/A | | | | |
| **Cl$^-$ Count:** | N/A | **Year:** | N/A | |
| **Condition When Leaving:** | | N/A | | |

| | |
|---|---|
| **Date In Museum:** | **26/04/2013** |
| **Date Out of Museum:** | **22/07/2014** |

| | | | | |
|---|---|---|---|---|
| **MRT #83-044** | | | **Sensor HS 096** | |
| **$O_2$ Consumption Rates (mg·year$^{-1}$·g$^{-1}$ )** | | | | |
| **20% RH** | **30% RH** | **40% RH** | **50% RH** | **60% RH** |
| 0.2024 | 0.2659 | 0.3768 | 1.7864 | 6.5051 |
| **Dia. (cm)** | **Mass (g)** | **Vol. (cm$^3$)** | **Dens. (g/cm$^3$)** | |
| 6.8 | 478.6 | 164.6 | 2.91 | |
| **Primary Treatment** | | | | |
| Washed in 2% Hostacor in water solution, dried using 50% Acetone:50%Water then 100% Acetone and finally coated with microcrystalline wax with a small amount of graphite powder. | | | | |
| **Cl$^-$ Count:** | 38ppm | **Year:** | 2010 | |
| **Secondary Treatment** | | | | |
| Wax removed with acetone and placed back in a wash of 2% Hostacor then coated with 15% Paraloid B48 w/v in Acetone. | | | | |
| **Cl$^-$ Count:** | 1500; 414; 266; 316; 126; 230; 659; 135; 247; 87; 51; 51; 54; 41ppm | **Year:** | 2011-2012 | |
| **Condition When Leaving:** | | Cracked | | |

| | |
|---|---|
| **Date In Museum:** | **N/A** |
| **Date Out of Museum:** | **N/A** |

| | | | | |
|---|---|---|---|---|
| **MRT #87-0062** | | | **Sensor RC 036** | |
| **$O_2$ Consumption Rates (mg·year$^{-1}$·g$^{-1}$ )** | | | | |
| **20% RH** | **30% RH** | **40% RH** | **50% RH** | **60% RH** |
| 0.0443 | 0.0470 | 0.0664 | 0.2879 | 1.0342 |
| **Dia. (cm)** | **Mass (g)** | **Vol. (cm$^3$)** | **Dens. (g/cm$^3$)** | |
| 6.8 | 1033.7 | 163.2 | 6.33 | |
| **Primary Treatment** | | | | |
| Washed in 2% Hostacor in water solution, dried using 50% Acetone:50%Water then 100% Acetone and finally coated with microcrystalline wax with a small amount of graphite powder. | | | | |
| **Cl$^-$ Count:** | 20ppm | **Year:** | 2010 | |
| **Secondary Treatment** | | | | |
| N/A | | | | |
| **Cl$^-$ Count:** | N/A | **Year:** | N/A | |
| **Condition When Leaving:** | | N/A | | |

| | |
|---|---|
| **Date In Museum:** | **26/04/2013** |
| **Date Out of Museum:** | **22/07/2014** |

## 9.2 APPENDIX B – RETREATED CANNONBALLS – CONDITION AND CORROSION RATES

The graph below is a plot of the primary oxygen consumption results of all 56 samples (in grey) and the consumption results of the 15 retreated samples (green), given as natural logarithms (ln, or $\log_e$). Following this, photos of all retreated cannonballs are shown along with their pre and post-retreatment oxygen consumption results (mg·year$^{-1}$·g$^{-1}$).

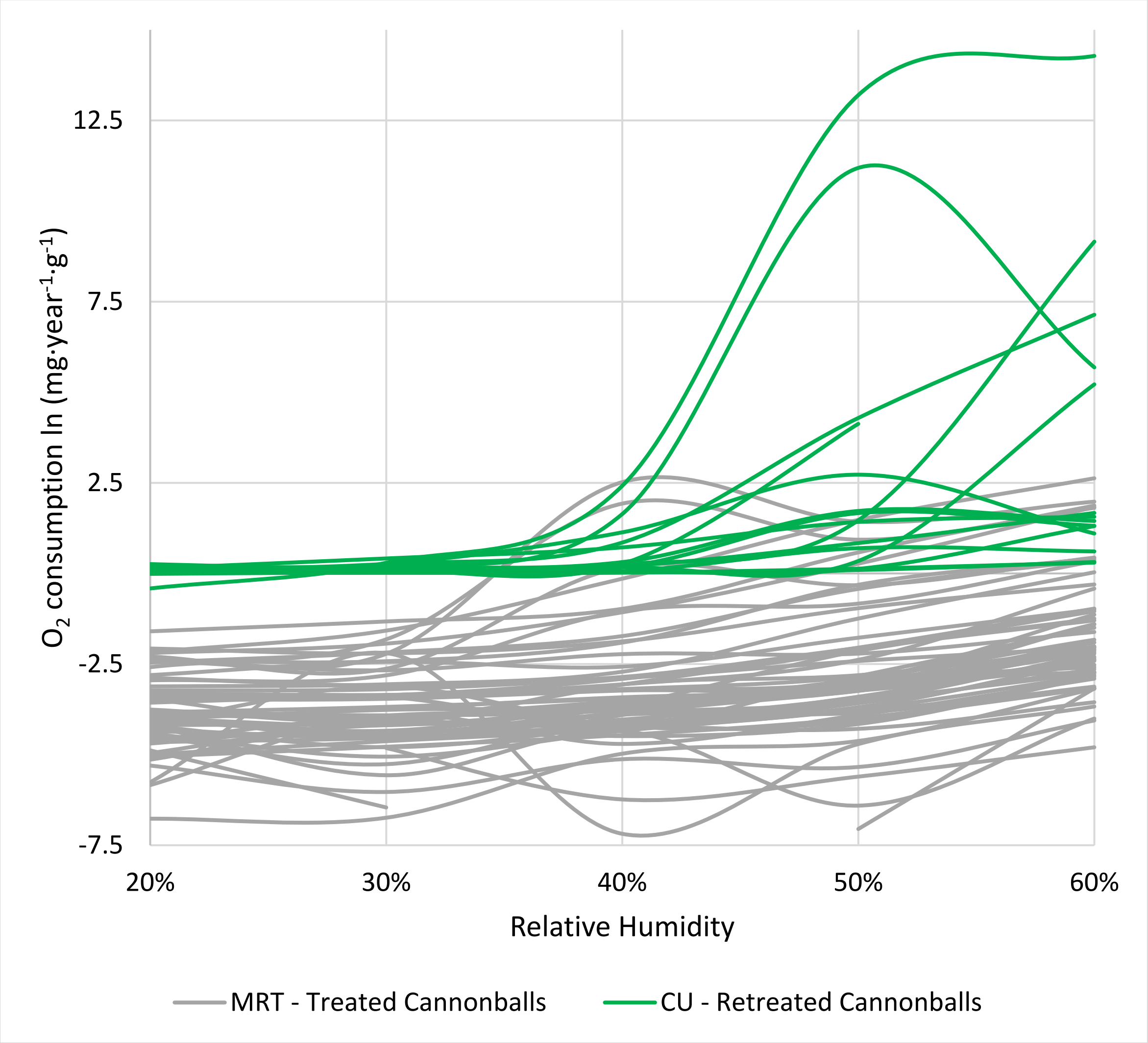

**Figure 9.1:** Primary (grey) and retreatment (green) $O_2$ data. Results given as natural logarithms.

**MRT #78A-0608**

| | 20% RH | 30% RH | 40% RH | 50% RH | 60% RH |
|---|---|---|---|---|---|
| Primary $O_2$ | 0.0312 | 0.0157 | 0.0468 | 0.0603 | 0.1265 |
| Retreat $O_2$ | 0.2578 | 0.0995 | 0.0633 | 0.6971 | 0.6077 |

**MRT #78A-0703**

| | 20% RH | 30% RH | 40% RH | 50% RH | 60% RH |
|---|---|---|---|---|---|
| Primary $O_2$ | -0.0261 | 0.0236 | 0.0328 | 0.0396 | 0.0803 |
| Retreat $O_2$ | 0.1486 | 0.1145 | 0.1719 | 1.6649 | 1.3136 |

**MRT #80A-0865**

| | 20% RH | 30% RH | 40% RH | 50% RH | 60% RH |
|---|---|---|---|---|---|
| Primary $O_2$ | 0.0235 | -0.0208 | 0.0219 | 0.0528 | 0.0755 |
| Retreat $O_2$ | 0.0621 | 0.1609 | 1.6396 | 11.1905 | 5.6861 |

**MRT #80A-1051**

| | 20% RH | 30% RH | 40% RH | 50% RH | 60% RH |
|---|---|---|---|---|---|
| Primary $O_2$ | 0.0152 | 0.0158 | 0.0169 | 0.0228 | 0.0423 |
| Retreat $O_2$ | 0.1845 | 0.1801 | 0.3132 | 1.7240 | 1.4483 |

**MRT #81A-3373**

| | 20% RH | 30% RH | 40% RH | 50% RH | 60% RH |
|---|---|---|---|---|---|
| Primary $O_2$ | 0.0855 | 0.1128 | 0.1776 | 0.6527 | 1.4575 |
| Retreat $O_2$ | -0.4135 | 0.2955 | 2.4186 | 13.1990 | 14.2813 |

**MRT #81A-3499**

| | 20% RH | 30% RH | 40% RH | 50% RH | 60% RH |
|---|---|---|---|---|---|
| Primary $O_2$ | 0.0524 | 0.0602 | 0.3517 | 0.4347 | 1.4031 |
| Retreat $O_2$ | -0.0114 | 0.0493 | 0.2431 | 1.4671 | 9.1549 |

**MRT #81A-3527**

| | 20% RH | 30% RH | 40% RH | 50% RH | 60% RH |
|---|---|---|---|---|---|
| Primary $O_2$ | 0.0907 | 0.0888 | 0.1484 | 0.7315 | 1.5207 |
| Retreat $O_2$ | 0.0808 | 0.2645 | 0.8524 | 4.2899 | 7.1387 |

**MRT #81A-6909**

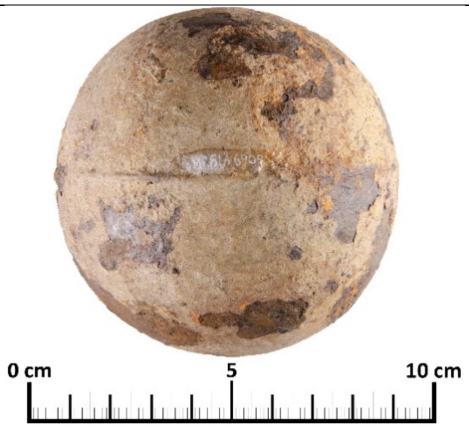

| | 20% RH | 30% RH | 40% RH | 50% RH | 60% RH |
|---|---|---|---|---|---|
| Primary $O_2$ | 0.1260 | 0.1102 | 0.1536 | 0.3829 | 0.7377 |
| Retreat $O_2$ | 0.0413 | 0.0928 | 0.1703 | 0.3437 | 5.2174 |

**MRT #82A-2547**

| | 20% RH | 30% RH | 40% RH | 50% RH | 60% RH |
|---|---|---|---|---|---|
| Primary $O_2$ | 0.0171 | 0.0130 | 0.0259 | 0.0425 | 0.1339 |
| Retreat $O_2$ | 0.0143 | 0.0178 | 0.0205 | 0.1306 | 0.2981 |

<table>
<tr><th colspan="6">MRT #82A-3594</th></tr>
<tr><td colspan="3"> </td><td colspan="3"></td></tr>
<tr><td></td><td>20% RH</td><td>30% RH</td><td>40% RH</td><td>50% RH</td><td>60% RH</td></tr>
<tr><td>Primary $O_2$</td><td>0.0752</td><td>0.1623</td><td>6.8720</td><td>2.5389</td><td>6.1091</td></tr>
<tr><td>Retreat $O_2$</td><td>0.0200</td><td>0.0729</td><td>0.2046</td><td>0.8377</td><td>1.6696</td></tr>
</table>

<table>
<tr><th colspan="6">MRT #82A-4235</th></tr>
<tr><td colspan="3"> </td><td colspan="3"></td></tr>
<tr><td></td><td>20% RH</td><td>30% RH</td><td>40% RH</td><td>50% RH</td><td>60% RH</td></tr>
<tr><td>Primary $O_2$</td><td>0.0212</td><td>0.0197</td><td>0.0292</td><td>0.0427</td><td>0.1146</td></tr>
<tr><td>Retreat $O_2$</td><td>0.0185</td><td>0.0224</td><td>0.0324</td><td>0.0952</td><td>0.3143</td></tr>
</table>

<table>
<tr><th colspan="6">MRT #83A-0176</th></tr>
<tr><td colspan="3"> </td><td colspan="3"></td></tr>
<tr><td></td><td>20% RH</td><td>30% RH</td><td>40% RH</td><td>50% RH</td><td>60% RH</td></tr>
<tr><td>Primary $O_2$</td><td>0.1013</td><td>0.0722</td><td>1.1861</td><td>0.7230</td><td>1.5486</td></tr>
<tr><td>Retreat $O_2$</td><td>0.0280</td><td>0.0789</td><td>0.2628</td><td>4.1279</td><td>43.9450</td></tr>
</table>

<table>
<tr><th colspan="6">MRT #83A-0275</th></tr>
<tr><td colspan="3"> </td><td colspan="3"></td></tr>
<tr><td></td><td>20% RH</td><td>30% RH</td><td>40% RH</td><td>50% RH</td><td>60% RH</td></tr>
<tr><td>Primary $O_2$</td><td>0.0354</td><td>0.0348</td><td>0.0469</td><td>0.0923</td><td>0.6585</td></tr>
<tr><td>Retreat $O_2$</td><td>0.0212</td><td>0.0274</td><td>0.0386</td><td>0.1266</td><td>1.3070</td></tr>
</table>

<table>
<tr><th colspan="6">MRT #83A-0441</th></tr>
<tr><td colspan="3"> </td><td colspan="3"></td></tr>
<tr><td></td><td>20% RH</td><td>30% RH</td><td>40% RH</td><td>50% RH</td><td>60% RH</td></tr>
<tr><td>Primary $O_2$</td><td>0.2024</td><td>0.2659</td><td>0.3768</td><td>1.7864</td><td>6.5051</td></tr>
<tr><td>Retreat $O_2$</td><td>0.1358</td><td>0.4139</td><td>0.7189</td><td>1.4221</td><td>1.5640</td></tr>
</table>

<table>
<tr><th colspan="6">MRT #87A-0062</th></tr>
<tr><td colspan="3"> </td><td colspan="3"></td></tr>
<tr><td></td><td>20% RH</td><td>30% RH</td><td>40% RH</td><td>50% RH</td><td>60% RH</td></tr>
<tr><td>Primary $O_2$</td><td>0.0443</td><td>0.0470</td><td>0.0664</td><td>0.2879</td><td>1.0342</td></tr>
<tr><td>Retreat $O_2$</td><td>0.0042</td><td>0.2625</td><td>1.1346</td><td>2.7251</td><td>1.1021</td></tr>
</table>

## 9.3 APPENDIX C – MATERIALS, EQUIPMENT, AND SOFTWARE

| MATERIAL | PURPOSE |
|---|---|
| Aluminium-Centred Honeycomb glass-reinforced plastic panel | Fibre optic cable plinth fabrication |
| Clas Ohlson (44-1319) 2-litre capacity, 10.8 cm aperture diameter, mild steel screw top lid glass vessel | Reaction vessels |
| Mouldlife PlatSil 10 2-part non-condensing silicone gel | Sealing reaction vessels, coating lid interiors |
| $N_2$ – OFN Oxygen Free Nitrogen, compressed (BOC suppliers) | Control gas |
| NaOH Sodium hydroxide pellets (Fischer Scientific) | Desalination treatment |
| $Na_2SO_3$ Sodium sulfite anhydrous (Fischer Scientific) | Desalination treatment |
| RS Silicon Mould Release Grease (RS 494-124) | Adhering $O_2$ sensor spots |
| Sherwood Chloride Meter Standard | Chloride measurement |
| Sherwood Combined Acid Buffer | Chloride measurement |
| Silica gel – 2.0 – 5.0 mm bead size, colour indicating (GeeJay Chemicals) | Internal climate replication |
| Steward 1/3 Size Gastronorm Container, 5.7L capacity | Desalination treatment |

| ANALYTICAL EQUIPMENT | PURPOSE |
|---|---|
| Binder KBF 720 (E6) climatic chamber | Climate reproduction and silica gel conditioning |
| Kern PCB 3500-2 balance (0.01g resolution) | Mass determination |
| MadgeTech RHTemp101A dataloggers (+/-0.5°C, +/- 3% RH) | Climate measuring |
| Nikon D7000 Camera body | Photography |
| Nikon FX AS-S NIKKOR 18-105 mm lens | Photography |
| PreSens SP-PSt3-NAU glass-mounted oxygen sensor spots (+/- .1hPa @ 2hPa, +/- 1hPa @ 207 hPa) | Oxygen monitoring |
| PreSens OXY-1 SMA Single Channel Fiber Optic Oxygen Transmitter | Oxygen monitoring |
| PreSens OXY-4 SMA 4 Channel Fiber Optic Oxygen Transmitter | Oxygen monitoring |
| Sherwood Chloride Analyser 926 | Chloride measurement |

| | |
|---|---|
| SNOL 60/300 LFN GP Laboratory Oven (+/- 0.2°C) | Drying silica gel, drying cannonballs after retreatment |

| SOFTWARE | PURPOSE |
|---|---|
| Adobe Acrobat Pro DC, Illustrator 2021, Photoshop 2021 | Image, graphics, and document processing |
| EndNote X9.2 | Referencing database and organisation |
| Madgetech 4 | Software for Madgetech dataloggers |
| Matlab 2020a | Data analysis |
| Microsoft Word, Excel | Document and spreadsheet creation, data organisation and analysis |
| Presence Measurement Studio 2, v.3.0.1.1413 | Oxygen monitoring |
| R Studio v.1.4.1717 | Statistical analysis, multilinear regression modelling |